University of Nottingham
UK | CHINA | MALAYSIA

Formulation strategies for the 3D extrusion printing of tablets containing a poorly soluble drug

Maria Inês Evangelista Barreiros

Thesis submitted to the University of Nottingham for the Degree of Doctor of Philosophy

March 2023

Abstract

Oral solid dosage forms are the most flexible and used route of delivery of medicines. 3D printing has allowed new manufacturing approaches to tablets, experimenting with personalised drug loading, combination of two or more drugs and types of drug release. Several 3D printing techniques have been used to produce tablets, with material extrusion being the most widely used in research and being explored in both clinical trials and industrial production.

Here, 3D material extrusion printing is used to manufacture tablets containing a poorly soluble drug, fenofibrate. While the same printer, a Cellink BioX bioprinter, was used for all experiments, different types of formulations, such as paste-based, polymer-based and eutectic mixture were explored. The first experimental chapter focuses on the utilisation of traditional excipients, such as lactose, microcrystalline cellulose, sodium starch glycolate, polyacrylic acid and hydroxypropyl methyl cellulose. Different formulations were designed for rapid and extended release of fenofibrate, making use of disintegrants and swellable polymers, respectively. While the formulation used for the fast release of fenofibrate led to a more rapid release of the drug in comparison to the pure drug, it was still a very slow release. Moreover, while the extended-release formulation led to a slower release of fenofibrate when compared to the pure drug, the release was too slow and not adequate for oral delivery. It was concluded that these types of system, where materials are used as received, formulations are simple to prepare with minimum steps required, are not the most suitable for a poorly soluble drug such as fenofibrate. To improve on this, the second experimental chapter explores the use of amorphous solid dispersions. Using a direct powder printing approach, tablets containing a mixture of fenofibrate and the pharmaceutical polymer Eudragit RL PO were produced. Moreover, the addition of a surfactant, Tween 80, was explored for its plasticising effect. All formulations led to tablets containing the amorphous form of the drug, which improved the release rate of fenofibrate when compared to its pure form. The addition of Tween 80 also facilitated the printing process. However, its addition also led to physical instability, as observed in a short-term stability study. To avoid the stability challenge of amorphous solid dispersions, the third experimental chapter focused on crystalline amorphous dispersions. A PEG 8000 – fenofibrate system was explored, and a eutectic point of this mixture was identified. While the mixture was printable, the

equipment used was not adequate for this material and only a small number of fairly homogenous prints could be obtained. However, the *in vitro* fenofibrate release was able to be assessed and an increase in the release rate of fenofibrate could be observed, which is due to the solubilisation of the drug by the polymer component and the decrease of the particle size of fenofibrate upon mixture preparation.

The explored strategies were chosen for their advantages in terms of formulation and/or processing but they have all been found to require further optimisation in either or both formulation and processing. Only when optimised can they be explored for higher drug loadings and combination of actives.

Acknowledgements

First, I would like to thank my supervisors, Ian Ashcroft, Ricky Wildman and Clive Roberts. A special thank you to Clive, who always had kind words and was there when I was feeling anxious and doubtful of it all. My supervisor at AstraZeneca, Johanna Laru, as well as Susanna Abrahmsén-Alami and Jonathan Booth. Our meetings were invaluable!

I would also like to thank the Marks (East and Hardy) and Adam at the CfAM lab for always being so helpful and making lab work much more fun with their jokes. A special thank you to Mark East for always having my back and going all out to find everything I needed, for always having the time to listen to me talk about my cats and for all the (successful) attempts to scare me. Jane McLaren for her training on the micro-CT, Nigel Neate on SEM and Anil Bastola for helping me with the rheometer.

Thank you to Anna Lion for being a mentor to me from the very first day, for our long chats while waiting for things to finally work in the lab and all the laughs we had. Kristian Plender for being such a great friend and colleague with whom I had such long discussions about work and life. The people in B19 and CDT cohort 5 for these challenging but fun past 4 years, and Mirela for always being there for us. Thank you to Anna Mitzakoff and Kevin Bandeira, who started this PhD journey with me and who became my family away from home. These past 4 years would not be the same without you and I'm so grateful to now have you in my life.

Thank you to my partner Ally, who I met during the PhD. Thank you for helping me design and print a metal nozzle cap for a printhead, for always listening to me, making me laugh and just making life better.

Lastly, I would like to thank my family, who are my everything: my parents, stepparents, my two brothers, and my grandmother. The most special thank you to my mum, to whom I dedicate this thesis, no one will ever compare to you, my best friend and best mother anyone could ever ask for. Thank you for the countless hours talking on the phone, cheering me up and for always believing in me even when I don't. I am beyond grateful for you, for everything you have taught me and continue to teach me every day. This thesis is also dedicated to my grandad, 'vô Manel. You were the kindest, funniest, and most special person I have ever met, and I hope you are proud, wherever you are.

Publications

Journal publications

Rivers, G., Lion, A., Putri, N. R. E., Rance, G. A., Moloney, C., Taresco, V., Crucitti, V. C., Constantin, H., **Barreiros, M. I. E.**, Cantu, L. R., Rose, F., Hague, R., Turyanska, L., Roberts, C. J., Wildman, R., He, Y. A water-soluble excipient for high fidelity inkjet 3D printing of personalized pharmaceutical tablets. (in preparation)

Salimi, S., Wu, Y., **Barreiros, M. I. E.**, Natfji, A. A., Khaled, S., Wildman, R., Hart, L. R., Greco, F., Clark, E. A., Roberts, C. J., & Hayes, W. (2020). A 3D printed drug delivery implant formed from a dynamic supramolecular polyurethane formulation. *Polymer Chemistry*, *11*(20), 3453–3464. https://doi.org/10.1039/d0py00068j

Book chapters

He, Y., **Barreiros, M. I. E.**; Cader, H. (2023). Personalized Medicine: Manufacturing Oral Solid Dosage Forms Through Additive Manufacturing. Additive Manufacturing, 113–150. https://doi.org/10.1007/978-3-031-04721-3_4

Conference attendance

<u>Poster presentations</u>

13th World Meeting on Pharmaceutics, Biopharmaceutics and Pharmaceutical Technology (PBP), March 2022, Rotterdam, The Netherlands – "*The importance of exploring the rheological properties of formulation inks for 3D printing dosage form manufacture*"

<u>Oral presentations</u>

13th World Meeting on Pharmaceutics, Biopharmaceutics and Pharmaceutical Technology (PBP), March 2022, Rotterdam, The Netherlands – "*3D Printed fenofibrate tablets using direct powder printing*"

Controlled Release Society (CRS) Annual Meeting 2022, July 2022, Montreal, Canada – "*The effect of a plasticiser on the printability and solubility of a poorly soluble drug in a 3D printed tablet*"

Table of contents

List of Figures

List of Tables

Glossary

3D	Three dimensional	DLP	Digital light processing
API	Active pharmaceutical Ingredient	DPP	Direct powder printing
AM	Additive manufacturing	DoD	Drop on demand
ASTM	American Society for Testing and Materials	EDX	Energy dispersion x-ray analysis
ASD	Amorphous solid dispersion	EMA	European Medicines Agency
ATR-FTIR	Attenuated total reflection Fourier transform infrared	EM	Eutectic mixture
BSE	Backscattered electrons	FEN	Fenofibrate
BCS	Biopharmaceutical classification system	FDA	Food and Drug Administration
CT	Computed tomography	FDM	Fused deposition modelling
CAD	Computer aided design	GRAS	Generally recognised as safe
DSC	Differential scanning calorimetry	GMP	Good manufacturing practices

HME	Hot melt extrusion	PEGDA	Polyethylene Glycol Diacrylate
HPMC	Hydroxy propyl methylcellulose	pXRD	Powder x-ray diffraction
HPMCAS	Hydroxy propyl methylcellulose acetate succinate	SEM	Scanning electron microscopy
IND	Investigational new drug application	SE	Secondary electrons
LED	Light-emitting diodes	SLS	Selective laser sintering
LCD	Liquid crystal display	SSE	Semisolid extrusion
MHRA	Medicines and Healthcare products Regulatory Agency	SSG	Sodium starch glycolate
MCC	Microcrystalline cellulose	S-SMEDDS	Solid self-microemulsifying drug delivery systems
NCEs	New chemical entities	SLA	Stereolithography
PLM	Polarised light microscopy	.stl	Stereolithography
PAA	Polyacrylic acid	TGA	Thermogravimetric analysis
PEG	Polyethylene glycol	USP	United States Pharmacopeia

UV	Ultraviolet	XRD	X-ray diffraction
UV/VIS	Ultraviolet/visible		

1. Introduction

1.1. Oral solid dosage forms

1.1.1. Traditional manufacturing techniques

Drug delivery systems, or medicines, are the vehicles that facilitate the delivery of therapeutic agents (or drugs) to the body. These are meant to be safe, effective, accurate, reproducible, and convenient. There are several ways – or routes - to administer drugs, such as oral, inhalation, topical, parenteral, amongst others. Each is designed to maximise the therapeutic response to the drug being administered [1]. The oral route of administrating drugs is the most common as it is the simplest, it is generally convenient for the patient, and it is cost effective for the manufacturer [1,2]. It is within oral solid dosage forms that we find tablets. They are usually prepared by compaction and contain not only the drug but other additives, or excipients, each with a specific function or functions [1,3]. These can be included to act as fillers [4,5], matrix formers [4,5], disintegrants[6], binders [5], or to mask flavour or provide colour [7]. Compared to liquid dosage forms, they tend to provide higher chemical and physical stability and are easier to handle [1,8]. However, as a large number of drugs have poor aqueous solubility, this type of system may lead to poor bioavailability in the gastrointestinal tract [1,3,9–11]. Depending on the solubility and intestinal permeability of drugs, the Biopharmaceutical Classification System (BCS) puts drugs into four different classes – drugs with high permeability and solubility are termed class I; in case of low solubility and high permeability the class is II; class III includes drugs with high solubility and low permeability; and lastly, drugs in class IV present both low solubility and permeability [12]. Most drugs and new chemical entities (NCEs) fit into classes II and IV [10].

There are several well-established steps in the manufacturing process of tablets, from processing raw materials to obtaining the final product. Raw materials may exist in different forms, such as crystalline or amorphous [5]. The different forms will have different physical, chemical and mechanical properties and therefore impact the processability of the materials and the characteristics of the final product [9]. While crystalline structures have very defined conformations and/or packing arrangements in the solid-state, amorphous materials do not have any distinguishable crystal lattice [1,8,13]. This lack of defined crystal structure tends to be associated with higher

thermodynamic activity and higher apparent solubility, though it is also associated with lower stability [3,8,14–18], both important characteristics of drugs. As there tends to be several steps in the manufacturing of tablets, as shown in Figure 1.1, there are many opportunities for these phase transitions to happen and this might be difficult to control [8].

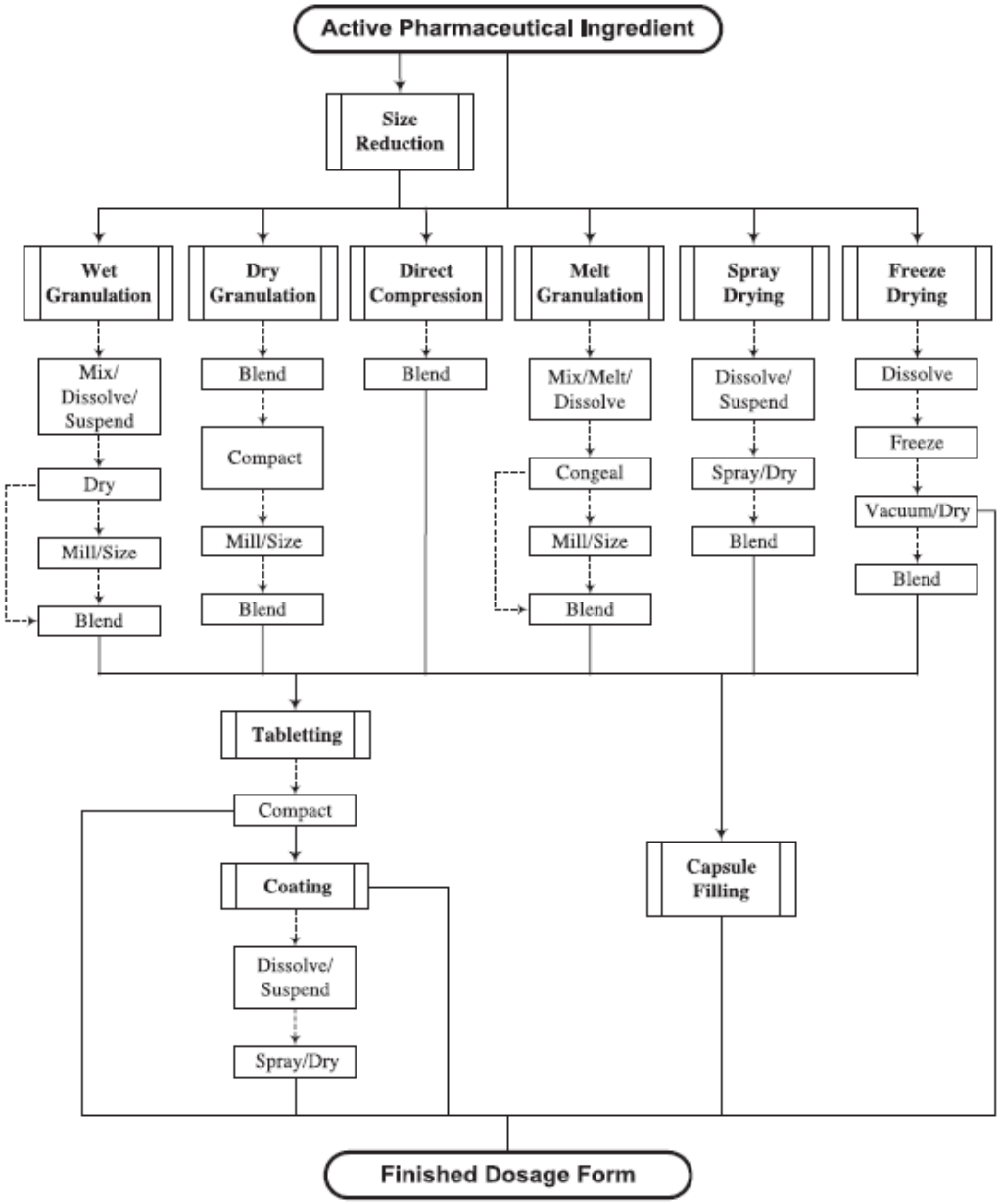

Figure 1.1 Schematic summarising the different routes for the traditional manufacturing of oral solid dosage forms [8]

Due to the poor solubility of many drugs, a size reduction step tends to be the first in the manufacturing process [11,19]. This increases the effective surface area compared to a given mass of drug particles which increases dissolution rate. This

also helps improving the next processability steps, as long as particle size does not become so small that powder cohesion/adhesion becomes dominant [11]. Size reduction processes, such as milling, can induce phase transitions [11,18]. Moreover, phase transitions can occur in many of the other processing techniques such as hot melt extrusion (HME) and spray-drying [19], and when compacting powder blends into tablets [3]. As these transitions can change the processability and properties of the materials and final product, this is something that should be monitored [8]. As many drugs possess poor solubility, several processing and formulation techniques are used to improve their solubilization prior to and during manufacturing. These include chemical modifications (prodrugs), cyclodextrin complexation, salt formation, particle size reduction, solid amorphous dispersion, amongst others [12,20,21]. One of the most used physical approaches is amorphization, in which an amorphous solid dispersion (ASD) is made [19]. As previously mentioned, an amorphous form of a drug is typically more soluble than its crystalline form, though it is also less stable [3,8,13–17]

The entirety of the process from raw materials to processing and packaging is governed by Good Manufacturing Practices (GMP), which describe “the minimum standard that a medicines manufacturer must meet in their production processes” [22]. The guidelines are made to ensure batch-to-batch reproducibility, safety and product quality, describing the necessary documentation, personnel training and the required tests to ensure product quality. These are adopted by national regulatory agencies such as the US Food and Drug Administration (FDA) [23], the Medicines and Healthcare products Regulatory Agency (MHRA) in the UK [24], and the European Medicines Agency (EMA) [22].

The excipients chosen and the manufacturing technique used can influence the type of mechanism through which the drug is released from the dosage form. Modified-release systems have been growing in popularity, especially for controlled-release systems [1] as these are designed to enhance drug therapy and can help increase patient compliance by reducing the frequency of administration [1,2]. Mechanisms that can control drug delivery include [2]:

- Dissolution – drug particles are transferred to the surrounding medium
- Diffusion – independent random movement of drug molecules from a high concentration region to another of lower concentration
- Osmosis – water flows through a semi-permeable membrane in order to equalise the concentration of impermeable solutes on either side of the membrane

- Swelling – the uptake of water by a delivery system causes an increase in the volume of the device, allowing for release of the drug particles through dissolution or diffusion
- Erosion and degradation – drug particles are released as a polymer disintegrates
- Regional delivery and targeting – drug delivery near or at the site of action.

1.2. Additive manufacturing of oral solid dosage forms

Additive manufacturing (AM), commonly known as 3D printing, is a process of building a 3D object by depositing material on a layer-by-layer basis by following a digital image, such as an .stl (stereolithography) file generated using computer aided design (CAD). According to the American Society for Testing and Materials (ASTM) group "ASTM F42 – Additive Manufacturing"; there are seven additive manufacturing process categories: vat photopolymerization, material jetting, binder jetting, material extrusion, powder bed fusion, sheet lamination and direct energy deposition [25]. Within each category, there are different techniques which have different processes and requirements.

Contrary to traditional powder-compression tablet manufacturing, 3D printing [26–31], allows for smaller batch production, personalised bespoke manufacture [32], a reduction of the number of excipients used [30], and the production process completed in one to two process steps. Personalisation can accommodate different drug loadings [33], the use of more than one active in a tablet – the concept of a *polypill* – [4,5,34], and also the control of the release profile through shape [27,30,35,36] or material deposition [37] rather than a formulation approach.

While AM is extensively used in several industries, including medical orthopaedics [38–43], its use for the manufacture of oral solid dosage forms is still in its infancy. Extensive research on the area has been done but only one product has received market approval. Spritam®, produced by Aprecia, was approved by the United States Food and Drug Administration (FDA) in 2015. The tablets are produced using binder jetting, a technique that allows for the manufacture of a high drug loading in a tablet with very rapid disintegration in minimal solvent. This is important for the clinical use of Spritam® and the active, levetiracetam, as it used to stop a seizure in patients that have difficulty swallowing [44,45]. While the manufacturing technique is new, the

materials used are not, and are generally recognised as safe (GRAS) [45]. Even though the only 3D printed marketed product is produced by binder jetting, the most commonly explored technique in research is material extrusion [4,5,7,26,29,32,35–37,46–86], followed by material jetting [27,30,31,87–91]. There have also been publications on vat photopolymerization [34,92–98], selective laser sintering [99–104] and binder jetting [45,105–109] printed tablets.

1.2.1. Techniques

1.2.1.1. Binder jetting

As mentioned, binder jetting, or drop-on-powder jetting, is the technique used to produce the only additive manufactured oral solid dosage form that is on the market [45]. In this technique, powder particles are selectively joined together using a liquid binder on a layer-by-layer process, as it is customary in the different AM techniques. Once a layer has been printed and the binder has solidified, the powder bed is lowered, another layer of powder is deposited, and the process repeats itself (Figure 1.2) [106,108].

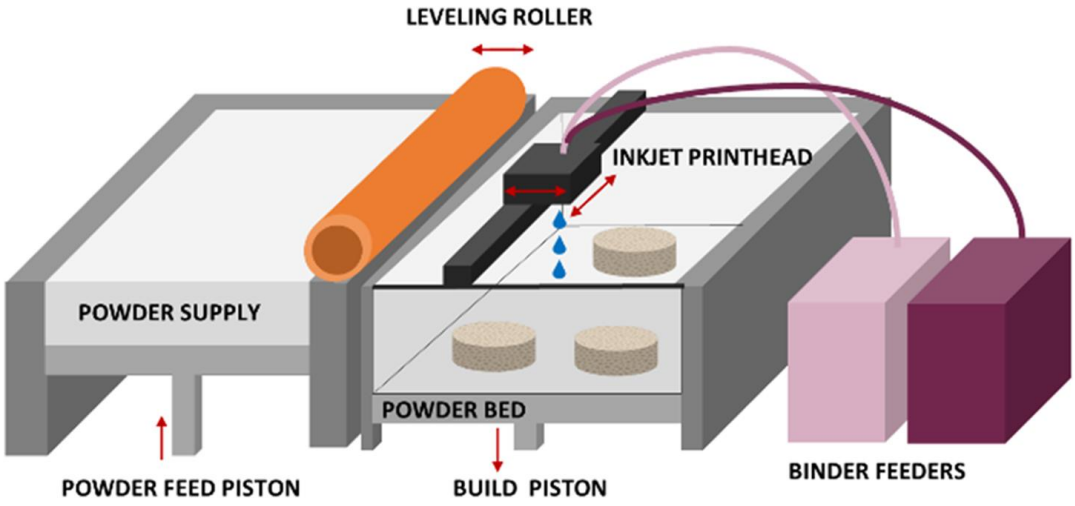

Figure 1.2 Schematic of the binder jetting process [108]

Just like a traditional wet granulation process [107], binder jetting does not require heat, which is an advantage when working with thermo-sensible drugs [107,109]. While the drug is usually placed in the powder mixture, in case of a low loading it can be placed within the binder ink [45]. However, if the drug has poor solubility this might crystallise and become dispersed in the ink which can lead to nozzle blockages [107,109]. As such, it is preferable to have inks containing no dissolved active substances [107]. Producing the binder ink is the main challenge with binder jetting,

something that is also encountered with material jetting. The ink must have adequate surface tension and viscosity [105,107]. The binding ink can contain organic solvents, which tend to have lower viscosity and surface tension than water-based binders and can solubilise poorly soluble drugs, be water-based or be a combination of both [108]. However, powder characterisation is also of utmost importance, as it can impact the penetration of the binding ink and consequently the disintegration speed of the final product. Moreover, the ink and powder interaction must be considered along with the drying steps [107], and the mechanical properties of the dry tablets as they are usually more friable considering the binder ink is the only force holding the powder together [105]. Examples of binder jetting printed tablets are shown in Figure 1.3.

Figure 1.3 Examples of binder jetting printed tables. **a)** Aprecia's Spritam® tablets in all of their four strengths [45]; **b)** SLS printed tablets utilising different grades of hydroxypropyl cellulose [105]

1.2.1.2. Material jetting

With inkjet, the feedstock material consists of a liquid ink that is selectively deposited onto a substrate, solidified and again, the object is built layer by layer. In continuous inkjet, a charge is applied to the fluid ink, causing it to break and eject as droplets. Charged droplets are directed to the desired location and non-charged ink is directed to a catcher to be used again. This, however, is not a commonly used approach as the exposure to the environment may lead to material degradation [110]. In Drop on demand (DoD) printing, the droplets of ink are produced in the nozzle, and their formation can be due to either a thermal resistor or a piezoelectric actuator [30,87],

as illustrated in Figure 1.4. When using a thermal resistor, the charge applied heats up the ink contained in the ink reservoir. This causes evaporation of the material, and therefore the formation of a bubble, which in turn leads to a change in volume, and pressures the material to be ejected from the nozzle in the form of a droplet. With a piezoelectric actuator, when a charge is applied to the material, it causes a mechanical deformation which in turn leads to droplet ejection. This type of actuator has the advantage of not requiring high temperatures which can cause material degradation [87]. Ink formulation is the biggest challenge in jet-based techniques such as inkjet and binder jetting. There are defined limits for ink properties that depend on the equipment used. To assist appropriate ink selection a printability factor Z, or its inverse value the Ohnesorge number (Oh), have been created. They are dependent on ink properties such as viscosity (η), density (ρ) and surface tension (Y), and on the printer itself, such as droplet size (a). The printability factor Z can be calculated as shown in Equation 1.1:

$$Z = \frac{1}{Oh} = \frac{(\gamma\, \rho\, a)^{\frac{1}{2}}}{\eta} \qquad \text{Equation 1.1}$$

Z should have a value between 1 and 10 and the values of viscosity and surface tension might also have requirements within each printer [87].

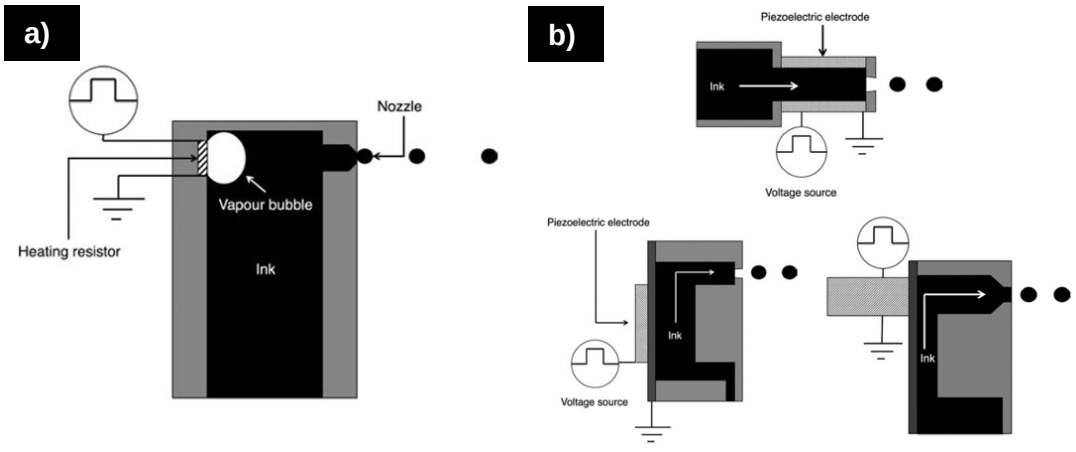

Figure 1.4 **a)** DoD inkjet printer with a thermal resistor controlling drop ejection, **b)** DoD inkjet printer with a piezoelectric resistor controlling drop ejection [110]

Tablets have been inkjet printed using a hot melt chamber with solidification occurring as the material cools after printing [30] (Figure 1.5 **a)**) or by using liquid formulations that can be solidified by other processes [27,31,87,88]. Solidification in the case of a liquid ink can happen by photopolymerization with UV light [27,88–91] (Figure 1.5 **b)**)

or solvent evaporation [31,87]. The current poor availability of safe materials for pharmaceutical applications that are photopolymerisable has slowed the take up of UV photocurable inks [27,88], the use of organic solvents in the inks can be a problem as these organic solvents can be toxic [30,31,87]. While being a lengthy printing process, Cader *et al.* have shown a way of using only water as a solvent for an inkjet printing ink. However, the use of water as solvent is only possible when dealing with water-soluble drugs and the drying step makes this a long process [87].

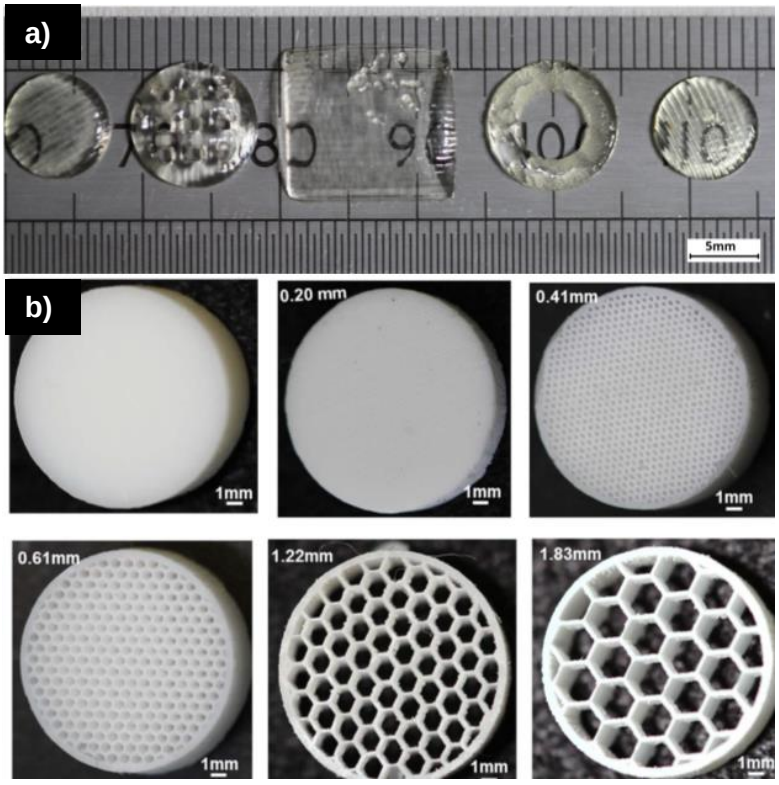

Figure 1.5 Examples of inkjet printed tablets. **a)** Inkjet printed tablets using a photocurable formulation [27]; **b)** hot-melt inkjet printed tables with different internal geometries [30]

Some of inkjet's main advantages are the high placement accuracy of droplets, its high spatial resolution, and low waste [30]. The possibility of controlling droplet deposition at a voxel level could enable high precision of dosages and the use of high potency/low dose drugs. It can be done at room temperature which is an advantage when using thermally sensitive drugs and can be used for manufacturing multi-active dosage forms [91]. However, there are limited materials that can be used for inkjet printing of pharmaceutical products [30] and the main challenge remains the production of a printable ink [87].

1.2.1.3. Vat photopolymerisation

In vat photopolymerization, a photocurable resin is scanned with UV radiation causing the monomers in the resin to polymerise and construct a solid object, one layer at a time [92,93,98]. Several techniques within this category are used to print oral solid dosage forms and these include stereolithography (SLA), digital light processing (DLP) and liquid crystal display (LCD). While their principle is similar, they can be differentiated into scanning (SLA) and projection-type process (DLP and LCD) [92]. While SLA uses a point laser as a light source, DLP uses a digital light projector and LCD [92,93,98] uses light-emitting diodes (LEDs) [92] (Figure 1.6).

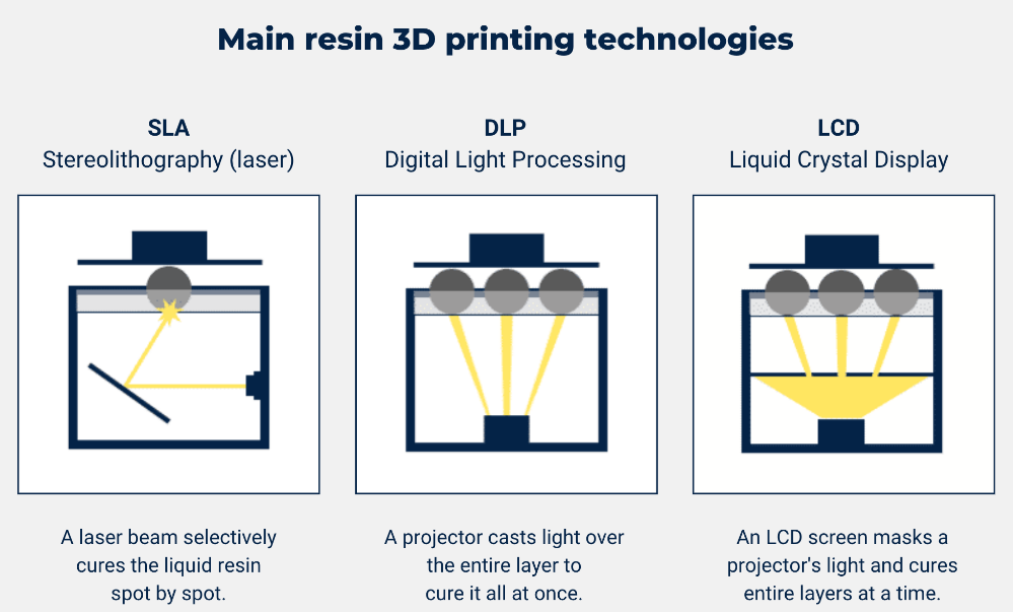

Figure 1.6 Vat photopolymerization technologies [111]

More recently there has been the exploration of volumetric 3D printing (Figure 1.7), in which the object is created in a single step by irradiating a container with a photocurable resin from multiple angles [94]. As there is a limit of light energy that needs to be absorbed in order for polymerisation to occur, this ensures that the polymerisation of the resin is limited to the area where there is the juxtaposition of the 2D images of the object [94,95]. This new vat photopolymerization technique allows for a faster printing speed with single tablets being printed in 7-17s [94]. More recently, and by changing the system to include the rotation of the resin containing vial so it is only irradiated from one angle and there is no juxtaposition of the 2D images of the object, it was possible to simultaneously print 2 dosage forms in just 12-23s [95].

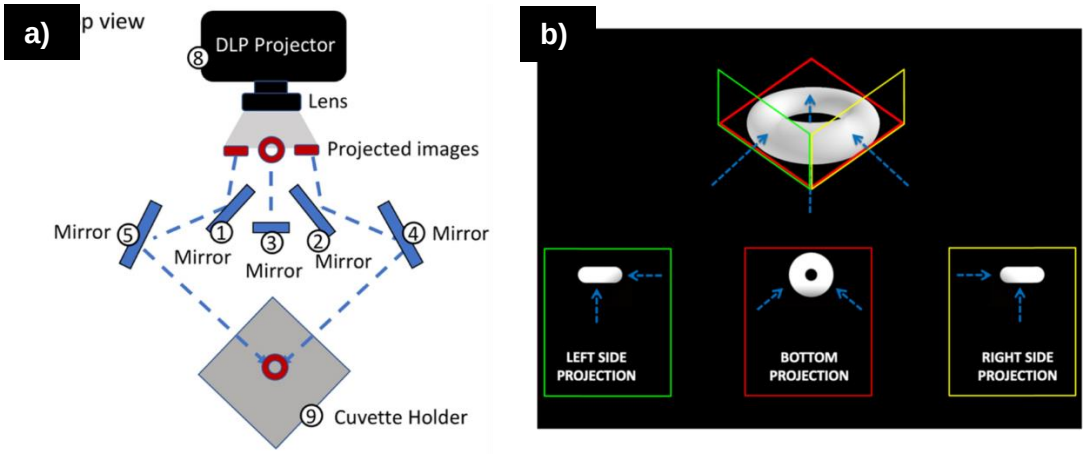

Figure 1.7 Schematics illustrating volumetric printing. **a)** Volumetric printing system; **b)** illustration of how the resin is irradiated and what the projected image is from different angles [94]

Both solutions [34,92,94–96,98] and suspensions [93,97] have been successfully used for the manufacture of oral solid dosage forms and tablets with multiple actives have been printed [34,96]. Examples are shown in Figure 1.8. While the different techniques within vat photopolymerization allow for smoother surfaces [92,97] and high resolution [34,92–95,97,98] when compared to other 3D printing techniques, the small number of materials that can be used and are GRAS are one of the drawbacks that make them less explored compared to other techniques [93,97,98].

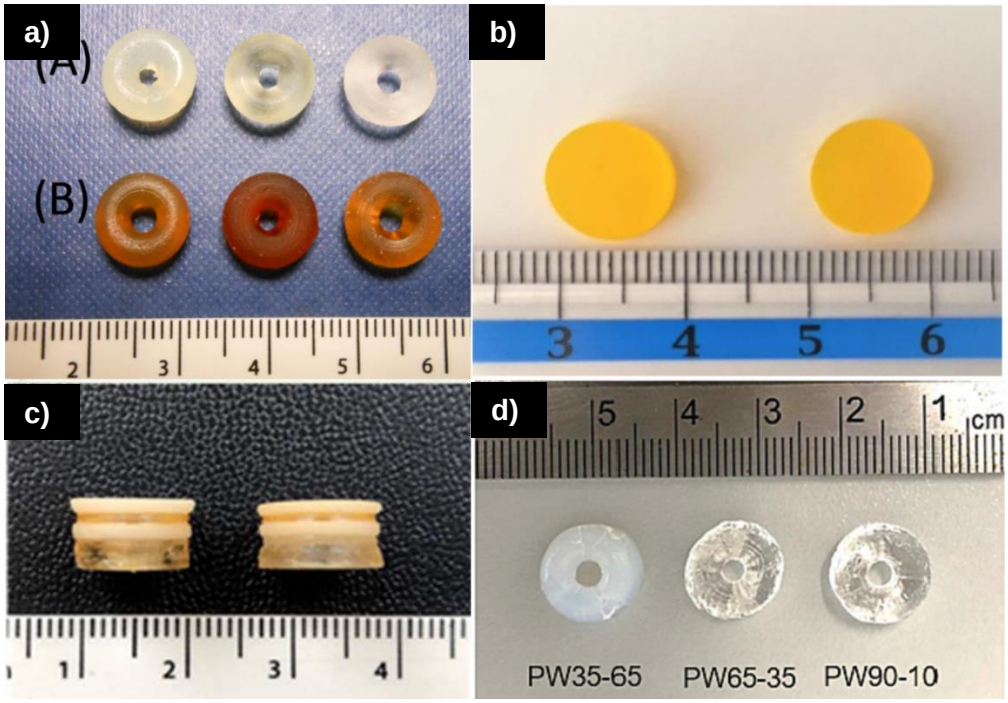

Figure 1.8 Examples of oral solid dosage forms manufactured using vat photopolymerization. **a)** SLA printed tablets loaded with (A) paracetamol and (B) 4-aminosalicylic acid and with varying PEGDA content [98]; **b)** LCD printed tablets containing ibuprofen [92]; **c)** SLA printed polypill containing 6 different actives [34]; **d)** Volumetric 3D printed tablets containing paracetamol and varying PEGDA content [95]

1.2.1.4. Selective laser sintering (SLS)

Selective laser sintering (SLS) is part of the powder bed fusion category. Figure 1.9 illustrates the process. In this technique, a laser is used to sinter selective parts of a powder that's contained in a powder bed in order to form the tablets. Once a layer has been printed, the printing platform is lowered and a new layer of powder is deposited, with the sintering process being repeated [99,101,102]. While this is a solvent free process, the high energy input required for the sintering of powders can cause drug degradation [102,104].

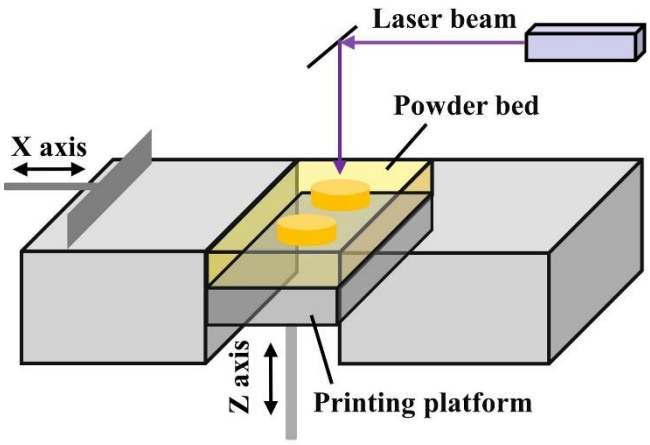

Figure 1.9 Schematic illustrating the selective laser sintering process [102]

In such technique, both the formulation and the powder particle properties are important. For example, particle size distribution can not only contribute to its processability, but it can also impact the density of the produced tablets and consequently the porosity, mechanical strength, and drug release profile [102].

Research has been done on the use of this technique for producing orodispersible tablets with release profiles comparable to commercial formulations with taste masking properties (Figure 1.10 **a)** and **b)**) [103] and with Braille and Moon patterns on their surface to aid visually impaired patients (Figure 1.10 **c)** and **d)**) [100].

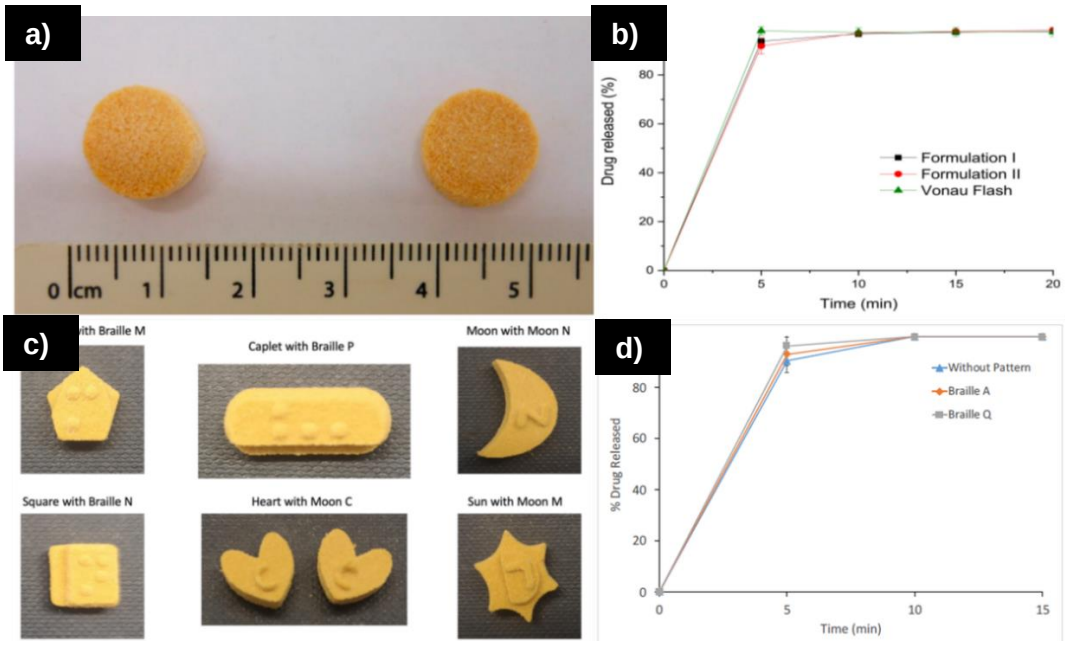

Figure 1.10 Examples of SLS printed tablets and drug release profiles. **a)** Orodispersible tablets with **b)** release comparable to a commercial product [103]; **c)**

Tablets with Braille and Moon patterns which **d)** do not affect the release profile of the drugs [100].

1.2.1.5. Material extrusion

No other AM technique has been used as much as material extrusion for the research of printed oral solid dosage forms. It is a versatile technique that can make use of different materials and achieve different results as there are three large printing modalities within it. They all work differently, require different materials with different material properties and can result in different products. These different modalities include fused deposition modelling (FDM), semi-solid extrusion (SSE) and direct powder printing (DPP).

In a typical FDM process, also called fused filament fabrication (FFF), the most explored technique for printing tablets, a thermoplastic filament is fed through a software controlled heated nozzle that melts the material and builds the object layer-by-layer that then solidifies on the printbed [51,52]. For the printing of tablets, these filaments have either been impregnated with the active substance [36,37,52,54], produced by hot melt extrusion in order to have a solid dispersion as the feedstock [26,55], or used to solely print a capsule device where the drug is then placed [48]. Additionally, drug-free printed tablets have been loaded with an active by soaking in a drug-loaded nanocapsule containing solution [57]. The different approaches are shown in Figure 1.11. Even though the drug loading tends to be limited [53,58], higher drug loadings of 30 % (w/w) have been achieved [54]. This is an inexpensive printing process that allows for the production of hollow objects with which several different polymers can be used. However, the high temperature necessary for both the HME and printing process might be a hurdle when dealing with thermally labile drugs [29,36,37,52]. Moreover, the available polymeric excipients can hardly achieve faster drug release profiles [32,49,53,58–61].

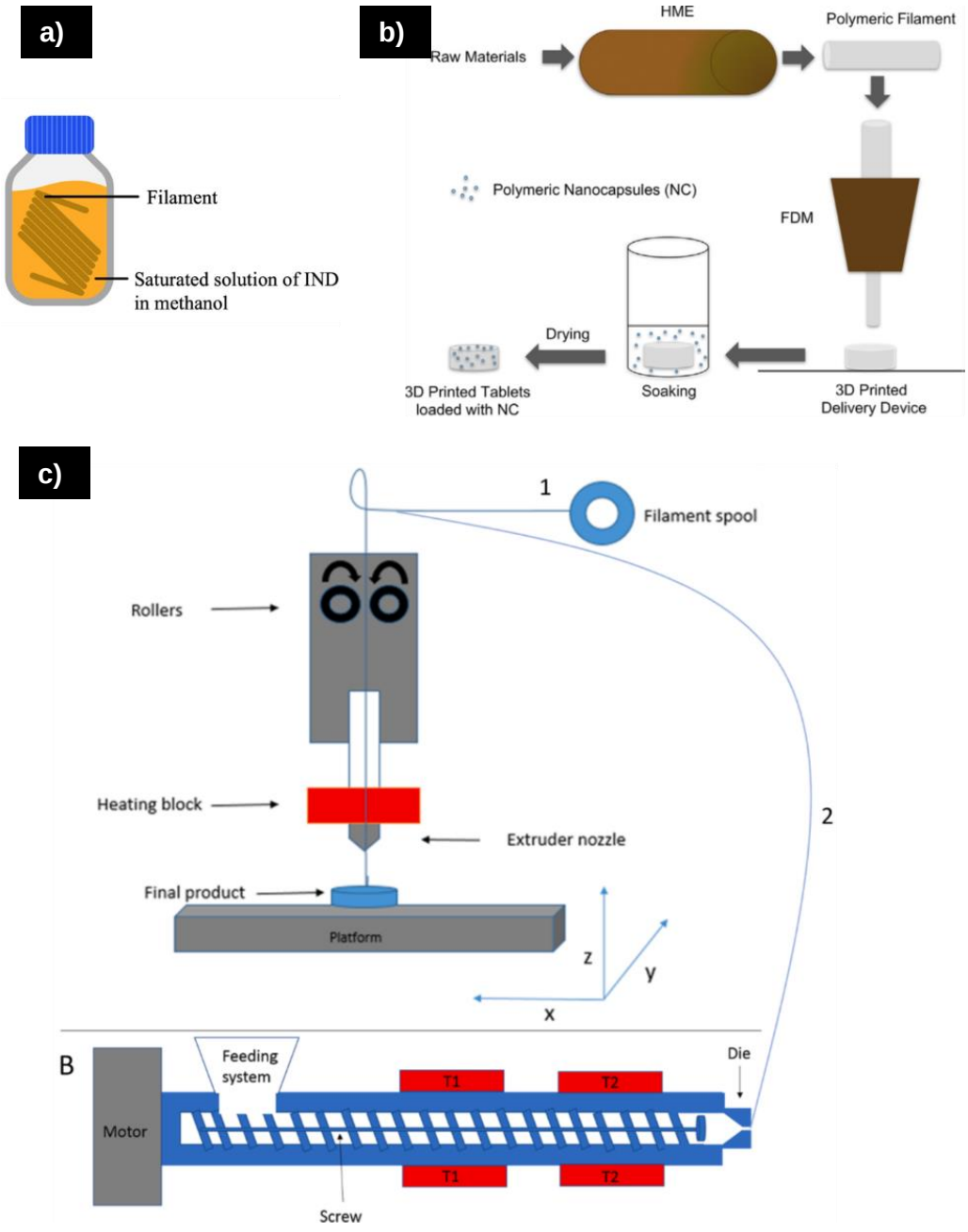

Figure 1.11 Drug loading methods for FDM printing. **a)** polymeric filament being impregnated with drug by soaking in drug containing solution [54]; **b)** drug-free printed tablet being soaked in drug containing nanocapsule solution [57]; **c)** typical HME + FDM process, with drug-loaded filament being produced by HME [62]

Another extrusion-based AM technique is the semi-solid extrusion process, in which material that is placed in a syringe or cartridge is extruded through a nozzle by compressed air [63] or with the aid of a stepper motor [64] (Figure 1.12).

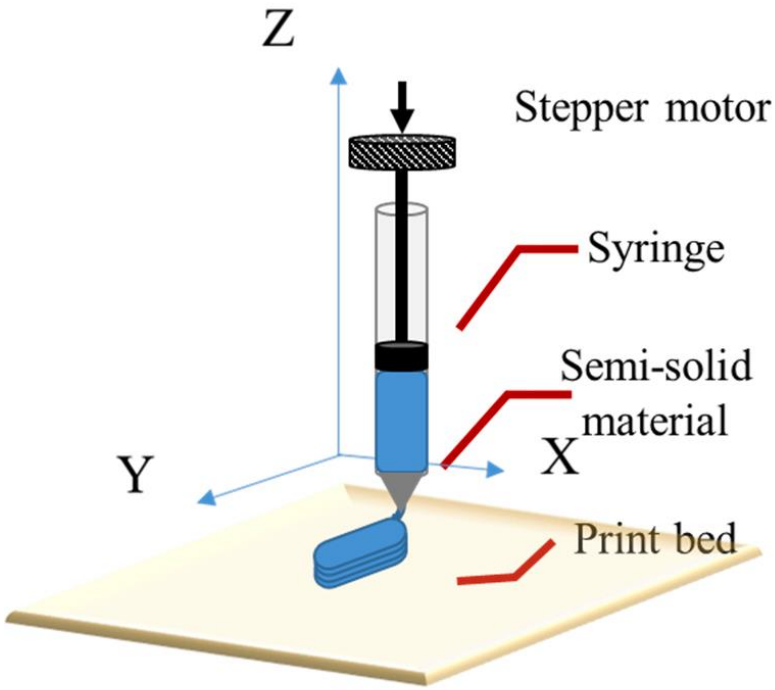

Figure 1.12 Schematic exemplifying a semi-solid extrusion printing process with a stepper motor [64]

For this type of process, a common feedstock material is a paste [4,5,35,46,47,65–69,86], gel [7,64,70], and chocolate [71,72]. Self-emulsifying drug delivery systems [73–77] have also been employed. Tablets printed using these different feedstock materials are shown in Figure 1.13. As the material does not need to be made into a filament using HME, the whole printing can be done at room temperature, overcoming the issue of temperature-induced degradation and increasing the number of materials that can be used [4,5,35,46,63,64,66]. For this type of process, as commonly used pharmaceutical excipients can be included in the formulations [4,5,35,46,67,112], the material availability is good, and higher drug loadings can be obtained [65,67]. The extruded material will then need to be solidified so that a solid pill can be achieved. This solidification process normally relies on the evaporation of liquid binders (e.g., volatile organic solvent, water etc.). The full printed tablet can be air dried at room temperature [65], air dried in a heated printbed [35,46] or placed to dry in an oven [63,66,78]. Alternatively, a drying step can be applied after each layer of material deposition [79]. Other methods such as microwave-assisted drying and vacuum drying have also been investigated [70].

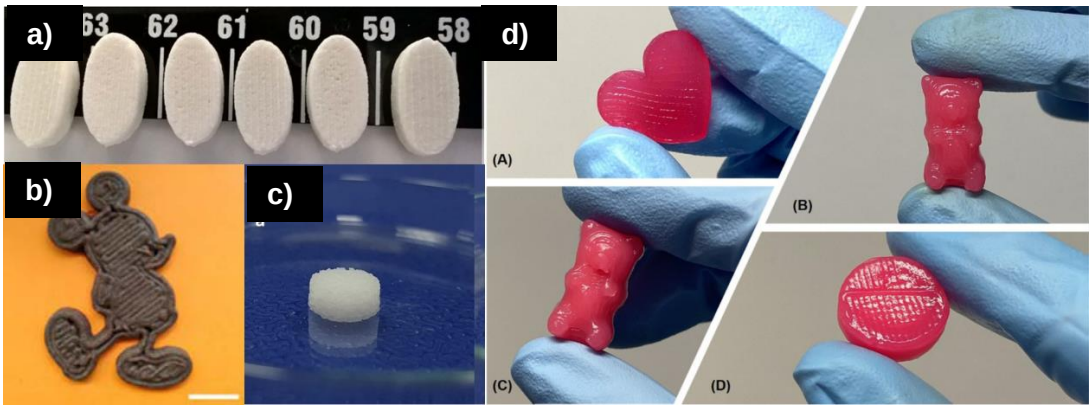

Figure 1.13 Examples of SSE printed tablets using different feedstock materials. **a)** paste-based tablets [46]; **b)** chocolate-based tablets [72]; **c)** self-emulsifying drug delivery system [77]; **d)** gel-based tablet [7].

It was semi-solid extrusion printing that was used in the first study of 3D printed dosage forms in a hospital setting [113]. Moreover, this technique has been trialled and implemented in a hospital in China for the administration of personalised dosages of spironolactone and hydrochlorothiazide, replacing subdivided tablets which have a less accurate dosage than the printed tablets [86].

A more recent extrusion technique is direct powder extrusion printing. Goyanes *et al.* reported an alternative to the need of prior production of filaments used in FDM by having a 1-step direct powder printing process [80]. While there is a previous step of mixing the formulation powders until homogenously distributed, the powder mixture is then fed into the endless screw where it is heated until able to directly extrude from the nozzle, creating the desired 3D shape. Alternatively, the material can be fed into an extruder connected to a nozzle that melts and mixes it [80–82]. The material is moved and extruded either via a screw extruder [80–82], by compressed air [83] or by being compressed with a piston [49,81,84] (Figure 1.14). This avoids the difficult process of preparing filaments that have the physical and mechanical properties needed for FDM printing [49,82,85], the double heating process that can affect temperature sensitive materials [49,83,85], and the use of solvents [85]. While not a direct powder printing process, a similar hot-melt process was used to print tablets containing a eutectic mixture of polyethylene glycol and puerarin which, whilst still using heat to produce an extrudable mixture, took advantage of the lower melting temperature that the system has due to it being a eutectic mixture [50]. Moreover, the formulation was transferred to the cartridge in liquid form rather than in powder form [50].

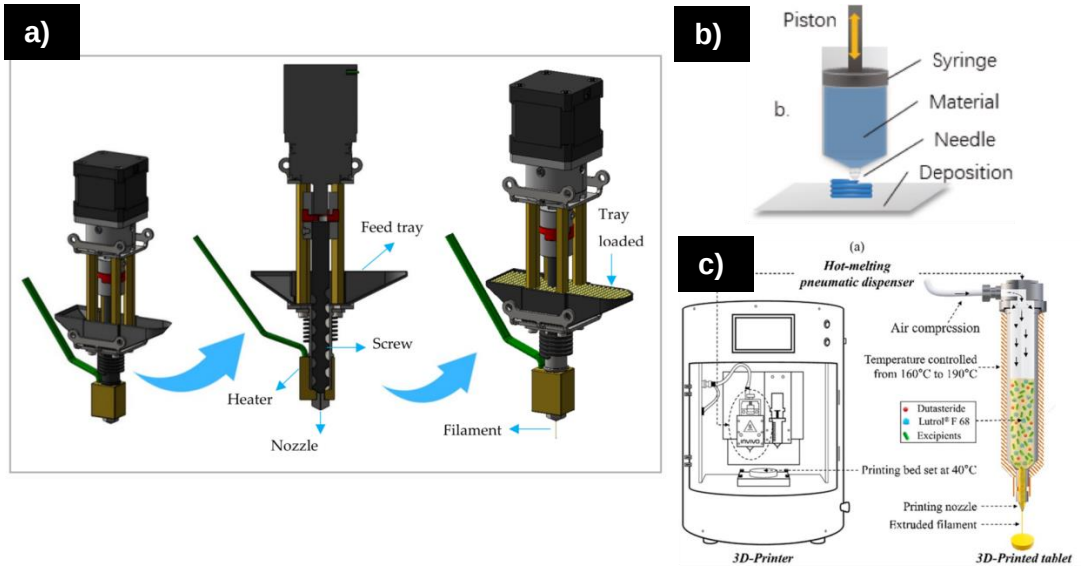

Figure 1.14 Schematics illustrating the different types of material feeding and extrusion in direct powder printing. **a)** single-screw direct powder extrusion printing [82]; **b)** extrusion via piston compression [84]; **c)** direct powder printing through air compression [83]

This has been employed to prepare both amorphous [80,82–84] and crystalline [49,50,85] solid dispersions (SD) with examples shown in Figure 1.15.

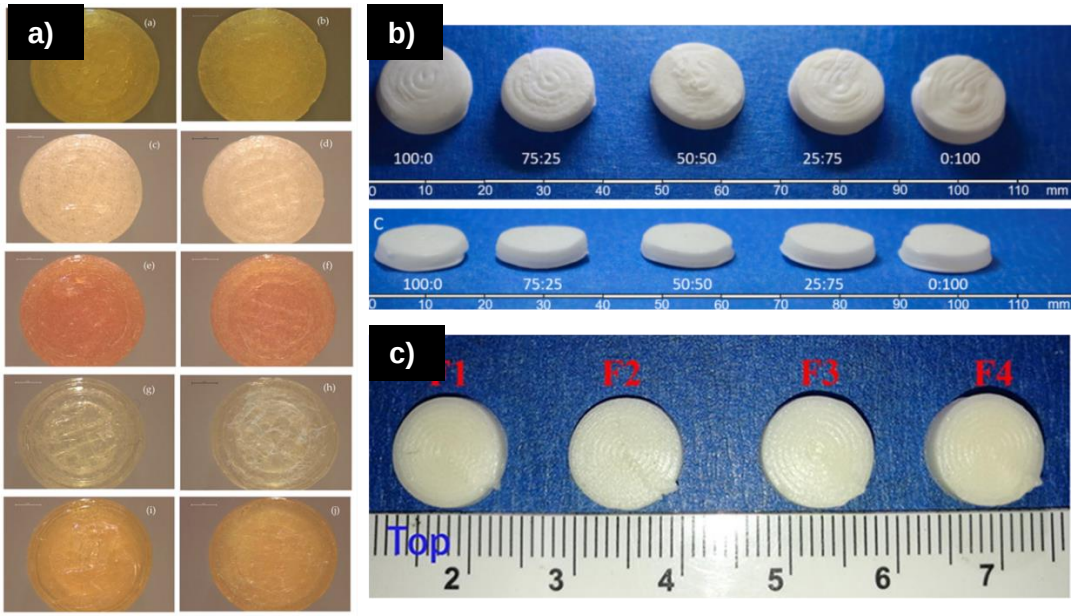

Figure 1.15 Examples of tablets prepared with a thermal extrusion process that differs from FDM. **a)** ASD printed tablets [82]; crystalline solid dispersion printed tablets consisting of **b)** a polymer mixture [85] and **c)** a eutectic mixture [50]

1.2.2. The future of additive manufactured tablets

As mentioned, there has been exhaustive research on the many possibilities that 3D printing has to offer for oral solid dosage forms, with companies pushing for this type of technology to be more widely used.

Starting with Aprecia, the producer of the only 3D printing product on the market. Their continuous binder jetting process allows for the production of large batches, which is not common for the additive manufacturing of pharmaceutical products. The requirement of high dosages was a hurdle when producing tablets through traditional compression, as the high compression forces would lead to poor dispersion of the tablets upon contact with water. The use of binder jetting has solved the issue [44,45].

In a traditional binder jetting process, the powder surrounding the printed parts is not used, but can be recycled and reused. Aprecia further developed their technology and presented Z-form, an 'in-cavity' printing process [44]. Independently of the manufacturing technique used for the production of oral solid dosage forms, there is always a packing step where the tablets are inserted into a blister cavity, which is then sealed with a sealing film [1,114]. This can lead to mass losses during the handling of the tablets, reason why tablets also go through a friability test, as required by pharmacopeias [1,115]. By manufacturing the tablets inside the blister, or as put by Aprecia, *'in-cavity'*, there is be no need for a packaging step as the tablet is already inside the blister. A small amount of liquid binder is jetted into the cavity while empty, followed by a first layer of powder blend, which is then dispersed in the cavity and levelled. These steps are repeated until a last layer of powder blend is deposited, tamped to smooth the top surface and finally, a layer of binder ink is jetted. Prior to sealing the blister, a drying step removes any residual moisture and solidifies the tablet. This improvement in their technology has several advantages, such as facilitating the changeover of materials such as actives, reducing the costs by only utilising what is needed for each tablet, and increasing the process yields [44].

In the same year that Aprecia got their market approval from the FDA for Spritam®, another company with a novel printing technology was founded. Triastek, a China-based company was founded in 2015 and it was its Melt Extrusion Deposition (MED^{TM}) for the manufacture of modified release oral solid dosage forms coupled with an automated process with process analytical technology tools and feedback controls that led to them being selected for the FDA Emerging Technology Program in 2020. Moreover, they have now become a participant in the discussions related to 3D

printing pharmaceutical standards led by the US Pharmacopeia (USP). This technology has granted them 55 patents worldwide and led to three of their products to be given investigational new drug application (IND) clearance from the FDA in the United States. These IND approvals allows them to move the 3 products into clinical trials, with products meant for the treatment of rheumatoid arthritis and ulcerative colitis [116].

MED^{TM} technology allows for the manufacture of controlled release drug delivery systems in a layer-by-layer manner, as it is customary with 3D printing technologies, with the possibility for both research and large-scale production of dosage forms. It can be a continuous and modular process and contrary to other forms of processes for the printing of tablets, there is no pre- or post-production step. The raw materials are directly mixed and fused in the extruder that is part of the equipment, which is attached to the printing station. This station is equipped with multiple printing heads so that several units can be printed at a time (Figure 1.16). This can be used for applications such as oral solid dosage forms and implants, and for several different active ingredients [81,116].

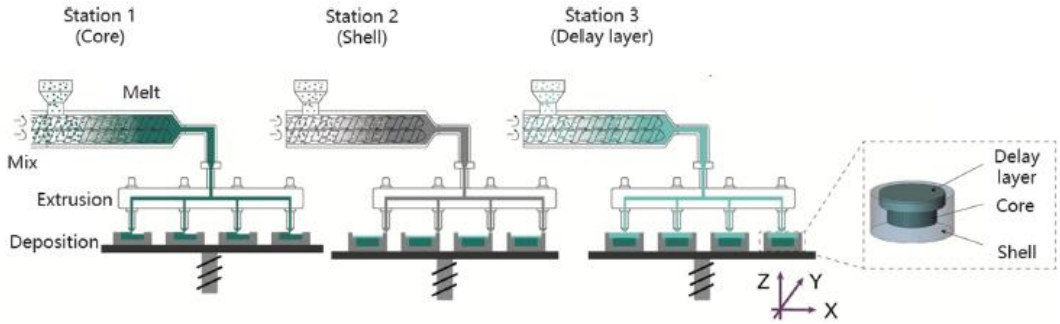

Figure 1.16 Schematic of the MED^{TM} printing process using multiple printing stations so that a tablet containing a delayed layer, core and shell can be manufactured [81]

By changing the design and/or the materials that are used in their printed dosage forms, they can achieve modified and delayed release of actives. A report by Zheng *et al.*, part of Triastek, introduced for the first time the MED^{TM} technology and what it can achieve. Examples are shown in Figure 1.17. In Figure 1.17 **a)**, tablets were produced with and without a pH-responsive layer so that the active could be released in a specific intestinal area after passing through the stomach, such as the duodenum (with pH 5.8) and the jejunum (with pH 6.8) [81]. Moreover, they have shown how multiple actives can be placed in one single tablet, and their release kinetics modulated to fit a certain type of release. In Figure 1.17 **b)** a single tablet containing two drugs, metoprolol and tofacitinib, is shown. Their concomitant administration does

not mean equal release profiles, as while metoprolol is released continuously over time, there is a pulsatile release of tofacitinib, hence the two peaks in plasma concentration [82].

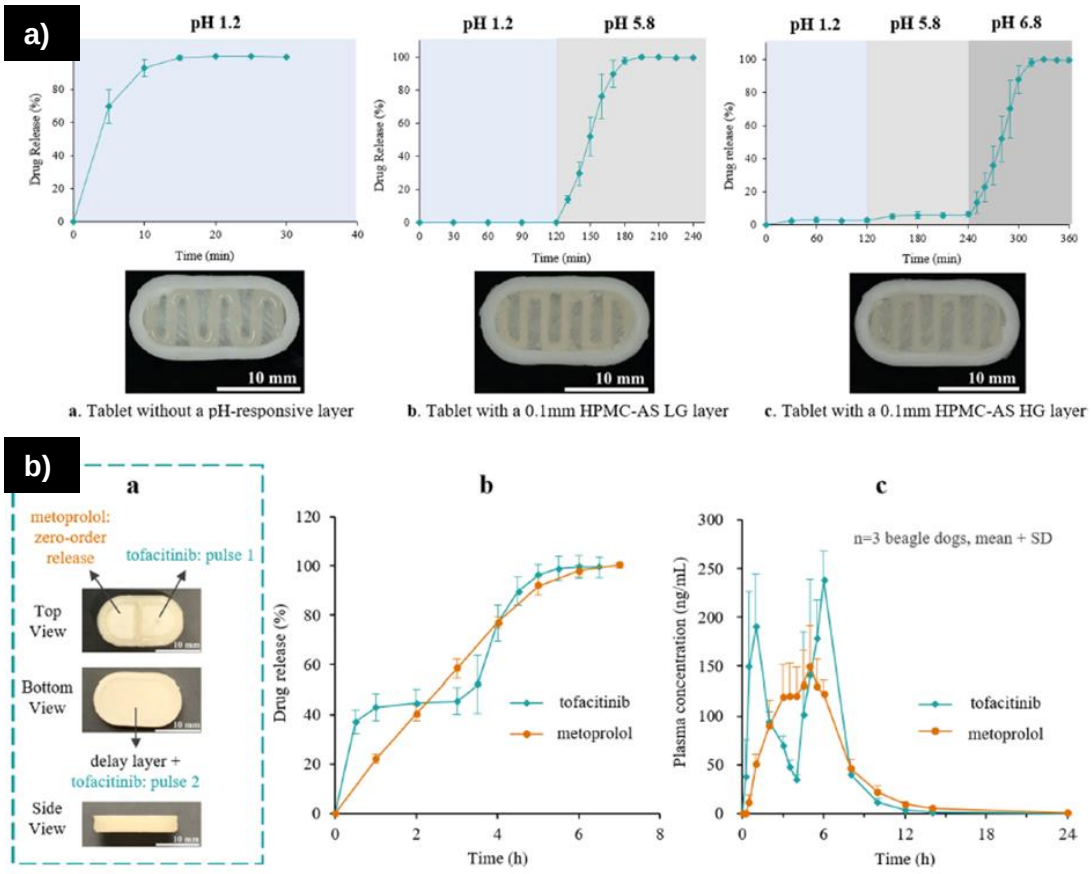

Figure 1.17 Examples of the capabilities of using MED^{TM} technology. **a)** tablets printed with and without pH-responsive layers and their corresponding release profile. **b)** in vitro and in vivo studies of a dual-active printed tablets [82]

Triastek has recently announced collaborations with companies such as Siemens and Eli Lilly. The first to aid automation and the digital transformation of the pharmaceutical industry, by aiding in issues such as manufacturing costs, quality and control. The second, to study excipients and their processability stability and to identify a structure design that will allow drug delivery to specific parts of the gastrointestinal tract in order to improve the bioavailability of administered drugs [116].

One of the leading companies pushing the 3D printing of pharmaceuticals forward is FabRx, a spinout company from University College London. They are involved with several research organisations, universities and pharmaceutical companies with certain projects already being at the clinical level. Not only did they release the world's

first pharmaceutical 3D printer, but they were also the first to complete a first-in-human clinical study using their proprietary Printlets™ technology, done in a hospital setting. 3D printing was used to produce an isoleucine supplementation therapy for patients with the rare metabolic disorder of Maple Syrup Urine Disease (MSUD). Isoleucine had no licensed formulation in the market and for this type of disorder, it needs to be tailored to patients depending on their age, weight and isoleucine blood levels. As such, 3D printing allowed an easy, quick and automated approach to produce the personalised dosage forms [113].

With their own printer, M3DIMAKER™ (Figure 1.18), an extrusion-based printer, they can produce different types of oral dosage forms, using either FDM, direct powder printing or a semi-solid extrusion technique. This printer was designed to be used from research to drug development and clinical practice, with security measures ensuring that only authorised personal make use of it. It also includes in-line quality control measures to detect any fault during manufacturing.

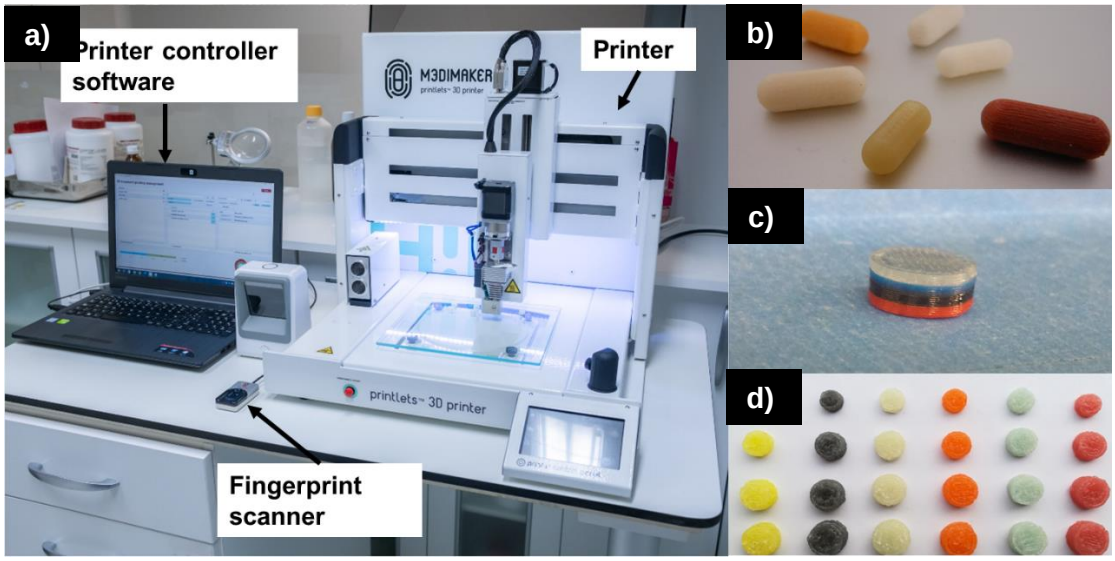

Figure 1.18 FabRx's equipment and examples of products. **a)** M3DIMAKER™ printer; **b)** example of FabRx's Printlets™; **c)** multi-active tablet; **d)** chewable formulation

Besides their printer, FabRx have also developed different types of software. Their M3DISEEN software has combined data on hundreds of formulations for 3D printing to help predict the production of filaments, printing of the filaments and dissolution profile from the produced tablets with such filaments. Figure 1.19 is one of the examples provided on their website, for the manufacture of a pregabalin containing dosage form. It sets out the required temperature for the hot melt extrusion process and the printing temperature, as well as showcasing the likely dissolution profile over

time. Moreover, it takes into account the material properties depending on the manufacturer [117,118].

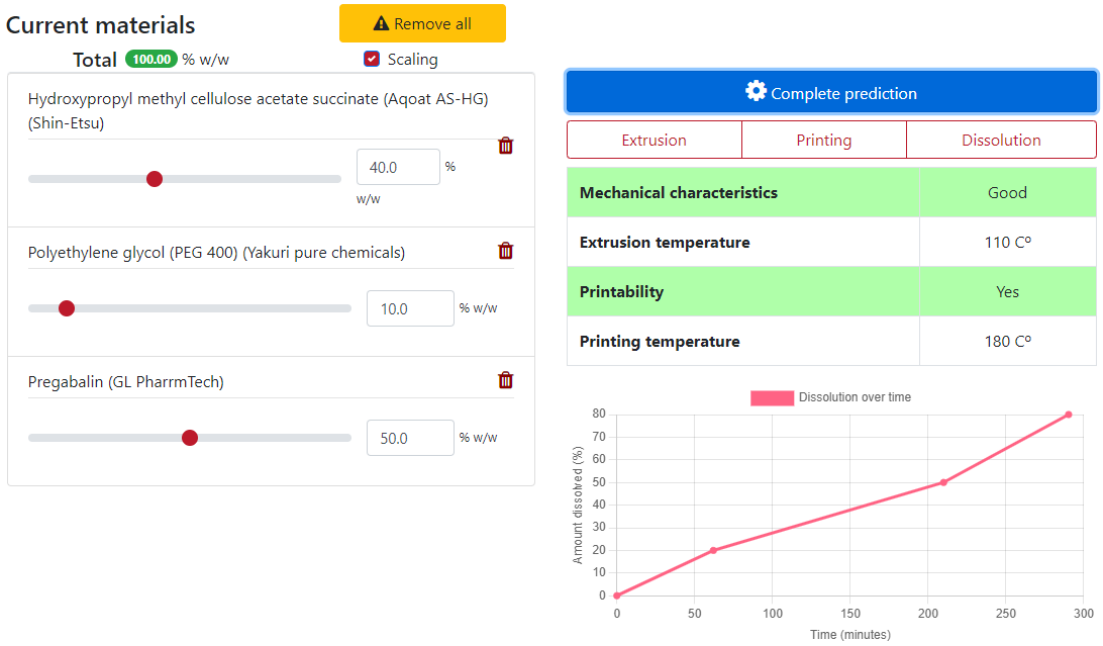

Figure 1.19 Example of FabRx's M3DISEEN software with suggested formulation and the predicted printability and release profile [117]

The company has been at the forefront of much of the research in additive manufacturing of oral solid dosage forms, being involved in the first publications on the use of FDM [52], SLS [104], direct powder printing [80] and recently volumetric printing [94] of oral solid dosage forms. Moreover, they were the first ones to investigate the effect that the shape of the 3D printed tablets could have on the patients' perception [56].

Along with companies like FabRx, existing bioprinter manufacturing companies are also taking the step to better their technology and software in order to ensure their printers can be used for the printing of pharmaceutical products. With translational research and clinical trials in mind, Cellink, a leading 3D bioprinting company, further developed their software, DNA Studio 4, in order to accommodate and follow good manufacturing practice (GMP) guidelines. Now, only authorised personal can make use of the printer, requiring their authentication prior to the use, and keeping digital records of its use, ensuring compliance with the regulatory requirements [119]. This demonstrates the willingness of existing companies to change their products to fit the regulations of the pharmaceutical industry. Other research companies who have diverse portfolios are also taking a step into additive manufacturing of personalised

medicines. The Dutch company TNO, with already years of experience in other areas of additive manufacturing, is collaborating with a hospital in Rotterdam in order to develop a method for the production of personalised paediatric dosage forms [120].

AM is also being used by companies such as Nourished to produce personalised nutrient gummies using material extrusion printing. These are tailored to each individual based on their diet, lifestyle, and health concerns [121].

Besides binder jetting and material extrusion, another type of printing technique is being used for the manufacture of dosage forms. In 2022, Evonik Venture Capital, a company that manufactures speciality chemicals, including excipients for the pharmaceutical industry, announced that they had invested in Laxxon Medical, a pharmaceutical company [122]. Laxxon Medical have developed a patented 3D screen printing technology that allows for the mass production, as well as small production, of oral, transdermal, and implantable dosage forms that can be tailored through their shape, distribution of the active ingredients and choice of materials. It allows for a much faster production of 3D printed dosage forms and it is called SPID® Technology, which stands for Screen Printed Innovative Drug Technology and is illustrated in Figure 1.20. While this technology follows the traditional layer-by-layer manufacturing way of other 3D printing technologies, its way of working is quite different. The medicated paste is dispensed into a screen with the shapes of the layers and then pressed through the screen onto the printing plate. The shape containing screen is then lifted and the platform containing the tablets moves onto the drying station, where the curing of the paste can be through solvent evaporation or UV curing. After the drying process is completed, the platform is moved back to the printing station and the height is automatically adjusted in order to print a subsequent layer. The cycle continues until the dosage forms are completed. The paste used in this process will need the right viscosity to pass through the screen and maintain the shape of the layer after the screen is lifted [123].

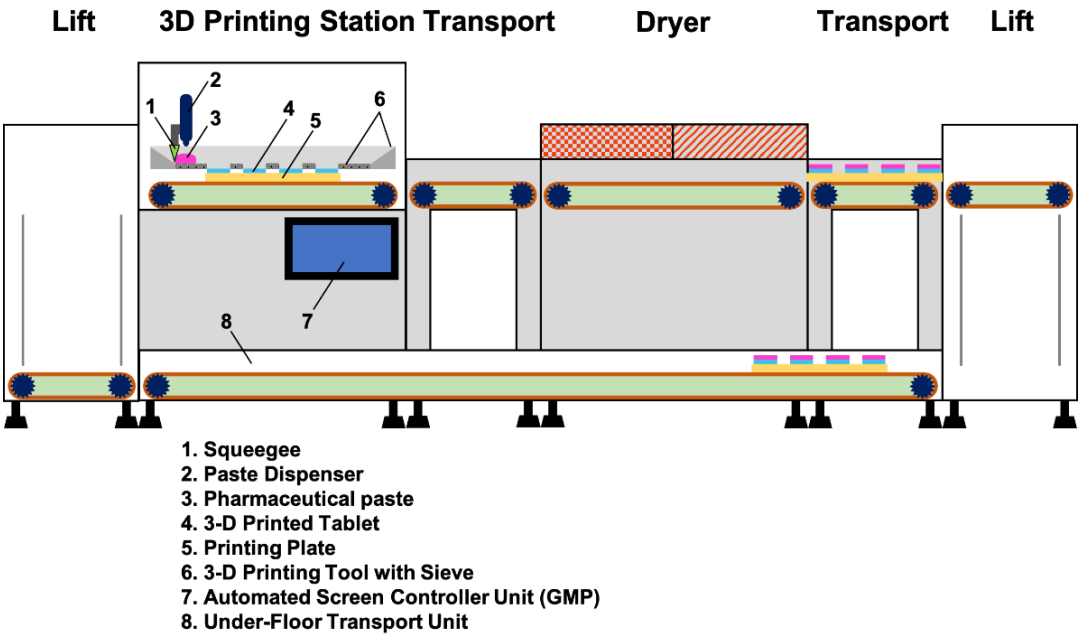

Figure 1.20 Schematic of the SPID® Technology

Together, the companies are establishing a GMP lab and production site in the United States. Some of the products that Evonik manufactures are coating excipients that can either lead to immediate, prolonged or delayed release of active pharmaceutical ingredients (APIs). Evonik's excipients are to be used in Laxxon's paste formulations, therefore allowing for a more controlled drug delivery and a decrease in side effects. With the control over geometry and material deposition, a single tablet can contain more than one dose and multiple actives can be administered in one single pill as well, which is meant to improve compliance [122].

This type of printing was reported by Moldenhauer *et al.* from Laxxon Medical in 2021, where this type of screen printing was used to manufacture delayed release paracetamol containing tablets. In one single production process, three different geometries in three different sizes were printed (Figure 1.21), demonstrating the capability of this technique to produce different dosage forms in one production process [124].

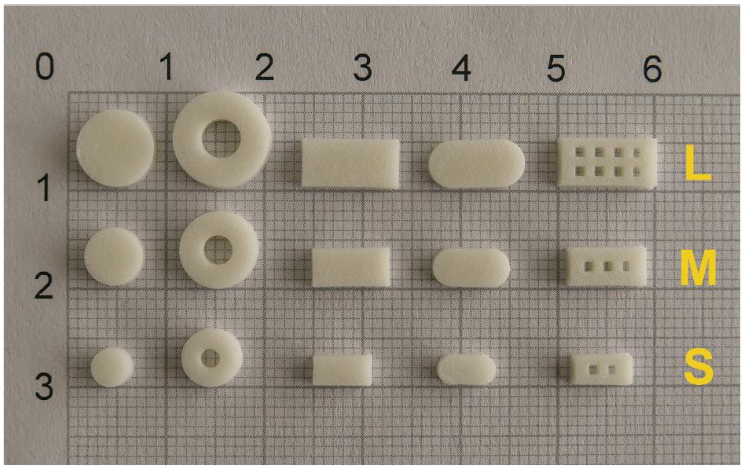

Figure 1.21 Screen printed paracetamol tablets [124]

All the advances led by companies such as Aprecia, Triastek, FabRx and Laxxon Medical and Evonik demonstrate the wish for new and existing pharmaceutical companies to make a wider use of additive manufacturing for the production of pharmaceutical products. And not for the replacement of traditional manufacturing but rather to help solve issues that cannot be easily solved with common manufacturing process, such as fast disintegration of high loading dosage forms and the manufacture of multi-active tablets.

1.3. Aims and objectives of this thesis

The aim of the research presented in this thesis is to explore different formulation strategies for the extrusion printing of oral solid dosage forms containing a poorly soluble drug, fenofibrate. This is a versatile manufacturing technique that is already being trialled and used in hospital settings. Therefore, it is important to explore which type of different formulations can be used with the different modalities of printing. Depending on the printer available, only certain modalities will be possible and these will require different feedstock materials.

As such, the thesis has the following objectives:

- To produce different fenofibrate containing formulations
    - Paste formulations for a fast and an extended release of fenofibrate that can be printed at room temperature, without organic solvents and with commonly used pharmaceutical excipients.

- An amorphous solid dispersion consisting of a drug-polymer mixture for an extended release of fenofibrate with and without the addition of a surfactant
- A eutectic mixture of fenofibrate and PEG 8000 as a crystalline solid dispersion

- To utilise all formulations and print tablets of the same size and shape with good uniformity of weight and friability
- To assess the mechanical and physical properties of the printed tablets
- To assess the dissolution profile of each printed formulation through in vitro dissolution studies
- To investigate the effect that the addition of a high concentration of surfactant has on the stability of 3D printed tablets

2. Materials and Methods

2.1. Materials

2.1.1. Active Pharmaceutical Ingredient (API)

2.1.1.1. Fenofibrate

Fenofibrate ($C_{20}H_{21}ClO_4$) (Figure 2.1) is a prodrug of fenofibric acid [10,125–127] used for the treatment of cholesterolemia, hypertriglyceridemia and mixed dyslipidaemia by reducing triglyceride levels and low-density lipoprotein cholesterol in the blood.

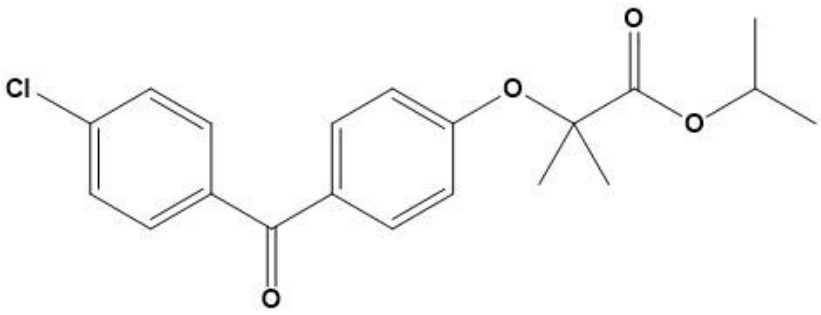

Figure 2.1 Chemical structure of fenofibrate

Fenofibrate is a poorly water-soluble drug with good permeability, meaning it is a BCS class II. Therefore, in oral delivery, solubility is its rate-limiting step during absorption *in vivo* [10,125–128]. As such, there have been several studies trying to improve fenofibrate's effective solubility and hence its bioavailability, mostly aiming to produce solid dispersions [10,125]. For example, Kallakunta *et al*. used a solvent-free hot melt extrusion technique to formulate an amorphous solid dispersion of fenofibrate and hydroxy propyl methylcellulose acetate succinate (HPMCAS), besides investigating the effect that drug loading had on drug release and formulation stability [10]. Fenofibrate's bioavailability has also been increased by using microemulsions, which are defined as thermodynamically stable liquid mixtures of oil, surfactant, a co-surfactant and an aqueous phase [9]. Liposomes are another formulation approach example, which consist of phosphatidylcholine and cholesterol lipid bilayers, the later carrying the hydrophobic drug. In Chen *et al*.'s work, not only did the fenofibrate containing liposomes increase the drug's solubility, the use of bile salts also increased this effect [129]. Other studies include the production of nanoparticles through

nanoencapsulation [130] and HME [131], while Patki *et al*. increased the solubility of fenofibrate by creating nanoemulsifying drug delivery systems with co-processed excipients [132]. Micronization of drug particles, co-grinding, spray-drying [133], nanocrystallisation [134], supercritical fluid impregnation [135], supercritical anti-solvent [136], pelletisation [128,137], electrospinning [126] and eutectic mixtures [15,17] are among other techniques used for the same purpose.

While fenofibrate has not been widely used as a model drug for the 3D printing of oral solid dosage forms, there are some examples across different printing techniques, all using lipid-based formulations. Taking advantage of the drug's low melting point, it was used in formulations using beeswax [30] and Compritol HD5 ATO [138] for hot melt inkjet printed tablets. In material 3D extrusion printing, it was a model drug in formulations for the manufacturing of solid self-microemulsifying drug delivery systems (S-SMEDDS) geometries [75,76,139]. However, none of the studies took advantage of the lower processing temperature that can be utilised when working with PEG-fenofibrate eutectic mixtures [15,17].

In summary, this poorly soluble drug has served as a model drug for lipid-based printed formulations, though its use in paste-based, polymer matrix and eutectic mixture formulations that are printed is still to be explored.

2.1.2. Excipients

2.1.2.1. Lactose

Lactose (Figure 2.2) is one of the most used excipients, both in oral solid dosage forms [140] and carrier-based dry powder inhalation formulations [141]. It has the advantage of being inexpensive and widely available, stable, water soluble, has low hygroscopicity [69,140] and no strong flavour [140]. It is a safe material [141], being non-toxic and non-irritant, even for paediatric use, though its use should be disclosed in case a patient has an intolerance [142]. While widely used, its general poor flowability in crystalline form and its particle-binding properties are hurdles to its use in direct compression tabletting processes. This results in the use of different lactose grades and co-processing lactose with other materials [140].

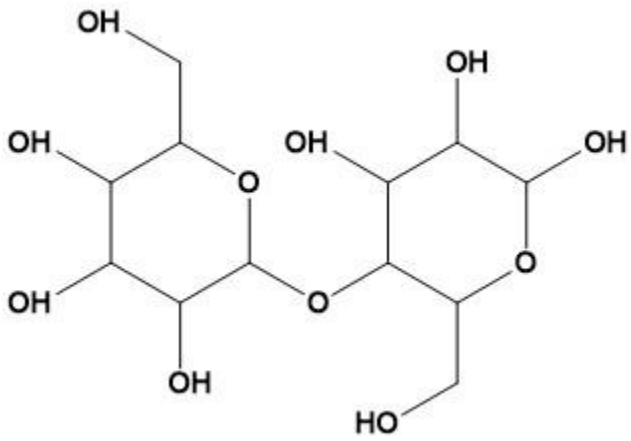

Figure 2.2 Chemical structure of lactose

As a commonly used excipient in commercialised tablets, lactose has been used in 3D powder bed printed oral solid dosage forms [107,143,144]. When using high temperatures, excipients such as lactose might degrade, which in turn can cause poor flow and lead to incomplete structures [145]. Hence, lactose has primarily been used in room temperature 3D extrusion processes using paste-based formulations [4,5,66,67,69,78,86,142]. Due to its water solubility and low hygroscopicity, lactose not only acts as a filler [5,67,86] in these formulations but also helps particles bond together [69,78,142], even in formulations containing insoluble particles [86]. As a filler material, it typically makes up less than 50% of the tablet's composition [5,66,67,69,78,86,142], though in Khaled *et al.*'s work, it went up to 70% [4]. And while its use might improve printability and decrease the extrusion pressure needed [69,86] due to its lubrication properties [69], lactose particles can also lead to low printing efficiency as they can block the nozzle [86]. Considering its wide use and its capability to aid printability, lactose was chosen here as a filler in the paste-based formulation produced in this work.

2.1.2.2. Microcrystalline cellulose

Microcrystalline cellulose (Figure 2.3) is a cellulose derivative that is commonly used in traditional manufacturing as a bulking agent in formulations meant for direct compression [146]. It is compatible with a wide range of actives, physiologically inert and easy to handle. Moreover, it is self-disintegrating as it is highly porous and can aid compaction and tableting in direct compression as it plastically deforms during the process, increasing the area of interparticle bonding [146]. As such, this has been used in formulations for 3D powder printing (or binder jetting) as a bulking/filler agent [108,144,147] and a disintegrant [108]. Its use in paste formulations has varied from

a bulking [66,67,69,73], binding [78], glidant [148] and disintegrant agent [5,112]. As a filler, it was meant to improve the extrudability of the paste [66], though higher amounts of this excipient can also hinder extrudability due to forming a more viscous paste [73] which requires higher printing pressure [69,73]. For its disintegrating properties, this excipient was used in this study in a paste formulation for the fast release of the selected model drug.

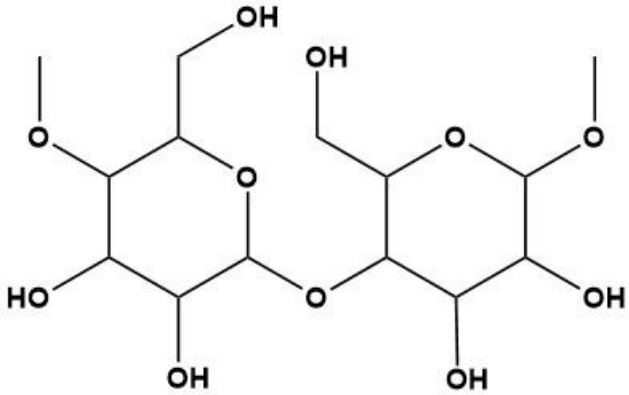

Figure 2.3 Chemical structure of microcrystalline cellulose

2.1.2.3. Sodium starch glycolate

Sodium starch glycolate (SSG) (Figure 2.4) is a hydrophilic and poorly soluble modified starch [149,150]. It is commonly used as a disintegrant, often also called super disintegrant, in oral solid dosage forms [4,5,32,107,112,149–151]. Another commonly used super disintegrant is croscarmellose sodium, another modified starch [65,78,150]. SSG and similar, aid disintegration by rapidly absorbing water and swelling, causing the rapid breaking of the tablet, therefore releasing the active [4,112,150]. While its disintegration mechanism is quite straightforward in powder formulations [149], paste-based printed tablets [4,5,112] and binder jetted tablets [107], its effect on FDM printed tablets does not seem to follow a trend [32,150,151]. Disintegrants such as SSG led to drug release 40% higher in FDM printed tablets compared to those without SSG in Hussain *et al.*'s work [151], though no significant effect was observed in Arafat *et al.*'s [32] and Đuranović *et al.*'s work [150]. Arafat *et al.* hypothesised that this is caused by the disruption of the disintegrating particles with the molten polymers during the thermal process [32]. As its use in this work is for a paste-based formulation, this is not thought to be a hurdle to the process.

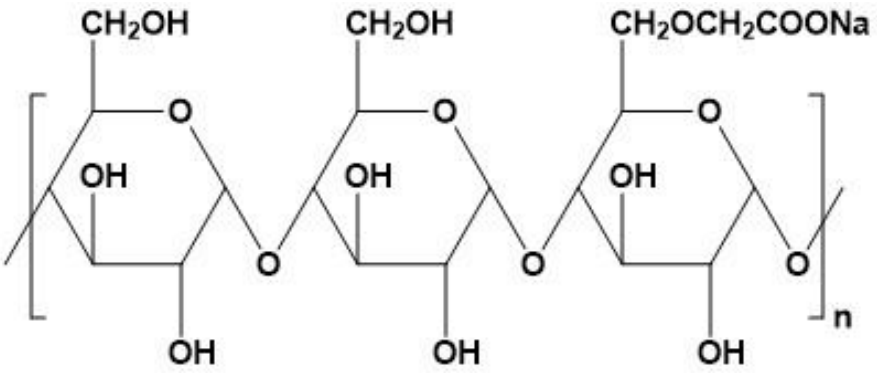

Figure 2.4 Chemical structure of sodium starch glycolate's repeating unit

2.1.2.4. Hydroxypropylmethyl cellulose

Hydroxypropyl cellulose, Hypromellose, or simply HPMC (Figure 2.5), is a water soluble non-ionic cellulosic polymer that is commonly used for its hydrophilicity and swellable gelling properties [28,78,152,153]. Upon contact with water, the polymer forms a thick viscous layer that can be used to modify drug release [28,66,73,152,154], with higher amounts of HPMC in a formulation leading to slower drug release as the gel that forms upon hydration is stronger [5,66,112]. Taking advantage of its gel forming abilities, a hydrogel can be formed and used as a binder in paste-based formulations for 3D printing, with the amount of gel formed dictating the formulations viscosity, the solid tablets' weigh, and hardness [153]. Depending on the HPMC grade that is chosen, as that will influence the ink's viscosity, the wet formulation might be too viscous to print and contain lumps that cannot be broken apart to produce a smooth homogenous ink that is printable [28]. It is due to its binding capability, as well as its ability to form hydrophilic matrices that this was chosen for a paste-based formulation.

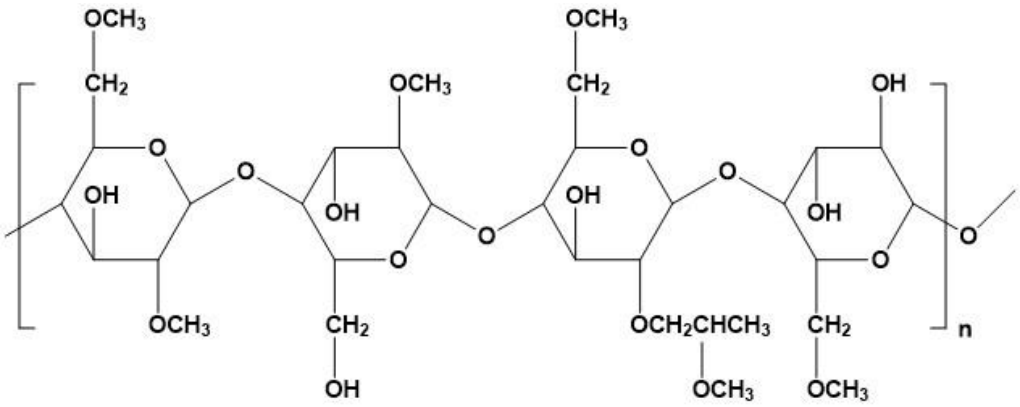

Figure 2.5 Chemical structure of hydroxypropyl cellulose's repeating unit

2.1.2.5. Polyacrylic acid

Polyacrylic acid (Figure 2.6), also known as carbomers, are high molecular weight polymers made of acrylic acid [155,156] used in cosmetics and in pharmaceutical applications [155], as a taste masking agent, an extended release agent, rheology modifier and tablet binder [157]. It is a non-toxic, stable and high thickening polymer [155]. Upon contact with water, it forms a hydrogel [69,112,155,156] with its swelling behaviour depending on different stimuli, such as temperature, pH, light or electric field [156]. However, it is the pH of the medium that determines its final dimensions [155,156], with alkaline pH leading to a maximum swelling of the produced hydrogel and allowing for the release of a higher drug concentration [156]. As it forms a hydrophilic matrix [69,112], it is used for controlled release formulations [69,112,156], sometimes used alongside HPMC [112]. As an excipient in formulations for 3D extrusion printing, the viscosity and swellability of the produced formulation should be considered as to not cause nozzle blockage and severe shrinkage of the printed tablets after drying [69]. Polyacrylic acid was chosen here to, alongside HPMC, to help create a smooth and printable paste that could be used to print extended release tablets containing fenofibrate.

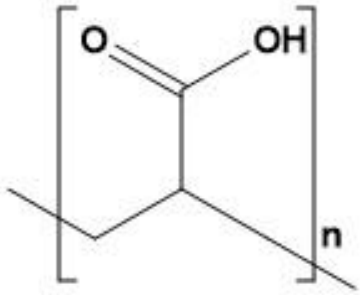

Figure 2.6 Chemical structure of polyacrylic acid's repeating unit

2.1.2.6. Eudragit® RL PO

Eudragit® are a group of polymethacrylates made for sustained release whose differences lay on their substituents. Eudragit RL PO (Figure 2.7) is an insoluble, pH independent and highly permeable polymer [158,159]. Being a stable polymer with good extrudability properties, it is often chosen as the sole polymer matrix or as part of a mixture of polymers in hot melt extrusion [158].

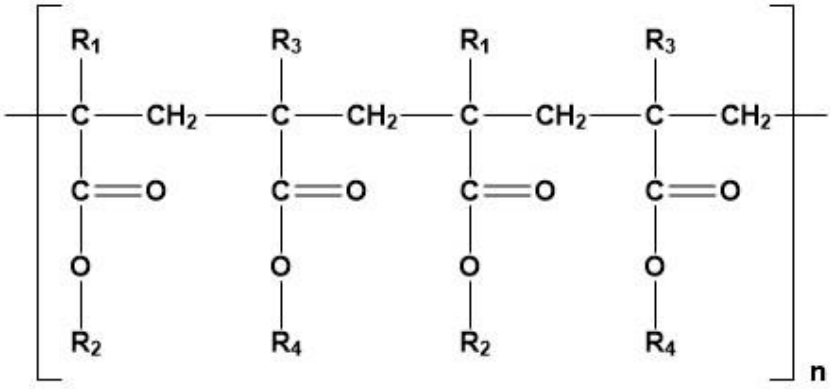

Figure 2.7 Main structure of Eudragit polymers. For Eudragit RL PO R_1 = H, CH_3; R_2 = CH_3, C_2H_5; R_3 = CH_3; R_4 = $CH_2CH_2N(NH_3)3^+$ Cl^- [158]

While other polymers in the Eudragit family have been widely explored as part of different types of formulations [26,83,104,160–164], Eudragit RL PO is infrequently discussed in literature, as mentioned in an extensive review by Santos *et al.* [158]. Still, its use in AM goes back to early publications on tablets manufactured using binder jetting [106,165] and more recently on a formulation for selective laser sintering as reported by Yang *et al.* [166]. When it comes to 3D material extrusion, it was part of Kuźmińska *et al.*'s work, where RL PO and RS PO, were used alone or in a mixture as part of a formulation to print solid tablets using a direct extrusion printing method utilising low printing temperature [85] and part of Gültekin *et al.*'s work, as part of a mixture with a low molecular weight polymer in order to produce flexible filaments suitable for use in FDM [167]. Due to the infrequent use of Eudragit RL PO in the literature, this polymer was chosen as the polymer matrix in an amorphous solid dispersion printed using direct powder printing.

2.1.2.7. Tween 80

Tween 80 (Figure 2.8), or polysorbate 80, is an amphiphilic polymer and non-ionic surfactant that is widely used in biopharmaceuticals and many dosage forms, including oral solid dosage forms [168]. As well as being used as a plasticiser, this material is also used as a solubilising agent for formulations containing poorly soluble drugs [26,168–170]. In processes such as hot melt extrusion, Tween 80 is capable of lowering the glass transition temperature (T_g) of a system, improving processability and extrudability of filaments [26,169], and preventing drug degradation [26]. Ghebremeskel *et al.* hypothesised that the smaller Tween 80 molecules dilute and weaken the cohesive chains of a povidone polymer, increasing the free volume in the polymer, therefore having a good plasticising effect and reducing the dissolution time

of an API by 6 times [169]. The addition of Tween 80 can indeed improve the dissolution rate of APIs, though only up to a certain extent [170]. However, there is a concern that using a surfactant, such as Tween 80, in processes such as HME could possibly impact the product's stability. Still, even at 10% loading, Ghebremeskel *et al.* have demonstrated that while the use of this material can indeed lower the glass transition temperature of the formulation and increase water uptake, the effect on stability of the product is minimal [171]. While this surfactant has been a part of formulations for HME and FDM printing [26], it has not been present in any of the formulations for direct extrusion printing. As this printing method can already require lower printing temperatures, Tween 80 is meant to further lower the printing temperature and facilitate the printing process.

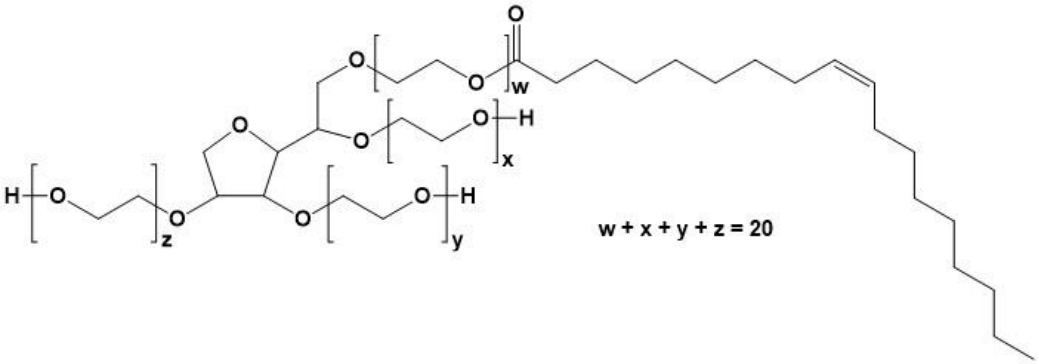

Figure 2.8 Chemical structure of Tween 80

2.1.2.8. Polyethylene glycol (PEG)

Polyethylene glycol (PEG) (Figure 2.9), or Macrogol, is a polymer family made of repeating ethylene glycol units, with different degrees of polymerisation granting different properties [172]. PEG is an amphiphilic polymer that has a highly flexible structure, is biocompatible [172], biodegradable [173] and whose high polarity increases hydrophilicity which in turns aids increasing water solubility. It is often used as a plasticiser [26,62,172,173] and solubility enhancer in polymer-based formulations [26,97]. Its low melt viscosity is an advantage in hot melt extrusion [26,62] and direct powder printing [49]. Smaller molecular weight PEGs, such as PEG 400, have also been found to be good plasticisers and solubility enhancers in photopolymerising formulations [97]. Moreover, certain solid PEGs have been found to produce eutectic mixtures with poorly soluble drug molecules such as fenofibrate [15,17] flurbiprofen [15] and puerarin [50], increasing their release rate [15,17]. This type of formulation has yet to be explored for the printing of oral solid dosage forms, hence this choice of material, more specifically, PEG 8000.

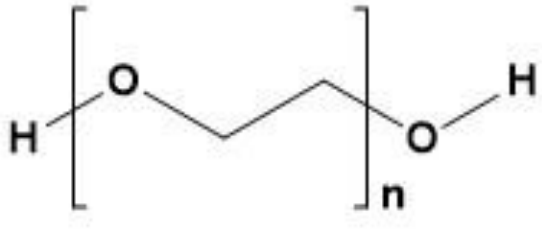

Figure 2.9 Chemical structure of polyethylene glycol's repeating unit

2.2. Methods

2.2.1. 3D extrusion printing

As stated previously, there are different modalities to 3D extrusion printing. In turn, this means that different types of formulations, with different preparations methods, cartridges and printing parameters' requirements are required. The printer chosen for this study is a BIO X bioprinter (Cellink). According to the manufacturer, the printer is capable of automating 3D cell cultures, print tissues and tissue models and test new dosage forms. Depending on the printhead chosen, printing can be done between 4°C and 250°C while maintaining a heated printbed. It is the flexibility in terms of formulation type that dictated the choice of equipment. As described by the manufacturer, this is a pneumatic-based extrusion printer that depends on the input of air pressure in order to extrude the formulation contained in the cartridges [174]. Figure 2.10 illustrates what the printer looks like.

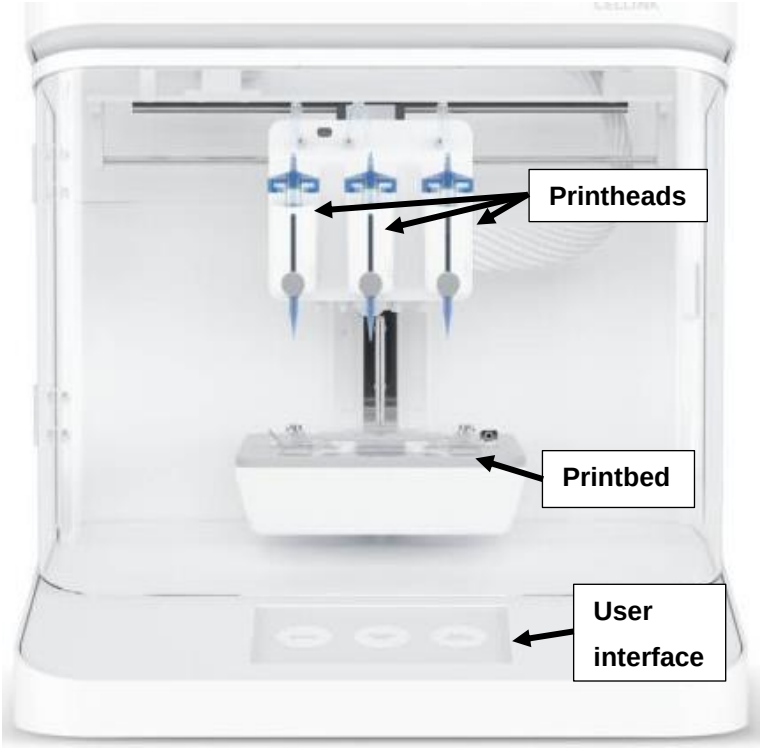

Figure 2.10 Image of the BIO X bioprinter [174]

Typically, 3D printers require a 3D model of the object to be designed and converted to an .stl file that can then be input into a slicing software. A slicing software allows the creation of a G-code stating the coordinates, movements, and actions that the printer must follow when printing. As the BIO X printer has its own slicing software included, an stl. file can be used as the input to the printer. Still, there is the possibility to input G-codes as well. Besides setting parameters as printing temperature and pressure on the printer itself, parameters such as infill geometry and its percentage can also be selected on the printer [174]. Simple 3D models, as the one used throughout the project, and that can then be saved as .stl files, were created using the free software Tinkercad®. Figure 2.11 illustrates a 3D image of a common tablet shape, a cylinder.

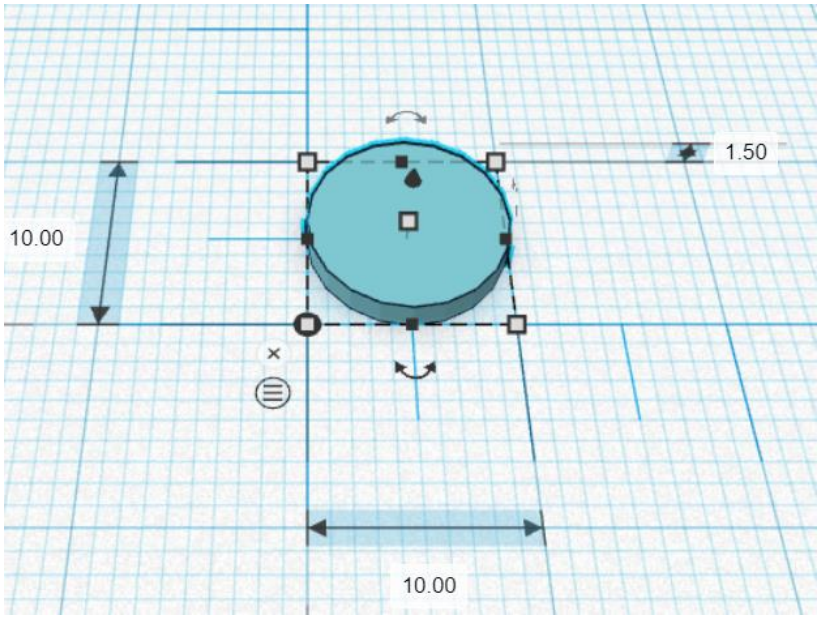

Figure 2.11 Illustrative example of a CAD model of a cylindrical tablet done using Tinkercad®. Dimensions shown are in mm

2.2.2. Attenuated total reflection Fourier transform infrared (ATR-FTIR)

Attenuated Total Reflection Fourier Transform Infrared (ATR-FTIR) spectroscopy is an infrared spectroscopy technique in which infrared light interacts with matter [175]. Molecular vibrations upon absorption of infrared light (mid-infrared region of 4000-400 cm^{-1}) by the samples are very characteristic [176] and give information on the chemical and structure of the entities present in the sample [175]. This is an important technique that can give information on the component materials in pharmaceutical formulations and also on finished products, reason why it is used in this study. When processing techniques such as material extrusion are used, it is important to assess whether there has been any degradation of the drug and that can easily be done with ATR-FTIR as the functional groups of the drug and excipient molecules will give very characteristic peaks in the spectra [4,5,35,46,112].

2.2.3. Viscosity measurements

Viscosity is an important property of printable inks, a parameter that should be within the range suggested by the printer manufacturer, especially for inkjet printing. However, it is also an important parameter for extrusion printing, as formulations that are too viscous will not be extruded even at the highest possible printing pressure. While viscosity can be determined with a viscosimeter and a rheometer [177], the

latter was used in this project. Rotational rheometers, such as the one illustrated in Figure 2.12, are the most common types.

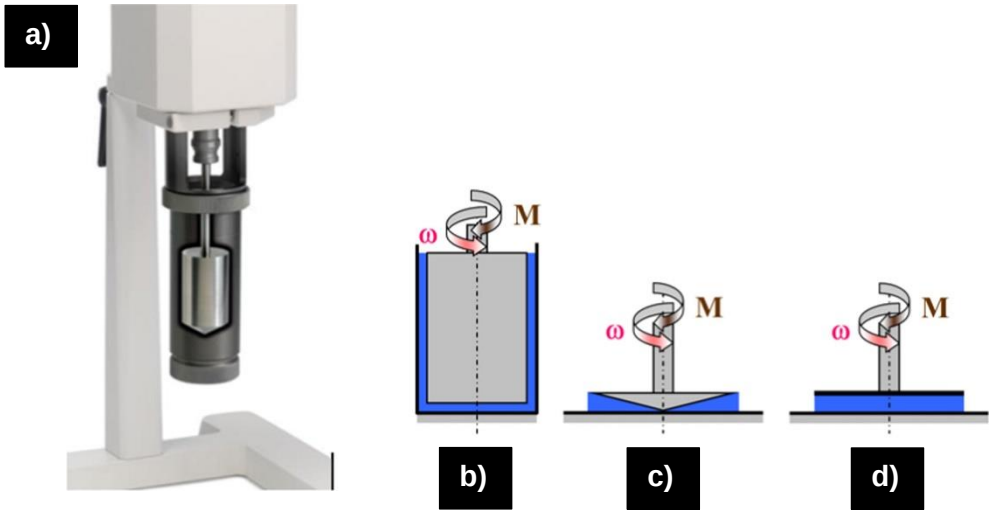

Figure 2.12 **a)** Image of a rotational rheometer, followed by the different geometries used. **b)** Cup and bob, **c)** cone and plate and **d)** parallel plates [54]

The first measuring slit shown in Figure 2.12 **b)** is more common for liquid inks, such as the ones used in inkjet printing [27,88]. The two following ones, cone and plate (Figure 2.12 **c)**) and parallel plate (Figure 2.12 **d)**), respectively, are commonly used for more viscous materials [64,68,75,84]. The measurement of viscosity (η) is intrinsically related to the shear stress of a fluid (τ) and the rate (shear rate ($\dot{\gamma}$)) at which it deforms. This relation is explained by Equation 2.1 [177]:

$$\tau = \eta \cdot \dot{\gamma} \leftrightarrow \eta = \frac{\tau}{\dot{\gamma}} \qquad \text{Equation 2.1}$$

In a rheometer, shear stress (τ) is applied to the sample and a graph of the shear stress as a function of the shear rate of the sample ($\dot{\gamma}$) is usually given by the rheometer software [177]. This is an equation derived from Newton's law of viscosity which consists of Equation 2.2 [178]:

$$\frac{F}{A} = -\mu \frac{\Delta v}{\Delta y} \leftrightarrow \tau = -\mu \frac{\Delta v}{\Delta y} \leftrightarrow \tau = -\mu \frac{dv}{dy} \qquad \text{Equation 2.2}$$

where F is the force (N), A is area (m^2), μ is a proportionality constant, Δv is the velocity ($m \cdot s^{-1}$) and Δy is the distance, with $\left(\frac{dv}{dy}\right)$ being shear rate. There are two types

of fluids, Newtonians, and non-Newtonians. Newtonian fluids, such as water, closely follow ideal Newton's law of viscosity (Equation 2.2) and their viscosity is for practical purposes independent of the shear rate applied. However, non-Newtonian fluids deviate from this relation and can be better described by a power law equation, Equation 2.3 [178]:

$$\tau = -k \left(\frac{dv}{dy}\right)^{n} \qquad \text{Equation 2.3}$$

where k is a proportionality constant. These can exhibit either shear-thinning behaviour (pseudoplastics) as viscosity decreases as shear forces are increased, or a shear-thickening behaviour (dilatants), as viscosity increases as shear forces increase. As a further consideration, a common characteristic of viscous formulations for 3D printing is that they exhibit time-dependant viscoelastic properties. This means they exhibit both solid and liquid properties and as such, this is important to characterise. As a material is deformed, its elastic behaviour is depicted as the storage modulus, measuring the amount of energy that has been stored. At the same time, energy is dissipated in the form of heat, which is quantified as loss modulus, its viscous element [178]. As conditions change during processing it is important to investigate how the change in parameters can influence an ink's viscosity and hence printability.

2.2.4. Powder X-ray diffraction (pXRD)

X-ray diffraction of powders is one of the most used methods to analyse materials [179], and one of the most important techniques in the pharmaceutical sciences [180]. It is a simple process [179], requiring minimal sample preparation and by being a non-destructive technique, makes it ideal for the analysis of finished products [180]. When a material is in its crystalline form, the atoms are arranged in an organised manner and will therefore diffract light. The diffraction of x-rays by the crystalline structure produces a diffraction pattern which will be characteristic from that material [13,179,180]. For amorphous materials with no long-range molecular organisation, no peak is seen in the diffraction pattern, rather a broad halo [4,13,83,180]. This is an important technique when analysing APIs, as different polymorphs of the same active, which will have different x-ray diffractograms as internal order is different, can exhibit different properties such as solubility and melting points. As such, it is important to identify which polymorph is present in formulations and finished products [26,28,37,49,59,63,83,180,181]. Considering the amorphization approach often used

for poorly soluble drugs, pXRD can be useful to show the absence of diffraction peaks (and hence crystalline order), though detection limitations should be considered (typically around 1% w/w crystalline material), especially when the drug loading in a formulation is low [83,167,182,183]. In part for this reason pXRD is often utilised along other techniques such as DSC [17,33,182,184], hot stage microscopy [17] and others [161,185] to study amorphicity or further confirm which polymorph of the material is being used and which one can be found in the final product. pXRD is also used to assess the stability of formulations with time under different conditions, as the drug particles can begin to crystallise and hence show diffraction peaks [83,186,187]. In this study, pXRD is used to investigate, alongside differential scanning calorimetry, the solid-state of raw materials and the printed tablets.

2.2.5. Differential scanning calorimetry (DSC)

Differential scanning calorimetry is a thermal analysis technique based on thermal transitions [26]. As temperature changes in a sample, the heat flow associated with a material transition is measured, as a function of time and temperature. DSC measures the heat quantity that is either lost or absorbed by the sample in comparison with a reference material as temperature changes [83,188]. It allows the assessment of the crystalline form of a material prior to processing and after and whether molecules are incorporated into a matrix, forming an amorphous dispersion [26,60,63,65,84,151,173,189,190]. Moreover, it allows for the measurement of the glass transition temperature [63,182]. The glass transition temperature is the temperature at which a solid material(s) is in a 'glass state' after cooling from its melting phase [191]. This method is usually used along other techniques such as pXRD [17,33,182], especially when the amount of crystallinity in a sample is below the limit of detection in the DSC (around 2% w/w) [184]. Other techniques used alongside DSC include polarised light microscopy [161,187] and hot stage microscopy [181]. While some materials in formulations are used specifically for their plasticising effect [83], which may be observed as a decrease in the T_g of the system, using DSC can also indicate whether other components [58], such as drug molecules [36,55], can also have a plasticising effect on a formulation. DSC is also useful when determining the eutectic point of a eutectic mixture as only one melting event will be observed in the DSC curve, while two melting peaks are observed away from the eutectic point [17,192–194]. In this study, DSC is used to investigate, alongside pXRD, the solid-state of raw materials and the printed tablets as well as to produce a phase diagram of a binary mixture in order to confirm the eutectic point of the mixture.

2.2.6. Polarised light microscopy (PLM)

Polarised light microscopy is an optical contrast-enhancing technique [195] that takes advantage of anisotropy of materials to visualise them [195,196]. The microscope is equipped with a polariser and an analyser (Figure 2.13). The polariser is placed between the light source and the analyser, with the analyser being placed in between the objective and the camera [195,196]. As a polarised light encounters an anisotropic (or birefringent) material, such as crystalline materials that display various refractive indexes, the polarised orientation of the incident light varies [195] leading to a difference in colour and colour intensity in the image that is obtained from the microscope (Figure 2.14 **a)**).

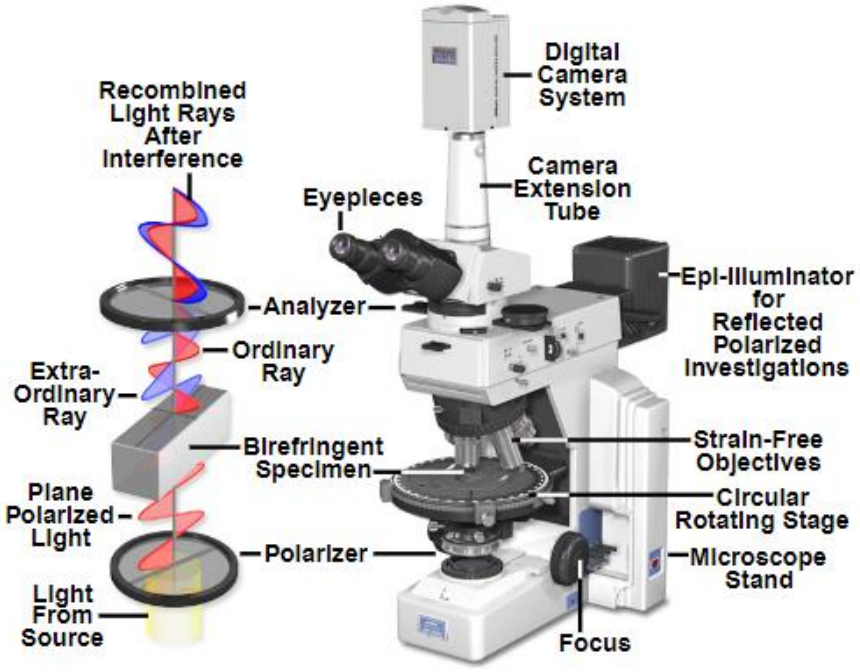

Figure 2.13 Configuration of a polarised light microscope [195]

Amorphous materials, which do not show anisotropy, only show one refractive index when light passes through them [195], with no colour being displayed on the captured image [27,195,196] (Figure 2.14 **b)**).

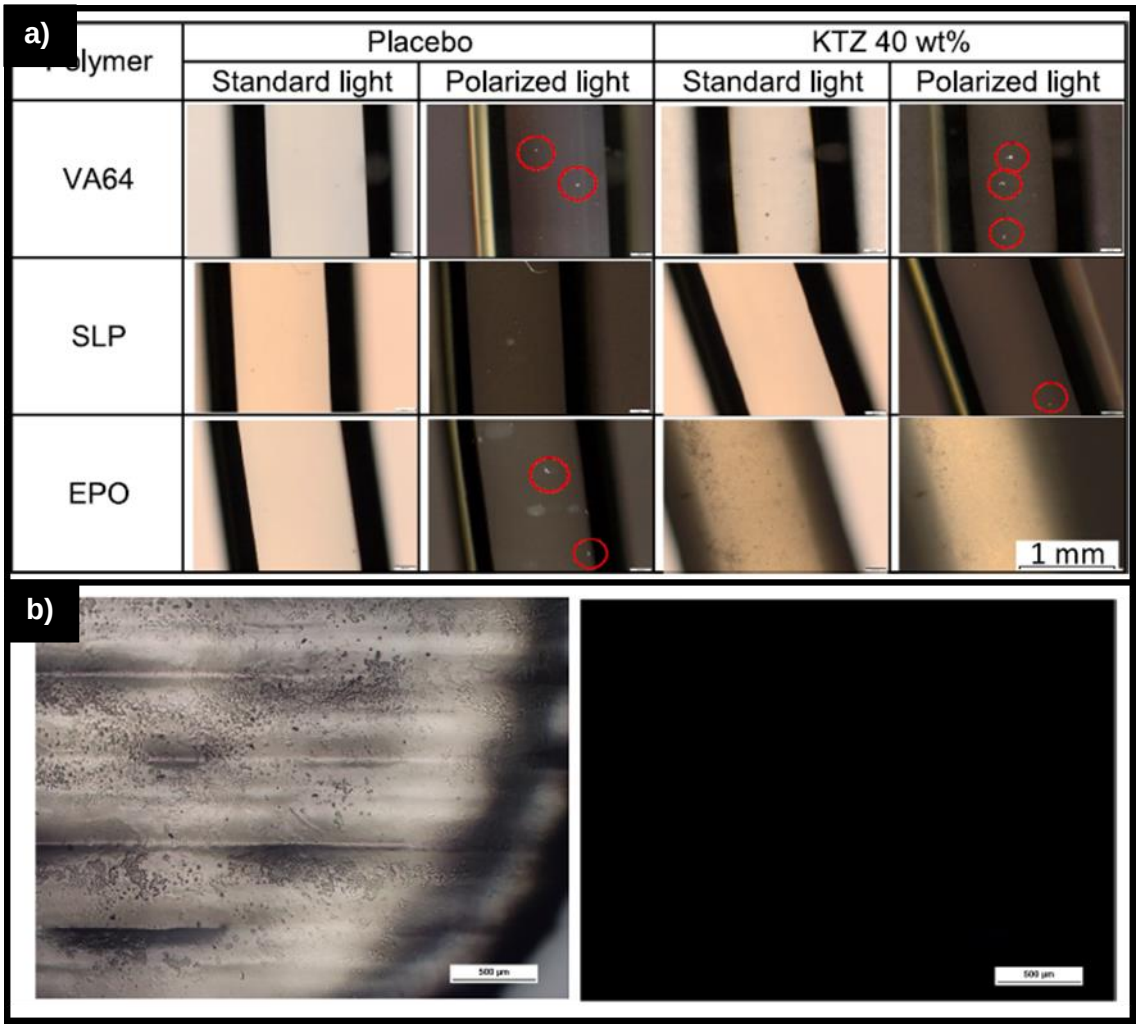

Figure 2.14 Examples of samples under standard light and polarised light; **a)** birefringent sports marked with circles [161]; **b)** amorphous material [27]

As printed tablets can sometimes be sufficiently transparent, this is a useful technique to assess and confirm whether the drug or excipients are present in crystalline form [27,197]. The same approach has been taken with HME produced filaments used for FDM 3D printing [161]. Whilst PLM is not a quantitative technique such as pXRD and DSC it can also be used with these techniques [27,161] to confirm whether materials and products are crystalline or amorphous, as it has a much more sensitive detection limit to crystallinity [161]. It is due to its higher sensitivity compared to DSC and pXRD and the fact that it is a non-destructive method that it was chosen for the detection of the onset of crystallinity in a stability study.

2.2.7. Thermogravimetric analysis (TGA)

In thermogravimetric analysis, a precision weight balance monitors the change in the sample's mass as the temperature changes. Generally, this is done as the

temperature is increasing, though some experiments are studied with decreasing temperature. The sample is placed in a furnace where gas is purged to maintain a controlled environment. TGA can quantify loss of water, and decomposition [198] and temperature materials start to decompose at, therefore determining the maximum processing temperature [32,62,199,200]. It can also be used to quantify any remaining solvent post printing [189,201] and residual water [57,60,62,162,202], which can be crucial to longer shelf-life formulations [62,162]. When unexpected mass differences are observed during processing, TGA analysis can give an indication of whether this was caused by material degradation, water evaporation or by one of the processing steps, thermal or not [203]. Moreover, it can help confirm the incorporation of a drug molecule into a polymer matrix, with the decomposition temperature changing from the drug itself [36,60]. TGA was use here to assess whether there was degradation of any of the raw materials and powder mixtures when printing at a high temperature.

2.2.8. Scanning electron microscopy (SEM)

Scanning electron microscopy is a type of electron microscopy that utilises an electron beam to produce images of the surface of materials up to a resolution of 1 nm [204–206]. A focused electron beam interacts with the atoms of a sample generating different types of ejected electrons and x-rays [204–206]. These signals are then captured by a detector and an image is produced [206]. The formed electrons are termed backscattered electrons (BSE) and secondary electrons (SE). While BSE come from deeper within the sample and give information on the sample's composition, SE come from the sample's surface, giving information on the topography and morphology of the sample. X-rays are produced from deeper within the sample [205,206] and give information on elemental composition [205]. Standard SEM generally requires the use of a high vacuum environment and the need for samples to be conductive [204,206]. In case of polymers, this means it is necessary to coat the sample with a conductive material such as a thin layer of gold, making this a destructive technique [204,206]. However, the sample can be kept and analysed multiple times [206].

In practical terms in this project, SEM allows for observation of the surface morphology [5,26,69,83,85] (Figure 2.15 **a)**), the fusion or lack thereof between printed layers [26,85] (Figure 2.15 **b)**) and to assess whether there is a physical change in the tablets after dissolution testing [5] (Figure 2.15 **c)**).

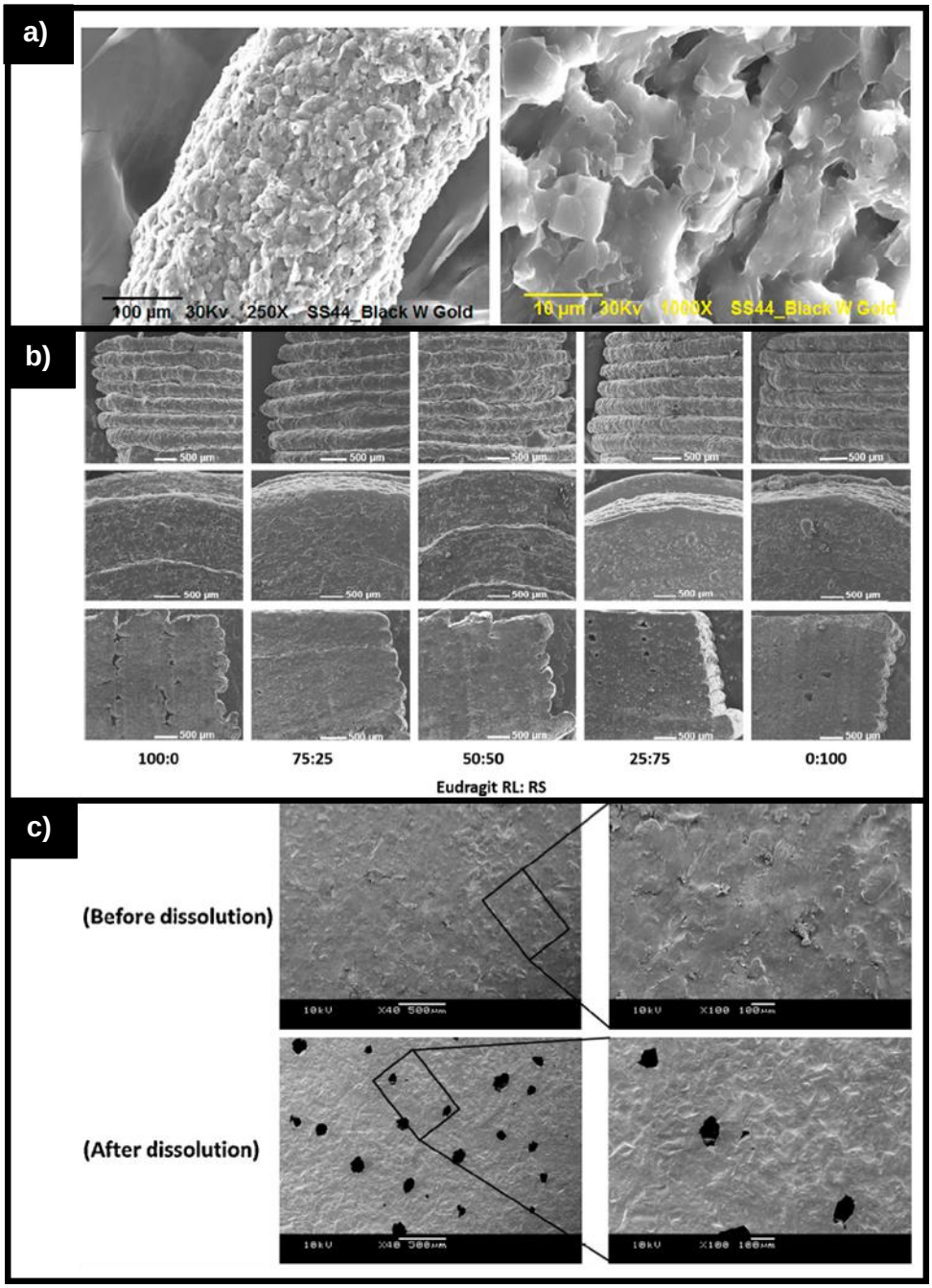

Figure 2.15 Examples of the use of SEM for observation of **a)** surface morphology of filaments [69], **b)** fusion of printed layers [85] and **c)** effect of channelling agents during dissolution testing [5]

2.2.9. X-ray micro-computed tomography (micro-CT) scanning

X-ray micro-computed tomography (micro-CT) is a powerful 3D imaging technique that is used in the medical field, engineering, the study of archaeological samples [204,207], in food, biology and geosciences [208], as well in the additive manufacturing field [26,27,69,209,210]. This is a non-invasive [207,208] and non-

destructive technique [204,208,211] that allows for the acquisition of two-dimensional (2D) x-ray images/projections of a rotating sample, which can be reconstructed into a 3D image [204,208,211] showing the inside and outside of a sample [204]. This provides information on internal cavities and porosity [204,210], as well as density estimation [210].

In a micro-CT scanner, there are three main components (Figure 2.16), an x-ray source, the sample, and a detector [204,208,210,211].

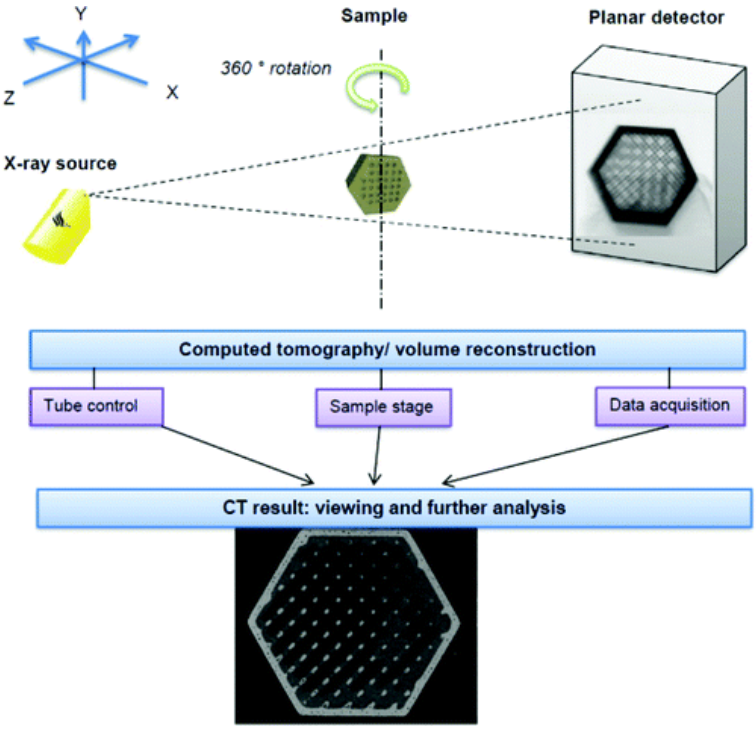

Figure 2.16 Schematic of an x-ray micro-CT scan components and process [210]

The x-ray source produces radiation that passes through the sample and is attenuated as it does so [208,211]. The detector then converts the attenuated radiation into visible light [211], producing 2D projection images [208,210,211]. These are then reconstructed into cross-section images [204], creating a volumetric data set, with the brightness of each volumetric pixel (or voxel) being related to the x-ray density of the material. After, 3D analysis can be performed, and the 3D image of the sample can be visualised [208,210]. A typical micro-CT resolution can be as low as 5 µm and the systems may vary depending on the type of detectors, x-ray sources and translation and rotation hardware, as well as the possible sample size [210]. Figure 2.17 Micro-CT images of inkjet printed tablets [27]

gives an example of reconstructed images of inkjet printed tablets and this technique was used in this study in order to non-destructively observe the interior and exterior of the printed tablets.

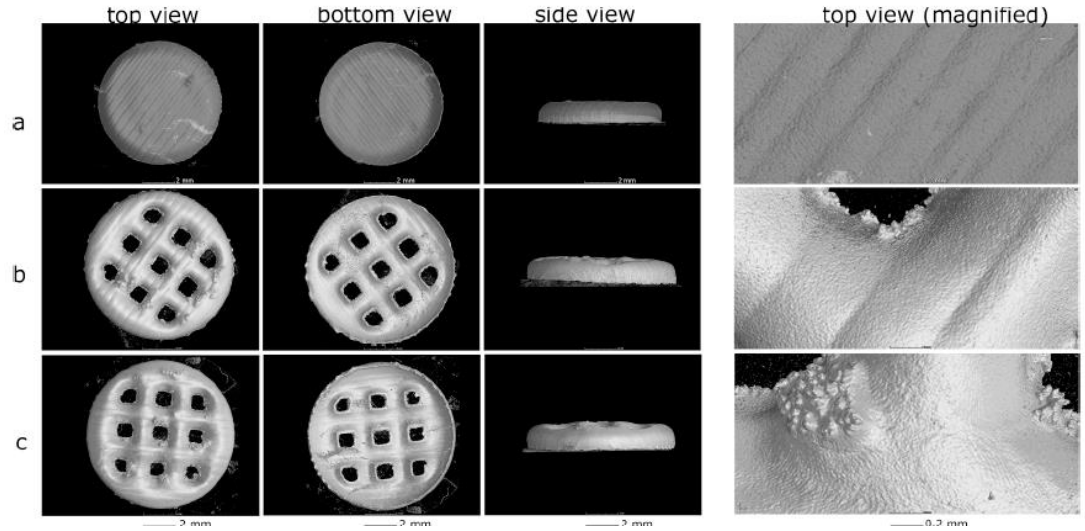

Figure 2.17 Micro-CT images of inkjet printed tablets [27]

2.2.10. Tablet friability tester

Another test described in pharmacopeias and that is important from a regulatory perspective to perform for oral solid dosage forms is friability. The friability test is done to mimic the handling of the tablets while going through the packaging process. When a tablet has high friability, it might lose particles (mass) due to abrasion, friction or mechanical shock which in turn might cause the actual drug loading to be lower than expected. It is generally accepted a maximum of 1% weight loss after the friability test [115].

2.2.11. *In vitro* drug release studies

For finished products, there are several quality tests that are usually described in the pharmacopeias. Different countries will have different monographs for each drug, though they are similar. One of them is the *in vitro* drug release (dissolution) studies. This is an important test in drug development and quality control as it is meant to (an extent) mimic and aid prediction of a drug's *in* vivo drug release [212]. Monographs for the different existing drugs recommend the type of dissolution apparatus and media, quantification method and assay tests, amongst others. While this is usually followed for conventional tablets, this cannot always be followed to the full regulatory extent when new formulations, excipients and release profiles are being tested [213].

2.2.11.1. UV/VIS quantification

Drug quantification in the samples collected from the *in vitro* drug release studies can usually be done by using UV/VIS spectroscopy, although HPLC is also used. When UV light is transmitted onto a specific material, the chromophores in the compound dictate at which wavelength of the group will absorb the light [214]. For example, fenofibrate absorbs UV light at 290 nm [30]. This is based on the Beer-Lambert law (Equation 2.4) where the absorbance of a compound depends on the molar absorption coefficient (ε), the light path (b) and the concentration of the compound that absorbs the light (c) [214].

$$A = \varepsilon b c \qquad \text{Equation 2.4}$$

For sample quantification, a calibration curve is usually done by reading the absorbance of standards at a known concentration.

3. Paste-based formulations for 3D printing of fenofibrate tablets

3.1. Introduction

3.1.1. Aims of chapter

To produce paste formulations that:

- Are easily prepared
- Incorporate commonly used pharmaceutical excipients and the drug as received
- Do not require organic solvents
- Can be printed at room temperature
- Enable a more rapid and extended release of a poorly soluble drug

3.1.2. Background

3D extrusion printing can make use of varying different types of formulations [28,75,83], with the most explored ones being used in FDM printing [36,183,215]. This approach requires heat which in turn requires polymers and active pharmaceutical ingredients to be stable at the extruding/printing temperature used [46,49,154]. However, paste-formulations have also been shown to work for the manufacture of different active tablets and multi-active tablets without the need for high temperatures and UV curing steps, while using pharmaceutical excipients commonly used in traditional manufacturing. After extrusion, the paste is left to solidify so that solid tablets can be obtained. The paste-based extrusion also demonstrated the possibility of using water and HPMC-gels as binding agents, which eliminates the need to use and remove organic solvents [35,46,112]. While water has been used to create these extrudable pastes [35,46,64,68,78,112,124,216], though hydroalcoholic gels and other organic solvents have also been reported to prevent product defects and nozzle blockage [4,5,65,67,154,189,190].

These types of paste-based formulations have been used for producing immediate release tablets [46,63], multi-active tablets [4,5,68], floating systems [154] and orodispersible systems for paediatric use [216]. It has also been explored for hospital dispensing of hydrochlorothiazide tablets and compared with tablets split by

pharmacists to tune the dose needed for patients [190]. Moreover, this type of formulation has also been used for the large-scale production of different tablets in a single production process in Laxxon Medical's screen printing technique [124].

Here, we explore a low temperature paste-based extrusion process to produce fenofibrate tablets with two different release rates, fast and extended. Excipients used in the commercially available tablets and other common pharmaceutical ones are also used in the two formulations.

3.2. Materials and Methods

3.2.1. Materials

Fenofibrate and α-lactose monohydrate were purchased from Merck Life Science (Gillingham, UK) and microcrystalline cellulose (MCC) was purchased from Fisher Scientific (Loughborough, UK). Hydroxypropyl methylcellulose 2910 (K4M) and 2208 (K100M CR), sodium starch glycolate type a (Primojel) and poly(acrylic acid) (Carbopol® 974P NF) were kindly gifted by Colorcon (Harleysville, USA), DFE Pharma (Goch, Germany) and Lubrizol (Wickliffe, USA), respectively.

3.2.2. Methods

3.2.2.1. Paste preparation and extrusion-based printing

Two different formulations, intended for fast release (FR) and extended release (ER), were prepared in accordance with Table 3.1. To act as a binder for the FR formulation, a HPMC 2910 (1%, w/v) gel was prepared. This was prepared as described in Khaled *et al.* [112]. For the FR formulation, fenofibrate (FEN), microcrystalline cellulose (MCC), sodium starch glycolate (SSG) and lactose were mixed for 15 min using a mortar and pestle until a homogeneous fine powder was obtained. After, a pre-adjusted volume of the HPMC gel was added and mixed until good paste homogeneity was obtained. The same method was used to prepare the ER paste. Fenofibrate, HPMC 2208, polyacrylic acid (PAA) and lactose were mixed for 15 min using a mortar and pestle and then a pre-adjusted volume of water (used as binder) was added and mixed thoroughly until a smooth paste was obtained. For each 1 g of solid, 0.5 mL of water was used.

Table 3.1 Composition (%) of the different solid formulations

Ingredient	Function	% (w/w) in FR	% (w/w) in ER
Fenofibrate	Active ingredient	10	10
Lactose	Filler	67.75	80
HPMC 2910	Binder (gel)	1.25	-
SSG	Disintegrant	9	-
MCC	Disintegrant	12	-
HPMC 2208	Hydrophilic matrix	-	5
PAA	Hydrophilic matrix	-	5

For both formulations, the fenofibrate paste was loaded into a syringe. A lock adapter was then attached between the syringe and a plastic 3 mL cartridge with a 0.610 mm diameter nozzle, where the paste was transferred to. An .stl file of a cylinder geometry (10 mm x 10 mm x 1.5 mm) was obtained using TinkerCAD®. The tablets were printed using a Cellink BioX printer (Gothenburg, Sweden). The printed infill geometry and percentage were selected prior to printing using the different parameters offered on the printer software. A concentric 100% infill (solid tablet) and a linear 40% infill (mesh tablet) were chosen. All formulations were printed at 20 °C and onto a 20 °C printbed using a temperature-controlled printhead. The remaining printing parameters are shown in Table 3.2. The tablets were dried in an incubation oven at 40 °C overnight and stored in a desiccator at room temperature until further tests. To assess the amount of water remaining on the tablets after drying, 10 tablets were selected. Their mass was taken right after printing and on the following morning.

Table 3.2 Printing parameters

Printing parameter	FR paste	ER paste
Speed (mm/s)	11	15
Pressure (kPa)	250	230

3.2.2.2. Weight uniformity

Twenty 3D printed tablets of the same batch of each formulation and geometry were selected, individually weighed and their average weight calculated, along with its relative standard deviation (RSD%).

3.2.2.3. Friability

For friability testing, ten solid tablets of each formulation were selected and weighed. The tablets were then put into the rotating drum for 100 revolutions at 25 rpm, following the Tablet Friability test recommendation by the United States Pharmacopeia [217]. After, the tablets were weighed again, and break and crack analysis were done visually by observation.

3.2.2.4. Attenuated total reflection Fourier transform infrared (ATR-FTIR)

A PerkinElmer Frontier ATR-FTIR (Waltham, USA) spectrometer was used to collect the infrared spectra of the drug fenofibrate, all excipients, the wet pastes and the printed tablets between 4000 cm^{-1} and 600 cm^{-1} with a scan resolution of 2 μm and a step size of 0.5 cm^{-1}.

3.2.2.5. X-ray diffraction (XRD)

X-ray diffraction patterns of fenofibrate, the solid excipients and the tablets were obtained at room temperature using a Bruker D8 Advance with DaVinci XRD instrument (Billerica, USA). This was set up in divergent beam mode running in Bragg–Brentano geometry and a Lynxeye 1D detector. A generator voltage of 40 kV was set, with a current of 40 mA. Samples were scanned over 2 theta range of 5° to 40° in a step size of 0.02° and time per step of 0.1 second.

3.2.2.6. Scanning electron microscopy (SEM)

SEM images of the printed tablets were obtained using a scanning electron microscope JEOL 6490LV (Tokyo, Japan) with a 10 kV voltage. The samples were mounted on stubs with carbon tape and then gold coated using an AGAR AGB7341 automatic sputter coater (Essex, UK).

3.2.2.7. Micro computed tomography (micro-CT) scanning

Micro-CT scanning was performed using a Skyscan 1174 Micro CT, with 50 kV voltage and 800 μA current, a resolution of 12.2 μm with a 0.4° rotating step. An

averaging frame of 6 was used. The samples were mounted on a stub containing an Eppendorph™ centrifuge lid as a sample holder. The obtained images were reconstructed using the NRecon, the analysis was done with CTAn and CTVox was used as a volume rendering software.

3.2.2.8. *In vitro* drug release dissolution studies

The studies were done using a United States Pharmacopeia (USP) type 1 apparatus Copley Dissolution system (Nottingham, UK). In each vessel, 500 mL of 0.1 M phosphate buffer (pH 7.40) with 0.05 M sodium lauryl sulphate as the dissolution medium was added and maintained at 37 °C. The rotation of the baskets was set to 50 rpm. 1 mL samples were collected at times 1, 2, 5, 10, 15, 30, 45, 60, 75, 90, 105 and 120 min for the fast release tablets and at times 5, 15, 30, 45, 60, 60, 120, 180, 240, 300 and 360 min for the extended-release tablets and pure fenofibrate. For pure fenofibrate, three 10 mg samples were used. All dissolution samples were filtered with a 0.45 µm MF-millipore membrane filter (Millex HA) before transferring to the collection vial. After each sample removal, an equivalent amount of fresh buffer kept at the same temperature was reintroduced in the dissolution vat. All dissolution tests were done in triplicate. Drug quantification was done using a TECAN Spark® (Zürich, Switzerland) multimode microplate reader UV–Visible spectroscopy (UV-VIS). A wavelength scan performed, and a wavelength of 290 nm was used for sample quantification.

3.3. Results and Discussion

3.3.1. Extrusion-based printing of tablets

For both formulations, FR and ER, two different geometries were printed. Figure 3.1 shows the images of the 3D printed tablets, solid and mesh, with the FR formulation (Figure 3.1 **a)**) and ER formulation (Figure 3.1 **b)**). While the solid tablets look identical and are cylindrical as the .stl file specified, the mesh ones have a gap on the outside. When choosing the printing parameters, there is an option to add a perimeter layer. This perimeter layer, which is just an outside layer, while not necessary for a solid tablet, is needed for a mesh tablet for rigidity. This allows it to have a more defined outside shape while maintaining the mesh geometry on the inside and it is the first part of the print. It begins with the printing of the perimeter, followed by the extrusion

of the infill. Due to the paste's viscosities, there was a continuous delay in the initial printing process, causing the gaps to be formed.

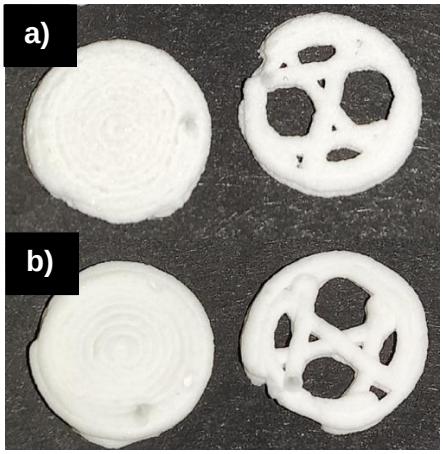

Figure 3.1 Images of 3D printed tablets. **a)** FR tablets, solid and mesh geometry; **b)** ER tablets, solid and mesh geometry

While a HPMC gel was used as a binding agent for the FR formulation, only water was necessary for the ER. There is a considerable difference in the formulation's components. Most of both formulations consist of lactose, a filler and bulking agent. Part of the fast release formulation are disintegrants. Both MCC and SSG are usually used as disintegrants, causing breakage of oral solid dosage forms upon contact with water and while MCC has been used as a binding agent [78], this was not enough to form a paste that could be extruded and sustain a 3D structure. As such, a hydrogel made with a lower viscosity HPMC [112] was used as a binding agent. On the other hand, two polymers known to swell upon contact with water and form a hydrophilic matrix were used for the extended release of fenofibrate in the ER formulation. Upon mixing the ER powder formulation with water, the swelling of these two polymers led to a smooth and elastic paste that could easily be extruded and sustain its shape. The effect of the swellable, hydrophilic polymers can be observed in Figure 3.2, with the surface of ER tablets being smoother and with defined layers. Large particles of similar shape can be seen in the SEM images of both tablets, most likely corresponding to the lactose particles, which along with the fenofibrate, are the only common ingredient in both formulations. Moreover, these appear to be of tomahawk shape, as typically associated with unprocessed α-lactose monohydrate crystalline lactose [218].

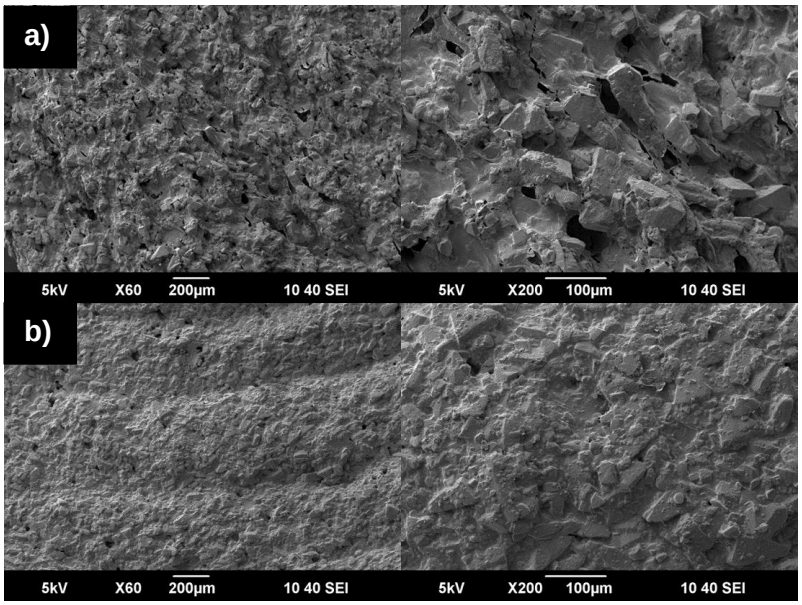

Figure 3.2 SEM images of the top layer of **a)** FR tablet (different magnifications) and **b)** ER tablet (different magnifications)

After printing, the tablets were all put to dry overnight in an incubation oven. The residual water post drying was quantified in 10 tablets of each formulation. With an initial water content of 55.56% (w/w) (from the HPMC gel), the FR tablets had around 3.71% of water remaining. For the ER paste, there was an initial 33.33% (w/w) of water, with tablets retaining around 3.39% (w/w). From the SEM images of each formulation (Figure 3.2) it is possible to observe small pores formed on the surface of each due to water evaporation. The dimensions of the tablets are shown in Table 3.3. While the height of the tablets is identical in both formulations and geometries the diameter of the ER printed tablets is larger than for the FR tablets. This is likely due to the use of the swelling polymers in the ER formulation, expanding while in contact with water, which led to the use of a faster printing speed and lower printing pressure than the ones used for the FR formulation.

Table 3.3 3D printed tablets' dimensions, measured with a Vernier caliper (n=10)

	Solid	**Mesh**
FR	Ø = 10.02 ± 0.04 mm H = 1.26 ± 0.04 mm	Ø = 9.97 ± 0.07 mm H = 1.24 ± 0.05 mm
ER	Ø = 10.47 ± 0.10 mm H = 1.27 ± 0.06 mm	Ø = 10.20 ± 0.10 mm H = 1.26 ± 0.06 mm

In Table 3.4 there is a summary of the calculated uniformity of weight for both formulations and geometries. While all are within the limits established by the British Pharmacopeia for tablets under 250 mg [219], there is a clear trend in a higher variation for tablets printed using the fast release formulation, especially for the mesh printed tablets.

Table 3.4 Uniformity of weight of printed tablets, RSD (%) (n=20)

	Solid	**Mesh**
FR	5.62%	7.22%
ER	4.80%	4.78%

From the micro-CT scans of both solid FR (Figure 3.3) and ER (Figure 3.4) tablets, it is possible to see the poor binding between extruded filaments in the FR tablet when compared to the ER one. This is presumably due to the sole use of the HPMC gel as a binding component, in comparison with the two swelling polymers in the ER formulation. The swelling of the paste for the ER formulation leads to a better binding between extruded filaments, leading to a more homogeneous solid tablet, lacking larger gaps or pores. Regardless of the formulation, both types of solid tablets had a mass difference of less than 1% when testing their friability, with no breakage or cracks observed.

Figure 3.3 Micro-CT scan of a solid FR printed tablet. **a)** top view, **b)** vertical cross section, **c)** horizontal cross sections at different heights of the tablet

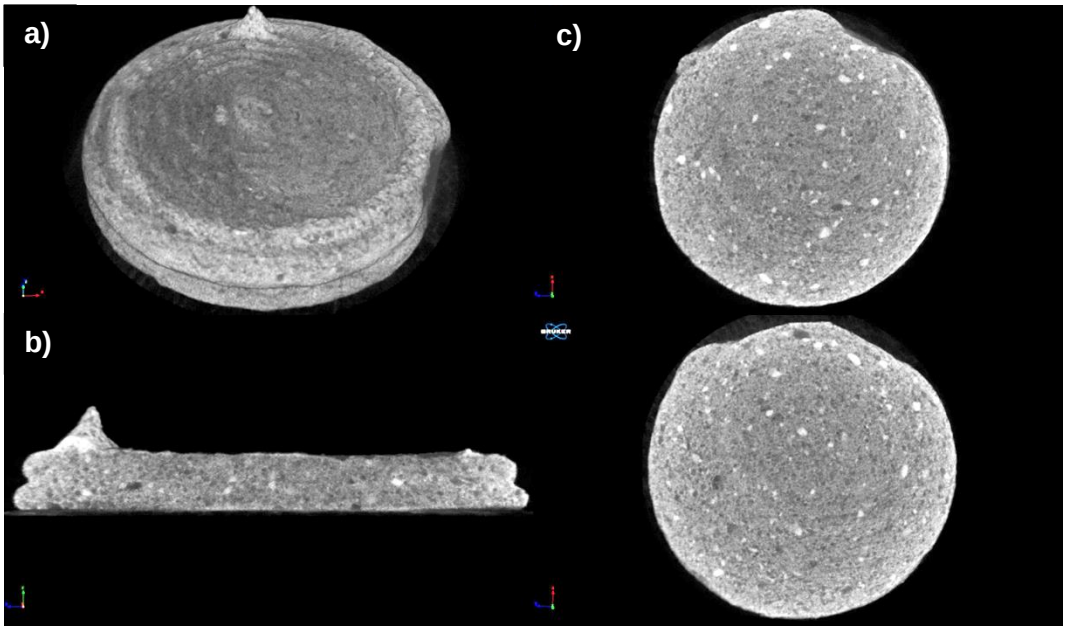

Figure 3.4 Micro-CT scan of a solid ER printed tablet. **a)** top view, **b)** vertical cross section, **c)** horizontal cross sections at different heights of the tablet

3.3.2. Attenuated total reflection Fourier transform infrared (ATR-FTIR)

FTIR was used to confirm the incorporation of the drug, fenofibrate, in both formulations. Figure 3.5 shows the spectra of fenofibrate, the FR wet paste and the FR printed tablet. Figure 3.6 shows, again, the spectra of fenofibrate, as well as the ER wet paste and the printed tablet using this formulation. Figure S 3.1 and Figure S 3.2 in the supplementary information show the FTIR spectra of FR and ER excipients, respectively.

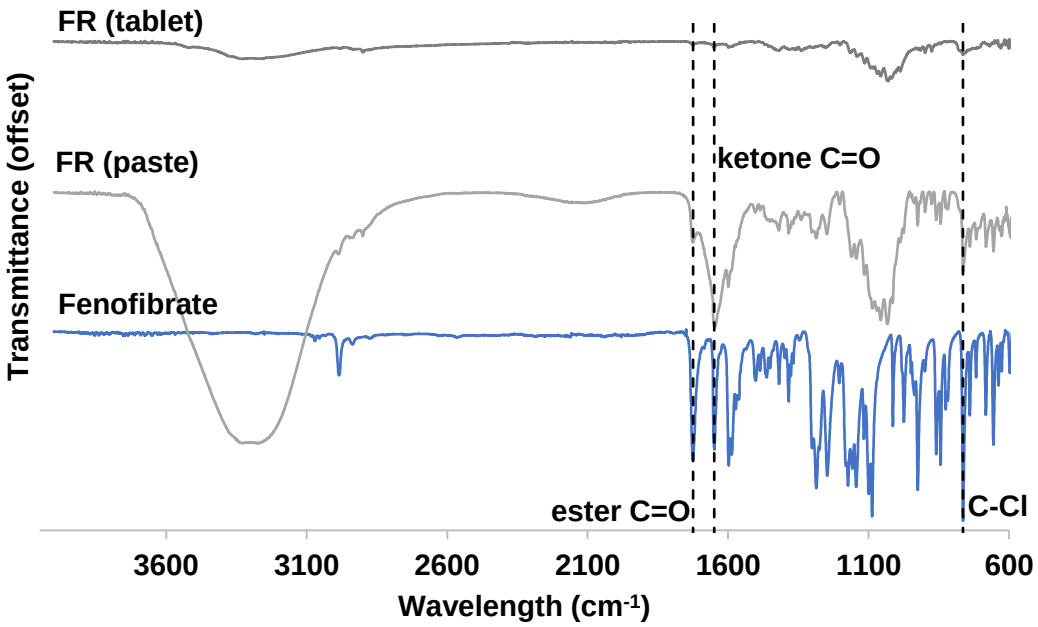

Figure 3.5 FTIR spectra of fenofibrate, the wet FR paste and the FR printed tablet

A clear indication of the incorporation of fenofibrate in the formulations is the peak corresponding to the C-Cl bond. In the fenofibrate spectra, shown in both Figure 3.5 and Figure 3.6, there is a sharp absorption centred at 764 cm^{-1}, which can also be seen, though with a weaker absorption considering a drug loading of less than 10%, on the spectra from both wet pastes and the printed tablets. Another two characteristic peaks of fenofibrate are the ester carbonyl stretching at 1725.7 cm^{-1} and the ketone carbonyl stretching at 1649.7 cm^{-1} [220]. Both can be observed in the spectra of fenofibrate, wet pastes and printed tablets which confirms the incorporation of the drug in the formulations, wet and dry.

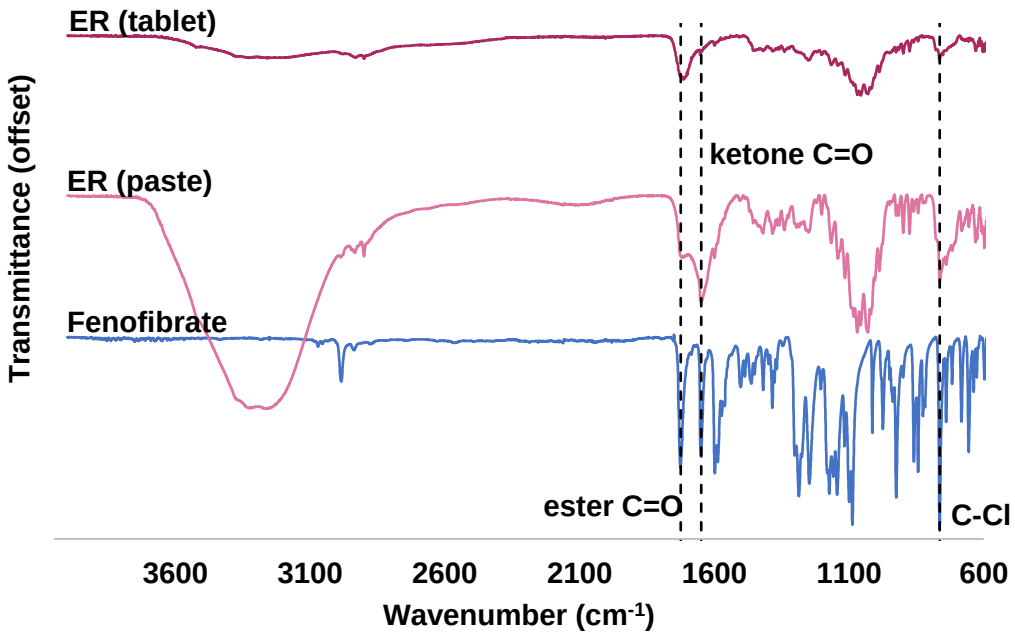

Figure 3.6 FTIR spectra of fenofibrate, the wet ER paste and the ER printed tablet

3.3.3. X-ray diffraction

The diffraction patterns of the drug, lactose and printed tablets are shown in Figure 3.7 and Figure 3.8, for FR and ER, respectively.

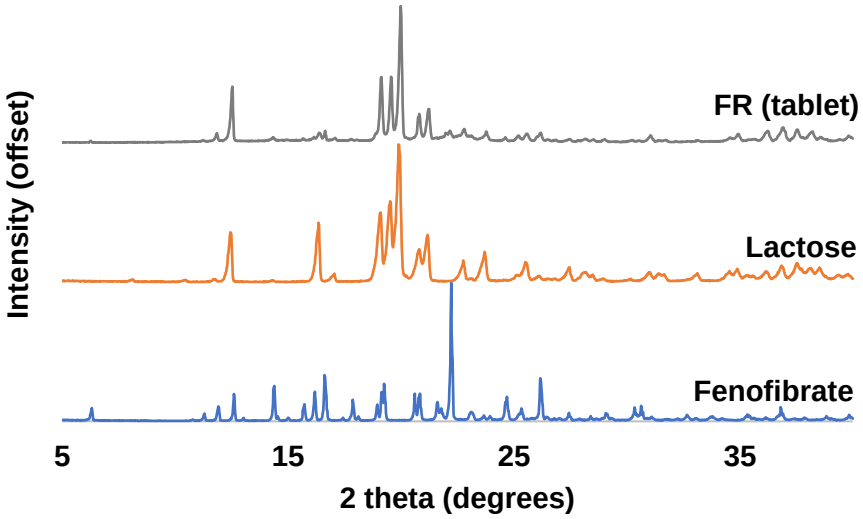

Figure 3.7 X-ray diffraction patterns of fenofibrate, lactose and the FR printed tablet

The diffraction pattern of fenofibrate shown in Figure 3.7 and Figure 3.8 matches the pattern from fenofibrate form I [27,30,31]. It is possible to see that fenofibrate has characteristic peaks at 11.9° (2θ), 14.5° (2θ), 16.2° (2θ), 16.6° (2θ) and 22.2° (2θ). In

both formulations, apart from fenofibrate and lactose, all other excipients are amorphous or semi-crystalline (Figure S 3.3, Figure S 3.4). The peak at 22.2° (2θ) from fenofibrate, for example, is not one that the drug molecule shares with lactose in the same 2θ range. However, it can be observed in the FR tablet diffractogram (Figure 3.7), as well as in the ER tablet diffractogram (Figure 3.8). As such, it can be assumed that the drug was incorporated in its crystalline form in both formulations. As the manufacturing process consisted purely of producing a paste using a hydrogel or water and extruding it, plus a drying step, the likelihood of a phase transition was minimal [8] and therefore not expected.

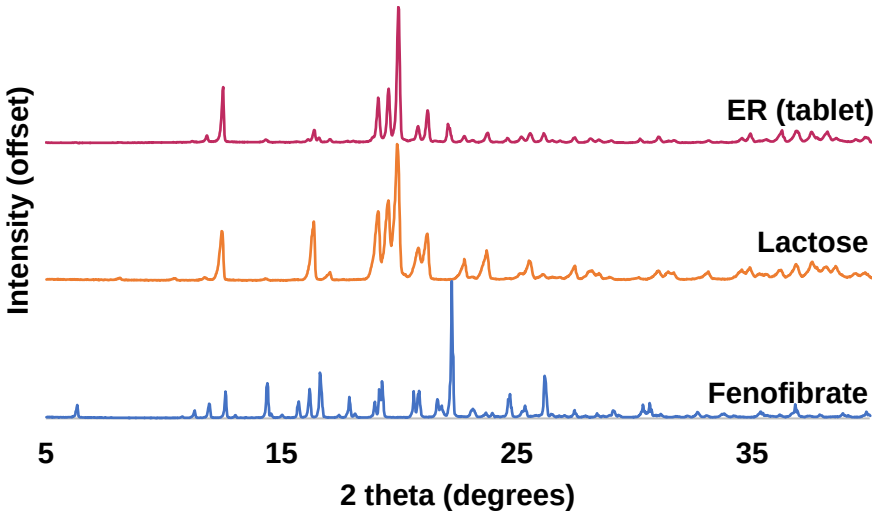

Figure 3.8 X-ray diffraction patterns of fenofibrate, lactose and the ER printed tablet

Still, as the amount of lactose is much higher than the amount of fenofibrate in the printed tablets, the decrease in peak intensity of fenofibrate was expected. Nonetheless, this shows how there has been no phase transition for the drug particles during the mixture and printing process.

3.3.4. In vitro drug release

Figure 3.9 shows the fenofibrate release profile from FR tablets, while Figure 3.12 corresponds to the release profile of fenofibrate from ER tablets. In both cases, there

is a comparison of the release of fenofibrate present in the tablets with pure fenofibrate.

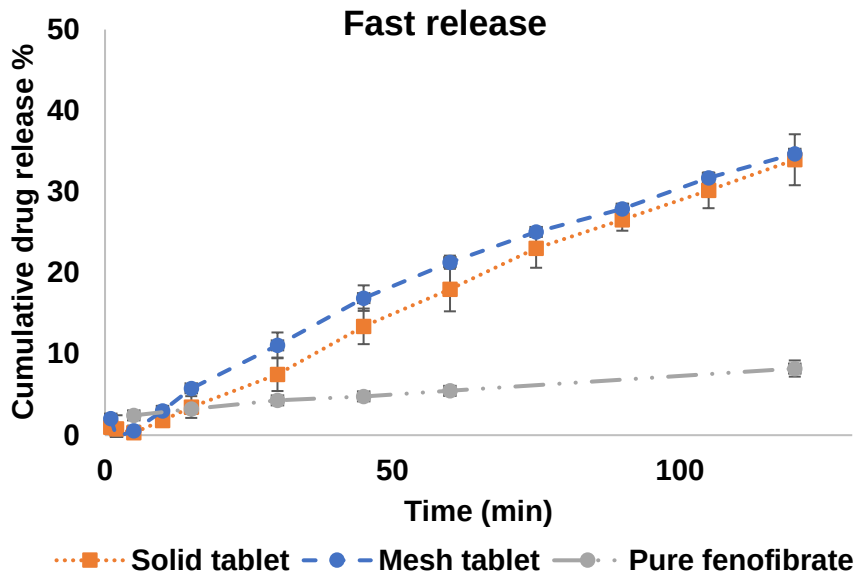

Figure 3.9 Dissolution data showing drug release profiles of FR printed tablets and comparison with pure fenofibrate (n=3)

Fenofibrate on its own, releases an average of 8% in 120 min, and 19% after 6h. In comparison, FR solid and mesh tablets released 34% and 35%, respectively after 120 min, and ER solid and mesh tablets released 11% and 18% after 6h, respectively.

What can be clearly seen is that the FR formulation did not ensure an immediate release of the active (Figure 3.9), but rather a faster release than the ER formulation (Figure 3.12). However, both did not achieve complete release after the defined time. The formulations chosen were inspired by the previous work of Khaled *et al.* [112] which used a water-soluble drug. Fenofibrate is a poorly soluble drug with a solubility of less than 1 mg/mL at 37 °C [134]. As the drug was used as received and no phase transformation occurred during the processing of the formulation, no change in its solubility was expected [8]. With a much lower solubility than the drug used in Khaled *et al.*'s work [112], it is clear that neither formulation would be suitable for the delivery of a drug such as fenofibrate. When using excipients such as the disintegrants MCC and SSG, upon contact with water there is the breakage of the tablets, and the drug is released. The consequence of this breakage can be seen on the image from a dissolution basket after the 120 min study (Figure 3.10 **a)**) as there is only residual material left. It is apparent from the release data of this formulation that a higher

surface area provided by the mesh infill does not lead to significant increase in the release of fenofibrate (Figure 3.9).

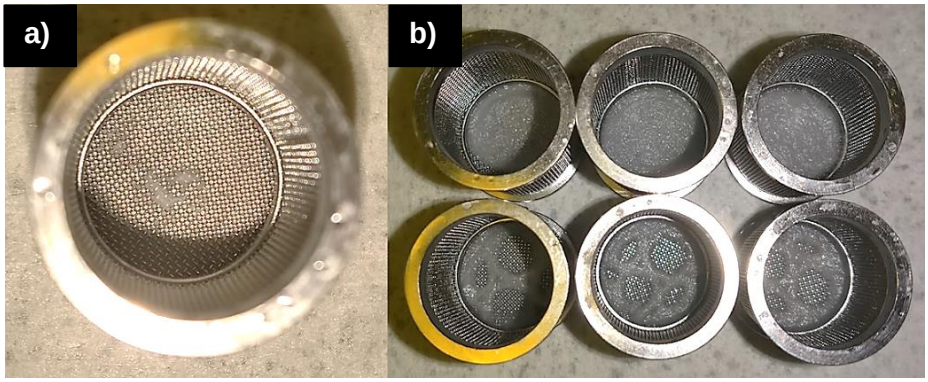

Figure 3.10 Images of the residual material in the dissolution baskets for **a)** FR tablet and **b)** ER tablets

This is likely due to the disintegrating nature of the excipients used. As such, there is a higher release from this formulation when compared to the pure drug. The drug release data was also fitted to existing mathematical models, zero and first order, Higuchi and Korsmeyer-Peppas [221], with the first order model better fitting the releases from both FR geometry tablets (Figure 3.11). This is characteristic of dosage forms in which it is assumed that the drug release rate is proportional to the remaining drug concentration [221]. A slow release was not intended with this chosen formulation, which is a clear indication that changes in the formulation and/or process are necessary.

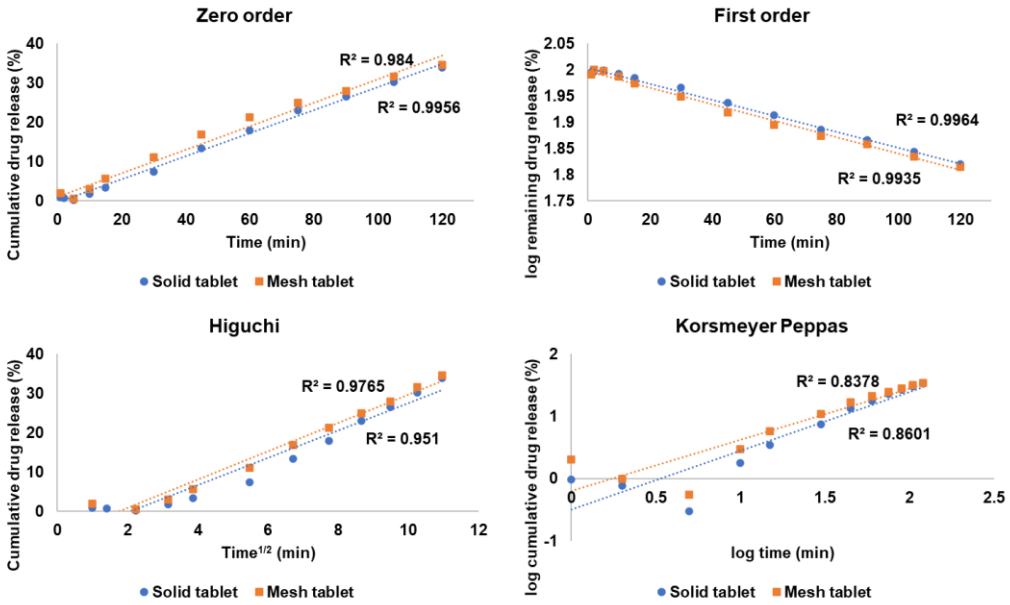

Figure 3.11 Dissolution models applied to the drug release data from FR printed tablets

With the ER formulation, it is clear that a difference in surface area by having a mesh geometry plays a role in increasing the release rate of fenofibrate from the matrix, as that led to a release of 18% in comparison with 11% from solid tablets (Figure 3.12). The swellable matrix which leads to a delay in release can still be observed in the photo taken of the tablets after a 6h study, by covering the bottom of the dissolution basket (Figure 3.10 **b)**). The matrix could retain the active inside and only allowing for its release to start between the 2-3h mark, which is in clear contrast with the pure active release in the medium (Figure 3.12). With such a small amount of drug being released when using this formulation demonstrates the need for a change in excipients and/or processability as well. Once again, the drug release data was fitted to existing mathematical models, with the zero order model also better fitting the releases from both ER geometry tablets (Figure 3.13).

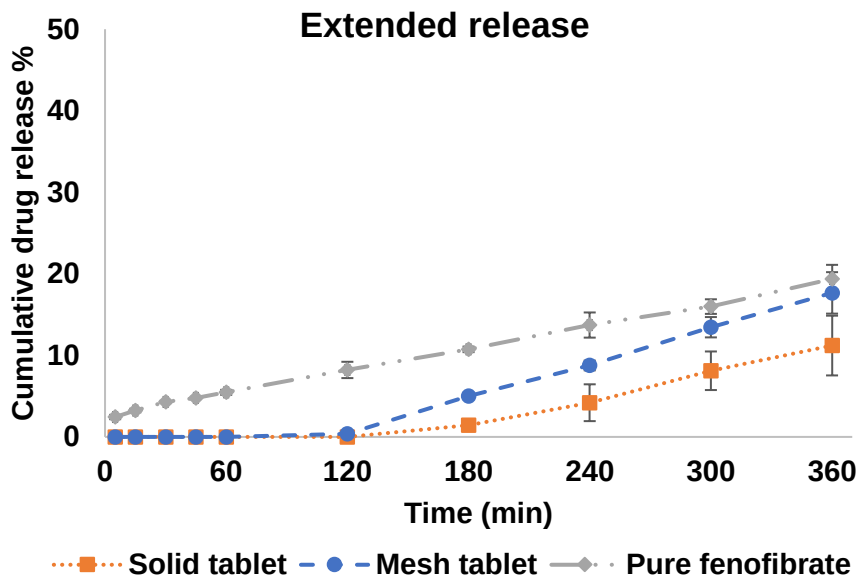

Figure 3.12 Dissolution data showing drug release profiles of ER printed tablets and comparison with pure fenofibrate (n=3)

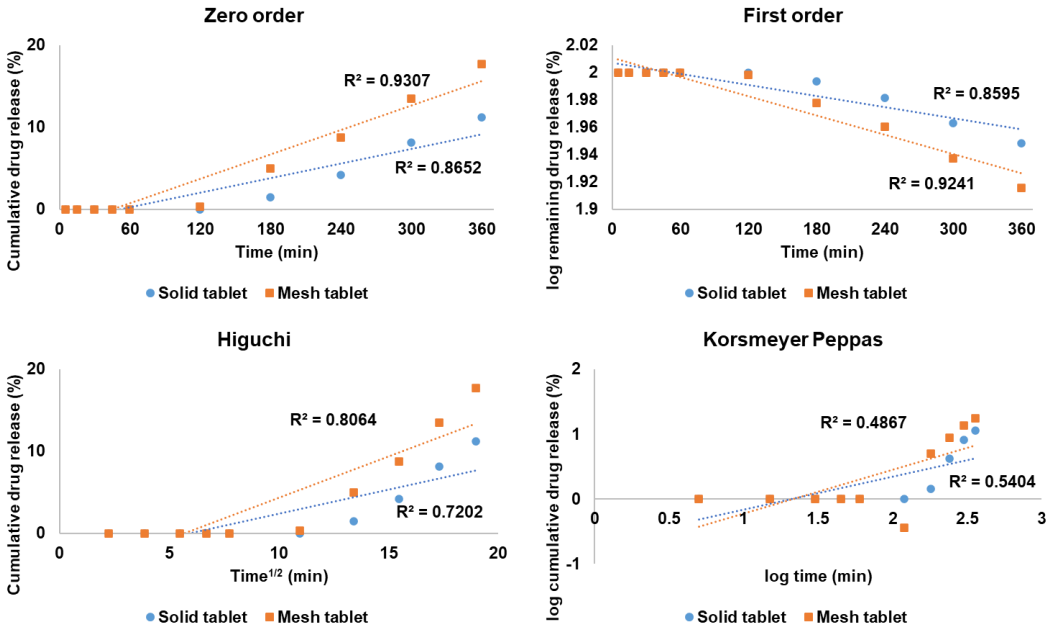

Figure 3.13 Dissolution models applied to the drug release data from ER printed tablets

The aim of this chapter was to investigate whether it was possible to produce tablets for a faster and extended release of fenofibrate, a poorly soluble drug, utilising commonly used pharmaceutical grade excipients as received and without the use of

organic solvents. It is clear from the results presented above that such this type of formulations are not the most suitable for the release of fenofibrate.

To improve release rate of a paste formulation containing fenofibrate, a first option would be the micronisation of the drug particles and/or the micronisation of the drug and excipients particles, instead of using all powders as received. Though with different excipients than the ones used in this work and with the intent of producing orally disintegrating tablets, higher dose fenofibrate formulations have been shown to have higher release rate when either jet-milling the drug prior to the blending step or jet-milling the powder mixture after blending all ingredients together, both prior to a granulation and tabletting process [11]. This micronisation of poorly soluble particles leads to a reduction in size and hence an increase of the surface area and the dissolution rate. The jet-milling of a powder blend of drug-excipients leads to a further increase in release rate as it increases its hydrophilicity and wettability due to the co-processing with the excipients [11]. As such, and without having to change the chosen formulation, this extra step could improve the results obtained.

A second possible approach, for a faster release of fenofibrate from 3D extruded tablets would be to increase the amount of sodium starch glycolate (SSG), as this is a superdisintegrant. Wet granulation of other poorly soluble drugs with high concentrations of this disintegrant has been shown to significantly improve drug release and bioavailability from both capsules and tablets. A concentration of 35% (w/w) of SSG was found to be optimum for the release of methylprednisolone, with this poorly soluble drug achieving complete release in less than 30 min. However, a too high concentration of SSG was also found to delay drug release, as it leads to the formation of a viscous barrier in the granules during dissolution [6]. As such, a change in the amount of each component of the FR formulation could lead to a faster release of fenofibrate.

A third option, which would work for both types of formulations, would be to use an organic solvent in which fenofibrate is soluble, as a prior step to forming the paste. In Chen *et al.* work, in which a paste-based formulation was used in the production of 3D printed floating core-shell systems to deliver the poorly soluble clarithromycin, ethanol was used. The excipients' mixture was dissolved and mixed with ethanol, with the drug then added and stirred in until solidification. This solid mass was then grounded and mixed with water to form the paste that would be used to produce the printed tablets [154]. This would be a simple step to be added to both processes, though it would include the use of an organic solvent.

There are many other approaches that can be used for improving the release rate of a poorly soluble drug [6,11,12,20,21,64], though they might not be the most suitable for a paste-based formulation that can be extruded at room temperature. Different approaches will be explored in the next chapters.

3.4. Conclusions

The following conclusions can be made from this chapter:

- Paste-based formulations were produced with different excipients to allow a faster and extended release of fenofibrate, a poorly soluble drug.
- The FR formulation, due to the materials used, led to the printing of tablets with a slightly higher variability between them, in comparison to the ER tablets. The poorer binding between extruded filaments led to gaps inside the tablets and the variability was also higher in mesh tablets.
- ER tablets, due to the swellable polymers used for the production of a hydrophilic matrix which are meant to delay the release of drugs dispersed in them, led to solid tablets with no clear gaps and with much smoother surfaces.
- The incorporation of fenofibrate in the wet pastes and in the dry tablets was confirmed, as well as its incorporation as crystalline form I.
- While the release of fenofibrate from FR tablets was indeed faster than from ER tablets, less than 40% had been released after 120 min. However, the incorporation of the disintegrants led to an increase in release rate when compared to pure fenofibrate.
- The use of swellable polymers such as HPMC and polyacrylic acid led to the formation of a hydrophilic matrix that delayed the release of fenofibrate completely up to 2 h, and led to a maximum release of 11% from solid tablets after 6 h.
- Both formulations and the process chosen were shown to not be the most suitable for the preparation and printing of tablets containing a poorly soluble drug.

3.5. Chapter appendix: supplementary information

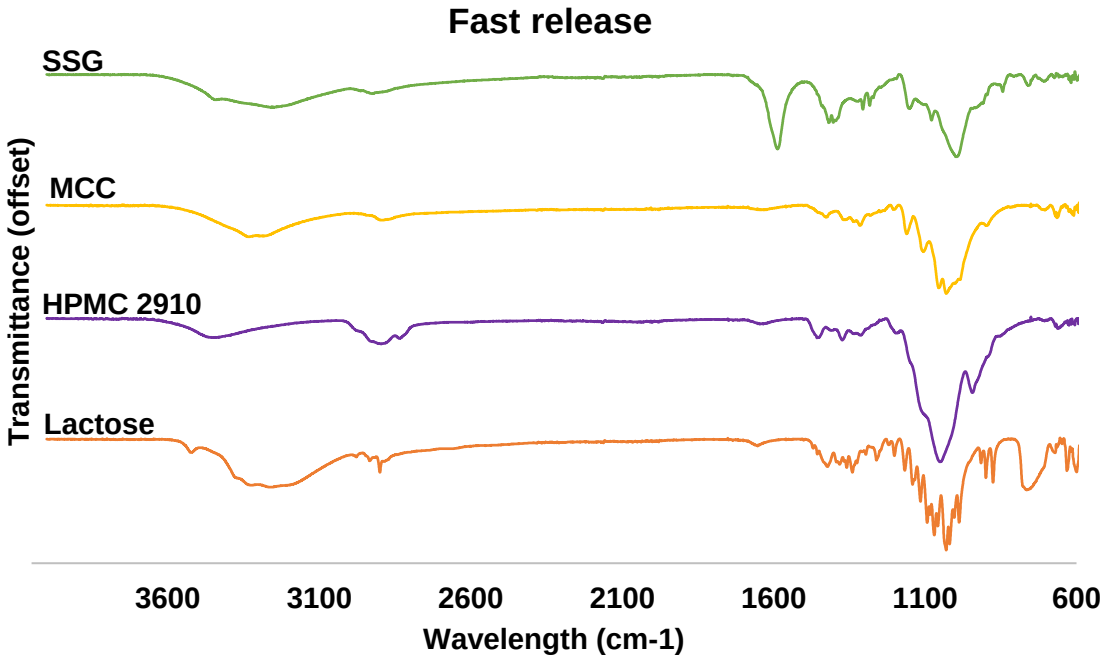

Figure S 3.1 FTIR spectra of excipients in FR formulation

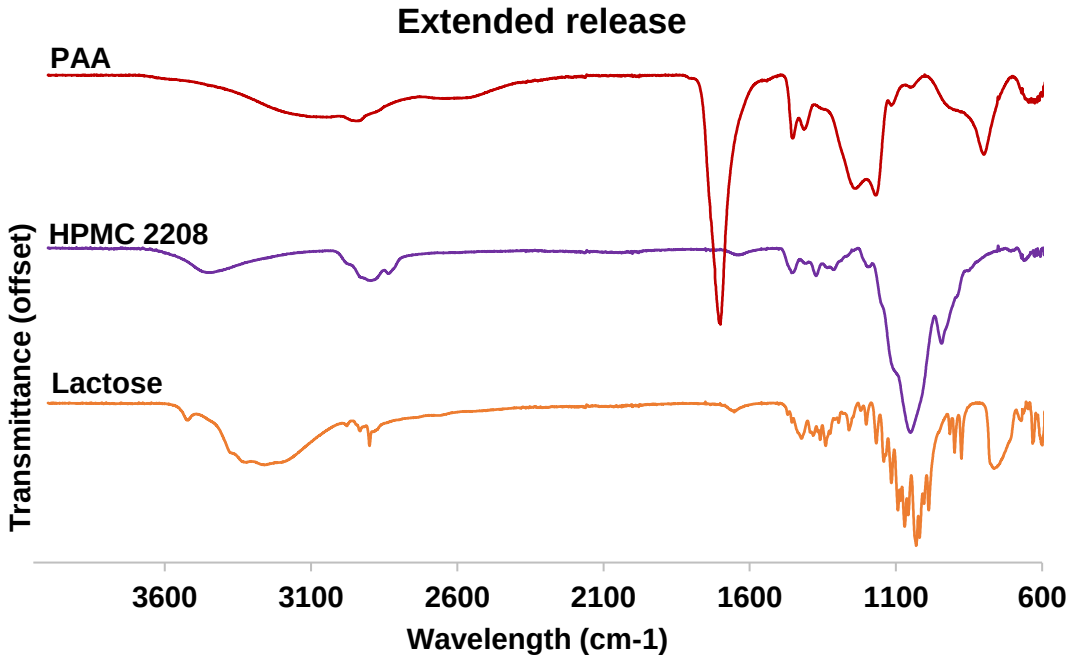

Figure S 3.2 FTIR spectra of excipients in ER formulation

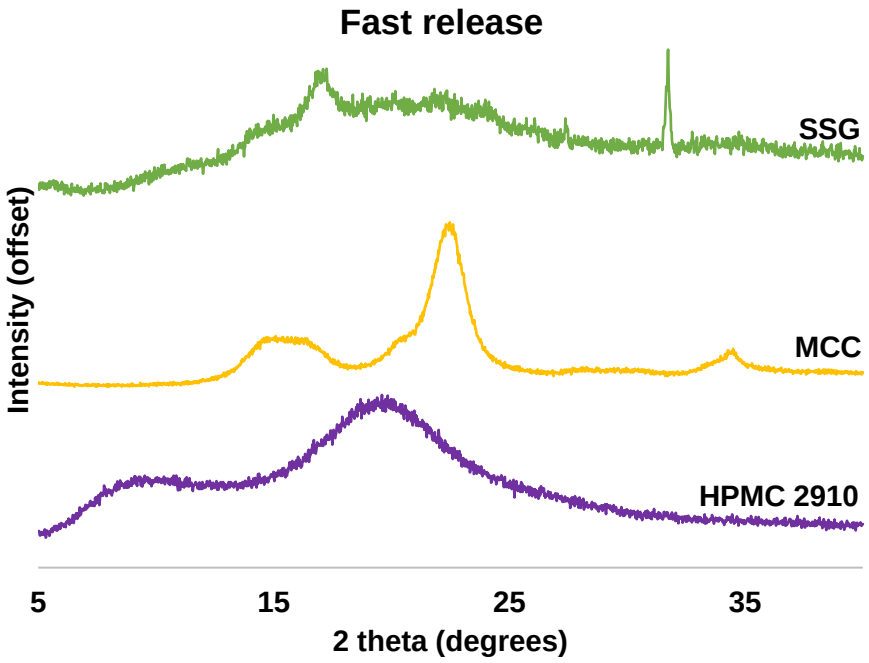

Figure S 3.3 X-ray diffraction patterns of excipients from the FR formulation

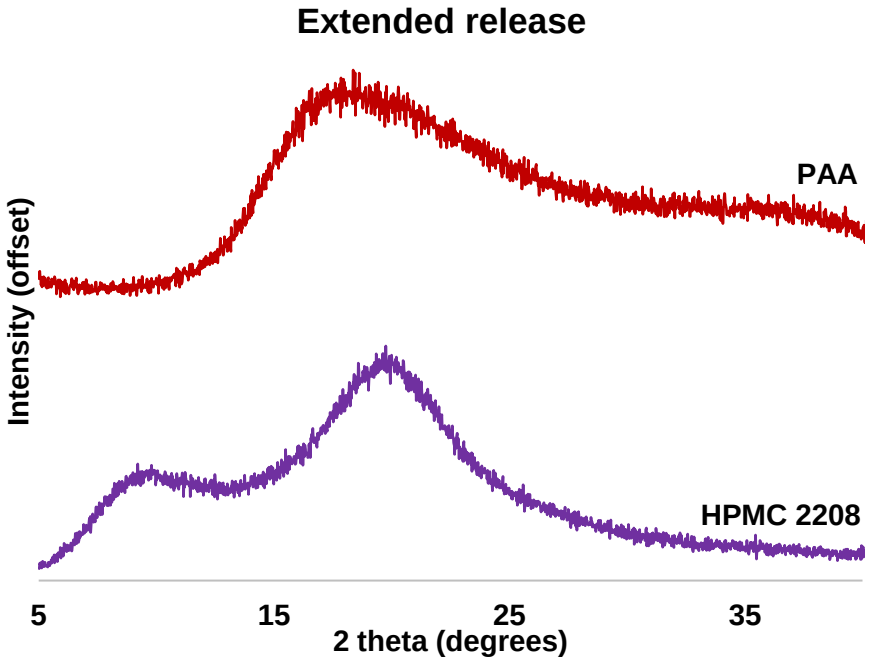

Figure S 3.4 X-ray diffraction patterns of excipients from the ER formulation

4. The effect of a surfactant on the printability, solubility and stability of a poorly soluble drug 3D printed tablet

4.1. Introduction

4.1.1. Aims of chapter

To investigate the impact of different concentrations of Tween 80, a commonly used pharmaceutical grade surfactant, on:

- The viscosity and printability of the inks
- The morphology of the printed tablets, assessing the existence of internal gaps
- Possibility of phase transformation of the model drug
- The release rate of the drug
- The physical stability of the printed tablets

4.1.2. Background

Amorphous solid dispersions (ASD) are one of the approaches used to increase the effective solubility and hence bioavailability of a poorly soluble drug. It involves the molecular dispersion of a poorly soluble drug into an inert polymeric matrix, often amorphous. Amorphous materials do not possess the ordered crystal lattice that crystalline materials do, in turn having "*the molecular conformation of a frozen-in higher temperature liquid*". Such materials have such high viscosity that they appear solid [222]. Consequently, they possess high free energy, which results in higher apparent solubility and dissolution rate though also resulting in higher thermodynamical instability [8,14–17,26,222]. Not only are ASD highly used in research using traditional manufacturing techniques [10,169,171,223], but they are also mentioned in studies where 3D printing is being used to manufacture oral solid dosage forms. ASD have been used in 3D printing in conjunction with traditional techniques such as hot melt extrusion (HME) in the case of fused deposition modelling (FDM) [26,224,225] or as a sole manufacturing technique in case of direct powder printing (DPP) [80,83,84]. While FDM requires a filament as feedstock material, direct powder printing solely requires a homogeneous mixture of powders.

This one step approach reduces the need for optimisation of the mechanical properties of the used filaments and the possibility of thermal degradation [49]. However, while lower printing temperatures can be used with DPP, ASD are not always obtained [49,82,85].

Different drugs have been used as model drugs and different polymers have also been explored as carriers for this system in DPP, though Eudragit RL PO has not been used as a carrier for the delivery of fenofibrate as it is employed here. Moreover, most formulations used in 3D printing, whether using FDM or DPP, require a plasticiser in order to be printable [26]. Plasticisers are used as they reduce the glass transition temperature of polymeric systems and their melt viscosity, therefore reducing the processing temperature [169,171]. Surfactants such as Tween 80 have been used in HME and FDM printing for their plasticising effects [26,169,171]. The amount of plasticiser material can vary vastly, with values that can go up to 25 % (w/w) [81]. Amorphous solid dispersions are in general more hygroscopic than crystalline ones as they tend to absorb moisture more easily. The absorbed moisture then tends to act as a plasticiser which leads to an increase in molecular mobility [8]. By adding a plasticising material to a formulation that is meant to form an amorphous solid dispersion, there might, hence, be too great of an increase in molecular mobility. As an ASD is already potentially physically unstable, this can more easily lead to a phase transition of materials in the formulation, such as the drug recrystallising, and hence losing the advantage in improved solubility. Therefore, it is very important to study the stability of this type of systems in different storage conditions [222]. While 3D printing has been argued as being for on-demand manufacture, the stability of these manufactured dosage forms should still be assessed, even if for a much shorter amount of time than the required for drug products [226].

This work explores the effect that the addition of a surfactant has on printability, solubility, and stability of fenofibrate tablets using direct powder printing.

4.2. Materials and Methods

4.2.1. Materials

Fenofibrate was purchased from Merck Life Science (Gillingham, UK). Tween 80 and Eudragit RL PO were kindly gifted by Croda (Cowick, UK) and Evonik Industries (Essen, Germany), respectively.

4.2.2. Methods

4.2.2.1. Rheology

Rheological characterisation of the powder mixtures at the printing temperature of 150 °C was done using a Malvern Kinexus Rheometer (Worcester, UK). 40 mm disposable parallel plates were chosen and a 0.4 mm gap to mimic the nozzle diameter was selected. Samples were placed on the bottom plate and allowed to melt and stabilise before analysis. An amplitude sweep was first conducted at 1 Hz in order to determine the range of linear viscoelasticity. This was then followed by a frequency sweep at a constant strain of 1%.

4.2.2.2. Ink preparation and extrusion-based printing

With the aid of a mortar and pestle, Eudragit RL PO , fenofibrate and Tween 80 were mixed for 15 min until a dry homogenous (by appearance) paste was obtained. The different formulation compositions are shown in Table 4.1. The formulation was then transferred to a stainless steel 10 mL cartridge with a 0.4 mm nozzle and placed in a thermoplastic print-head. An .stl file of a cylinder geometry (10 mm x 10 mm x 1.5 mm) was obtained using TinkerCAD®. The tablets were printed using a Cellink BioX printer (Gothenburg, Sweden). The printed infill geometry and percentage were selected prior to printing using the different parameters offered on the printer software. A concentric 100% infill (solid tablet) was chosen for all formulations and a linear 40% infill (mesh tablet) was also used for the 10% (w/w) Tween 80 containing formulation. All formulations were printed at 150 °C, with a printbed temperature of 65 °C and a printing pressure of 700 kPa. The printing speed varied between 1-14.5 mm/s, depending on the Tween 80 % (w/w). The tablets were allowed to solidify at room temperature and were stored in a desiccator at room temperature until further tests.

Table 4.1 Composition (%) of the different formulations

Formulation name	Fenofibrate % (w/w)	Eudragit RL PO % (w/w)	Tween 80 % (w/w)
0T	10	90	0
1T	10	89	1
10T	10	80	10

4.2.2.3. Weight uniformity

Twenty 3D printed tablets of each formulation and geometry from the same batch were selected, individually weighed and their average weight calculated, along with its relative standard deviation (RSD%).

4.2.2.4. Friability

For friability testing, ten tablets of each formulation and geometry were selected and weighed. The tablets were then put into the rotating drum for 100 revolutions at 25 rpm, following the Tablet Friability test recommendation by the United States Pharmacopeia [217]. After, the tablets were weighed again, and break and crack analysis were done visually by observation.

4.2.2.5. Attenuated total reflection Fourier transform infrared (ATR-FTIR)

A PerkinElmer Frontier ATR-FTIR (Waltham, USA) spectrometer was used to collect the infrared spectra of fenofibrate, Eudragit RL PO, Tween 80, and the printed tablet between 4000 cm^{-1} and 600 cm^{-1} with a scan resolution of 2 μm and a step size of 0.5 cm^{-1}.

4.2.2.6. X-ray diffraction (XRD)

X-ray diffraction patterns of fenofibrate, Eudragit RL PO and printed 0T, 1T and 10T tablets were obtained using a Bruker D8 Advance with DaVinci XRD instrument (Billerica, USA).

Further experimental details can be found in section 3.2.2.5.

4.2.2.7. Thermal analysis

4.2.2.7.1. Thermogravimetric analysis (TGA)

To assess the thermal stability at the printing temperature of the raw solid materials and the powder mixtures a TGA 4000 thermogravimetric analyser (Perkin Elmer, Waltham, USA) was used. Samples of 10-15 mg were placed in the instrument crucible and scanned between 20 and 700 °C at 20 °C/min.

4.2.2.7.2. Differential scanning calorimetry (DSC)

In order to characterise the thermal properties of the solid constituents, the powder mixtures and the 3D printed tablets, a Perkin Elmer DSC 8000 (Waltham, USA) was used at a heating rate of 10 °C/min between 0 °C to 160 °C. The samples were heated and cooled through this cycle twice. 4-7 mg of each material was weighted onto an aluminium pan and hermetically sealed using an aluminium lid. To identify a baseline and remove the peaks associated with the aluminium pan, an empty pan was analysed prior to the materials. The gas flow was controlled at a flow rate of 20 mL/min of N_2 and the DSC was calibrated using iridium (T_m =156 ± 5 ˚C, ΔHf = 28.71 ± 5 % J/g). The results were analysed using the Pyris software, provided with the DSC equipment.

4.2.2.8. Scanning electron microscopy (SEM)

SEM images of the printed tablets were obtained using a scanning electron microscope JEOL 6490LV (Tokyo, Japan) with a 10 kV voltage. The samples were mounted on stubs with carbon tape and then gold coated using an AGAR AGB7341 automatic sputter coater (Essex, UK).

4.2.2.9. Micro computed tomography (micro-CT) scanning

Micro-CT scanning was performed using a Skyscan 1174 Micro CT.

See section 3.2.2.7 for experimental details.

4.2.2.10. *In vitro* drug release studies

The studies were done using a United States Pharmacopeia (USP) type 1 apparatus Copley Dissolution system (Nottingham, UK). Drug quantification was done using a TECAN Spark® (Zürich, Switzerland) multimode microplate reader UV–Visible spectroscopy (UV-Vis).

Details on the dissolution media and drug quantification can be found in section 3.2.2.8. 1 mL samples were collected at 5, 15, 30, 45, 60, 120, 180, 240, 300 and 360 mins and filtered with a 0.45 µm MF-millipore membrane filter (Millex HA) before transferring to the collection vial. After each sample removal, an equivalent amount of fresh buffer at the same temperature was added to the dissolution vat. All dissolution tests were done in triplicate.

4.2.2.11. Stability studies

As 3D printing can be viewed as an on-demand manufacturing technique, a 4-week study (28 days) was done for all three formulations at accelerated conditions, 40 °C/ 75% relative humidity (RH), following part of ICH guidelines [226]. Five solid tablets of each formulation, 0T, 1T and 10T were placed in 20 mL vials, with closed lids. The vials were placed in a closed container in an incubation oven set at 40 °C (Figure 4.1 **a)** and **b)**). The container had a concentrated sodium chloride solution to create the high humidity atmosphere, as described in [227]. Furthermore, five samples of each formulation were also kept in a desiccator to assess their stability in normal laboratory storage conditions ((Figure 4.1 **c)**). The amorphous form of printed tablets of each formulation was confirmed at the start of the stability study. After, a tablet from each formulation and storage condition was analysed at 24h, 48h, 1 week, 2 weeks and 4 weeks. Polarised light microscopy (PLM) was used as a sensitive method for detecting the onset of crystallisation. All tablets were printed on the same day so the study could start on the day they were produced.

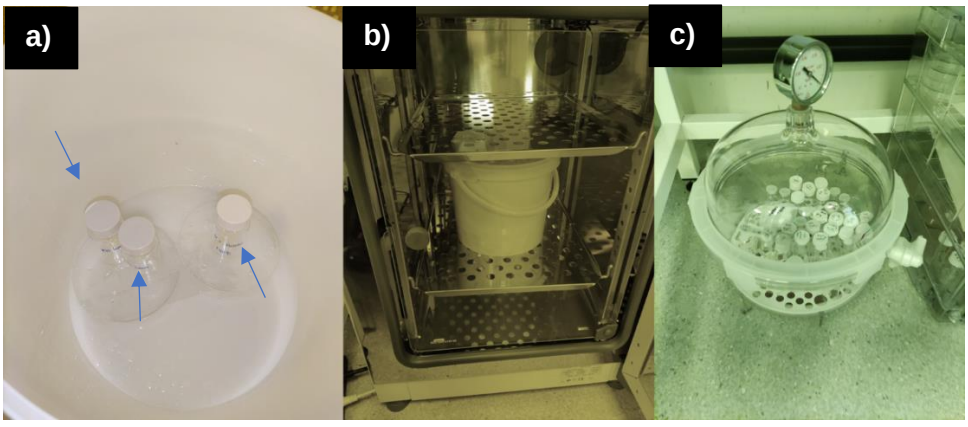

Figure 4.1 **a)** Stability samples (blue arrow) placed in vials inside container, **b)** closed container in incubation oven, **c)** samples placed in desiccator

The presence of crystalline material was analysed using a Nikon Eclipse LV100ND Optical Microscope with polarising filters. Individual tablets were placed in a glass

slide and examined using both polarised and non-polarised light. Images of different areas of each tablet in both lights were recorded. Crystalline material was defined as bright white or a coloured spot under polarised light, while making sure this had a defined shape and was not caused due to a physical defect of the examined surface or any contamination (for example fibres from the isopropanol wipes used to clean the cartridges). Material was considered crystalline material if exhibiting a geometric shape such as star-like, a square or rectangle.

4.3. Results and Discussion

4.3.1. Extrusion-based printing of tablets

Figure 4.2 shows two printed tablet geometries of the 10T formulation, a concentric 100% infill solid tablet (Figure 4.2 **a)**), and a linear 40% infill mesh tablet (Figure 4.2 **b)**). The process starts with the printing of a perimeter layer first, followed by the infill printing in a geometry and percentage that the user chooses. It is possible to observe that where the perimeter printing starts, there is a smaller indentation on the outside of both types of tablets from a delayed start of extrusion. This is marked on Figure 4.2 with a blue arrow and it is likely due to the viscosity of the material. This is more noticeable in the micro-CT scans of both printed geometries, shown in Figure 4.3 and Figure 4.4. A possible way to solve this issue would be to add a pre-flow delay in the print, which means the material would be extruded for a specified amount of time prior to the start of the printhead moving. This would be required during the infill printing phase also. While this pre-flow delay would potentially solve the small gap in the perimeter, it would lead to an accumulation of material in the centre of the tablet from excess material deposition. Therefore, no pre-delay was used. Both geometries were printed at the same speed, 14.5 mm/s. Their average sizes are shown in Table 4.2. From twenty printed solid tablets, uniformity of tablet weight was calculated at 3.05 % (RSD%) for an average mass of 131 mg, with the mesh tablet at 4.33% (RSD%) and an average mass of 75 mg. This is within the limits established by the British Pharmacopeia for tablets under 250 mg [219]. The increase in RSD% for the mesh tablet might be explained by the geometry of the infill, which is more prone to gaps, as can clearly be seen in the micro-CT of the tablet in Figure 4.4.

Table 4.2 10T tablets' dimensions, measured with a Vernier caliper (n=10)

Geometry	Solid	Mesh
Dimensions	Ø = 9.41 ± 0.11 mm H = 1.79 ± 0.17 mm	Ø = 9.29 ± 0.15 mm H = 1.72 ± 0.18 mm

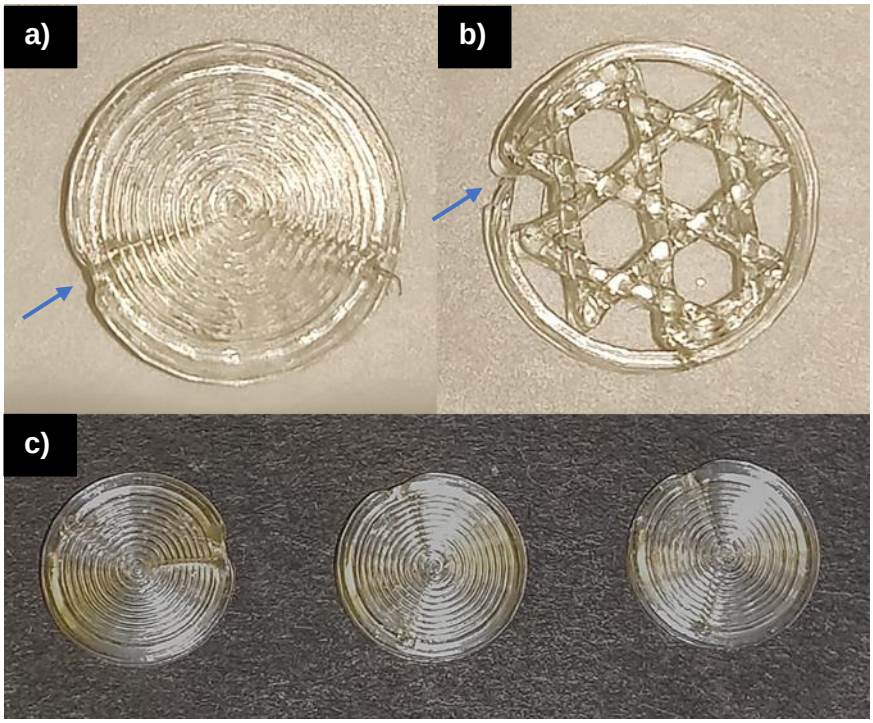

Figure 4.2 Images of 3D printed tablets: **a)** solid 10T; **b)** mesh 10T; **c)** solid 0T, 1T and 10T tablets, respectively

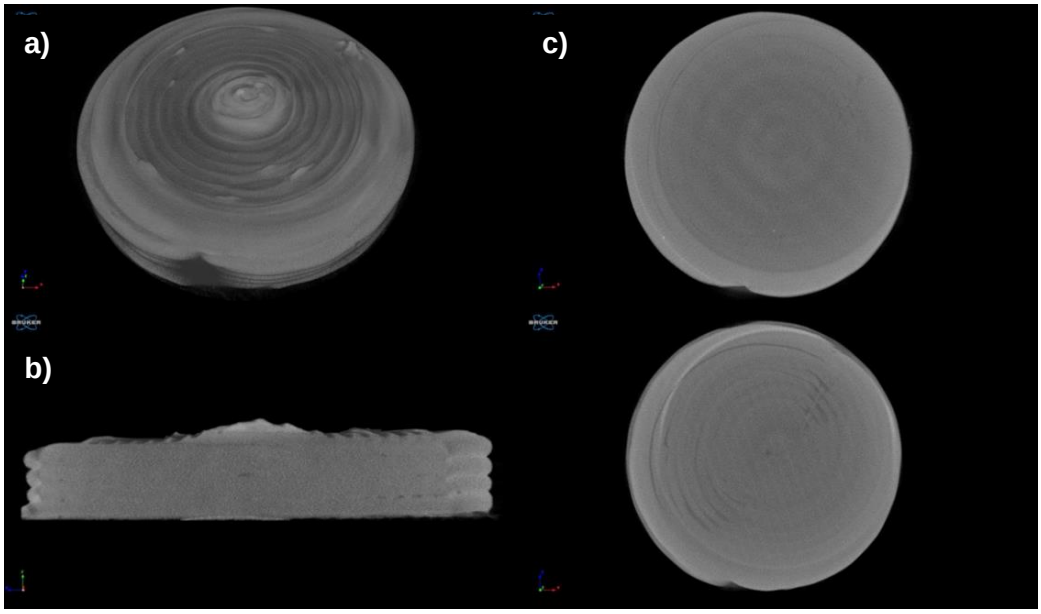

Figure 4.3 Micro-CT scan of a solid 10T printed tablet. **a)** top view, **b)** vertical cross section, **c)** horizontal cross sections at different heights of the tablet

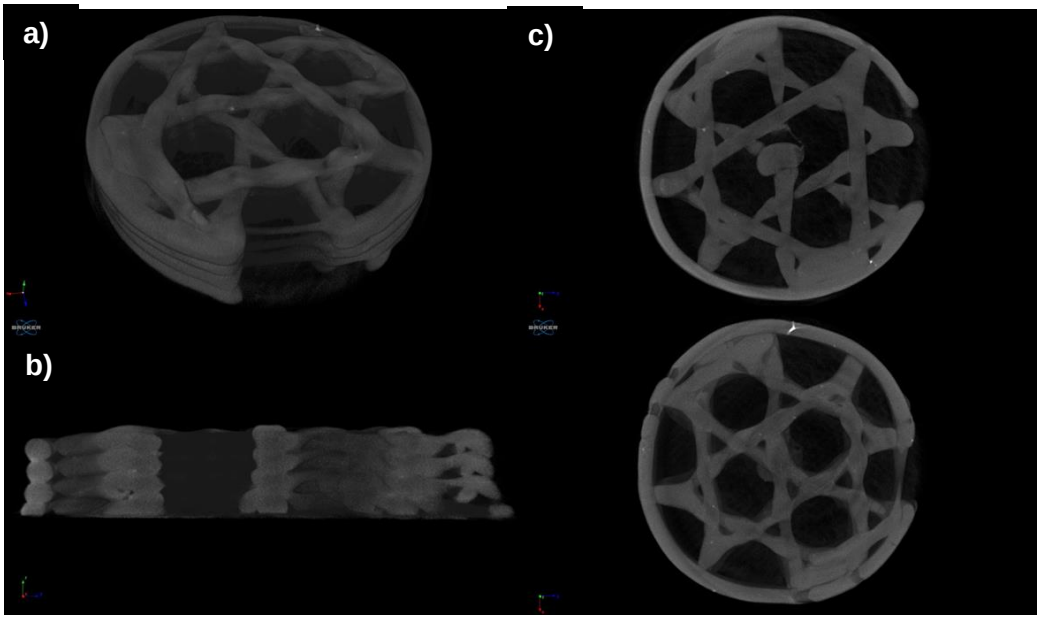

Figure 4.4 Micro-CT scan of a mesh 10T printed tablet. **a)** top view, **b)** vertical cross section, **c)** horizontal cross sections at different heights of the tablet

Friability testing of the solid tablets was also performed to assess the robustness of tablets and in particular their resistance to weight loss on physical agitation, which may happen from production until administration [1]. After the test, the difference in mass met regulatory standards, being less than 1% with no cracks or breakage being observed in the tablets.

Tablets without Tween 80 (0T) and with a smaller percentage of Tween 80 (1T) were also printed (Figure 4.2 **c)**). A comparison of the complex viscosity of each formulation is shown in Figure 4.5, with frequency sweep test data being shown in the supplementary information (Figure S 4.1). High frequencies simulate a faster motion over a shorter amount of time, while lower frequencies simulate a slower motion for a longer period of time, which can be the material at rest [228]. For all three formulations, the viscosity decreases as frequency increases, which indicates shear thinning at higher shear rates. This shear thinning effect would lead to an easier extrusion of the materials [225]. As the melt viscosity of these formulations was much higher than the formulation containing a higher percentage of Tween 80, a much lower printing speed had to be utilised. The smaller amount of Tween 80 did not lead to a significant difference in printing speed, consistent with the almost identical viscosities (Figure 4.5). 0T was printed at 1 mm/s, the slowest speed possible, and 1T was printed at 1.5 mm/s. This marks the viscosity limit for using the same nozzle size and printing pressure. By being printed at the lowest possible speed, this demonstrates that a printing process for a formulation of Eudragit RL PO and fenofibrate without a plasticising material would not be possible at lower temperatures, unless a larger nozzle was used, as it was in Kuźmińska *et al.*'s work [85]. A larger nozzle diameter can decrease the shear stress suffered by the material being extruded, therefore allowing for a more viscous material to be printed [229], although it reduces the spatial resolution of the printing.

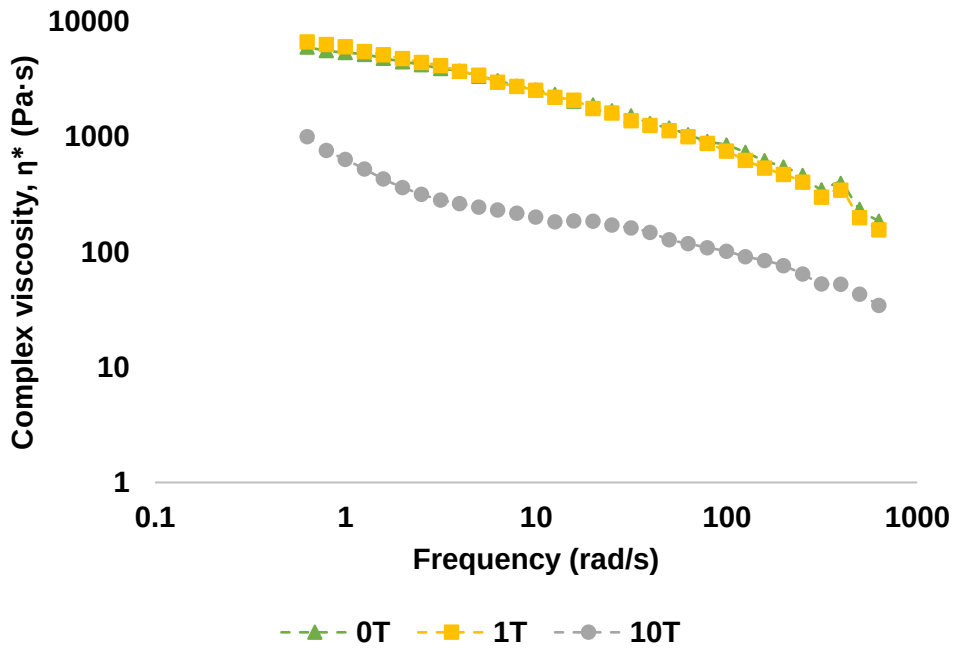

Figure 4.5 Effect of frequency on the viscosity of the different formulations

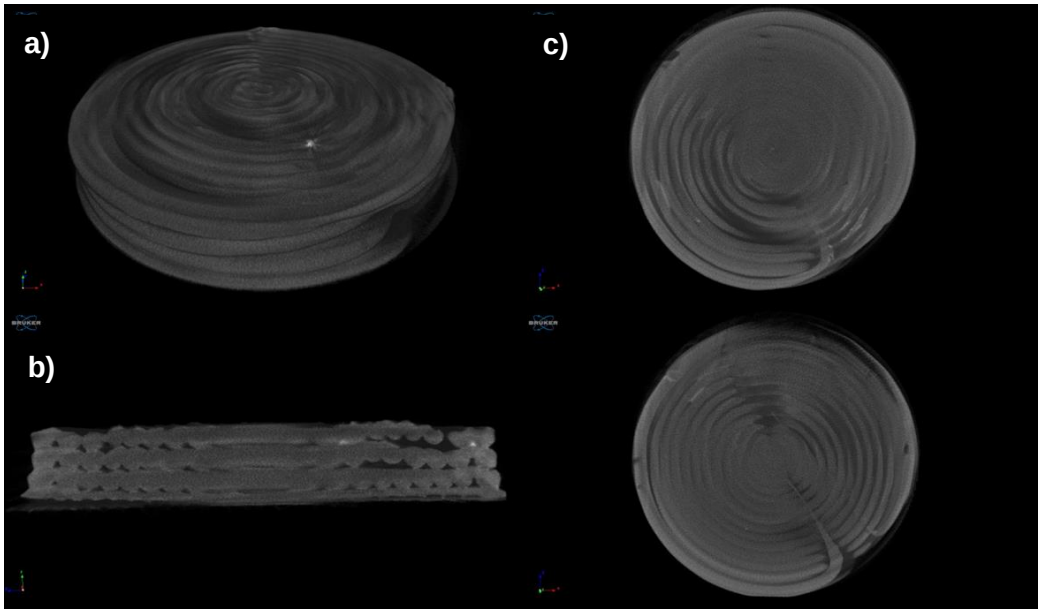

Figure 4.6 Micro-CT scan of a solid 0T printed tablet. **a)** top view, **b)** vertical cross section, **c)** horizontal cross sections at different heights of the tablet

However, the addition of Tween 80 (1T) did reduce the gaps found inside the tablets when compared to the formulation with no Tween 80. In the micro-CT scan (Figure 4.6) and SEM of a vertical cross section of a 0T tablet (Figure 4.8 **b)**) it is possible to see the gaps in between filaments and layers, these were usually near the outside of the tablet. Even though they can still be seen for the 1T tablets (Figure 4.7 and Figure 4.8 **b)**), they are considerably smaller and consistent throughout the entirety of the tablet rather than the much larger gaps near the edges. The improved viscosity of the material also led to a better contact and binding of the layers. As such, 1T tablets had an average mass of 128 mg and uniformity of weight of 4.60% (RSD%), whereas 0T had an average of 128 mg as well but with a uniformity of weight of 5.08% (RSD%). A summary of the 0T and 1T tablet's dimensions is shown in Table 4.3.

Table 4.3 0T and 1T tablets' dimensions, measured with a Vernier caliper (n=10)

	0T	**1T**
Dimensions	Ø = 9.53 ± 0.16 mm H = 1.56 ± 0.17 mm	Ø = 9.63 ± 0.14 mm H = 1.67 ± 0.17 mm

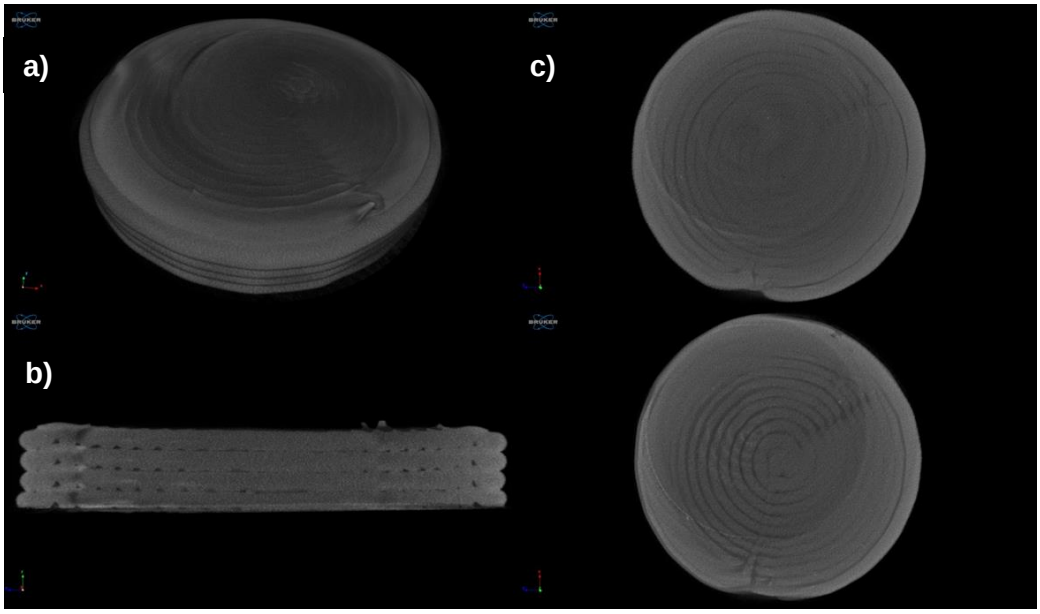

Figure 4.7 Micro-CT scan of a solid 1T printed tablet. **a)** top view, **b)** vertical cross section, **c)** horizontal cross sections at different heights of the tablet

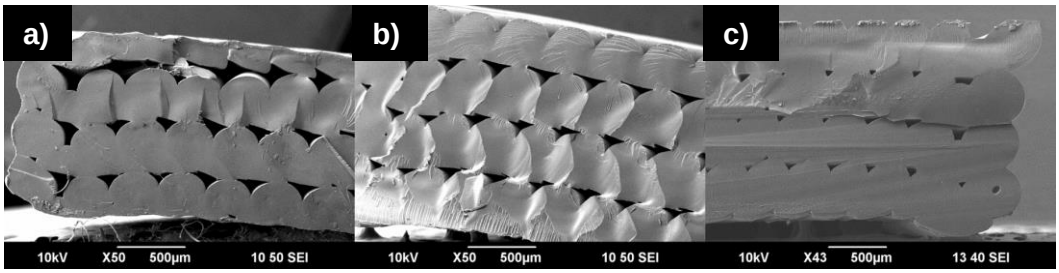

Figure 4.8 SEM images of vertical cross sections of tablets. **a)** 0T, **b)** 1T, **c)** 10T

4.3.2. Attenuated total reflection Fourier transform infrared (ATR-FTIR)

FTIR was used to investigate the incorporation of the drug, fenofibrate, in all formulations, as well as its change from Form I to an amorphous form. Figure 4.9 shows the spectra of the formulation's raw materials (fenofibrate, Eudragit RL PO and Tween 80) and the printed tablets.

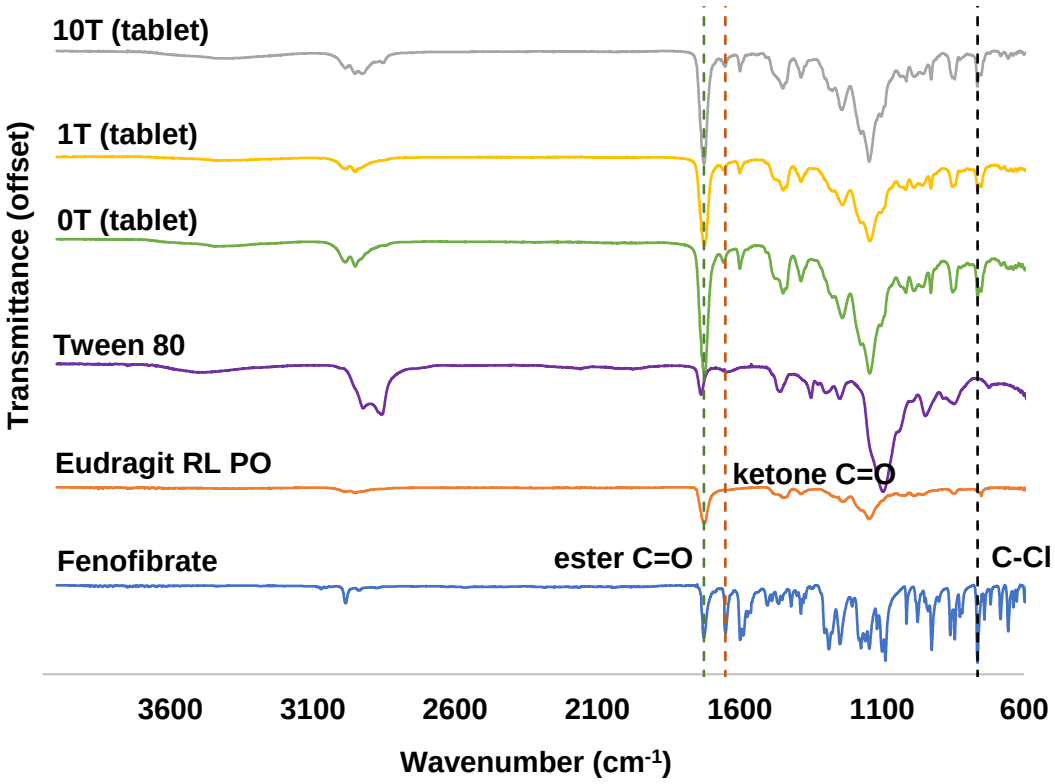

Figure 4.9 FTIR spectra of the raw materials fenofibrate, Eudragit RL PO and Tween 80, and the printed tablets of each formulation

Considering fenofibrate, Table 4.4 summarises some of the characteristic absorption peaks. As mentioned previously (3.3.2), a clear indication of its incorporation in the formulations is the peak corresponding to the C-Cl bond. In the fenofibrate spectra, there is a sharp absorption centred at 764 cm^{-1}, which can also be seen, though with a weaker absorption considering a drug loading of only 10% w/w, on the spectra in all of the printed tablets. Two other characteristic peaks can be seen at 1725.7 cm^{-1} for an ester carbonyl stretching, and 1649.7 cm^{-1} for a ketone carbonyl stretching [220]. Literature shows that between form I and the amorphous form of fenofibrate there are shifts in the absorption peaks [220,230]. This can also be observed in the spectra of fenofibrate and the printed tablets. There is a downward peak shift for the ester carbonyl stretching and an upward shift for the ketone carbonyl stretching (Table 4.4). The upwards shift for the ketone carbonyl stretching peak is consistent in the literature, as well as it being a more significant shift [220,230]. Sailaja *et al.* hypothesises that this upward shift for the ketone carbonyl stretching suggested a stronger hydrogen bond in the crystalline phase when compared to the amorphous phase of fenofibrate [230]. However, both upwards [220] and downwards shifts [230] have been reported for the peaks corresponding to the ester carbonyl stretching peak

of crystalline form I and amorphous fenofibrate. Regardless, the shift reported for the ester carbonyl stretching is smaller in both reported cases [220,230], which is also observed in the printed tablets as shown in Table 4.4. The absorption peaks corresponding to the two carbonyl groups and the C-Cl bond, are the most distinctive peaks and confirm the presence of amorphous fenofibrate in the printed formulations.

Table 4.4 Summary of fenofibrate's characteristic absorption peaks in pure component and printed tablets

Functional group	**Wavenumber (cm^{-1})**			
	Fenofibrate spectra	0T spectra	1T spectra	10T spectra
C=O (ester)	1725.7	1724.4	1723.6	1725.5
C=O (ketone)	1649.7	1656.8	1657.9	1658.9
C-Cl	764.0	763.5	763.5	764.4

4.3.3. X-ray diffraction (XRD)

X-ray diffraction of the raw solid components and the printed tablets of each formulation were performed to examine the physical state of the drug in the final product (Figure 4.10). As Eudragit RL PO is amorphous, its diffraction pattern exhibits a broad halo [186]. As shown in section 3.3.3, fenofibrate's diffraction pattern demonstrates it is crystalline and matches form I [9,194,220]. Peaks are observed at 11.9° (2θ), 14.5° (2 θ), 16.2° (2 θ), 16.6° (2Θ) and 22.2° (2 θ). In Figure 4.10, the data for all tablets confirm the amorphous form of fenofibrate within the formulations, with the presence of a broad halo and no distinctive peaks. Moreover, this demonstrates that the presence of Tween 80 is not required for the amorphicity of the drug-polymer printed system.

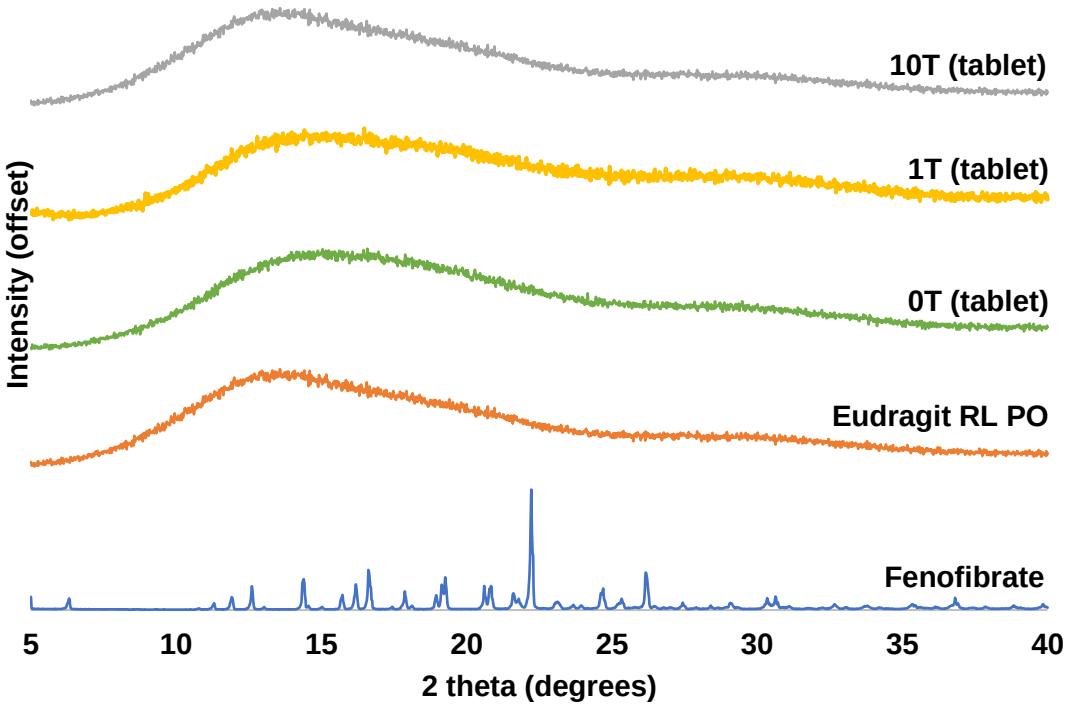

Figure 4.10 X-Ray diffraction patterns of raw solid components fenofibrate and Eudragit RL PO and printed tablet

4.3.4. Thermal analysis

To assess the stability of the raw solid materials and powder mixtures at the printing temperature (150 °C), TGA was used. A partial thermogram up to 200 °C can be seen in Figure 4.11, with the entire thermogram available in the supplementary information (Figure S 4.3). Eudragit RL PO and the powder mixtures with (10T) and without Tween 80 (0T) showed a 2.3% weight loss at 150 °C, as has been reported previously and that is thought to be associated with moisture evaporation [60,85]. Fenofibrate appears to start degrading at 200 °C, in agreement with literature [125].

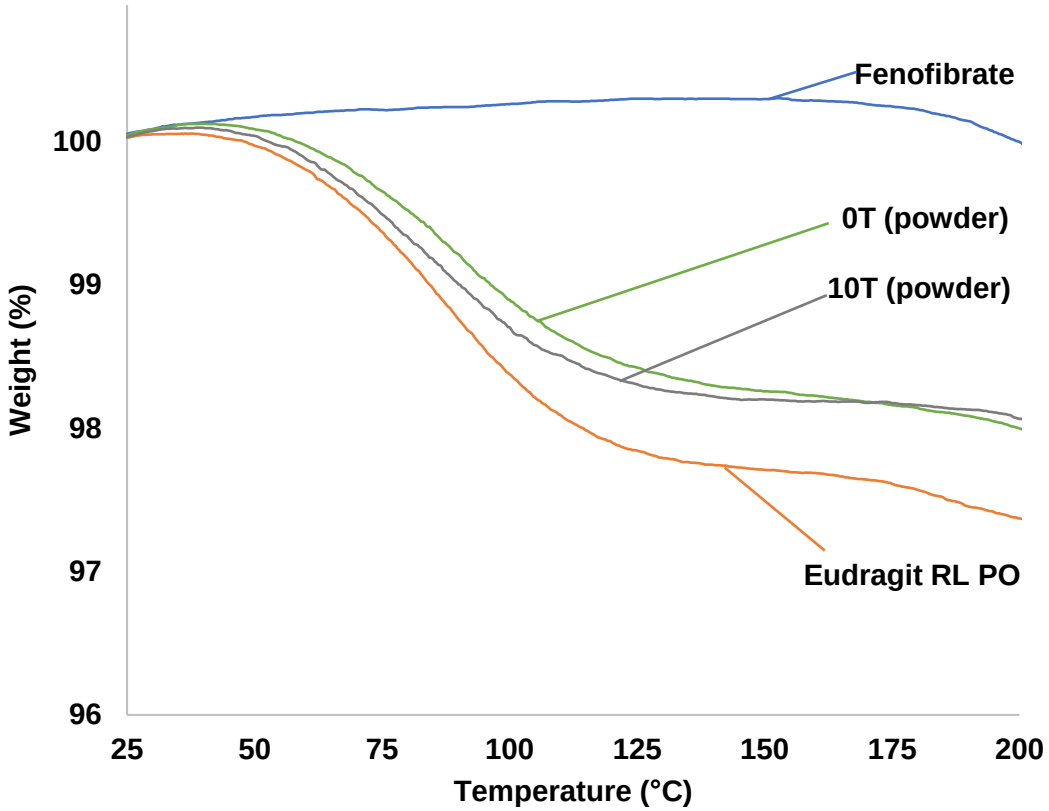

Figure 4.11 Partial TGA thermal degradation profiles of raw solid materials and powder mixtures

Figure 4.12 shows DSC thermograms of fenofibrate, including its first and second heating cycle and Figure 4.13 show the DSC thermogram of the solid raw materials, the powder mixtures, and the printed tablets. The fenofibrate thermogram shows a sharp endotherm peak at 82.2 °C in the first heating cycle, with the onset melting temperature at 80.7 °C, but the same feature was not observed in the second heating cycle. Even though the accepted melting point of fenofibrate form I is 80.5 °C [194], different melting points have been reported previously [9,10,194,231], including 83.4 °C [125], still believed to be indicative of fenofibrate form I. There is a lack of an endothermic peak for the melting of fenofibrate on the second heating run. Gorniak *et al.*, at the same heating and cooling rate used here, also did not observe the endothermic peak of fenofibrate in the second heating cycle, but rather an exothermic peak indicating the crystallisation of amorphous fenofibrate [194]. This was not observed here indicating a slow recrystallization of fenofibrate and hence the lack of an exothermic or endothermic peak. As such, and in order to investigate whether crystalline fenofibrate is present, the 1st heating cycle was analysed for the physical mixtures. However, and in order to eliminate the polymer's thermal history, the second cycle was used for Eudragit RL PO and the prints, as long as no endothermic peak

corresponding to the melting of crystalline fenofibrate was observed in the first heating cycle.

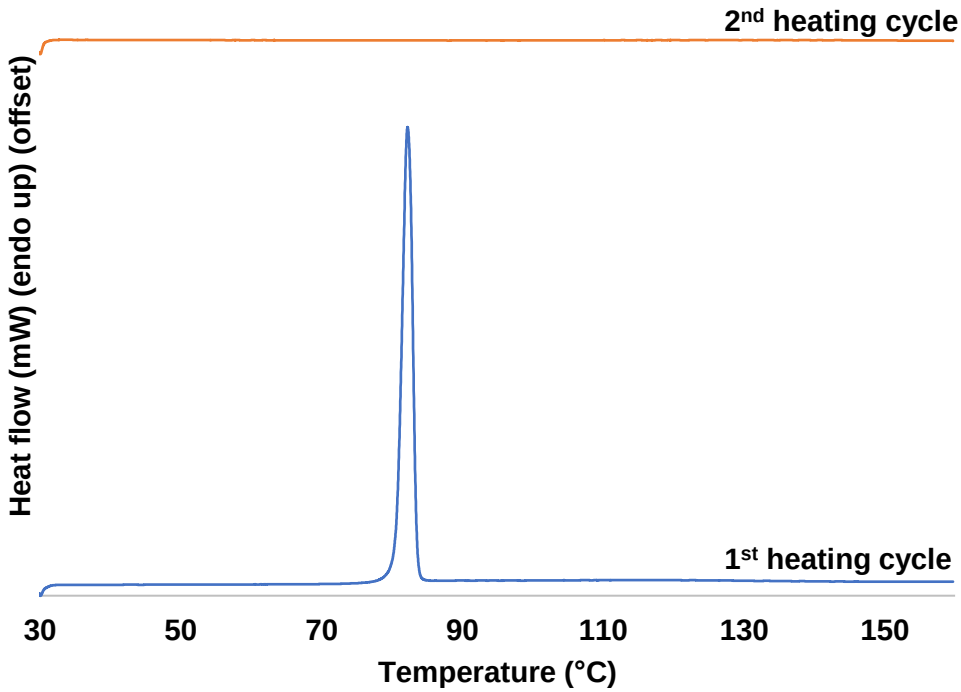

Figure 4.12 DSC thermogram of fenofibrate showing the 1st and 2nd heating cycle

Eudragit RL PO, as seen already by its diffraction pattern, is an amorphous material and did not show any characteristic peak in the thermogram (Figure 4.13). As with fenofibrate's melting point, different glass transition temperature values have been reported in the literature [85,158,232,233], ranging from 62 to 70 °C. However, it was not possible to detect this in this analysis, nor was it possible to detect the glass transition temperature of the other samples. Though not possible to see, what is expected is a decrease in T_g for the mixtures and prints with Tween 80, especially for the one containing 10% (w/w), as this surfactant was used with the intention to decrease the melt viscosity of the system, which was already demonstrated (subsection 3.3.1). A loading of 10% (w/w) of this type of surfactant has been seen to decrease the glass transition temperature of a drug-polymer system by up to 30 °C [169]. However, a significant difference was not expected to be seen for 1T, as a 2% (w/w) loading has not significantly impacted on the glass transition temperature of a drug-polymer systems [169]. Fenofibrate has also been found to act as a plasticiser in amorphous solid dispersions, though in higher concentrations (30% (w/w) and with different carrier polymers than used here [10]. Therefore, a decrease in glass

transition temperature for Eudragit RL PO with fenofibrate might be expected as well. For the physical mixtures, what was observed is a single endothermic event corresponding to the melting of the crystalline fenofibrate present in these mixtures. The onset temperature was detected at 80.30, 80.45 and 79.10 °C for 0T, 1T and 10T, respectively. The decrease in the endothermic peak height of the powder formulations and printed tablets compared to fenofibrate is due to the drug being only 10% (w/w) of the mixtures. The lack of endothermic peak, as observed for the carrier polymer, shows that the drug is amorphous in the printed formulation, at least below the limit of detection of DSC of around 2% w/w [184]. The DSC results further confirm what was observed with the XRD pattern of the printed tablets, which show that the drug in the printed tablets, regardless of the formulation, to be in its amorphous form. Eudragit RL PO therefore allows the transition of fenofibrate from its stable crystalline form I to an amorphous form which remains stable and unchanged for the period of observation.

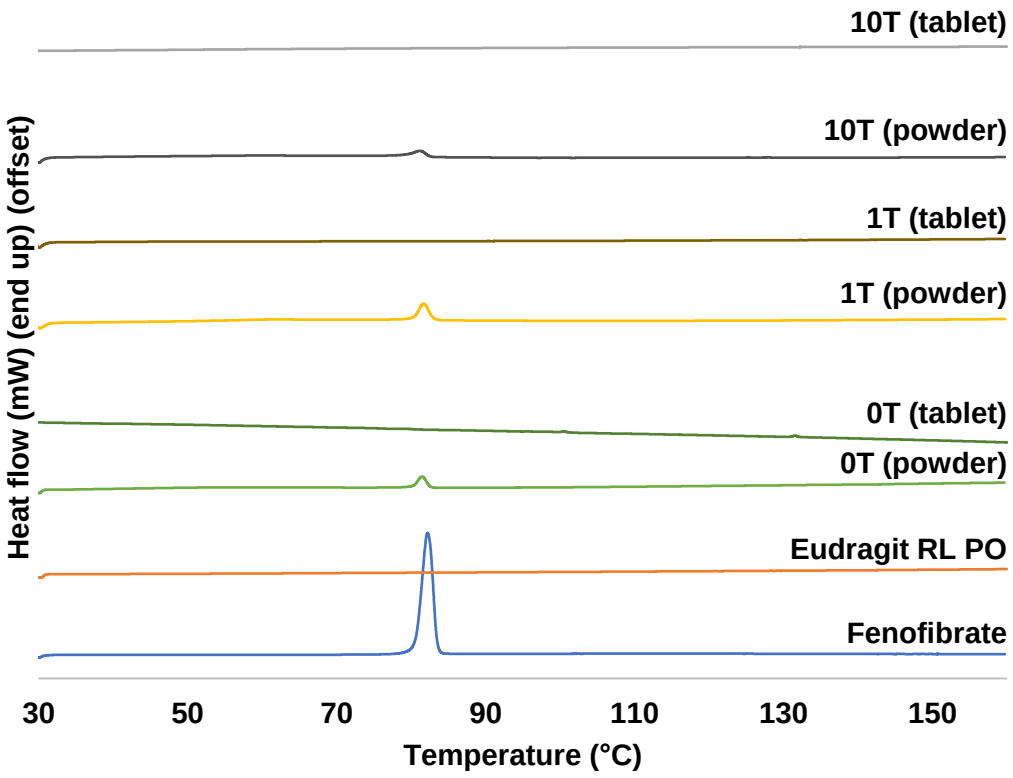

Figure 4.13 DSC thermogram of fenofibrate, Eudragit RL PO and the printed tablet

4.3.5. *In vitro* drug release

Figure 4.14 **a)** shows the cumulative % release of fenofibrate from the two different geometries that were printed with the 10T formulation. As it has been extensively shown in the literature for non-disintegrating tablets [52,231,234], when a lower infill % has been used to print a tablet, the surface area available for the release of the drug from the tablet matrix increases, therefore increasing the rate at which said drug is released. Notably, the mesh tablets show full release after 360 min (6hrs), while the solid tablets only exhibit a release of around 57% of fenofibrate after 6hrs. It is worth noting that the .stl file used for printing the tablets was the same, which means the shape is similar, though the amount of drug in the mesh tablets is pro rata less.

Figure 4.14 **b)** shows the comparison of cumulative % release of fenofibrate from the solid tablets from all three formulations. As expected, due to its solubilising effect [26,169–171], the tablets with the highest amount of Tween 80, the 10T tablets, have the highest release of drug in the 6 hours of the study. However, it is surprising to see the addition of 1% Tween 80 (1T) has no significant impact on the release of the drug in the same amount of time when as compared to the formulation with no Tween 80 (0T). Both released an average of 36% after 6h. One might argue that this was to be expected as the impact it had on the formulations' viscosity and printability was not significant but the addition of this material at a concentration as low as 1% has been reported to have a positive effect in the solubilisation of a poorly soluble drug and its consequent release rate, almost as much as the addition of a higher concentration of Tween 80 [170]. However, there have been reports of an addition of 10% (w/w) Tween 80 having no positive effect on the release rate of a poorly soluble drug when compared to the same drug-polymer system without the surfactant. In that case, the extrusion temperature of the drug-polymer-Tween 80 system was higher than 150 °C, which might have caused the degradation of the Tween 80, preventing its potential solubilising effect [169,171]. Still, the temperature used here for printing was lower than the one used in Ghebremeskel *et al.*'s work [169,171] and from the TGA thermogram (Figure 4.11) no thermal degradation of the surfactant occurred. Nonetheless, a positive effect with a higher concentration of Tween was observed. The difference in amount released in the first 5 min between all samples, but specifically for the 0T samples, could be due to a higher amount of the drug near the surface of these tablets, something that could be investigated in the future using techniques such as energy dispersive x-ray analysis (EDX) [138].

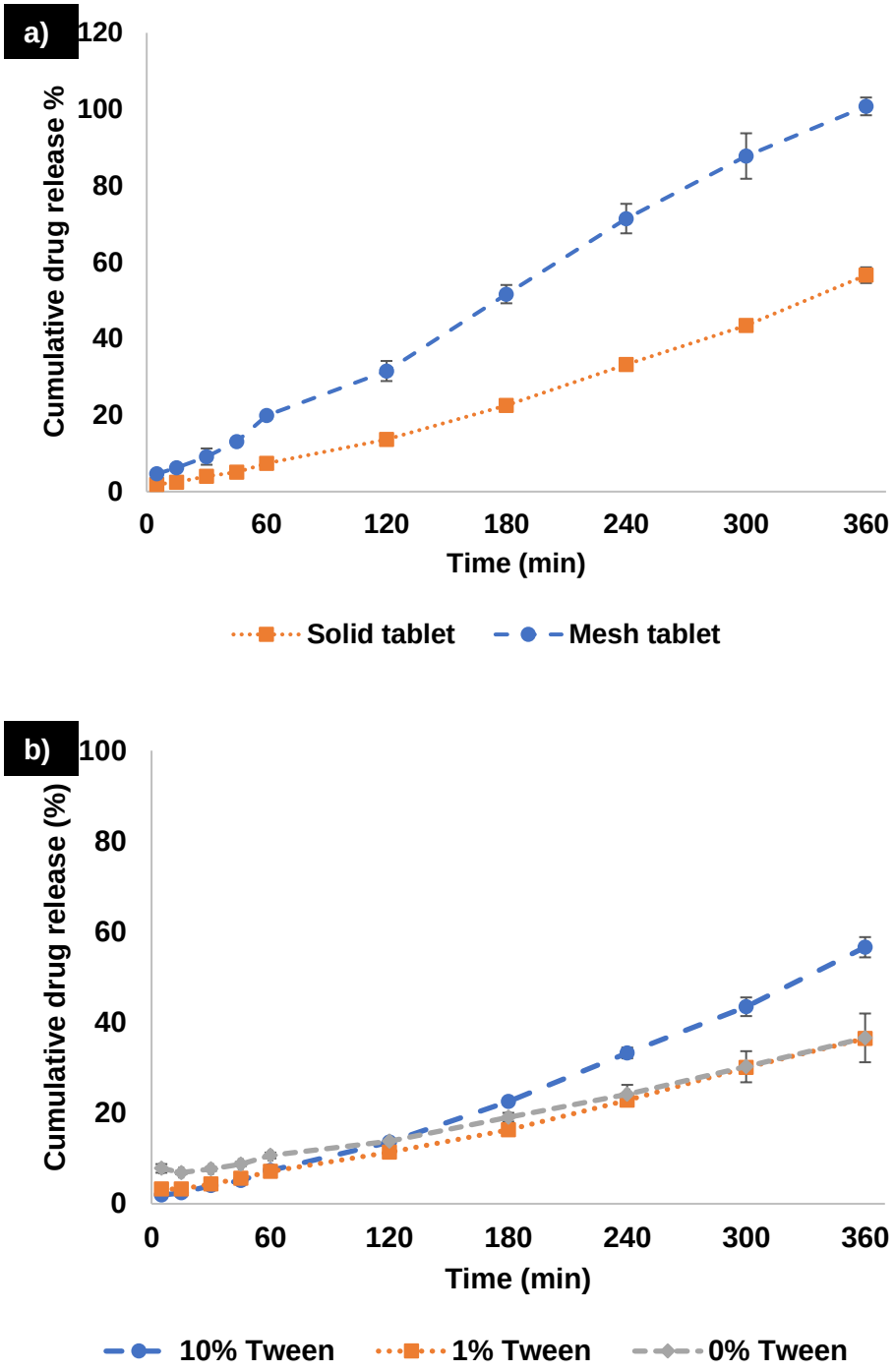

Figure 4.14 Dissolution data showing drug release profiles of the 3D printed tablets (n=3). **a)** 10% Tween 80 containing tablet with the two printing geometries; **b)** comparison of the release from tablets containing the different formulations

To better understand this difference in release profiles, a tablet of each formulation was removed from a dissolution vat after 3hr and analysed using micro-CT scanning and SEM imaging. The effect of 10% (w/w) Tween 80 can be seen in the micro-CT

scan of this tablet (Figure 4.15) and on the SEM image of a vertical cross section of the same tablet (Figure 4.18 **c)**). In both, several pores can be observed.

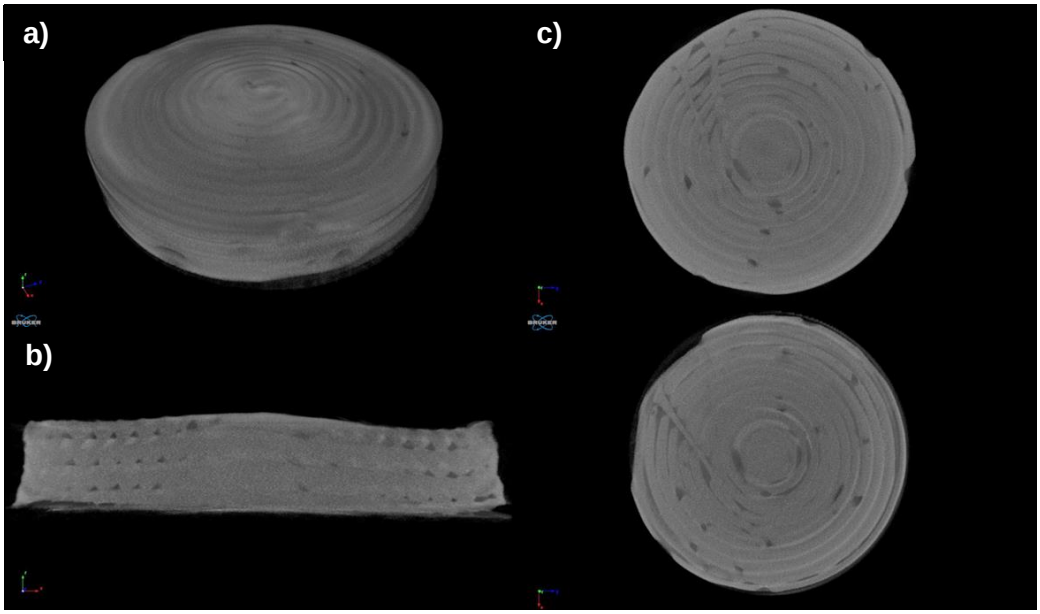

Figure 4.15 Micro-CT scan of a partial dissolved solid 10T printed tablet. **a)** top view, **b)** vertical cross section, **c)** horizontal cross sections at different heights of the tablet

As seen previously in the micro-CT scan (Figure 4.3) and SEM of a vertical cross section of a 10T tablet (Figure 4.8), the existence of pores and gaps in tablets printed with this formulation were minimal. They were mostly found in the filament interphase and were much smaller than the ones found in the other two tablets. We can therefore presume that these larger pores have appeared during the dissolution testing and are likely caused by a leaching of the Tween 80 into the dissolution media, something that has been seen by Tween 80 present in hydrogels [235]. The appearance of these pores is increasing the surface area of the tablet. Consequently, the release rate of fenofibrate increases as well and that leads to a much higher release from that tablet when compared to tablets 0T and 1T. Figure 4.16 and Figure 4.17 show the micro-CT scans of both 0T and 1T tablets after dissolution, respectively and Figure 4.18 shows the SEM image of vertical cross sections of the same tablets in the same condition. Besides the normal gaps found in these type of tablets in the interphase of the extruded filaments, from the high viscosity of material and (Figure 4.6 and Figure 4.7), no pores of significant size have formed in either 0T and 1T, consistent with the lower and similar amount of drug released.

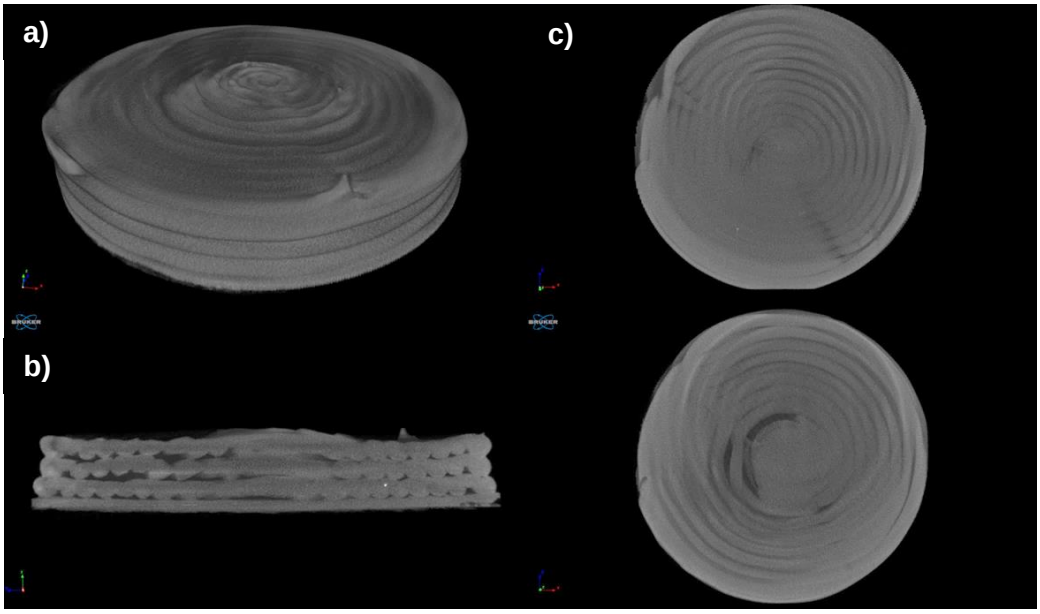

Figure 4.16 Micro-CT scan of a partial dissolved solid 0T printed tablet. **a)** top view, **b)** vertical cross section, **c)** horizontal cross sections at different heights of the tablet

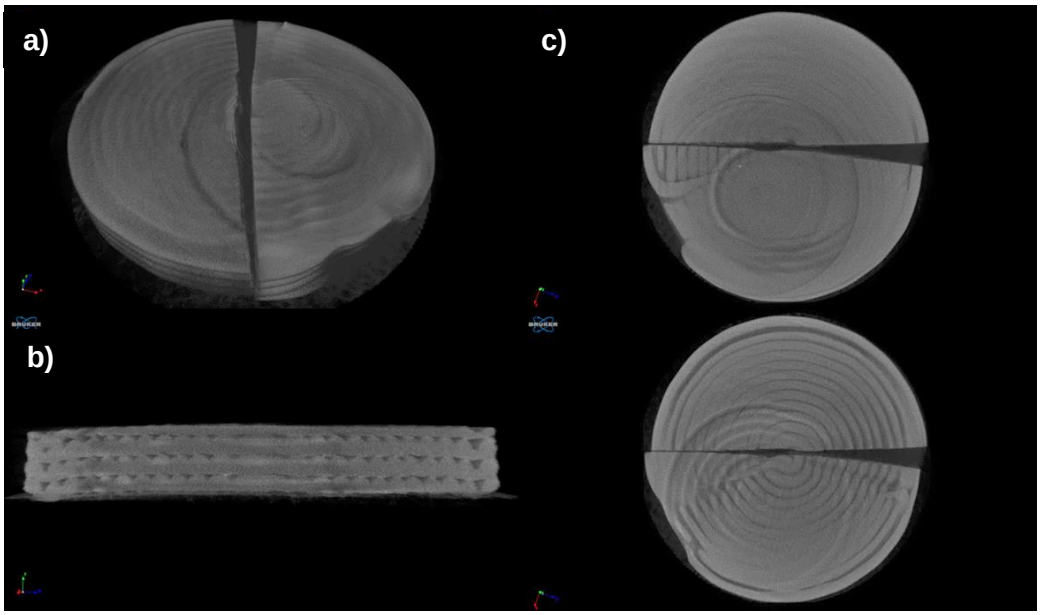

Figure 4.17 Micro-CT scan of a (broken) partial dissolved solid 1T printed tablet. **a)** top view, **b)** vertical cross section, **c)** horizontal cross sections at different heights of the tablet

Cross sectional SEM images of the same tablets (Figure 4.18) show that few pores or cracks have been formed during dissolution, as compared to their form prior to dissolution (Figure 4.8).

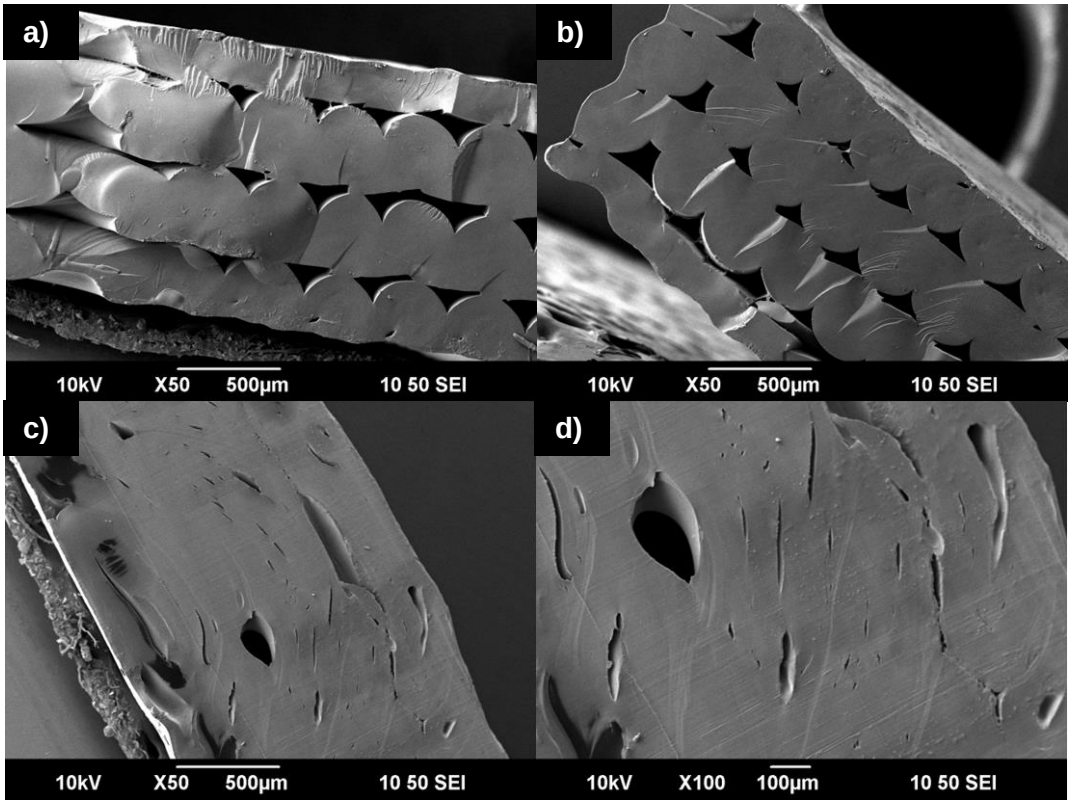

Figure 4.18 SEM images of vertical cross sections of partial dissolved tablets. **a)** 0T, **b)** 1T, **c)** 10T, **d)** 10T (higher magnification)

Independently of the geometry chosen and the addition of a plasticiser, the use of a polymeric matrix such as Eudragit RL PO leads to a sustained release of the drug. The drug release data was fitted to existing mathematical models, zero and first order, Higuchi and Korsmeyer-Peppas [221], with the zero order model better fitting the release profiles from all types of tablets (Figure 4.19, Figure 4.20 and Figure 4.21). This is characteristic of dosage forms with a slow drug release that is not caused by disintegration of the dosage form, where the same amount of drug is released per unit of time [221].

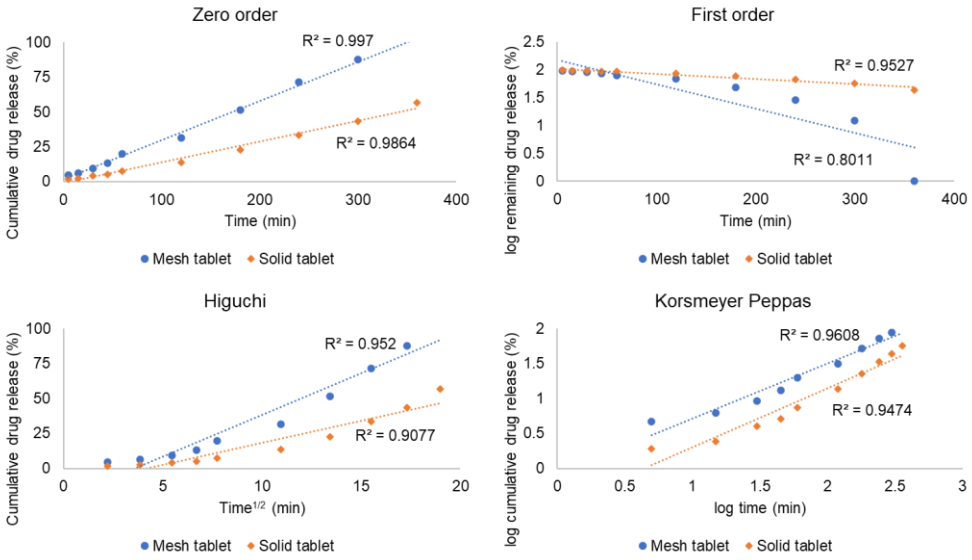

Figure 4.19 Dissolution models applied to the drug release data from 10T printed tablets (both solid and mesh ones)

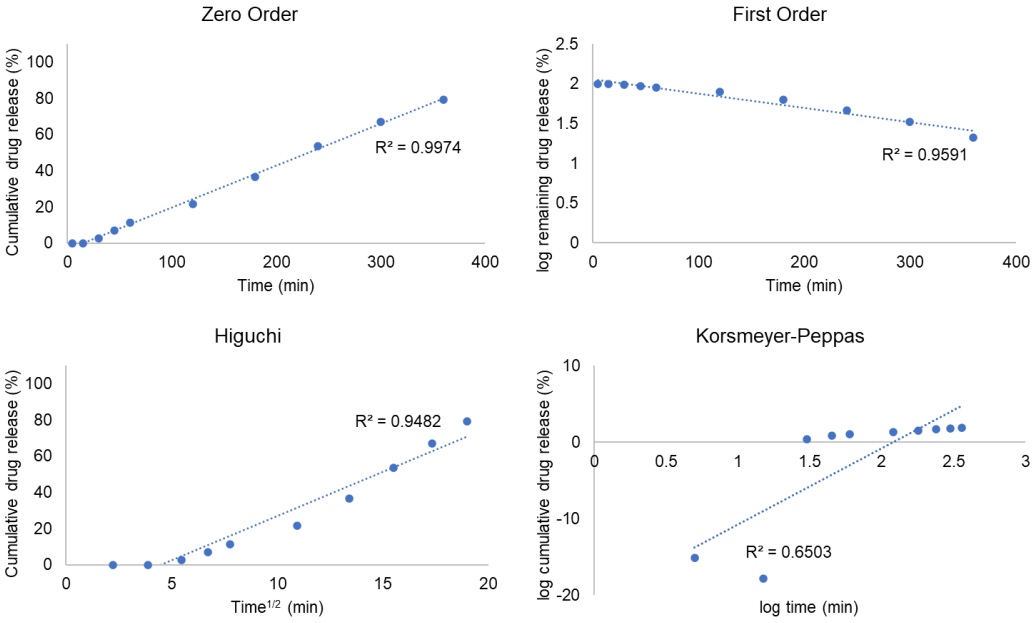

Figure 4.20 Dissolution models applied to the drug release data from 0T printed tablets

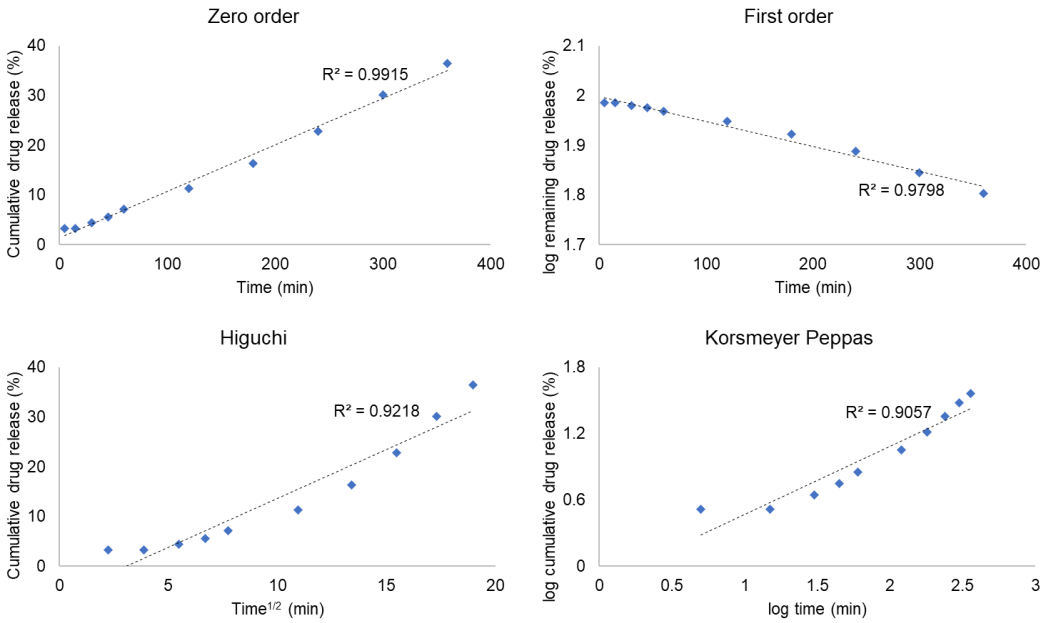

Figure 4.21 Dissolution models applied to the drug release data from 1T printed tablets

4.3.6. Stability study

The stability test started soon after printing. A photo of tablets at the beginning of the study is shown in Figure 4.22 **a)**.

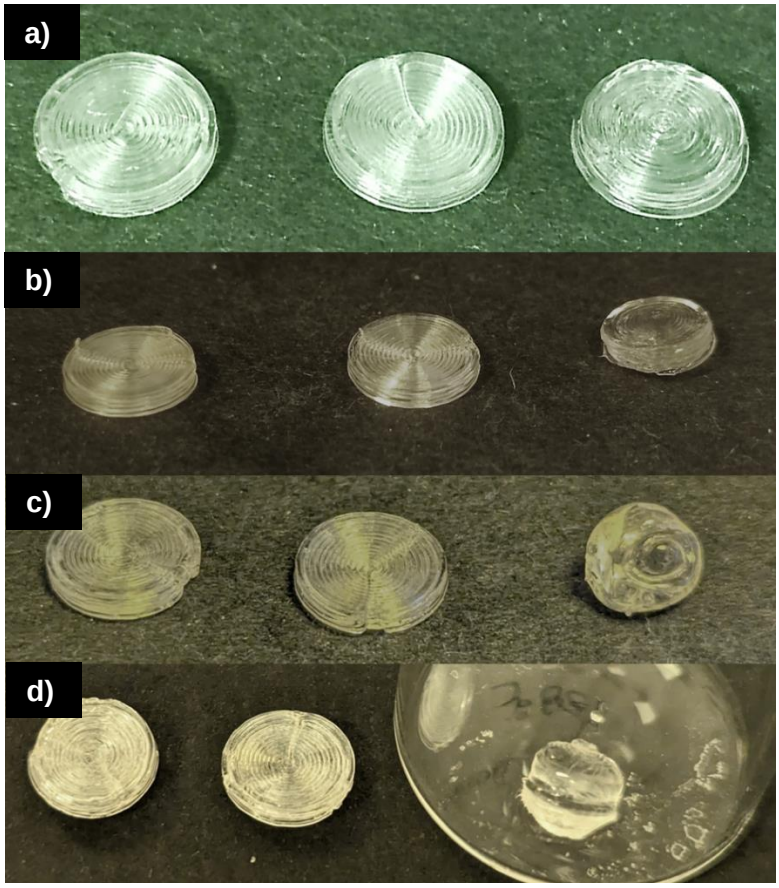

Figure 4.22 Printed tablets (0T on the left, 1T in the centre and 10T on the right) over time under accelerated conditions. **a)** day 0, **b)** day 7, **c)** day 14, **d)** day 28

These samples were analysed using optical microscopy and polarised light microscopy to characterize amorphicity upon printing (Figure 4.23). While some bright spots could be seen, these were not of defined geometrical shape and were not considered to be recrystallised drug, but rather features caused by localised scattering. The difference that the addition of 10% (w/w) Tween 80 makes can be seen from the same day they are printed, as the tablets are more transparent (Figure 4.23 **c)**). It is also with this formulation (10T) that more significant changes can be seen over time, for both storage conditions.

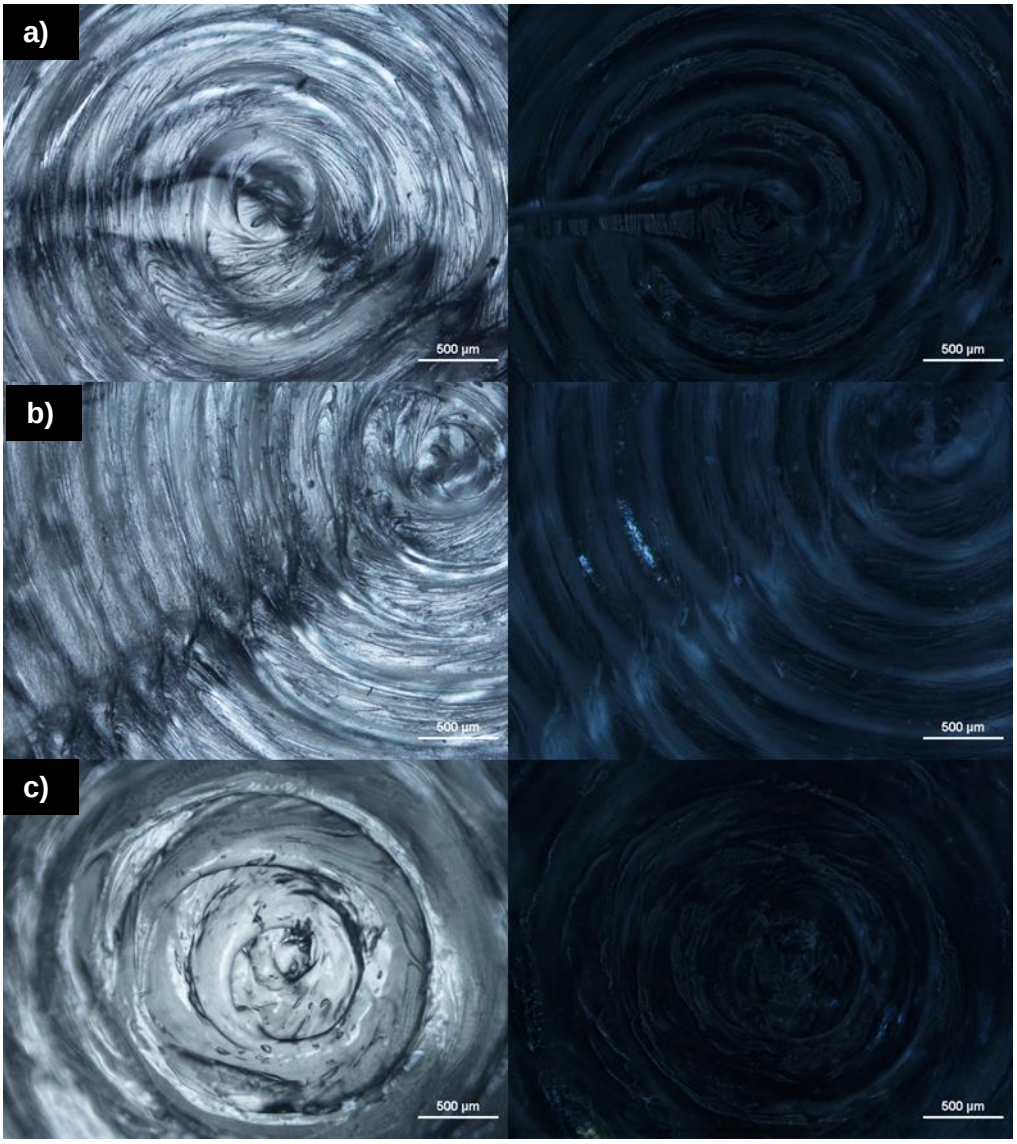

Figure 4.23 Images of the printed tablets on day 0 using optical microscopy followed by the same image under cross polarised optical microscopy. **a)** 0T, **b)** 1T and **c)** 10T

Starting with the study under accelerated conditions, there were no significant differences observed for the 0T and 1T tablets over the 28-day period (Figure S 4.4 and Figure S 4.5, respectively). The tablets retained their shape and appearance throughout the experiment (Figure 4.22). For the 10T tablets, the appearance changed significantly over time (Figure 4.22). On day 7, they had lost part of their shape, as can be seen from their optical microscopy image in Figure 4.24 **c)**. By day 14 their shape had been lost and under both polarised and non-polarised light, the sample appeared 'glassy' (Figure 4.24 **d)**). As previously mentioned, amorphous materials have higher hygroscopicity, with absorbed moisture acting as a plasticiser and leading to increased molecular mobility [8]. The system without Tween 80 is already an amorphous dispersion, in which the high humidity of the accelerated

conditions could be used as a plasticiser. By adding a high concentration of Tween 80 (10T), a plasticiser, the uptake of moisture might have led to an even greater plasticisation effect and consequent increase in molecular mobility. Moreover, as discussed previously (section 4.3.4), the addition of such a high concentration of Tween 80 might have decreased the glass transition temperature of the system considerably. With a temperature of 40 °C, likely near the T_g of the system, this would lead to a softening of the material [169]. Surfactants with higher glass transition temperatures and semi-solid in nature that provide higher viscosity to drug-polymer systems have been reported to have a higher stabilising effect of felodipine, another poorly soluble drug, when compared to Tween 80 [215]. As such, this combination of high temperature and high humidity led to the loss of shape of these tablets with higher concentration of Tween 80.

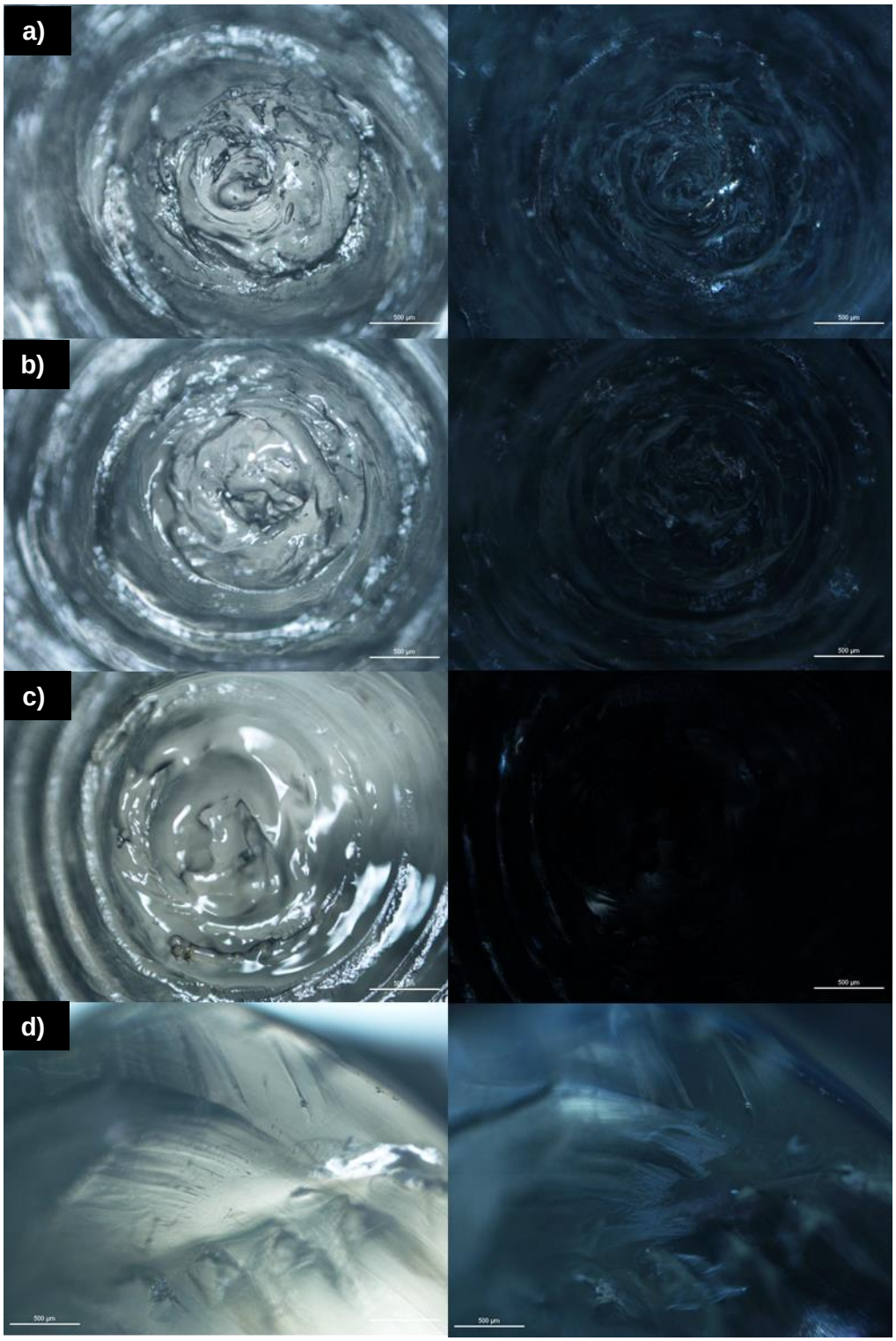

Figure 4.24 Images of the 10T tablets under accelerated conditions using optical microscopy, followed by the same image under cross polarised optical microscopy. **a)** day 1, **b)** day 2, **c)** day 7, **d)** day 14

At room temperature and in the desiccator significant recrystallisation was observed. While not much difference was observed for samples of 0T and 1T over time (Figure

S 4.6 and Figure S 4.7, respectively), clear crystallisation can be observed in the centre and outside border of a 10T sample starting on day 7 (Figure 4.25 **a)**). Spread of the crystallisation is seen on day 14 (Figure 4.25 **b)** and Figure S 4.8 **a)**), becoming even more spread throughout the entirety of the tablet by day 28 (Figure 4.25 **c)** and Figure S 4.8 **b)**). So, once again, the high amount of a plasticiser lead to an increase of mobility and instability.

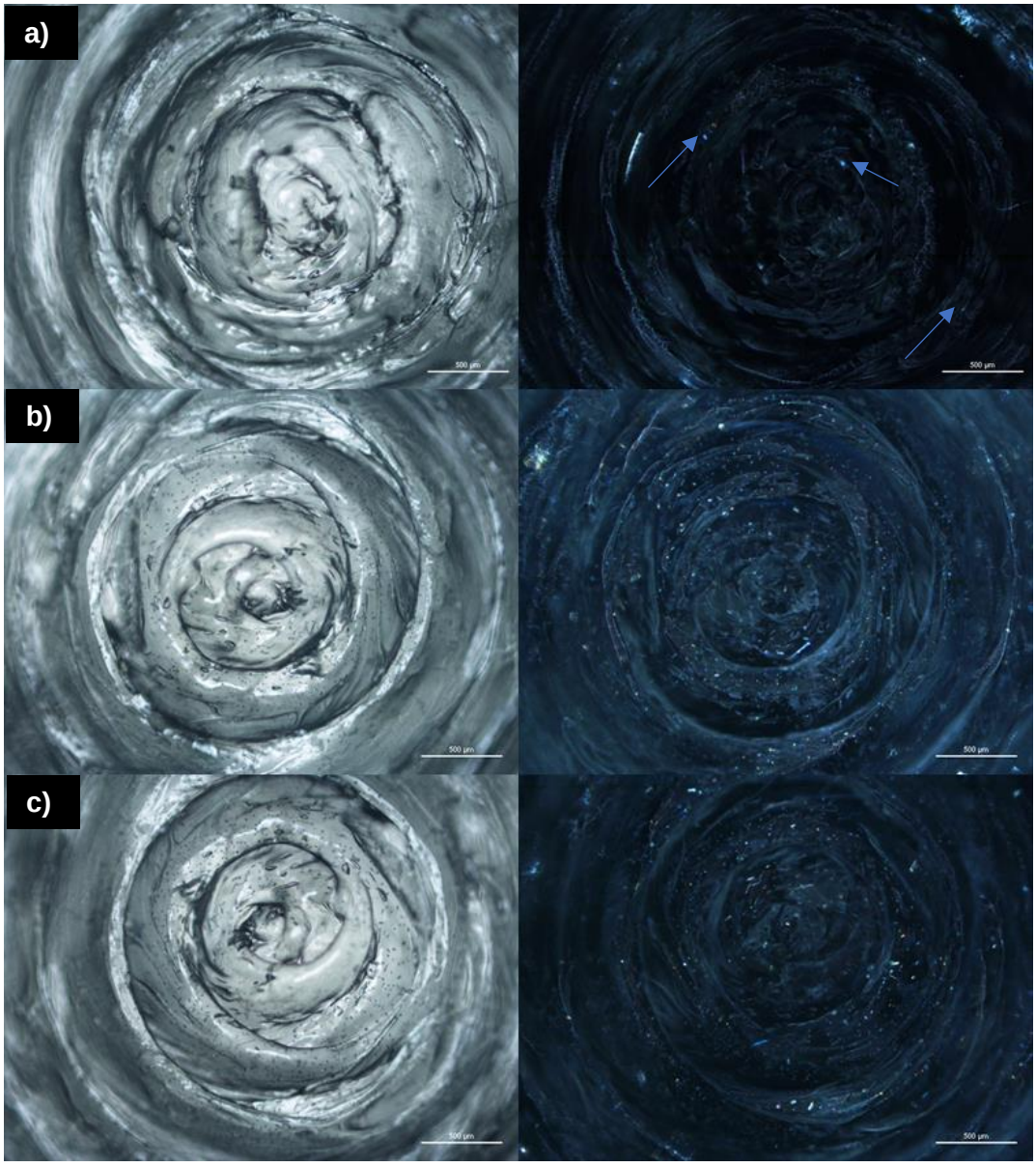

Figure 4.25 Images of the 10T tablets stored in desiccator using optical microscopy, followed by the same image under cross polarised optical microscopy. **a)** day 7 (blue arrows marking probable crystallisation), **b)** day 14, **c)** day 28

4.4. Conclusions

The following statements and conclusions can be made from this chapter:

- Direct powder printing is a modality of 3D material extrusion in which the material is melted, as with FDM printing, but where the prior production of a filament is not required, and a lower printing temperature can usually be employed.
- Amorphous solid dispersions of poorly soluble drugs can be achieved using this approach.
- Adding Tween 80, a surfactant, as a plasticiser can significantly decrease the viscosity of the melt, increase the printing speed of the mixture and improving the binding of the printed filaments and layers, leading to a more contiguous and uniformly solid tablet.
- The addition of Tween 80 has a significant effect on the release rate of fenofibrate. The surfactant aids solubilisation of the poorly soluble drug, and it is proposed to preferentially leach out the tablet during dissolution, creating pores that increase the surface area and consequently increase release rate.
- A change in geometry from a solid to a mesh tablet increases the surface area of the tablet which leads to an increase in release rate of fenofibrate.
- The formulations without Tween 80 and with a 1% (w/w) concentration of Tween 80 remain stable, whereas the one with 10% (w/w) of Tween 80 leads to physical instability under the same conditions. At higher temperatures and humidity, the tablets lose their shape as there is an increase in molecular mobility due to the temperature being close to the glass transition temperature of the system and the additional plasticising effect of absorbed water. While stored in the desiccator and at room temperature, Tween 80 leads to an increase in mobility though leading to an onset of crystallisation of fenofibrate, between day 2 and day 7.
- In order to print at lower temperatures and further optimise this process, there is a need to explore different plasticising materials. As such, it is imperative that their impact on the printability, solubility and stability of poorly soluble drugs is also studied.

4.5. Chapter appendix: supplementary information

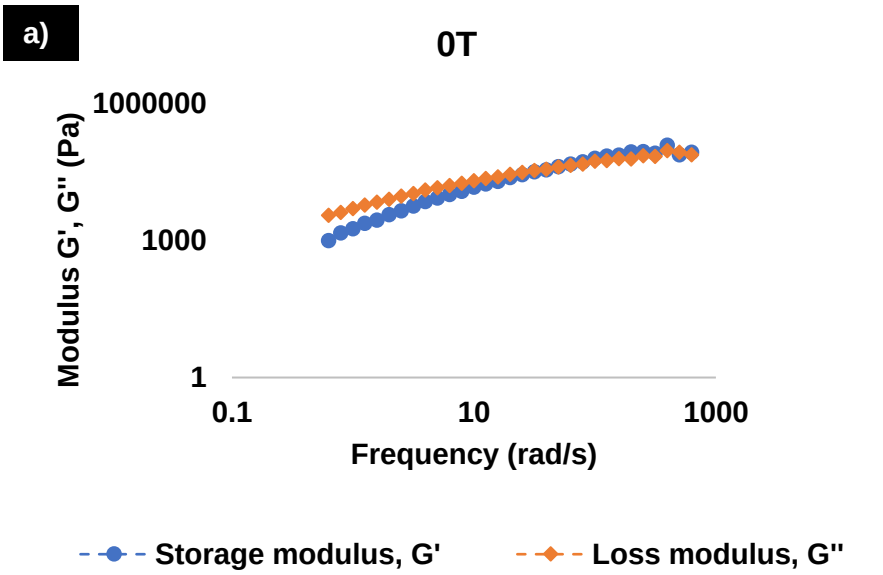

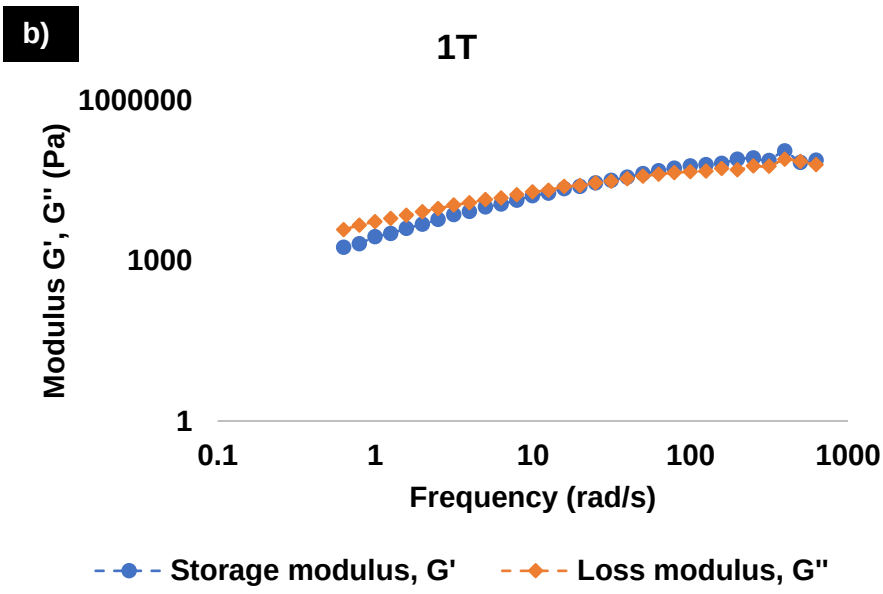

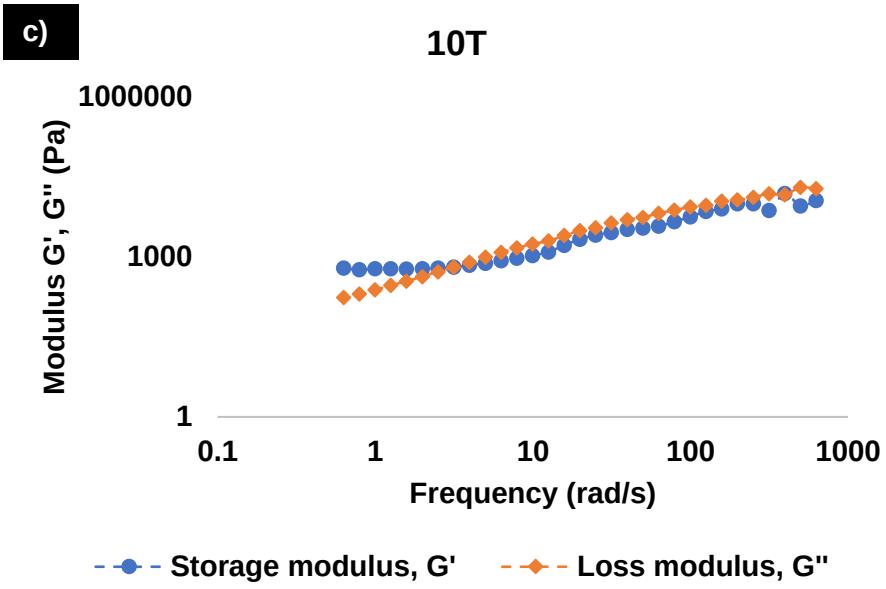

Figure S 4.1 Frequency sweep curves for **a)** 0T, **b)** 1T and **c)** 10T

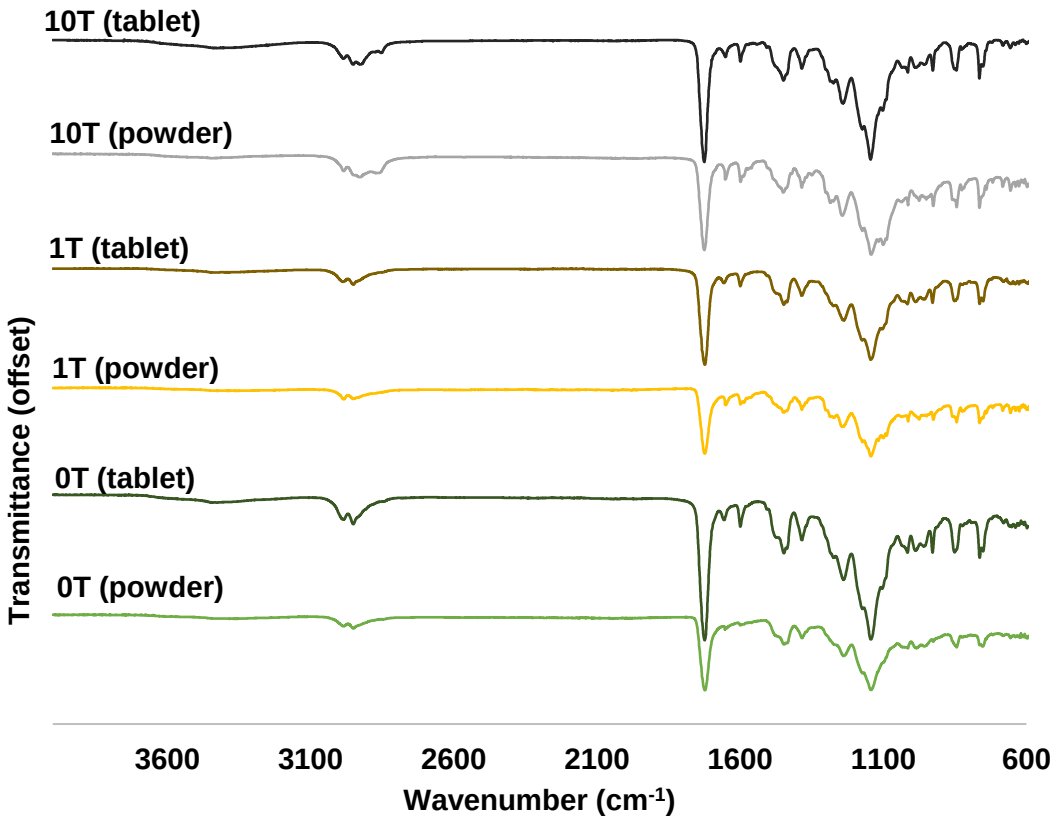

Figure S 4.2 FTIR spectra of all formulations, in powder form and printed tablets

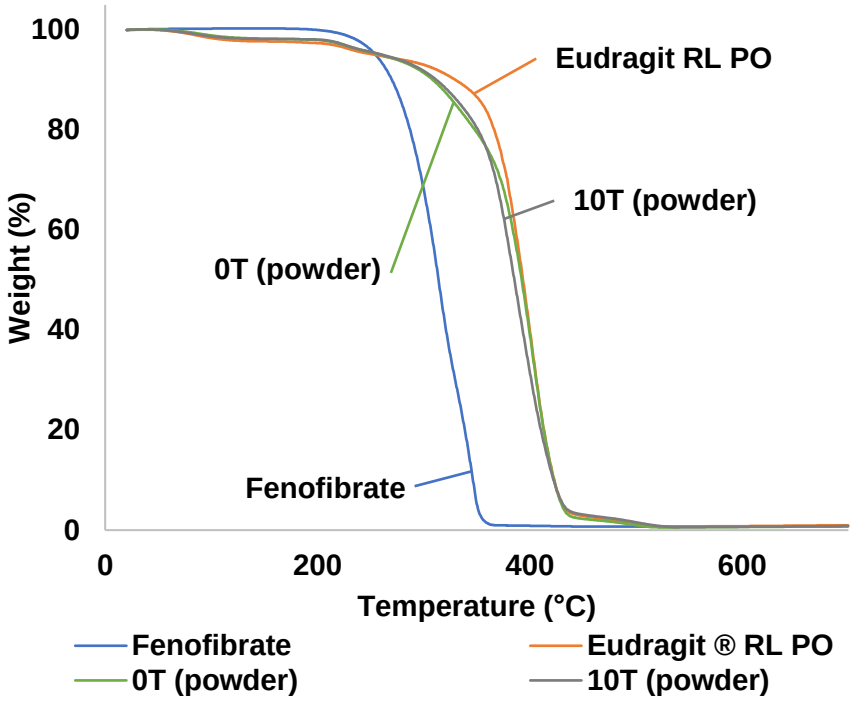

Figure S 4.3 TGA thermal degradation profiles of raw solid materials and powder mixtures

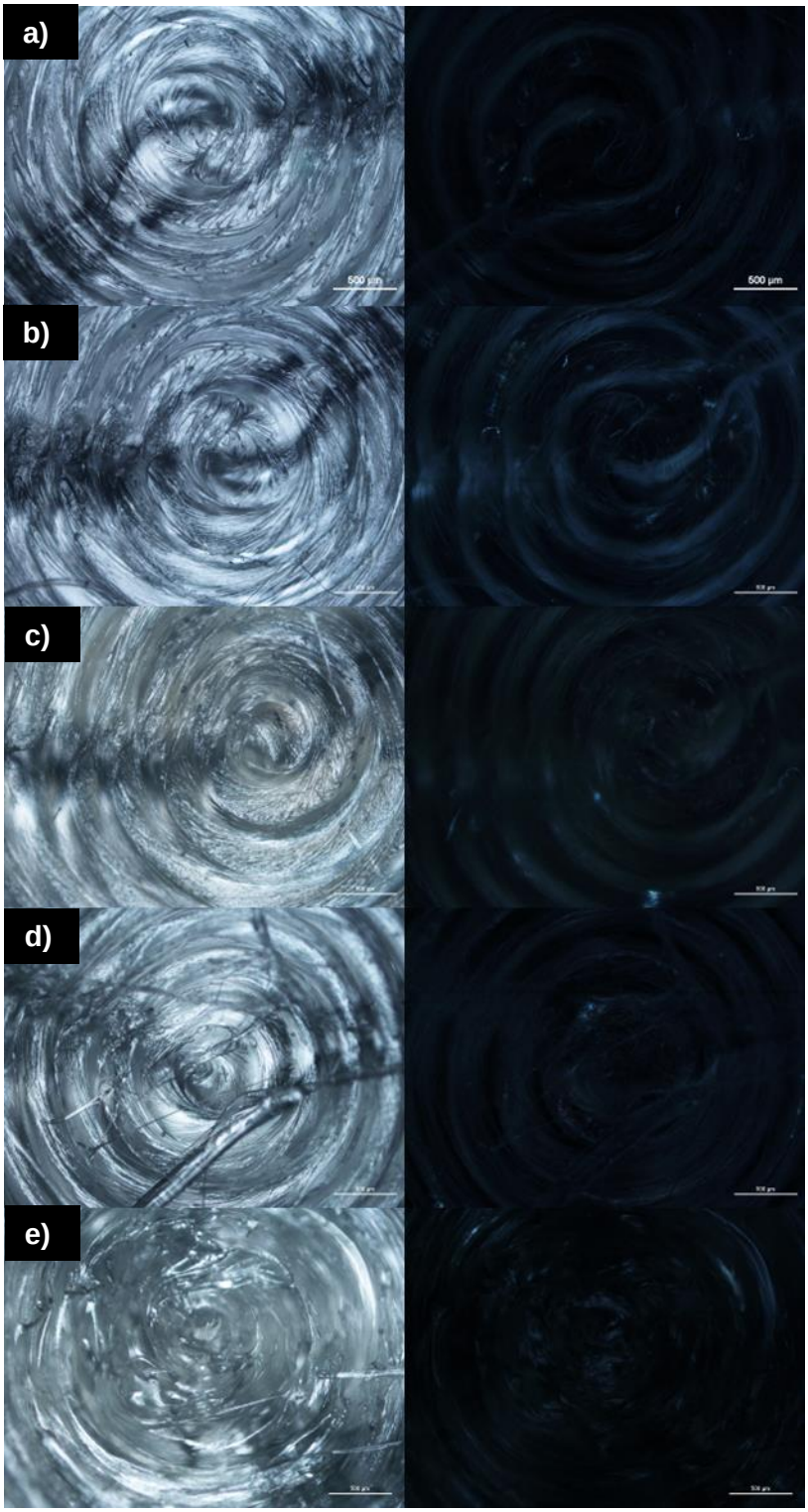

Figure S 4.4 Images of the 0T tablets under accelerated conditions using optical microscopy, followed by the same image under cross polarised optical microscopy. **a)** day 1, **b)** day 2, **c)** day 7, **d)** day 14, **e)** day 28

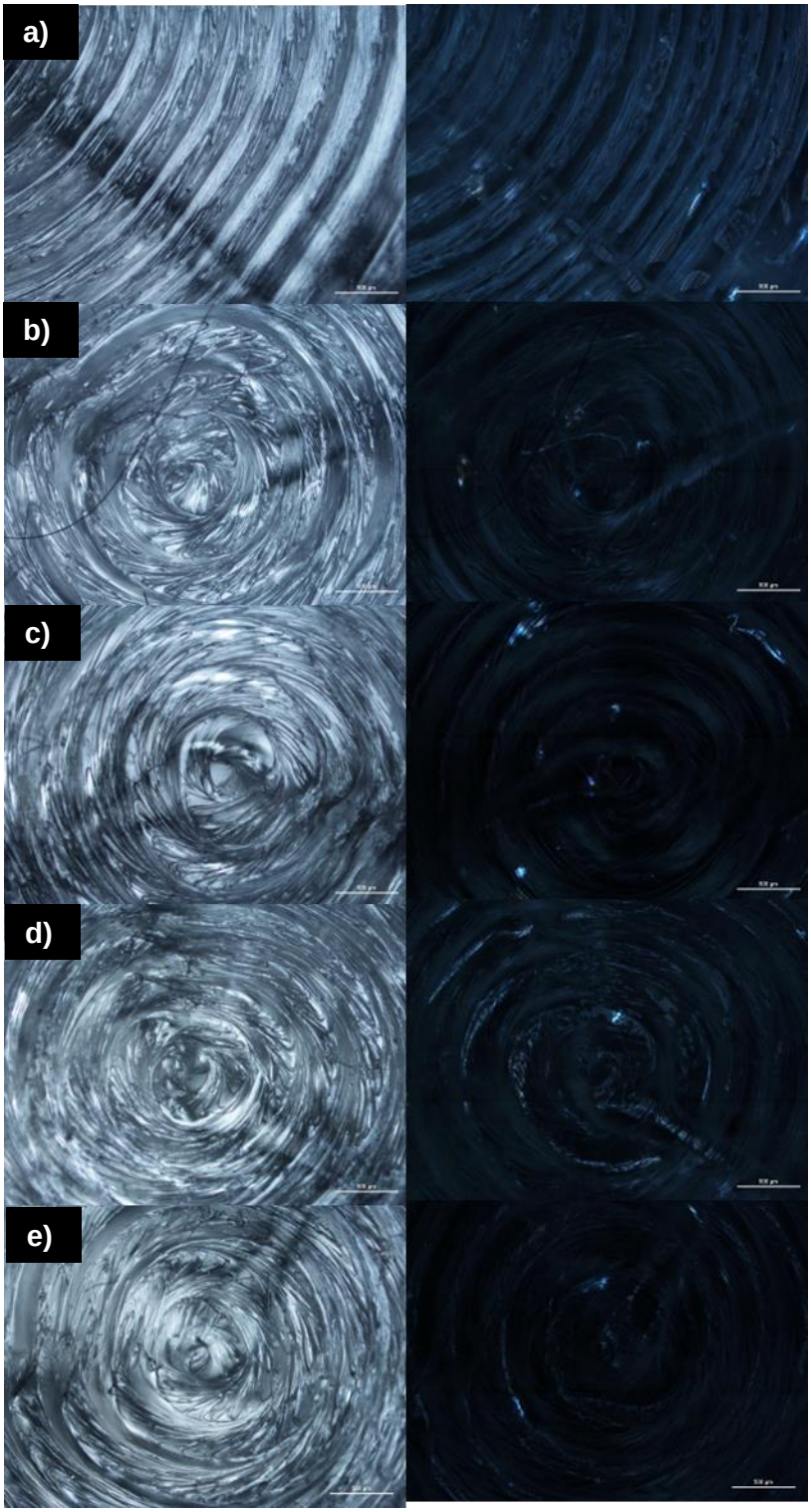

Figure S 4.5 Images of 1T tablets under accelerated conditions using optical microscopy, followed by the same image under cross polarised optical microscopy. **a)** day 1, **b)** day 2, **c)** day 7, **d)** day 14, **e)** day 28

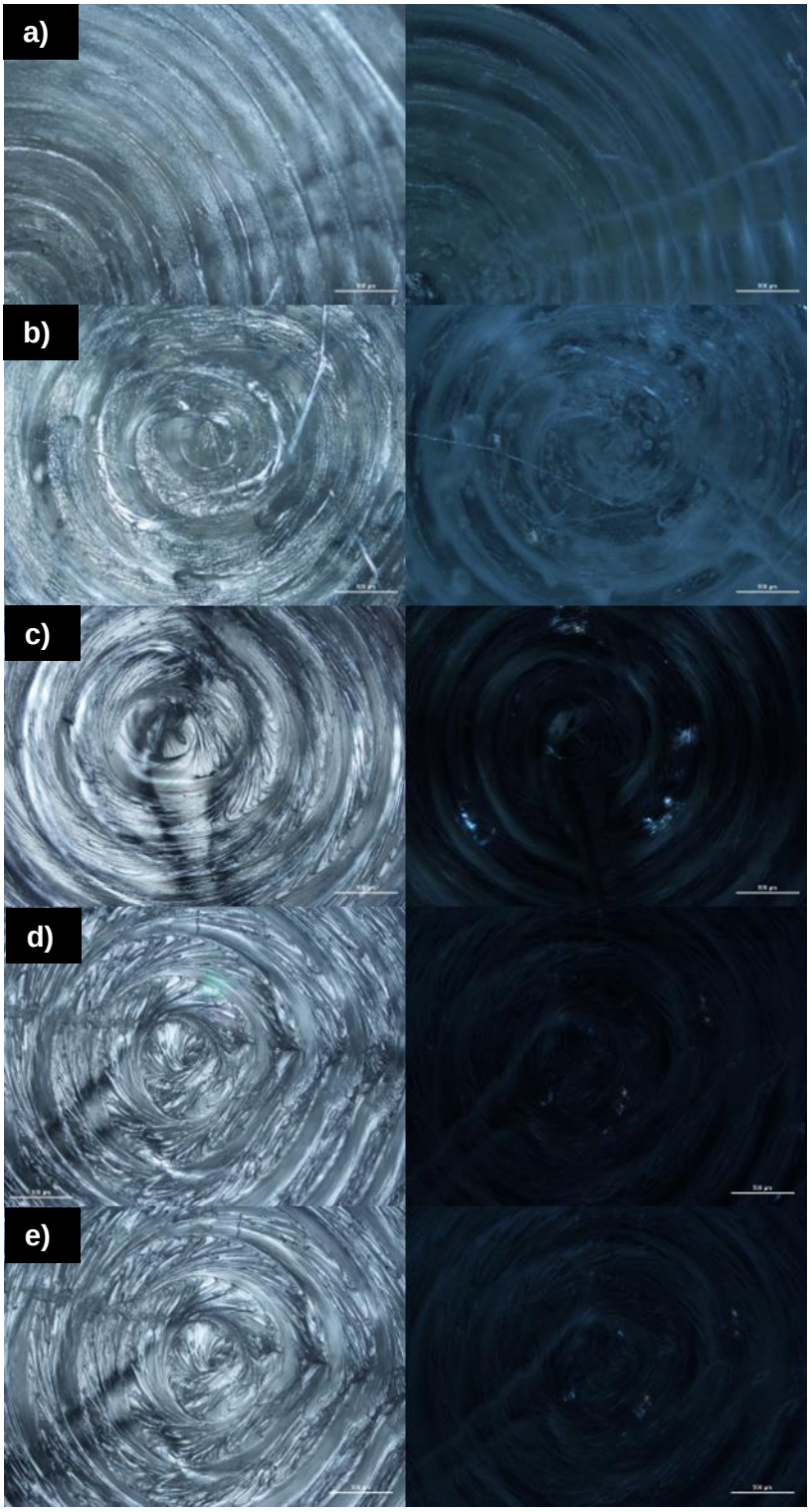

Figure S 4.6 Images of the 0T tablets stored in the desiccator using optical microscopy, followed by the same image under cross polarised optical microscopy. **a)** day 1, **b)** day 2, **c)** day 7, **d)** day 14, **e)** day 28

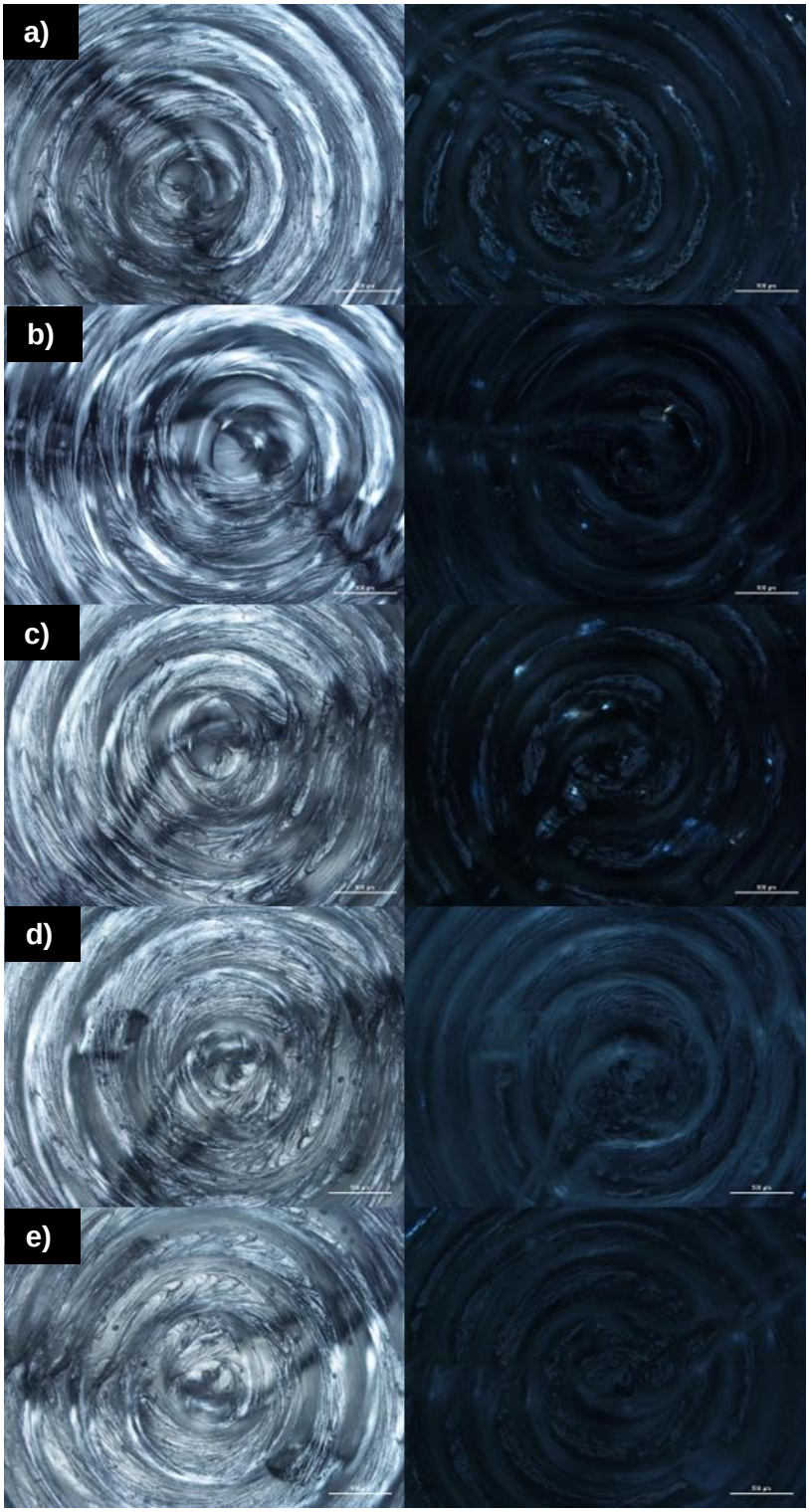

Figure S 4.7 Images of 1T tablets stored in the desiccator using optical microscopy, followed by the same image under cross polarised optical microscopy. **a)** day 1, **b)** day 2, **c)** day 7, **d)** day 14, **e)** day 28

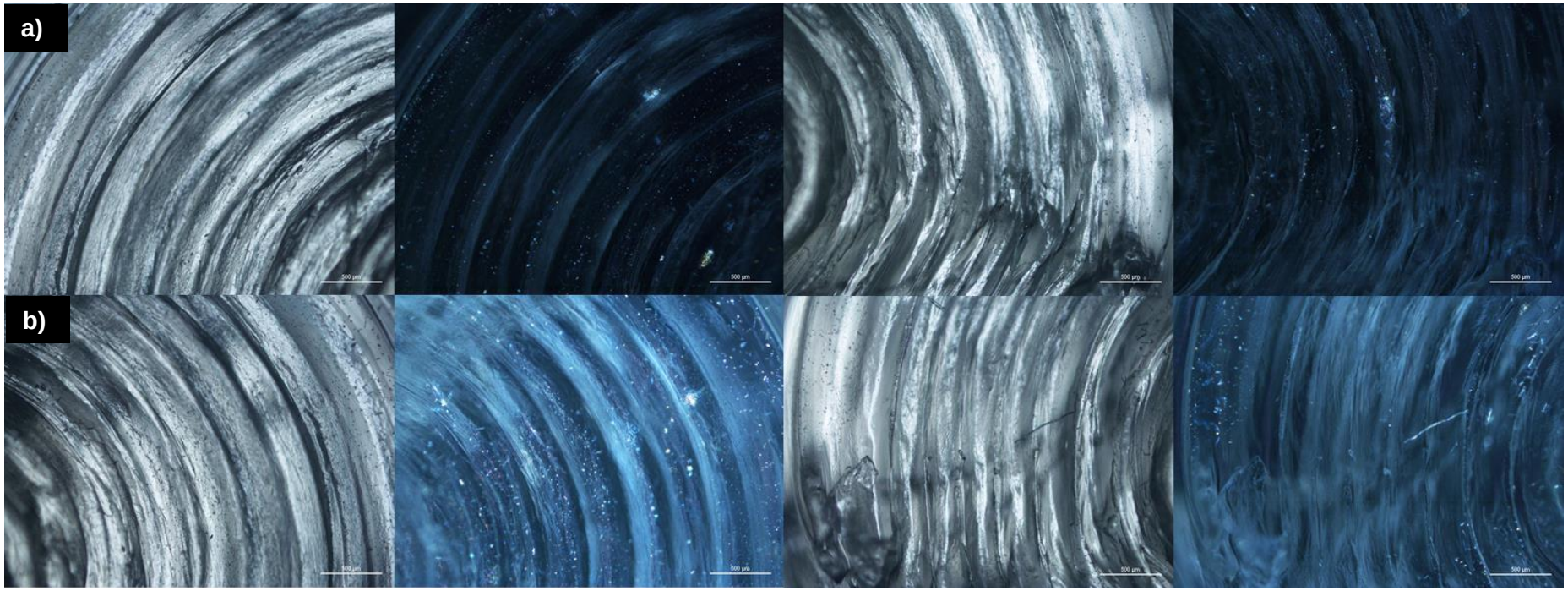

Figure S 4.8 Images of a 10T tablet stored in the desiccator using optical microscopy, followed by the same image under cross polarised optical microscopy. **a)** day 14 and **b)** day 28

5. Printing of a PEG–FEN eutectic system

5.1. Introduction

5.1.1. Aims of chapter

- Produce a phase diagram of a binary mixture of PEG 8000 and fenofibrate to confirm the eutectic point
- Assess the printability of a eutectic mixture using an extrusion-based printer
- Show that release of fenofibrate is enhanced by using this type of system

5.1.2. Background

In the previous chapter, the focus was on the use of amorphous solid dispersions in order to improve the release rate of fenofibrate from extrusion 3D printed tablets. Solid dispersions can be amorphous, partially crystalline or crystalline in nature. Indeed, solid dispersions can be thought of as being in the following categories, eutectic mixtures (EM), solid solutions, glass solutions/suspensions, amorphous regions of drug in a crystalline carrier, and where the drug and matrix strongly interact with each other in aqueous environment to form complexes.

A eutectic is defined as the combination of two crystalline compounds with a melting temperature below the melting temperature of each of the components [14–16,194]. In a eutectic system, where the drug and carrier are completely miscible in the liquid state but negligibly in the solid state, the drug is maintained in a normal crystalline state in a soluble crystalline matrix [16,194]. Such a system can be thermodynamically stable with a much lower possibility of phase transformations compared to amorphous systems [14–17]. Besides increased stability, eutectic mixtures have reduced particle size [15,17,194] and this increase in surface area leads to an increase in dissolution rate [194]. Moreover, as one of the components of the binary mixture is chosen to be hydrophilic, it can help solubilise the poorly soluble drug dissolution [16]. As a way to improve the solubility of poorly soluble drugs, this is not a widely explored option [192]. The lower melting temperature of the system can be an advantage for its processability, something that does not seem to have been explored much in 3D printing of pharmaceuticals [50].

Several methods have been reported to produce eutectic mixtures, with many using fusion followed by a grinding step in order to obtain a powder mixture that can be further used for analysis and drug release evaluation, as well as it facilitates the particle size reduction of the drug particles aiding an increase in solubility [15–17]. Others have used solely grinding for the preparation of the binary mixtures [194,236].

Continuing with the use of fenofibrate as a model drug, there have been studies with fenofibrate as part of eutectic systems. Both Law *et al.* [17] and Vippagunta *et al.* [15] have explored the eutectic mixture formed between PEG 8000 and fenofibrate (PEG – FEN), the first focusing on the eutectic microstructure and the enhancement of release rate, and the second focusing on the factors that affect the formation of eutectic systems, such as polymer molecular weight and possible drug-polymer interactions. Both used a fusion process followed by grinding as their preparation methods. Vippagunta *et al.* reported that there were no observable interactions between PEG 8000 and fenofibrate and that the molecular weight of the PEG polymer had no significant effect on the formation of the eutectic or on the release rate of the drug [15]. Both studies concluded that the eutectic point determined the upper limit for drug loading which would benefit from increase solubility and that the eutectic point was situated at around 25% (w/w) fenofibrate [15,17]. PEG 8000 has been found to also form eutectics with flurbiprofen and ibuprofen [15], with other molecular weight PEGs also forming eutectics with drugs such as temazepam [236], ibuprofen [16] and puerarin [50]. Eutectic systems can not only be formed between a drug and a polymer but also between different drugs. Gorniak *et al.* reported a eutectic system formed between fenofibrate and acetylsalicylic acid with a threefold increase in fenofibrate release when compared with pure fenofibrate [194].

5.2. Materials and Methods

5.2.1. Materials

Fenofibrate was purchased from Merck Life Science (Gillingham, UK) and Kollisolv® PEG 8000 was kindly gifted by BASF Pharma (Ludwigshafen, Germany).

5.2.2. Methods

5.2.2.1. Binary mixture preparation

With the aid of a mortar and pestle, fenofibrate and PEG 8000 were mixed for 15 min in ratios of 10:90, 15:85, 20:80, 25:75, 30:70, 40:60, 50:50, 70:30 and 90:10. The powder mixture was then transferred to a glass vial with a magnetic stirrer and placed in a water bath on a hot plate, as shown in Figure 5.1. The bath was heated to 70 °C and the mixture was mixed for 1h until all materials were melted and a clear visibly homogeneous mixture was obtained. This was left to cool overnight and the mixtures were then ground using a mortar and pestle and left in a desiccator until further use.

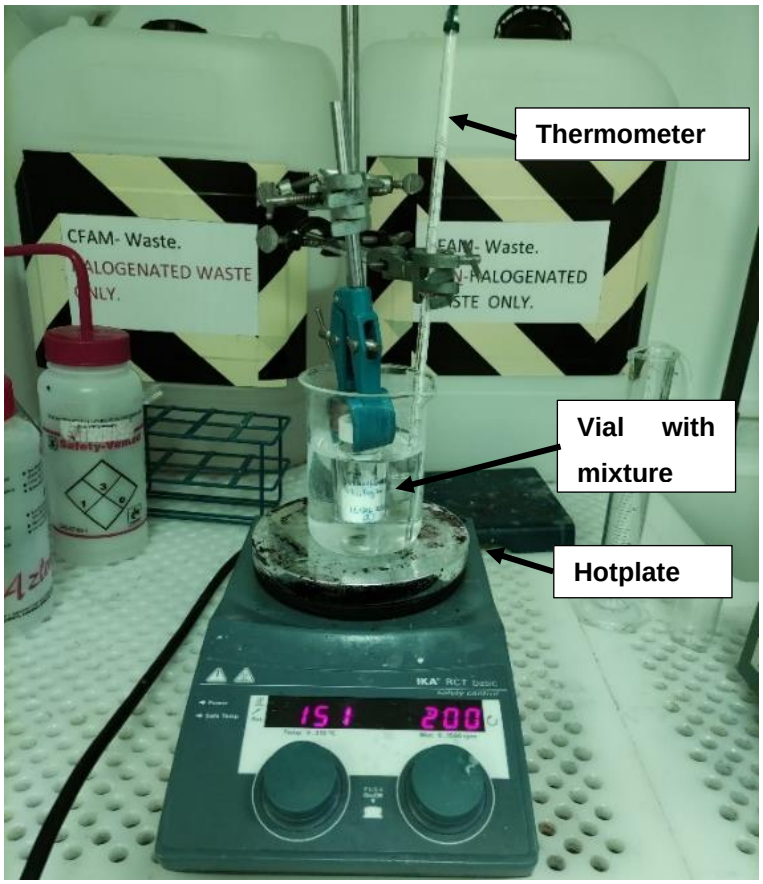

Figure 5.1 Melting and mixing of the binary mixture

5.2.2.2. Differential scanning calorimetry (DSC)

The binary mixtures from section 5.2.2.1, fenofibrate and PEG 8000 were analysed in a Perkin Elmer DSC 8500 (Waltham, USA). A heating rate of 5 °C/min between 30 °C to 90 °C was used and samples of 4-7 mg of each material were weighed onto an aluminium pan and hermetically sealed using an aluminium lid. To identify a

baseline and remove the peaks associated with the aluminium pan, an empty pan was analysed prior to the materials. The gas flow was controlled at a flow rate of 20 mL/min of N_2 and the DSC was calibrated using iridium (Tm =156 ± 5 ˚C, ΔHf = 28.71 ± 5 % J/g). The results were analysed using the Pyris software provided with the DSC.

5.2.2.3. Ink preparation and extrusion-based printing

For printing, the eutectic mixture consisting of fenofibrate (25 wt %) and PEG 8000 (75 wt %) was prepared as in section 5.2.2.1. Prior to printing, this mixture was remelted in a water bath as shown in Figure 5.1 and then transferred to an aluminium 3 mL INKREDIBLE+ cartridge with a 0.5 mm stainless steel micro metal precision nozzle and placed in a temperature-controlled print-head with a custom-made nozzle cap. The custom nozzle cap was designed using Autodesk® Fusion 360™ considering the measurements of the nozzle cap that comes with the printhead. The same .stl file of a cylinder geometry (10 mm x 10 mm x 1.5 mm) used in the previous chapters was used for the tablets. The tablets were printed using a Cellink BioX printer (Gothenburg, Sweden). Tablets with a concentric 100% infill were printed at 57 °C, with a printbed temperature of 40 °C, a pressure of 240 kPa and a speed of 4 mm/s. The tablets were allowed to solidify at room temperature and were stored in a desiccator at room temperature until further tests.

5.2.2.4. Weight uniformity

Ten 3D printed tablets of the same batch with 100% infill were selected, individually weighed and their average weight calculated, along with its relative standard deviation (RSD%).

5.2.2.5. Attenuated total reflection Fourier transform infrared (ATR-FTIR)

A PerkinElmer Frontier ATR-FTIR (Waltham, USA) spectrometer was used to collect the infrared spectra of pure fenofibrate, PEG 8000, the different mixtures and the printed tablet between 4000 cm^{-1} and 600 cm^{-1} with a scan resolution of 2 µm and a step size of 0.5 cm^{-1}.

5.2.2.6. X-ray diffraction (XRD)

X-ray diffraction patterns of pure fenofibrate, PEG 8000, the eutectic mixture and the printed tablet were obtained using a Bruker D8 Advance with DaVinci XRD instrument (Billerica, USA).

Further experimental details can be found in section 3.2.2.5.

5.2.2.7. Micro computed tomography (micro-CT) scanning

Micro-CT scanning was performed using a Skyscan 1174 Micro CT.

See section 3.2.2.7 for experimental details.

5.2.2.8. *In vitro* drug release studies

The studies were done using a United States Pharmacopeia (USP) type 1 apparatus Copley Dissolution system (Nottingham, UK). Drug quantification was done using a TECAN Spark® (Zürich, Switzerland) multimode microplate reader UV–Visible spectroscopy (UV-Vis).

Details on the dissolution media and drug quantification can be found in section 3.2.2.8. Samples were collected at times 0, 1, 2, 5, 10, 15, 30, 45, 60, 75, 90, 105 and 120 mins and filtered with a 0.45 µm MF-millipore membrane filter (Millex HA) before transferring to the collection vial.

5.3. Results and Discussion

5.3.1. Differential scanning calorimetry (DSC)

The first step in analysing the PEG–FEN system was to produce thermograms at different fenofibrate concentrations to determine the eutectic point (Figure 5.2 **a)**). Although this has been reported in literature [15,17], it was important to confirm these findings for the materials used in this work to further decide on the parameters to be used in the printing process.

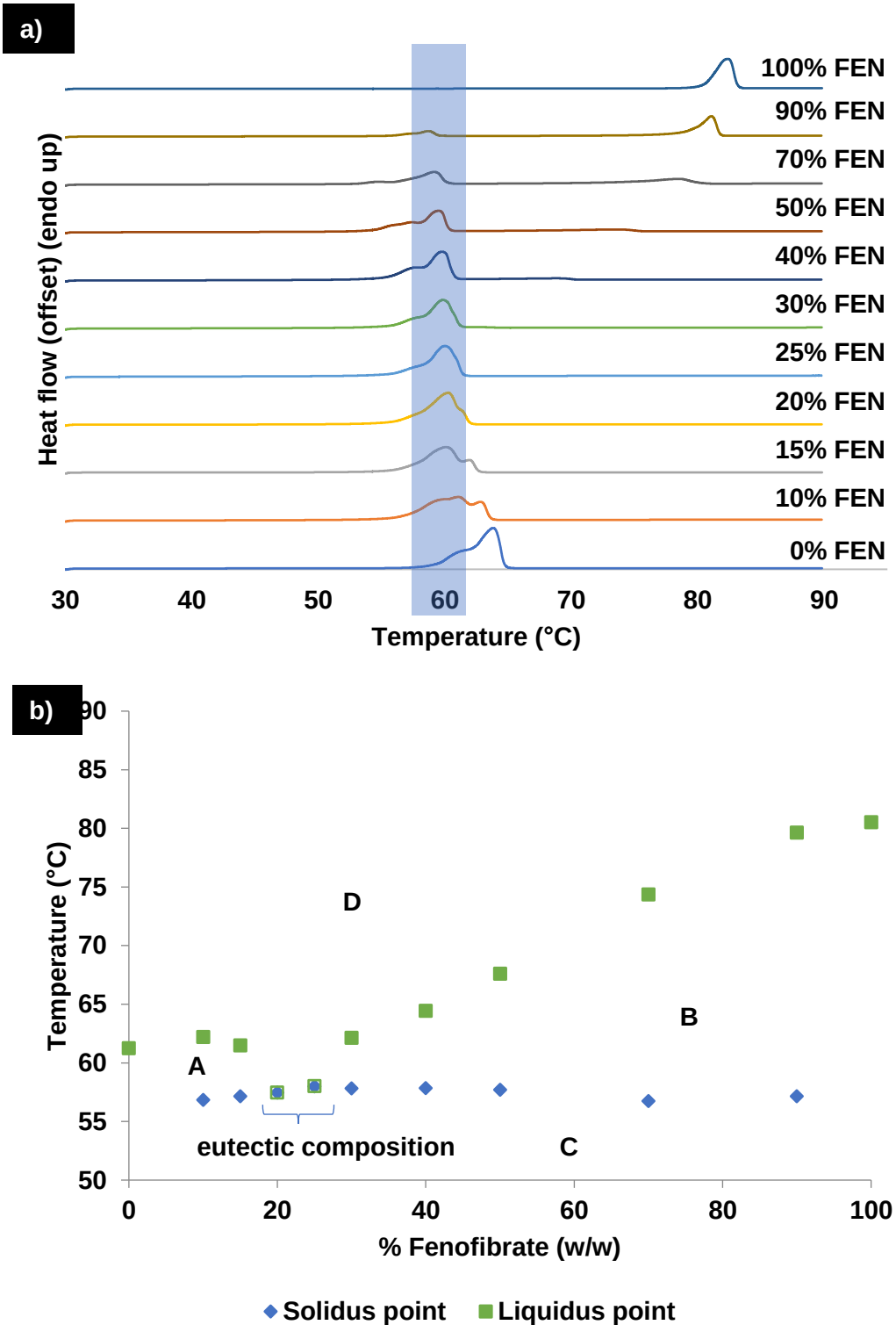

Figure 5.2 **a)** Stacked DSC thermograms of PEG 8000 – FEN systems and **b)** phase diagram of the PEG 8000 – FEN system (A – melted EM and excess solid fenofibrate, B – melted EM and solid excess PEG 8000, solid PEG 8000 and fenofibrate, D – liquid PEG 8000 and fenofibrate)

The PEG 8000 had an onset melting temperature of 61.3 °C and fenofibrate of 80.5 °C, both consistent with literature [15,17], it was hence expected that the eutectic system would have a melting point lower than these two values. Moreover, a fenofibrate concentration lower than 50% (w/w) was also expected due to the difference in melting temperatures [15]. Law *et al.* reported single endothermic events at 20 and 30% (w/w) fenofibrate when using DSC and 20 and 25% (w/w) when using hot stage microscopy, therefore determining that the eutectic composition was between 20 and 25% (w/w) fenofibrate [17]. Using solely hot stage microscopy, Vippagunta *et al.* determined that 25% (w/w) fenofibrate was the eutectic composition [15]. From our DSC analysis (Figure 5.2 **a)**, it is possible to observe single endothermic events for the pure components, PEG 8000 and fenofibrate, and the mixtures with 20 and 25% (w/w) fenofibrate. With the melting temperature of PEG 8000 and the eutectic mixture so close together, there are peaks overlapping. These are more easily distinguishable and analysed with the Pyris software that is available with the DSC equipment. The single endothermic event of 20% (w/w) fenofibrate occurred at 57.86 °C, with the one of 25% (w/w) at 58 °C, which is in agreement with the literature [15,17]. With the values obtained from the DSC analysis, a phase diagram was constructed (Figure 5.2 **b)**). This allows for the visualisation of the eutectic composition, which can be found where there is one single endothermic event and the lines for solidus and liquidus points meet. As with Law *et al.*, this is between 20-25% (w/w) [17]. As it would be desirable to have the highest drug loading possible, the printing experiments were done with a concentration of fenofibrate of 25%.

5.3.2. Extrusion-based printing of tablets

The eutectic mixture of PEG 8000 and fenofibrate at room temperature is solid. A solid object or powder cannot be printed, it must be semi-solid or melted. Considering the requirement for a higher temperature than room temperature, the first attempt was with the thermoplastic printhead (Figure 5.3 **a)**) as with a melting temperature of 58 °C, there would be no need for an excessively high printing temperature. The peculiarity of the thermoplastic printhead is that it was made to be used with thermoplastic polymers, preferably in a granulated form [237]. The heating element of the printhead is right above the nozzle, meaning the material further away from the nozzle is at a lower temperature.

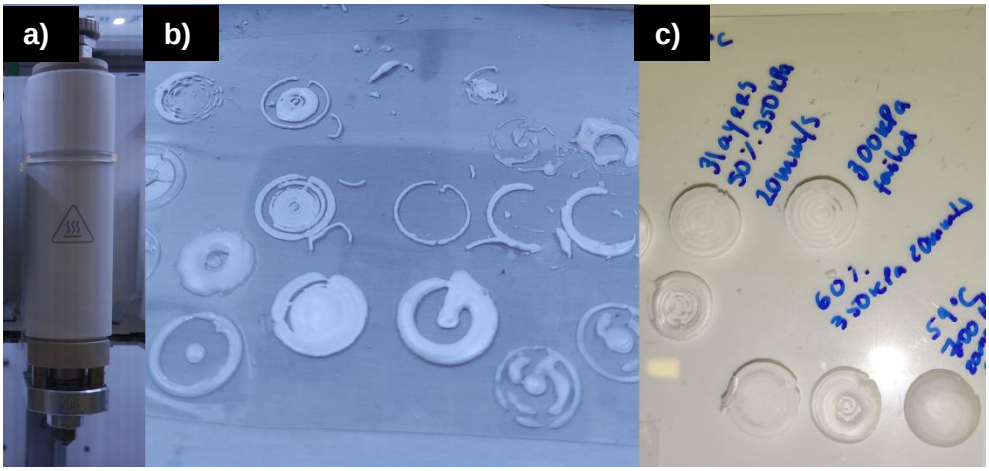

Figure 5.3 **a)** Thermoplastic printhead, **b)** initial printing attempts, **c)** possible prints with this set-up showing top and bottom of printed tablets

This can be seen in Figure 5.4. This difference in temperatures within the printhead meant that part of the ink was fully melted, and another part was solid. The solid material would create a solid lid inside the cartridge, preventing the soft or melted material from being extruded. To prevent the creation of this lid, the ink material was heated up to 60 °C. However, this caused the material to be completely melted. When using extrusion printing, the material cannot be too viscous, or it will not be extruded but, it equally cannot have too low a viscosity, or it will not retain its shape [63]. With the mixture being in a molten state, the printed tablet could not retain the desired shape and instead of using a 100% infill geometry, a 50% infill would have to be used, as the diameter of the extruded filament was much larger than the desired 0.4 mm, which was the size of the used nozzle. The effect of this can be observed in Figure 5.3 **c)**, as the tablets printed were not of a cylindrical shape but rather a round top. Moreover, in Figure 5.3 **b)**, inconsistency in the printing can be observed. Inkjet printing potentially would be a more suitable printing technique to use with this formulation in a melted form as its viscosity would be low, the material deposition would be more selective, and the resolution would be higher [138,231].

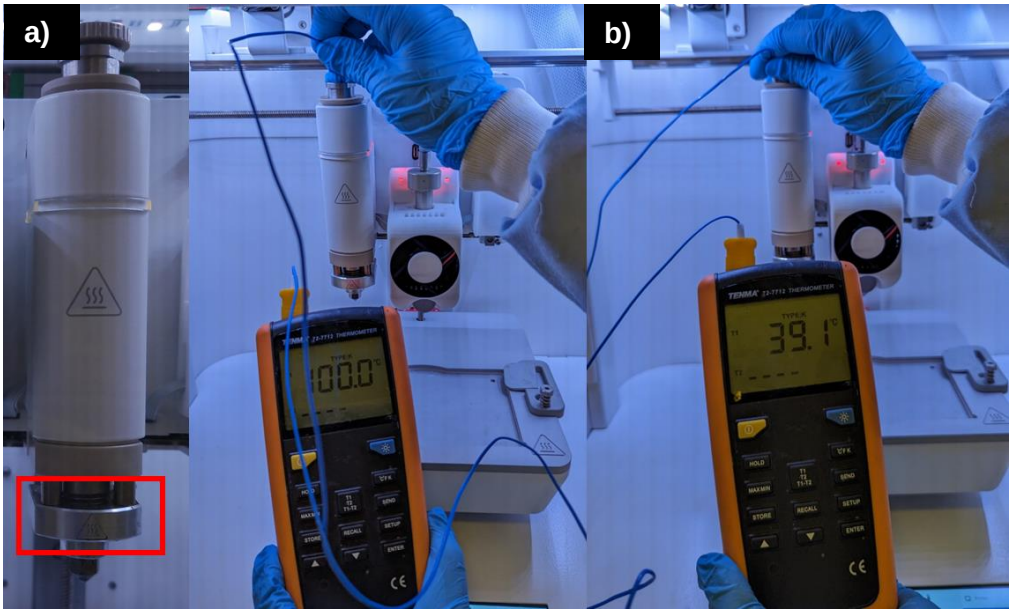

Figure 5.4 Temperature measurements in thermoplastic printhead (set to 100 °C as example): **a)** heating element highlighted with red rectangle, **b)** temperature measured inside nozzle, **c)** temperature measured on the walls in the middle of the cartridge

Considering this difference in temperature within the cartridge (Figure 5.4), the temperature-controlled printhead was chosen. Moreover, to help with the heat transfer within the material, an aluminium cartridge from another Cellink printer model, the Inkredible + was used as well. However, as this cartridge is meant for another printer, the nozzle cap that comes with the temperature-controlled printhead did not fit. The nozzle cap is meant to help with controlling the temperature within the nozzle, as this part is not inside the printhead. As such, the nozzle was completely exposed without a nozzle cap, causing a blockage of said nozzle as material was solidifying (Figure 5.5).

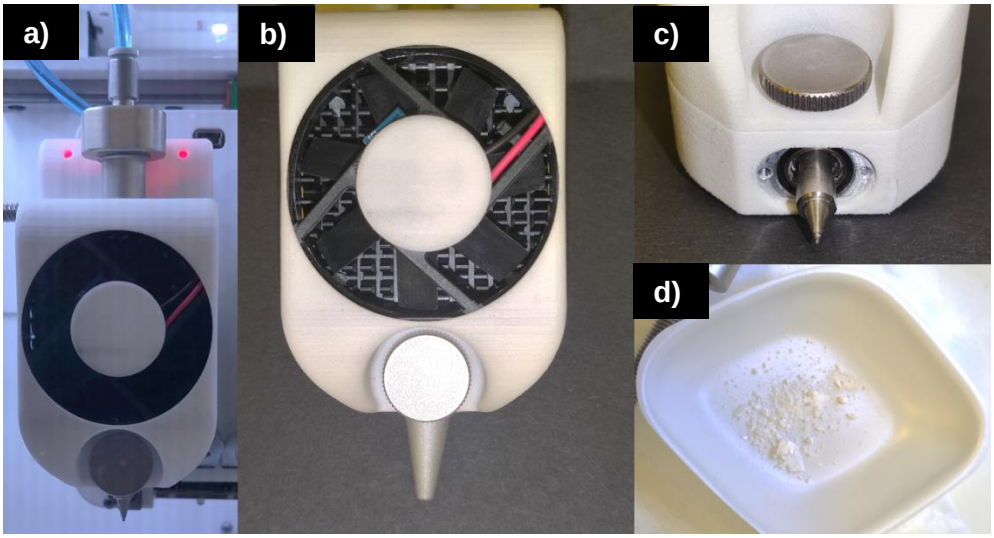

Figure 5.5 Images showing the use of the Inkredible + aluminium cartridge in a BioX temperature-controlled printhead. **a)** fitting of cartridge in printhead, **b)** printhead with nozzle cap, **c)** nozzle exposed to room temperature, **d)** solidified material blocking exposed nozzle

A first attempt to solve this issue was made using aluminium foil to cover the nozzle and help retain heat (Figure 5.6).

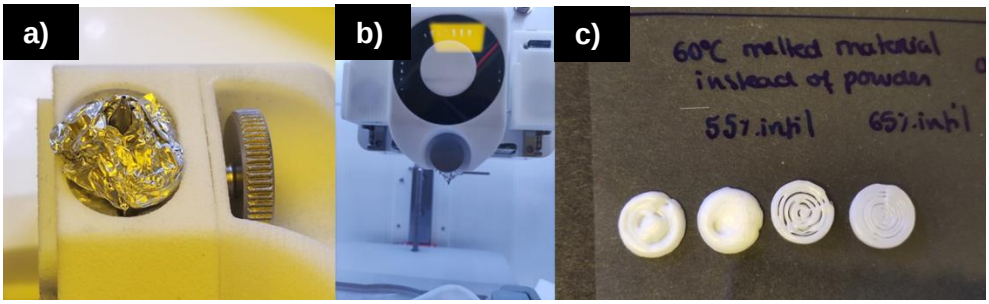

Figure 5.6 First try at covering nozzle to prevent ink solidification: **a)** placement of aluminium foil, **b)** image showing tip of nozzle is not covered, **c)** first printing attempt at 60 °C showing different infill percentages

As this seemed to have a positive effect but was not a viable permanent solution, a custom-made nozzle cap was made. Measurements of the existing nozzle cap were taken and used to design a new nozzle cap. The CAD model made from the existing nozzle cap and the new version can be seen in Figure 5.7.

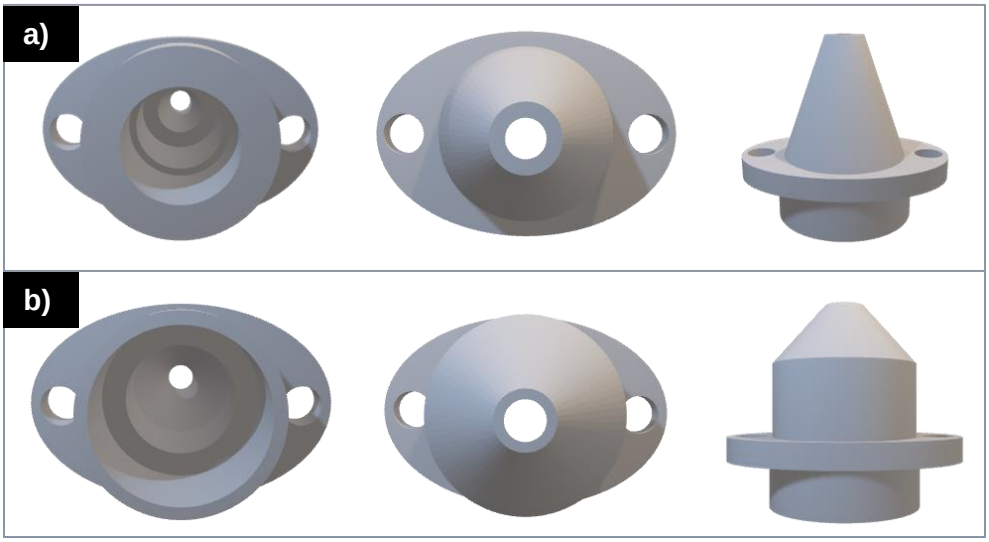

Figure 5.7 Different views of the CAD models of the **a)** existing nozzle cap and **b)** custom-made nozzle cap

A first prototype was printed with polylactic acid (PLA) using an FDM printer, the Ultimaker 2+ (Ultimaker B.V, Utrecht, The Netherlands) (Figure 5.8 and Figure 5.9) and the final version was printed in 316L stainless steel using a laser powder bed fusion printer, the AconityMIDI+ (Aconity3D, Herzogenrath, Germany) (Figure 5.10). Stainless steel was chosen due to its lower thermal conductivity (13.40 W/m K) [238] compared to the other available options, titanium and copper alloys.

Figure 5.8 Side to side comparison of existing nozzle cap (**grey**) and PLA printed custom made nozzle cap (**yellow**)

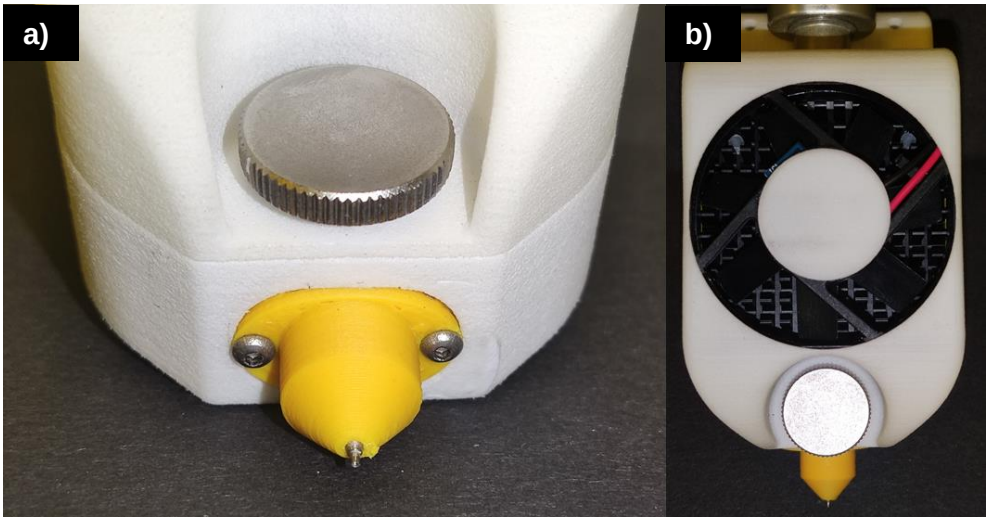

Figure 5.9 Fitting of FDM printed nozzle cap prototype: **a)** close-up of inserted nozzle cap, **b)** printhead with inserted cartridge and nozzle cap

The first EM printing attempts were made at a temperature higher than the melting point but as the printing parameters were optimised, it was possible to print at 57 °C, using 240 kPa of pressure and a printing speed of 4 mm/s (Figure 5.11). In this case, the material was semi-solid and an infill of 100% was possible. Still, and even though the printing was possible, there were inconsistencies in the prints and gaps can be seen in the tablets (Figure 5.11).

Figure 5.10 Different angles of laser powder bed fusion printed nozzle cap

Moreover, it was not possible to successively print as material would stop extruding mid print. 10 tablets were printed, with an average mass of 111 mg and a RSD(%) of 6.2%. Their dimensions are summarised in Table 5.1. While this relative standard deviation value is not too far from the generally accepted 5% for uniformity of weight, it is still within the limit established in the British Pharmacopeia of 7.5% for tablets under 250 mg [219]. This variation might be explained by the gaps that can be seen in the tablets (Figure 5.11) and in the micro-CT scan of the tablet (Figure 5.12). The extruded material would consistently curl near the centre of the print, which could have been more strongly impacted by the concentric infill geometry that was chosen.

This can be seen in Figure 5.12 on the top view of the tablet (Figure 5.12 **a)**) and the vertical cross-section (Figure 5.12 **c)**), where there is a large gap in between the extruded filaments. The printing inconsistency can also be seen in the bottom view of the tablet (Figure 5.12 **b)**) and in the horizontal cross-sections of the tablet (Figure 5.12 **d)**), all acquired using micro-CT scanning. These considerable-sized gaps are likely to differ between all printed tablets, which will consequently impact the mass uniformity and the release rate of the drug dispersed in it.

Figure 5.11 Successful printing attempts of eutectic printed tablets

Table 5.1 EM tablets' dimensions, measured with a Vernier caliper (n=10)

	Diameter (Ø)	**Height (H)**
Dimensions (mm)	9.61 ± 0.14	H = 1.56 ± 0.11

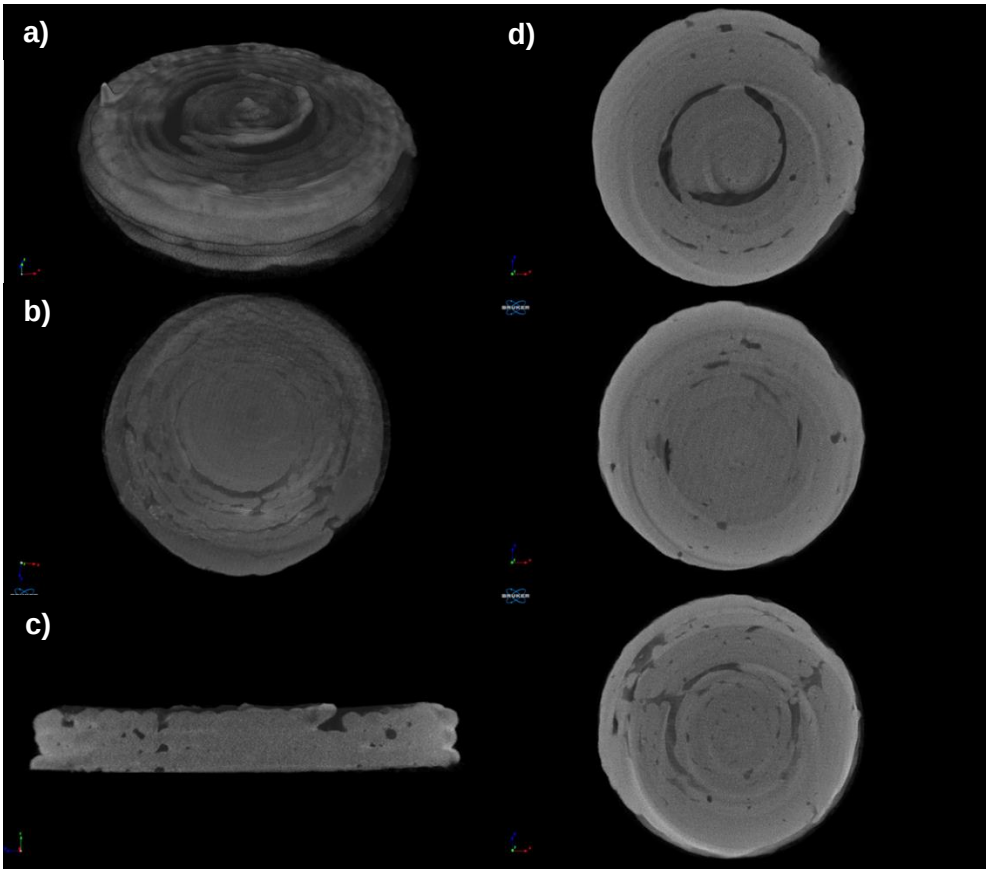

Figure 5.12 Micro-CT scan of one of the printed tablets: **a)** top view, **b)** bottom view, **c)** vertical cross-section, **d)** horizontal cross-sections at different heights of the tablet

Inconsistencies and differences in the temperature inside the cartridge and nozzle were still observed, even though a temperature-controlled printhead and a nozzle cap were used (Figure 5.13 and Figure 5.14). While some part of the material inside the cartridge was melting, other parts were solid (Figure 5.14). As such, in a few seconds there would be purging of liquid material even when using low pressure and an extrusion of a well-defined filament. The solid parts were also preventing the ink from being properly extruded, which in turn would lead to leakage. The material would quickly go from solid to melted and from melted to solid with the slightest temperature change. Another possible influence was the temperature inside the laboratory. Depending on the day and time of day this seemed to change, which could also be contributing to such inconsistencies. As this seemed to vary greatly and could not be controlled, this was something that could be monitored but not easily improved.

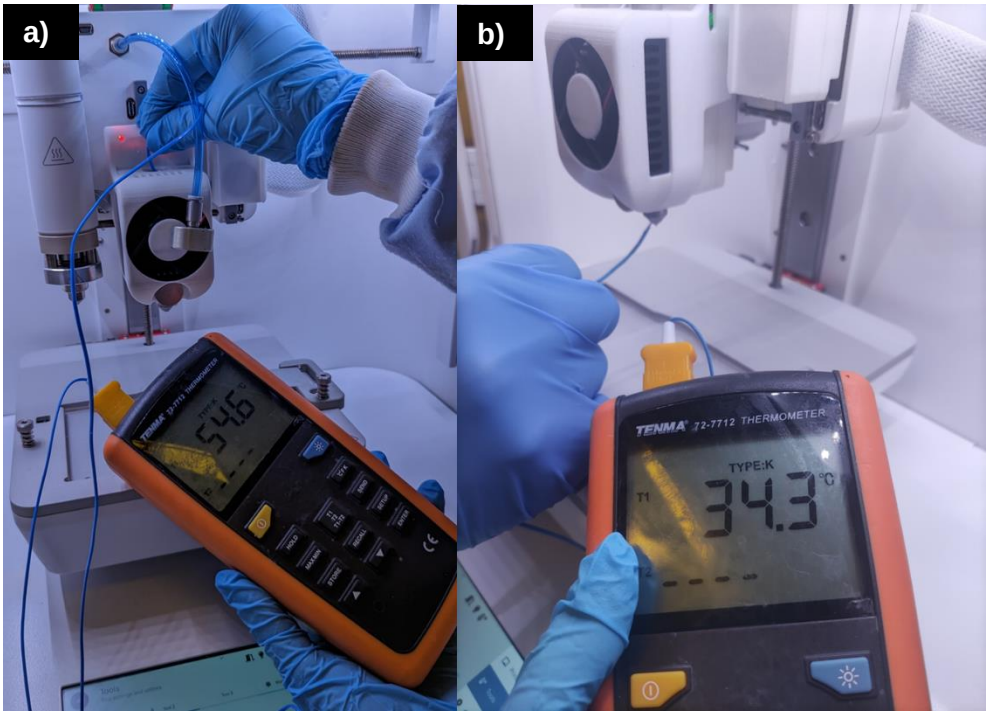

Figure 5.13 Temperature differences **a)** inside and **b)** outside of nozzle cap

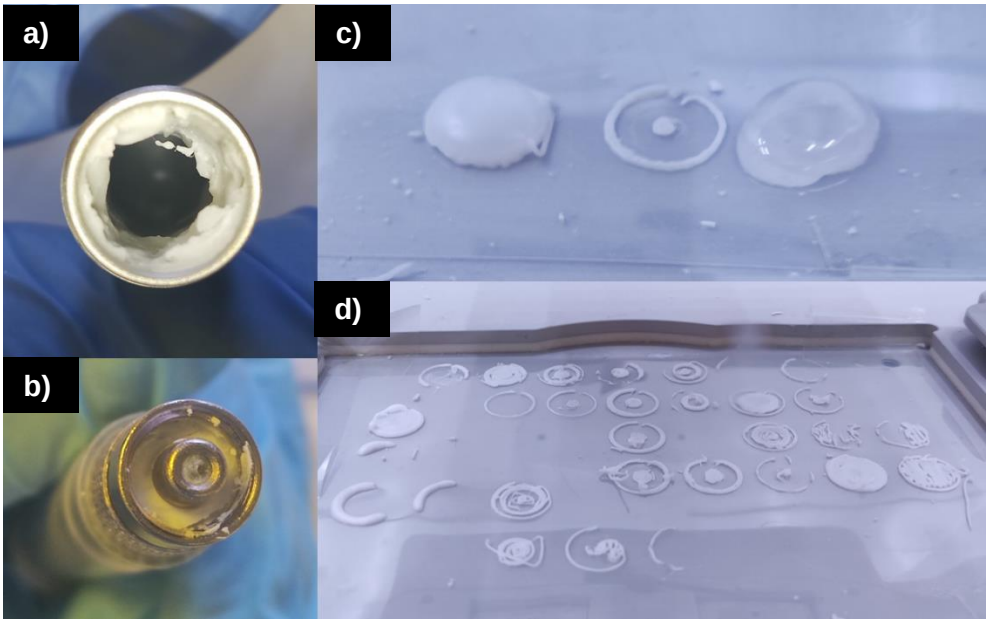

Figure 5.14 **a)** Solid material on sides of cartridge, **b)** material leakage, **c)** material purge and defined print, and **d)** printing inconsistency

To try and overcome the described issues, to improve the printing process and to increase the loading of fenofibrate, the addition of a tertiary material, PEG 400, was considered. This has previously been used as a plasticiser in filaments produced via hot melt extrusion [239]. Even though this is in the same chemical compound as the PEG 8000 but lower molecular weight, this would no longer be the printing of a binary

eutectic mixture but rather a ternary one. PEG 400, in this case, was to act as a plasticizer and its concentration would be 1% (w/w) of the total weight. The relevant DSC thermograms can be seen in the supplementary information, as well as a phase diagram (Figure 5.15 **a)** and **b)**, respectively). Because of the small number of samples data interpretation is not as clear as that for the data in Figure 5.2.

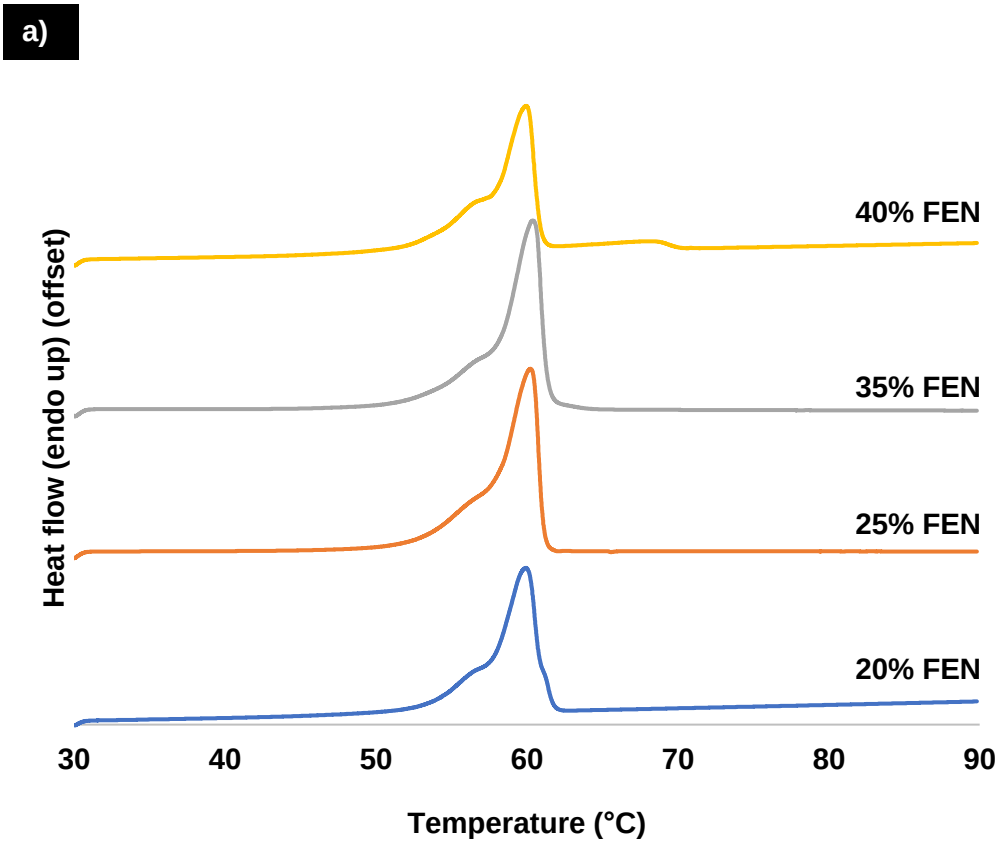

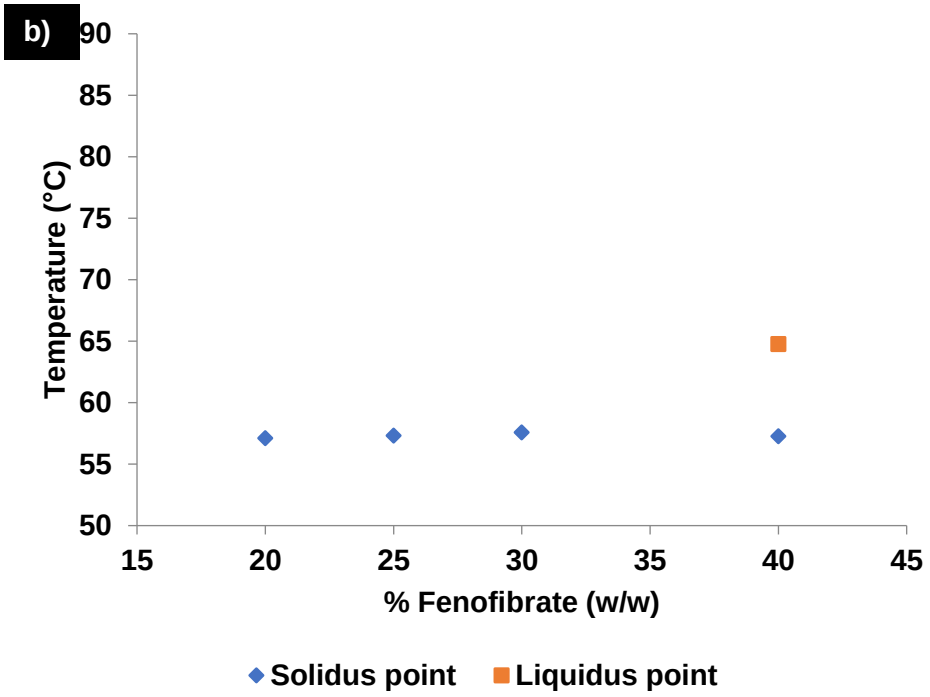

Figure 5.15 **a)** Stack of DSC thermograms of ternary mixtures of PEG 8000:FEN:PEG 400, with proportion shown being of PEG 8000:FEN and total mixture containing 1% (w/w) PEG 400; **b)** Partial phase diagram of the ternary mixture

However, it is clear that there was a shift in the eutectic composition towards a higher fenofibrate loading for this ternary mixture and a decrease in the temperature needed to melt the system. Moreover, there is a single endothermic event in the mixtures that contain 20, 25 and 30% (w/w) fenofibrate (with the PEG 8000-FEN accounting for 99% of the mixture), while two endothermic events are observed in the 40% (w/w) fenofibrate mixture. Therefore, there was an attempt to print a mixture of 70:30 PEG 8000:fenofibrate with 1% (w/w) PEG 400. However, this did not improve the printing process as hoped. It led to the material melting even at a temperature of 55 °C, while still being heterogeneous in texture. Moreover, it caused a leakage and the material to be extruded from the middle of the cartridge while solid material remained on the sides of it (Figure 5.16), which in turn led to an uncontrolled splatter of the ink (Figure 5.17).

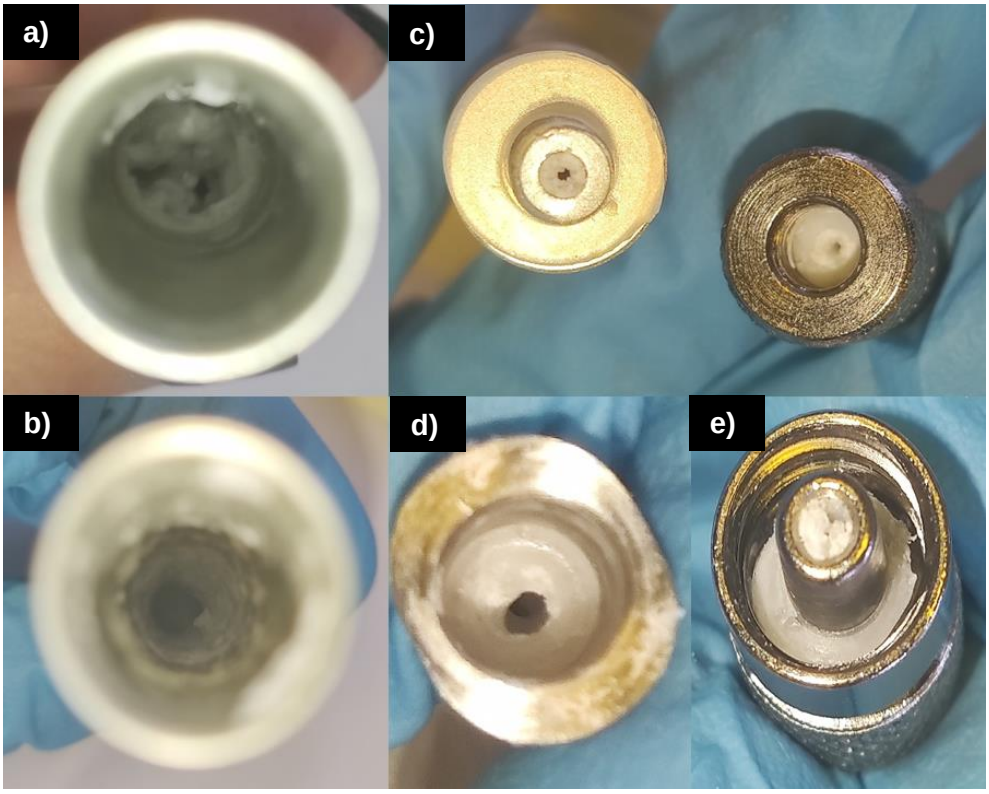

Figure 5.16 Tertiary mixture: **a)** material agglomeration and displacement to the sides of the cartridge, **b)** material sticking to sides of cartridge, **c)** material remaining on sides **d)** material on nozzle remaining on sides and solidifying **e)** material leakage and solidification near nozzle

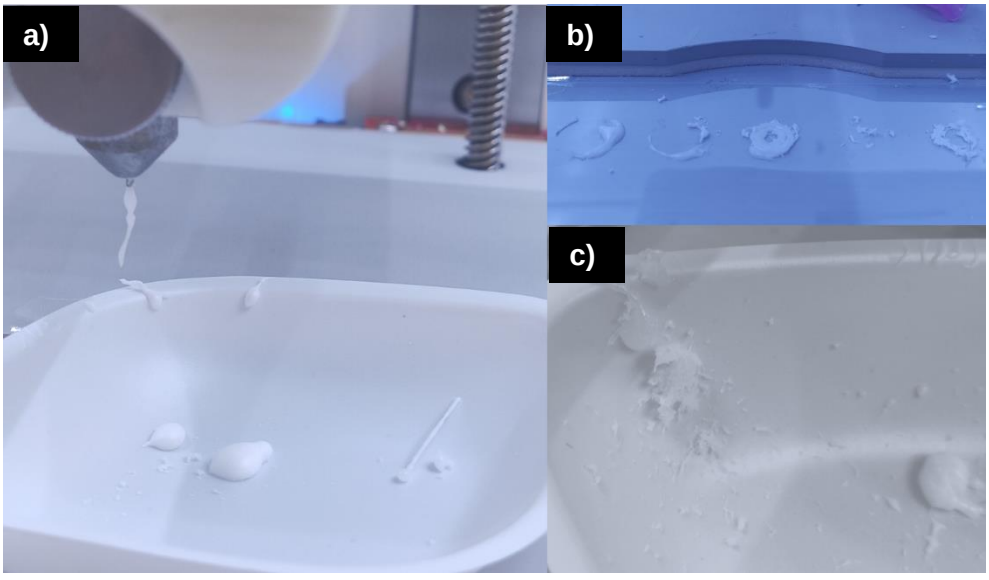

Figure 5.17 Attempt to print a tertiary mixture of 1:29.5:69.5 PEG 400:FEN:PEG 8000. **a)** Extruded filament inconsistency, **b)** printing attempts, **c)** splattering of material

The addition of PEG 400 was included to help soften the ink more homogeneously and improve the printability of it. However, this was not the case and the material remained on the sides of the cartridge. A possible future improvement could be to design and print a plunger that would be inserted in the cartridge to help press the material down near to the nozzle. An exploration of other possible plasticisers or change in PEG 400 could also be assessed, in order to achieve a more homogeneous semi-solid mixture that is more easily extruded while not being in a molten state. However, the purpose of using such formulation was due to its simplicity in preparation and number of excipients so that the modification and improvement of the printing equipment could be seen as a first step moving forward. The influence of a more easily controlled temperature in the equipment has proven to lead to more consistent tablets printed using a eutectic mixture. The printer used in Li *et al.*'s work had two hot ends, allowing the setting of a temperature for both the chamber and the nozzle [50]. Additionally, exploring different materials with which fenofibrate could form a eutectic mixture could be trialled.

Considering the described difficulties and because of time constraints, there was no further attempt to improve this process and the binary eutectic mixture printed tablets were analysed in order to assess if this type of formulation in a solid tablet was viable.

5.3.3. Attenuated total reflection Fourier transform infrared (ATR-FTIR)

The FTIR spectra of the pure components, the eutectic mixture in powder form and the EM printed tablet can be found in Figure 5.18. With FTIR it is possible to assess whether there are intermolecular interactions between the two components of the mixture [192]. In section 3.3.2, three of the most distinctive peaks from fenofibrate had already been identified. These peaks are shown in Figure 5.18 and corresponded to fenofibrate's ester carbonyl stretching, ketone carbonyl stretching and its C-Cl bond. These can all be identified in the spectra from the eutectic powder mixture and the printed tablet. Moreover, peaks from the PEG 8000 molecule can also be observed in those two spectra, indicating no interaction between the two components. This is in agreement with what is reported in Vippagunta *et al.*'s work, that there was no interaction between the two [15].

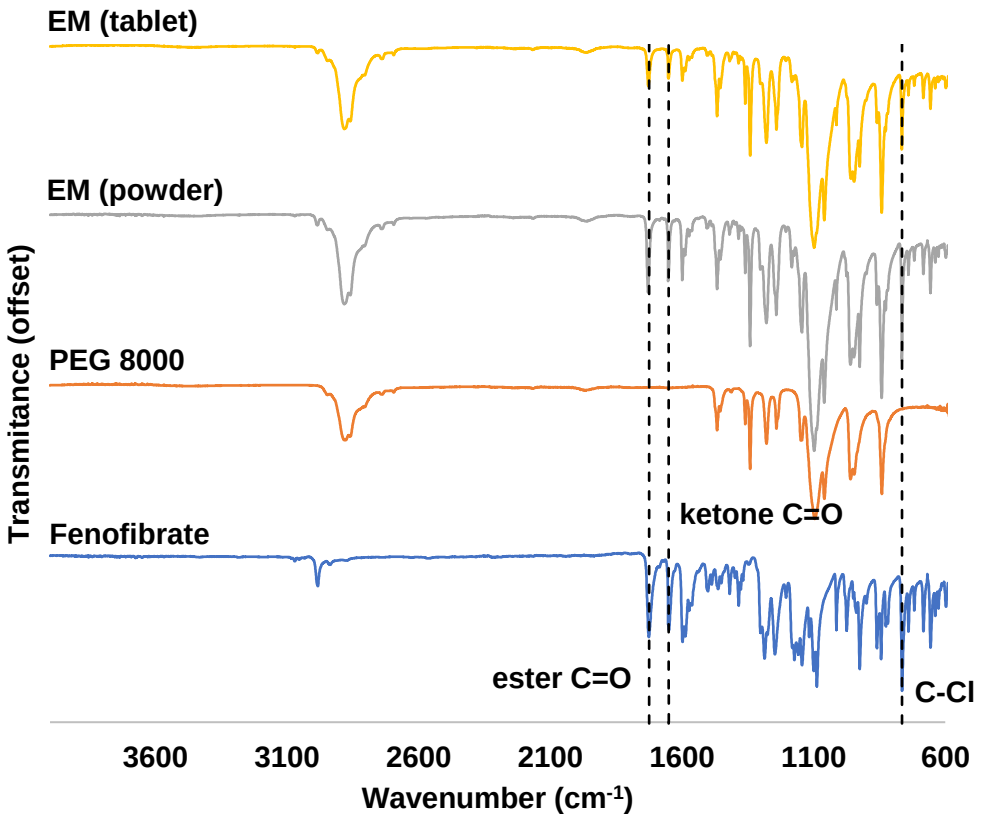

Figure 5.18 FTIR spectra of pure components fenofibrate, PEG 8000, the EM powder and EM printed tablet

5.3.4. X-ray diffraction (XRD)

X-ray diffraction of the pure solid components, the eutectic composition (EM) powder and the printed tablet were also performed to examine the state of the drug in the final formulation (Figure 5.19). At room temperature, the two components of the mixture are phase separated and both are crystalline [17], which can be observed in the EM (mixture) diffractogram. As stated before (section 3.3.3), the diffraction pattern of the used fenofibrate matches form I. Its characteristic peaks at 11.9° (2Θ), 14.5° (2Θ), 16.2° (2Θ), 16.6° (2Θ) and 22.2° (2Θ) can all be observed in the pure, mixture and printed tablet diffractograms. While no peak shift was observed, there is a clear difference in peak intensities. As stated by Chaturvedi *et al.*, the difference in peak intensity between the pure components and the EM could be due to preferred orientation of the crystals and the particle size reduction [16]. Still, this confirms the presence of crystalline fenofibrate in the mixture and printed tablet and that there seems to not have been any phase transformation of the drug in question.

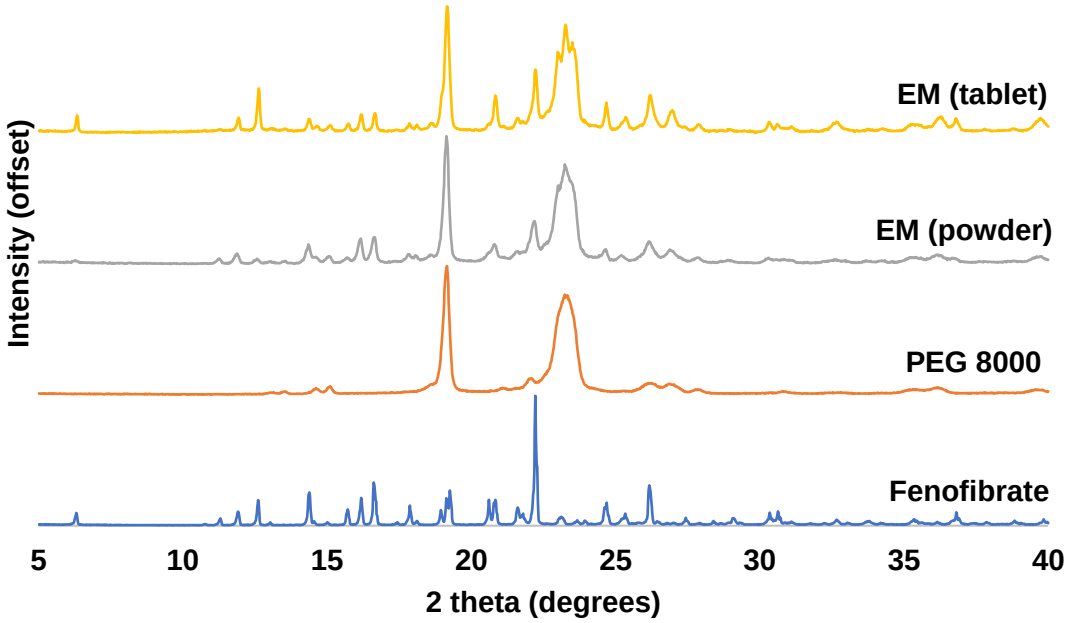

Figure 5.19 X-ray diffraction patterns of the pure solid components fenofibrate and PEG 8000, the powdered eutectic system and the printed tablet

5.3.5. *In vitro* drug release

Despite the difficulties presented in section 5.3.2, from the possible printed tablets, three of the most similar ones (Figure 5.20) were chosen for dissolution testing to assess the drug release from a eutectic mixture printed tablet.

Figure 5.20 3D printed tablets used for dissolution

Figure 5.21 shows the cumulative % release of fenofibrate from the printed tablets. As expected with using a eutectic mixture of PEG 8000 and fenofibrate, a faster release of the drug was achieved when compared with pure fenofibrate as shown in

section 3.3.4. Even though there was no observed phase transition of fenofibrate, as it is stated in Law *et al.*'s [17] and in Vippagunta *et al.*'s [15] work, as the two components of a eutectic mixture crystallize simultaneously, there is a consequent expected size reduction of the fenofibrate particles [17]. Therefore, improving the dissolution rate of this poorly soluble drug. However, contrary to their work where almost 100% of fenofibrate had been released after 60 min, only an average of 69% had been released from the 3D printed tablets after 120 min. This might be explained by the fact that in their work, dispersions in powder form had been placed in capsules [15,17], while here solid printed tablets were used. The use of powder, while inside capsules, increases the surface area which in turn, as explained previously [194], increases the release rate.

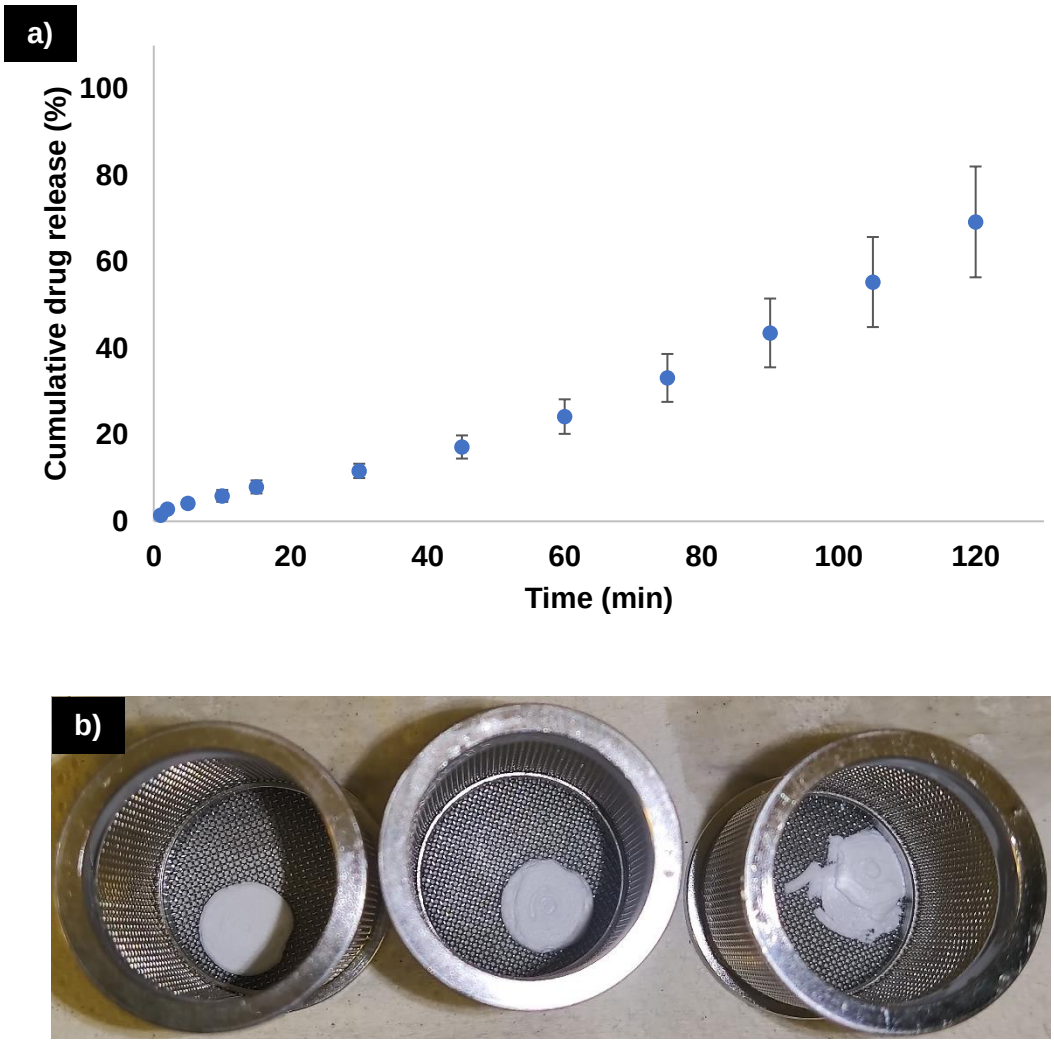

Figure 5.21 **a)** Release profile from eutectic mixture printed tablets (n=3) and **b)** 3D printed tablets after 2h of dissolution testing

From Figure 5.21 it can also be observed that the error bars, related to the standard variation of the drug released from the 3 samples during the study, became larger as the study went on. In the bottom image in Figure 5.21, it is possible to see that one tablet began to suffer delamination between the horizontal printed layers. This breakage causes an increase in surface area available for the release of the drug which would explain a release of 80% after 2h, compared with the average of 69%. Moreover, as was seen from the Micro-CT scan (Figure 5.12), there are several gaps inside the tablets. Considering the printing difficulties, these gaps are not thought to be consistent throughout each print, which would explain different release rates from different tablets. As in previous chapters, the release data was fitted to existing mathematical models, with the data being better fitted to a zero order model (Figure 5.22).

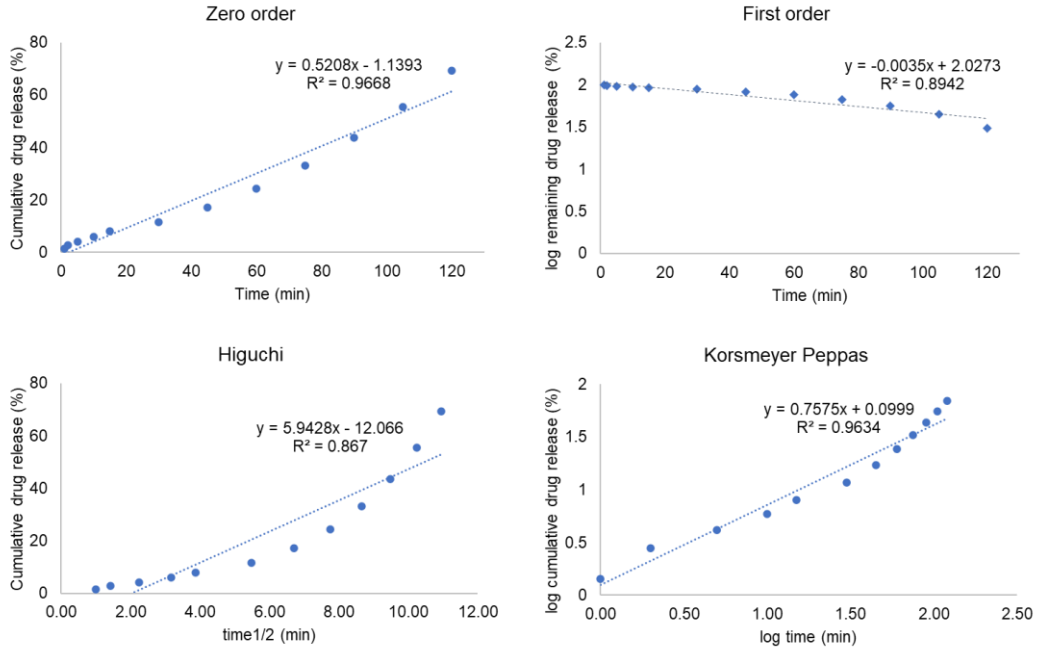

Figure 5.22 Dissolution models applied to the drug release data from EM 3D printed tablets

Additionally, the stability of this type of printed formulation should be investigated. As previously mentioned, one of the advantages of using this type of crystalline solid dispersion is the longer stability that it ensures as crystalline materials are more thermodynamically stable and less prone to phase transformations [16]. While Law *et al.* reported that there was no change in the thermal analysis, XRD and *in vitro* release studies of a 15% (w/w) fenofibrate dispersion [17], it would be important to verify that the same can be observed for the 3D printed tablets.

5.4. Conclusions

The following conclusions can be made from this chapter:

- PEG 8000 and fenofibrate form a eutectic mixture at a drug concentration between 20-25% (w/w), with no observed interaction occurring between the two components at the molecular level.
- With the eutectic mixture having a lower melting temperature, the temperature required for printing this mixture is correspondingly lower which eases the processability of this material. However, there is a fine line between its solid and molten state which causes a rapid change in viscosity of the system. In its molten state, the mixture does not possess viscosity to sustain a 3D printed structure, such that a semi-solid state of this formulation is preferred for printing 3D objects.
- A printhead that can more accurately control the temperature of the cartridge and the nozzle is necessary to ensure the material is found in a single form, preventing purging and/or the creation of a solid lid inside the cartridge that prevents the extrusion of the material. This better control of the equipment would ensure that the environment surrounding it would not have an influence on the temperature inside the printhead.
- While adding a plasticiser and forming a ternary mixture could aid shifting the eutectic point of the mixture to higher concentrations of the drug, this did not seem to have a significant effect on the printability of this type of system. As such, a higher concentration of a plasticiser and/or the exploration of other types of viscosity modifiers could be done.
- Exploring other materials such as different molecular weight PEGs with which fenofibrate form a eutectic mixture should be investigated for 3D printing tablets.
- Reproducibility of this printing process is an issue and should be improved by optimising the process. When printing is possible, tablets can be printed within the defined limits for uniformity of weight. However, tablets are not uniform all throughout and large gaps can be observed inside, as was possible to see with micro-CT scanning.
- Dissolution testing showed that this type of eutectic system does have a positive effect on the effective solubility of a poorly soluble drug such as fenofibrate, increasing its release rate considerably when compared with the pure drug. As such, this type of formulation can be further explored for the 3D printing of poorly soluble drugs. Still, the heterogeneity of the tablets and consequently delamination between printed layers can lead to a significant variation in drug released and this needs to be optimised.
- Further to processing optimisation, the stability of the printed tablets should be assessed over time.

5.5. Chapter appendix: supplementary information

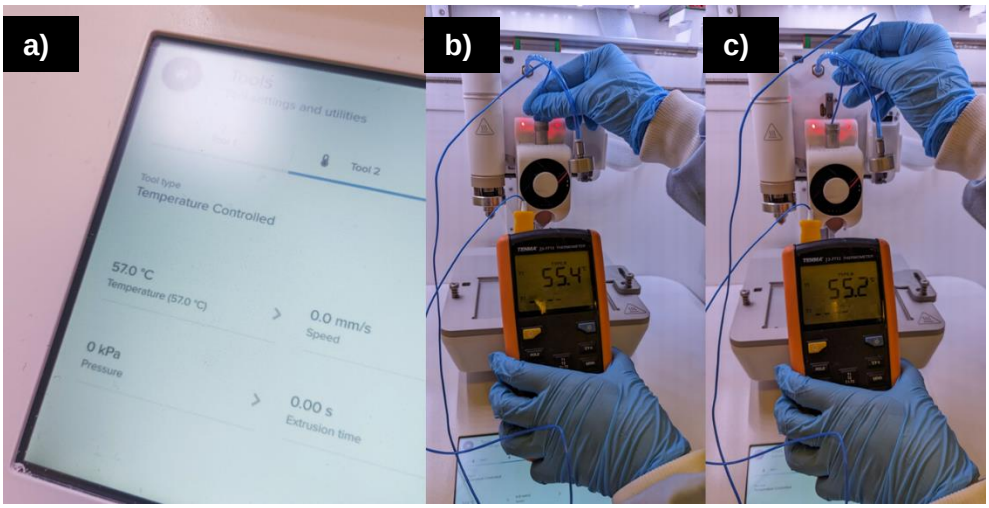

Figure S 5.1 **a)** Temperature setting in the printer, **b)** temperature inside nozzle, **c)** temperature inside cartridge

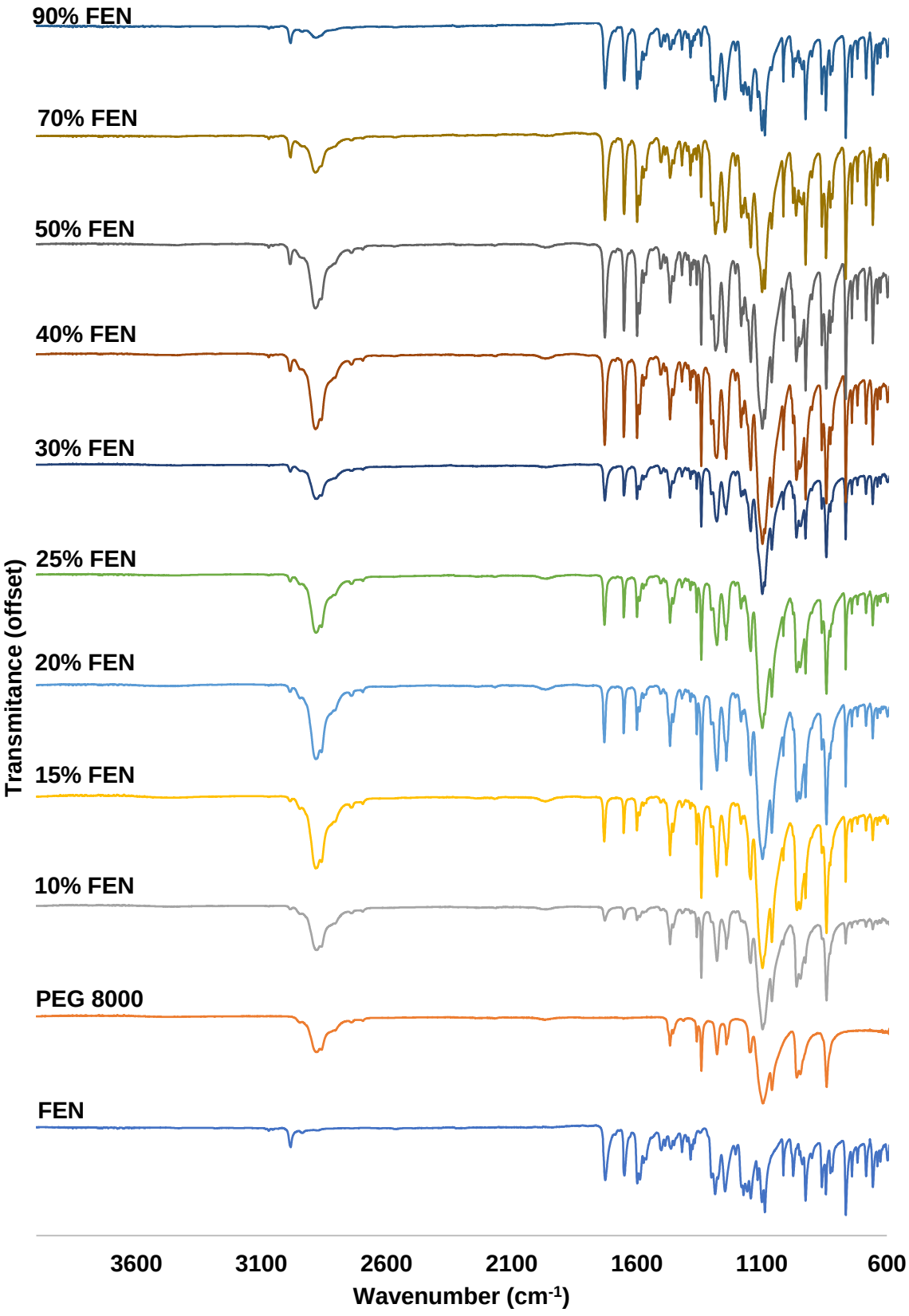

Figure S 5.2 FTIR spectra of pure fenofibrate (FEN) and PEG 8000 and all mixtures used for phase diagram

6. Conclusions and Future Work

In this thesis, different formulation strategies, with different materials and utilising different printing modalities within material extrusion printing were to be explored for the manufacturing of tablets containing a poorly soluble drug, fenofibrate. The formulations were to be produced, optimised for printing and the tablets characterised.

Firstly, paste-based formulations were produced with commonly used pharmaceutical excipients with no material manipulation, they were all used as received. Two different formulations were produced, so that a fast and an extended release of fenofibrate could be obtained. As no organic solvents were to be used, water was used as the binding agent. While pure water could be used as a binding agent for the extended release tablets as these contained swellable polymers that allowed for good binding between layers, a hydrogel was necessary for the fast release tablets as these mostly contained lactose as filler as well as disintegrants. With no phase transformation happening to fenofibrate during the room temperature manufacturing process (i.e., remained in crystalline state), this led to a very slow release of the drug for both paste-based formulation strategies, though each with a different release profile which was dependent on the excipients used. As neither formulation was shown to be the most suitable for the release of this poorly soluble drug, different approaches were proposed for future investigation. A first approach, which would allow the formulations used to be the same as the ones explored in this work, would be micronization. The use of an organic solvent prior to the past formation could also be explored, as well as the use of high concentrations of superdisintegrants for a fast release of fenofibrate.

Another approach to improve the release of poorly soluble drugs was explored in chapter 4, amorphous solid dispersions. This was achieved by printing a polymer-drug formulation with direct powder printing. This modality of material extrusion solely requires the production of a powder mixture prior to printing and can be used at lower temperatures when compared to the most explored thermal material extrusion process, FDM. The addition of a surfactant, Tween 80, at different concentrations was also explored, in order to assess the effect it has on the printability of the mixture, the release rate of fenofibrate and on the short-term stability of the printed tablets. The addition of Tween 80, which acts as a plasticiser, at a higher concentration led to a

decrease in the melt viscosity of the formulation, increase of the printing speed of the mixture and the improvement of layer binding. It also led to a much faster release of fenofibrate by aiding solubilisation and creating pores which increased the tablet's surface area. The addition of a small amount of Tween 80 did not lead to any significant effects. This was also observed in terms of the tablets' stability, as an addition of 10% (w/w) Tween 80 led to an increase in molecular mobility and loss of shape in higher humidity and temperature and an onset of crystallisation while stored in a desiccator. As such, it was proposed that for future work, different plasticising materials should be explored while assessing the effect on the printability and stability of printed tablets.

As amorphous solid dispersions can display physical instability, the third formulation strategy that was explored to address this was crystalline solid dispersions. As PEG 8000 and fenofibrate form eutectic mixtures and the system forms at a lower temperature than the melting point of the individual components, this was used to produce tablets. However, it was found that the printing system that was available was not adequate for this type of material and while improvements were made, more would be needed. However, this type of formulation did produce tablets that while heterogeneous amongst them, did lead to a fast, though not immediate, release of fenofibrate. As such, it was proposed that further optimisation of the printing system could be made in order to continue exploring the printing of eutectic systems, as well as assessing the stability of these systems over time.

In summary, while all formulation strategies have their advantages, the ones explored in this work should all be further optimised if to be taken forward in scale up or eventual clinical studies. Upon optimisation, higher drug loadings can be explored for personalisation, as well as the combination of different types of actives. These types of simple formulations that can be easily prepared and used to print oral solid dosage forms are the types of formulations that could be explored in compounding pharmacies, hospital and clinical trials settings.

From the work done and presented in this thesis, it is possible to see how versatile 3D material extrusion can be, in terms of formulation and process. It could be argued that it is the most versatile AM technique as no other technique can accommodate the use of such different materials and processing parameters, from pastes to gels to powders and polymeric filaments using a wide range of printing temperatures. Liquid feedstocks with limited rheological specifications are required for material jetting, vat photopolymerization and binder jetting, while powder feedstocks are used in selective laser sintering as well as binder jetting. Its versatility

makes this technique useful for the preparation of tablets containing all types of drugs, whether soluble or poorly soluble. While requirements for the different types of drugs differ, and careful consideration must be given when using poorly soluble drugs, as was proven with this study, the types of formulations that can be used within the modality pool of 3D material extrusion are able to accommodate them. It makes it a strong contender for the manufacturing of tablets during clinical trials as drug loading and release profile can be easily personalised. Moreover, it could be useful for the manufacturing of oral solid dosage forms containing orphan drugs as the amount of feedstock material needed can be as little or as much as needed. As such, this is a promising technique that is worth continuing to explore, especially in clinical and hospital settings.

7. References

[1] K.M.G. Taylor, M.E. Aulton, Aulton's Pharmaceutics, Elsevier Health Sciences, London, 2013.

[2] J. Siepmann, Fundamentals and Applications of Controlled Release Drug Delivery, Springer, New York ; London, 2013.

[3] N.G. Solanki, M. Kathawala, A.T.M. Serajuddin, Effects of Surfactants on Itraconazole-Hydroxypropyl Methylcellulose Acetate Succinate Solid Dispersion Prepared by Hot Melt Extrusion III: Tableting of Extrudates and Drug Release From Tablets, J Pharm Sci. 108 (2019) 3859–3869. https://doi.org/10.1016/J.XPHS.2019.09.014.

[4] S.A. Khaled, J.C. Burley, M.R. Alexander, J. Yang, C.J. Roberts, 3D printing of five-in-one dose combination polypill with defined immediate and sustained release profiles, Journal of Controlled Release. (2015). https://doi.org/10.1016/j.jconrel.2015.09.028.

[5] S.A. Khaled, J.C. Burley, M.R. Alexander, J. Yang, C.J. Roberts, 3D printing of tablets containing multiple drugs with defined release profiles, Int J Pharm. (2015). https://doi.org/10.1016/j.ijpharm.2015.07.067.

[6] G.K. Bolhuis, K. Zuurman, G.H.P. te Wierik, Improvement of dissolution of poorly soluble drugs by solid deposition on a super disintegrant. II. The choice of super disintegrants and effect of granulation, European Journal of Pharmaceutical Sciences. 5 (1997) 63–69. https://doi.org/10.1016/S0928-0987(96)00256-4.

[7] H. Herrada-Manchón, D. Rodríguez-González, M. Alejandro Fernández, M. Suñé-Pou, P. Pérez-Lozano, E. García-Montoya, E. Aguilar, 3D printed gummies: Personalized drug dosage in a safe and appealing way, Int J Pharm. 587 (2020) 119687. https://doi.org/10.1016/j.ijpharm.2020.119687.

[8] G.G.Z. Zhang, D. Law, E.A. Schmitt, Y. Qiu, Phase transformation considerations during process development and manufacture of solid oral dosage forms, Adv Drug Deliv Rev. 56 (2004) 371–390. https://doi.org/10.1016/J.ADDR.2003.10.009.

[9] A. Heinz, K.C. Gordon, C.M. McGoverin, T. Rades, C.J. Strachan, Understanding the solid-state forms of fenofibrate – A spectroscopic and

computational study, European Journal of Pharmaceutics and Biopharmaceutics. 71 (2009) 100–108. https://doi.org/10.1016/J.EJPB.2008.05.030.

[10] V.R. Kallakunta, S. Sarabu, S. Bandari, A. Batra, V. Bi, T. Durig, M.A. Repka, Stable amorphous solid dispersions of fenofibrate using hot melt extrusion technology: Effect of formulation and process parameters for a low glass transition temperature drug, J Drug Deliv Sci Technol. 58 (2020) 101395. https://doi.org/10.1016/j.jddst.2019.101395.

[11] R.A. Jain, L. Brito, J.A. Straub, T. Tessier, H. Bernstein, Effect of powder processing on performance of fenofibrate formulations, Eur J Pharm Biopharm. 69 (2008) 727–734. https://doi.org/10.1016/J.EJPB.2007.12.006.

[12] Y. Kawabata, K. Wada, M. Nakatani, S. Yamada, S. Onoue, Formulation design for poorly water-soluble drugs based on biopharmaceutics classification system: Basic approaches and practical applications, Int J Pharm. 420 (2011) 1–10. https://doi.org/10.1016/j.ijpharm.2011.08.032.

[13] A. Chauhan, Powder XRD Technique and its Applications in Science and Technology, J Anal Bioanal Tech. 5 (2014) 1–5. https://doi.org/10.4172/2155-9872.1000212.

[14] M.T. França, T. Martins Marcos, P.F.A. Costa, G.C. Bazzo, R. Nicolay Pereira, A.P. Gerola, H.K. Stulzer, Eutectic mixture and amorphous solid dispersion: Two different supersaturating drug delivery system strategies to improve griseofulvin release using saccharin, Int J Pharm. 615 (2022) 121498. https://doi.org/10.1016/J.IJPHARM.2022.121498.

[15] S.R. Vippagunta, Z. Wang, S. Hornung, S.L. Krill, Factors affecting the formation of eutectic solid dispersions and their dissolution behavior, J Pharm Sci. 96 (2007) 294–304. https://doi.org/10.1002/JPS.20754.

[16] K. Chaturvedi, H.S. Shah, K. Nahar, R. Dave, K.R. Morris, Contribution of Crystal Lattice Energy on the Dissolution Behavior of Eutectic Solid Dispersions, ACS Omega. 5 (2020) 9690–9701. https://doi.org/10.1021/ACSOMEGA.9B03886/ASSET/IMAGES/MEDIUM/AO9B03886_M006.GIF.

[17] D. Law, W. Wang, E.A. Schmitt, Y. Qiu, S.L. Krill, J.J. Fort, Properties of rapidly dissolving eutectic mixtures of poly(ethylene glycol) and fenofibrate: The

eutectic microstructure, J Pharm Sci. 92 (2003) 505–515. https://doi.org/10.1002/jps.10324.

[18] M. D. Ticehurst, P. A. Basford, C. I. Dallman, T. M. Lukas, P. v. Marshall, G. Nichols, D. Smith, Characterisation of the influence of micronisation on the crystallinity and physical stability of revatropate hydrobromide, Int J Pharm. 193 (2000) 247–259. https://doi.org/10.1016/S0378-5173(99)00347-6.

[19] B. v. Schönfeld, U. Westedt, K.G. Wagner, Compression of amorphous solid dispersions prepared by hot-melt extrusion, spray drying and vacuum drum drying, Int J Pharm X. 3 (2021) 100102. https://doi.org/10.1016/J.IJPX.2021.100102.

[20] Y. Umemoto, S. Uchida, T. Yoshida, K. Shimada, H. Kojima, A. Takagi, S. Tanaka, Y. Kashiwagura, N. Namiki, An effective polyvinyl alcohol for the solubilization of poorly water-soluble drugs in solid dispersion formulations, J Drug Deliv Sci Technol. 55 (2020) 101401. https://doi.org/10.1016/j.jddst.2019.101401.

[21] K. Göke, T. Lorenz, A. Repanas, F. Schneider, D. Steiner, K. Baumann, H. Bunjes, A. Dietzel, J.H. Finke, B. Glasmacher, A. Kwade, Novel strategies for the formulation and processing of poorly water-soluble drugs, European Journal of Pharmaceutics and Biopharmaceutics. 126 (2018) 40–56. https://doi.org/10.1016/j.ejpb.2017.05.008.

[22] Good manufacturing practice | European Medicines Agency, (n.d.). https://www.ema.europa.eu/en/human-regulatory/research-development/compliance/good-manufacturing-practice (accessed January 23, 2023).

[23] Current Good Manufacturing Practice (CGMP) Regulations | FDA, (n.d.). https://www.fda.gov/drugs/pharmaceutical-quality-resources/current-good-manufacturing-practice-cgmp-regulations (accessed January 23, 2023).

[24] Good manufacturing practice and good distribution practice - GOV.UK, (n.d.). https://www.gov.uk/guidance/good-manufacturing-practice-and-good-distribution-practice (accessed January 23, 2023).

[25] ISO/ASTM 52900:2021, Additive manufacturing — General principles — Fundamentals and vocabulary, 2021.

[26] M. Alhijjaj, P. Belton, S. Qi, An investigation into the use of polymer blends to improve the printability of and regulate drug release from pharmaceutical solid dispersions prepared via fused deposition modeling (FDM) 3D printing, European Journal of Pharmaceutics and Biopharmaceutics. (2016). https://doi.org/10.1016/j.ejpb.2016.08.016.

[27] E.A. Clark, M.R. Alexander, D.J. Irvine, C.J. Roberts, M.J. Wallace, J. Yoo, R.D. Wildman, Making tablets for delivery of poorly soluble drugs using photoinitiated 3D inkjet printing, Int J Pharm. 578 (2020). https://doi.org/10.1016/j.ijpharm.2019.118805.

[28] J. Conceição, X. Farto-Vaamonde, A. Goyanes, O. Adeoye, A. Concheiro, H. Cabral-Marques, J.M. Sousa Lobo, C. Alvarez-Lorenzo, Hydroxypropyl-β-cyclodextrin-based fast dissolving carbamazepine printlets prepared by semisolid extrusion 3D printing, Carbohydr Polym. (2019). https://doi.org/10.1016/j.carbpol.2019.05.084.

[29] G. Kollamaram, D.M. Croker, G.M. Walker, A. Goyanes, A.W. Basit, S. Gaisford, Low temperature fused deposition modeling (FDM) 3D printing of thermolabile drugs, Int J Pharm. (2018). https://doi.org/10.1016/j.ijpharm.2018.04.055.

[30] M. Kyobula, A. Adedeji, M.R. Alexander, E. Saleh, R. Wildman, I. Ashcroft, P.R. Gellert, C.J. Roberts, 3D inkjet printing of tablets exploiting bespoke complex geometries for controlled and tuneable drug release, Journal of Controlled Release. (2017). https://doi.org/10.1016/j.jconrel.2017.06.025.

[31] Y. Thabet, D. Lunter, J. Breitkreutz, Continuous inkjet printing of enalapril maleate onto orodispersible film formulations, Int J Pharm. 546 (2018) 180–187. https://doi.org/10.1016/j.ijpharm.2018.04.064.

[32] B. Arafat, M. Wojsz, A. Isreb, R.T. Forbes, M. Isreb, W. Ahmed, T. Arafat, M.A. Alhnan, Tablet fragmentation without a disintegrant: A novel design approach for accelerating disintegration and drug release from 3D printed cellulosic tablets, European Journal of Pharmaceutical Sciences. (2018). https://doi.org/10.1016/j.ejps.2018.03.019.

[33] S. Lamichhane, J.B. Park, D.H. Sohn, S. Lee, Customized novel design of 3D printed pregabalin tablets for intra-gastric floating and controlled release using fused deposition modeling, Pharmaceutics. (2019). https://doi.org/10.3390/pharmaceutics11110564.

[34] P. Robles-Martinez, X. Xu, S.J. Trenfield, A. Awad, A. Goyanes, R. Telford, A.W. Basit, S. Gaisford, 3D Printing of a Multi-Layered Polypill Containing Six Drugs Using a Novel Stereolithographic Method, Pharmaceutics. 11 (2019) 274. https://doi.org/10.3390/pharmaceutics11060274.

[35] S.A. Khaled, M.R. Alexander, D.J. Irvine, R.D. Wildman, M.J. Wallace, S. Sharpe, J. Yoo, C.J. Roberts, Extrusion 3D Printing of Paracetamol Tablets from a Single Formulation with Tunable Release Profiles Through Control of Tablet Geometry, AAPS PharmSciTech. (2018). https://doi.org/10.1208/s12249-018-1107-z.

[36] A. Goyanes, P. Robles Martinez, A. Buanz, A.W. Basit, S. Gaisford, Effect of geometry on drug release from 3D printed tablets, Int J Pharm. (2015). https://doi.org/10.1016/j.ijpharm.2015.04.069.

[37] A. Goyanes, J. Wang, A. Buanz, R. Martínez-Pacheco, R. Telford, S. Gaisford, A.W. Basit, 3D Printing of Medicines: Engineering Novel Oral Devices with Unique Design and Drug Release Characteristics, Mol Pharm. 12 (2015) 4077–4084. https://doi.org/10.1021/acs.molpharmaceut.5b00510.

[38] L'Oréal 2017: Improving agility, from prototyping to distribution, (n.d.). https://www.loreal-finance.com/en/annual-report-2017/operations/industry-4_0-agility-phototyping-distribution (accessed February 28, 2023).

[39] 3D printing at DB, (n.d.). https://www.deutschebahn.com/en/3d_printing-6935100 (accessed February 28, 2023).

[40] G.M. Tartaglia, A. Mapelli, C. Maspero, T. Santaniello, M. Serafin, M. Farronato, A. Caprioglio, Direct 3D Printing of Clear Orthodontic Aligners: Current State and Future Possibilities, Materials. 14 (2021). https://doi.org/10.3390/MA14071799.

[41] Geared for Success: Ford Now Operates 3D Printers Autonomously, Increasing Efficiency and Reducing Cost | Ford Media Center, (n.d.). https://media.ford.com/content/fordmedia/fna/us/en/news/2022/03/16/ford-now-operates-3d-printers-autonomously.html (accessed February 28, 2023).

[42] Additive Layer Manufacturing (ALM) Services | Airbus Aircraft, (n.d.). https://aircraft.airbus.com/en/services/expand/engineering-design-services/aerospace-integrated-research-test-centre/additive-layer-manufacturing (accessed February 28, 2023).

[43] Additive Manufacturing Machines & Materials | GE Additive, (n.d.). https://www.ge.com/additive/ (accessed February 28, 2023).

[44] ZipDose Technology | Spritam | Aprecia, (n.d.). https://www.aprecia.com/technology/zipdose (accessed December 9, 2019).

[45] T.G. West, T.J. Bradbury, 3D Printing: A Case of ZipDose® Technology – World's First 3D Printing Platform to Obtain FDA Approval for a Pharmaceutical Product, 3D and 4D Printing in Biomedical Applications. (2018) 53–79. https://doi.org/10.1002/9783527813704.CH3.

[46] S.A. Khaled, M.R. Alexander, R.D. Wildman, M.J. Wallace, S. Sharpe, J. Yoo, C.J. Roberts, 3D extrusion printing of high drug loading immediate release paracetamol tablets, Int J Pharm. (2018). https://doi.org/10.1016/j.ijpharm.2018.01.024.

[47] S.A. Khaled, J.C. Burley, M.R. Alexander, C.J. Roberts, Desktop 3D printing of controlled release pharmaceutical bilayer tablets, Int J Pharm. (2014). https://doi.org/10.1016/j.ijpharm.2013.11.021.

[48] N. Genina, J.P. Boetker, S. Colombo, N. Harmankaya, J. Rantanen, A. Bohr, Anti-tuberculosis drug combination for controlled oral delivery using 3D printed compartmental dosage forms: From drug product design to in vivo testing, Journal of Controlled Release. (2017). https://doi.org/10.1016/j.jconrel.2017.10.003.

[49] M. Fanous, S. Gold, S. Muller, S. Hirsch, J. Ogorka, G. Imanidis, Simplification of fused deposition modeling 3D-printing paradigm: Feasibility of 1-step direct powder printing for immediate release dosage form production, Int J Pharm. (2020). https://doi.org/10.1016/j.ijpharm.2020.119124.

[50] P. Li, H. Jia, S. Zhang, Y. Yang, H. Sun, H. Wang, W. Pan, F. Yin, X. Yang, Thermal Extrusion 3D Printing for the Fabrication of Puerarin Immediate-Release Tablets, AAPS PharmSciTech. 21 (2020) 1–10. https://doi.org/10.1208/S12249-019-1538-1/FIGURES/5.

[51] J. Skowyra, K. Pietrzak, M.A. Alhnan, Fabrication of extended-release patient-tailored prednisolone tablets via fused deposition modelling (FDM) 3D printing, European Journal of Pharmaceutical Sciences. (2015). https://doi.org/10.1016/j.ejps.2014.11.009.

[52] A. Goyanes, A.B.M. Buanz, A.W. Basit, S. Gaisford, Fused-filament 3D printing (3DP) for fabrication of tablets, Int J Pharm. (2014). https://doi.org/10.1016/j.ijpharm.2014.09.044.

[53] A. Goyanes, A.B.M. Buanz, G.B. Hatton, S. Gaisford, A.W. Basit, 3D printing of modified-release aminosalicylate (4-ASA and 5-ASA) tablets, European Journal of Pharmaceutics and Biopharmaceutics. (2015). https://doi.org/10.1016/j.ejpb.2014.12.003.

[54] K. Thanawuth, L. Sutthapitaksakul, S. Konthong, S. Suttiruengwong, K. Huanbutta, C.R. Dass, P. Sriamornsak, Impact of Drug Loading Method on Drug Release from 3D-Printed Tablets Made from Filaments Fabricated by Hot-Melt Extrusion and Impregnation Processes, Pharmaceutics 2021, Vol. 13, Page 1607. 13 (2021) 1607. https://doi.org/10.3390/PHARMACEUTICS13101607.

[55] A. Goyanes, F. Fina, A. Martorana, D. Sedough, S. Gaisford, A.W. Basit, Development of modified release 3D printed tablets (printlets) with pharmaceutical excipients using additive manufacturing, Int J Pharm. (2017). https://doi.org/10.1016/j.ijpharm.2017.05.021.

[56] A. Goyanes, M. Scarpa, M. Kamlow, S. Gaisford, A.W. Basit, M. Orlu, Patient acceptability of 3D printed medicines, Int J Pharm. (2017). https://doi.org/10.1016/j.ijpharm.2017.07.064.

[57] R.C.R. Beck, P.S. Chaves, A. Goyanes, B. Vukosavljevic, A. Buanz, M. Windbergs, A.W. Basit, S. Gaisford, 3D printed tablets loaded with polymeric nanocapsules: An innovative approach to produce customized drug delivery systems, Int J Pharm. (2017). https://doi.org/10.1016/j.ijpharm.2017.05.074.

[58] M. Ibrahim, M. Barnes, R. McMillin, D.W. Cook, S. Smith, M. Halquist, D. Wijesinghe, T.D. Roper, 3D Printing of Metformin HCl PVA Tablets by Fused Deposition Modeling: Drug Loading, Tablet Design, and Dissolution Studies, AAPS PharmSciTech. (2019). https://doi.org/10.1208/s12249-019-1400-5.

[59] M. Fanous, S. Gold, S. Hirsch, J. Ogorka, G. Imanidis, Development of immediate release (IR) 3D-printed oral dosage forms with focus on industrial relevance, European Journal of Pharmaceutical Sciences. (2020). https://doi.org/10.1016/j.ejps.2020.105558.

[60] K. Pietrzak, A. Isreb, M.A. Alhnan, A flexible-dose dispenser for immediate and extended release 3D printed tablets, European Journal of Pharmaceutics and Biopharmaceutics. (2015). https://doi.org/10.1016/j.ejpb.2015.07.027.

[61] S. Chung, P. Srinivasan, P. Zhang, S. Bandari, M.A. Repka, Development of ibuprofen tablet with polyethylene oxide using fused deposition modeling 3D-printing coupled with hot-melt extrusion, J Drug Deliv Sci Technol. 76 (2022) 103716. https://doi.org/10.1016/J.JDDST.2022.103716.

[62] S. Ayyoubi, J.R. Cerda, R. Fernández-García, P. Knief, A. Lalatsa, A.M. Healy, D.R. Serrano, 3D printed spherical mini-tablets: Geometry versus composition effects in controlling dissolution from personalised solid dosage forms, Int J Pharm. 597 (2021). https://doi.org/10.1016/j.ijpharm.2021.120336.

[63] I. el Aita, J. Breitkreutz, J. Quodbach, On-demand manufacturing of immediate release levetiracetam tablets using pressure-assisted microsyringe printing, European Journal of Pharmaceutics and Biopharmaceutics. (2019). https://doi.org/10.1016/j.ejpb.2018.11.008.

[64] Y. Cheng, H. Qin, N.C. Acevedo, X. Jiang, X. Shi, 3D printing of extended-release tablets of theophylline using hydroxypropyl methylcellulose (HPMC) hydrogels, Int J Pharm. (2020). https://doi.org/10.1016/j.ijpharm.2020.119983.

[65] M. Cui, H. Pan, D. Fang, S. Qiao, S. Wang, W. Pan, Fabrication of high drug loading levetiracetam tablets using semi-solid extrusion 3D printing, J Drug Deliv Sci Technol. 57 (2020) 101683. https://doi.org/10.1016/j.jddst.2020.101683.

[66] D. Fang, H. Pan, M. Cui, S. Qiao, X. Li, T. Wang, Q. Meng, L. Xu, W. Pan, Fabrication of three-dimensional-printed ofloxacin gastric floating sustained-release tablets with different structures, J Drug Deliv Sci Technol. 67 (2022) 102992. https://doi.org/10.1016/J.JDDST.2021.102992.

[67] M. Cui, Y. Yang, D. Jia, P. Li, Q. Li, F. Chen, S. Wang, W. Pan, P. Ding, Effect of novel internal structures on printability and drug release behavior of 3D printed tablets, J Drug Deliv Sci Technol. 49 (2019) 14–23. https://doi.org/10.1016/J.JDDST.2018.10.037.

[68] W.J. Goh, S.X. Tan, G. Pastorin, P.C.L. Ho, J. Hu, S.H. Lim, 3D printing of four-in-one oral polypill with multiple release profiles for personalized delivery

of caffeine and vitamin B analogues, Int J Pharm. 598 (2021) 120360. https://doi.org/10.1016/j.ijpharm.2021.120360.

[69] A. Zidan, A. Alayoubi, S. Asfari, J. Coburn, B. Ghammraoui, C.N. Cruz, M. Ashraf, Development of mechanistic models to identify critical formulation and process variables of pastes for 3D printing of modified release tablets, Int J Pharm. 555 (2019) 109–123. https://doi.org/10.1016/J.IJPHARM.2018.11.044.

[70] G. Falcone, M. Saviano, R.P. Aquino, P. del Gaudio, P. Russo, Coaxial semi-solid extrusion and ionotropic alginate gelation: A successful duo for personalized floating formulations via 3D printing, Carbohydr Polym. 260 (2021) 117791. https://doi.org/10.1016/J.CARBPOL.2021.117791.

[71] K. Chachlioutaki, C. Karavasili, E.E. Mavrokefalou, C.I. Gioumouxouzis, C. Ritzoulis, D.G. Fatouros, Quality control evaluation of paediatric chocolate-based dosage forms: 3D printing vs mold-casting method, Int J Pharm. 624 (2022) 121991. https://doi.org/10.1016/J.IJPHARM.2022.121991.

[72] C. Karavasili, A. Gkaragkounis, T. Moschakis, C. Ritzoulis, D.G. Fatouros, Pediatric-friendly chocolate-based dosage forms for the oral administration of both hydrophilic and lipophilic drugs fabricated with extrusion-based 3D printing, European Journal of Pharmaceutical Sciences. 147 (2020) 105291. https://doi.org/10.1016/J.EJPS.2020.105291.

[73] T.A. Ahmed, R.I. Felimban, H.H. Tayeb, W.Y. Rizg, F.H. Alnadwi, H.A. Alotaibi, N.A. Alhakamy, F.I. Abd-Allah, G.A. Mohamed, A.S. Zidan, K.M. El-Say, Development of Multi-Compartment 3D-Printed Tablets Loaded with Self-Nanoemulsified Formulations of Various Drugs: A New Strategy for Personalized Medicine, Pharmaceutics 2021, Vol. 13, Page 1733. 13 (2021) 1733. https://doi.org/10.3390/PHARMACEUTICS13101733.

[74] T.A. Ahmed, H.A. Alotaibi, W.S. Alharbi, M.K. Safo, K.M. El-Say, Development of 3D-Printed, Liquisolid and Directly Compressed Glimepiride Tablets, Loaded with Black Seed Oil Self-Nanoemulsifying Drug Delivery System: In Vitro and In Vivo Characterization, Pharmaceuticals 2022, Vol. 15, Page 68. 15 (2022) 68. https://doi.org/10.3390/PH15010068.

[75] J. Johannesson, J. Khan, M. Hubert, A. Teleki, C.A.S. Bergström, 3D-printing of solid lipid tablets from emulsion gels, Int J Pharm. 597 (2021) 120304. https://doi.org/10.1016/J.IJPHARM.2021.120304.

[76] B.W. Barber, C. Dumont, P. Caisse, G.P. Simon, B.J. Boyd, A 3D-Printed Polymer–Lipid-Hybrid Tablet towards the Development of Bespoke SMEDDS Formulations, Pharmaceutics 2021, Vol. 13, Page 2107. 13 (2021) 2107. https://doi.org/10.3390/PHARMACEUTICS13122107.

[77] M.S. Algahtani, A.A. Mohammed, J. Ahmad, M.M. Abdullah, E. Saleh, 3D Printing of Dapagliflozin Containing Self-Nanoemulsifying Tablets: Formulation Design and In Vitro Characterization, Pharmaceutics 2021, Vol. 13, Page 993. 13 (2021) 993. https://doi.org/10.3390/PHARMACEUTICS13070993.

[78] N. Callede, T. Masciotti, L. Casettari, N. Loosveldt, J. Goole, Development and evaluation of a 3D printing protocol to produce zolpidem-containing printlets, as compounding preparation, by the pressurized-assisted microsyringes technique, Int J Pharm. 621 (2022) 121756. https://doi.org/10.1016/J.IJPHARM.2022.121756.

[79] J. Elbl, J. Gajdziok, J. Kolarczyk, 3D printing of multilayered orodispersible films with in-process drying, Int J Pharm. (2020). https://doi.org/10.1016/j.ijpharm.2019.118883.

[80] A. Goyanes, N. Allahham, S.J. Trenfield, E. Stoyanov, S. Gaisford, A.W. Basit, Direct powder extrusion 3D printing: Fabrication of drug products using a novel single-step process, Int J Pharm. (2019). https://doi.org/10.1016/j.ijpharm.2019.118471.

[81] Y. Zheng, F. Deng, B. Wang, Y. Wu, Q. Luo, X. Zuo, X. Liu, L. Cao, M. Li, H. Lu, S. Cheng, X. Li, Melt extrusion deposition (MED^{TM}) 3D printing technology – A paradigm shift in design and development of modified release drug products, Int J Pharm. 602 (2021) 120639. https://doi.org/10.1016/J.IJPHARM.2021.120639.

[82] J. Boniatti, P. Januskaite, L.B. da Fonseca, A.L. Viçosa, F.C. Amendoeira, C. Tuleu, A.W. Basit, A. Goyanes, M.I. Ré, Direct Powder Extrusion 3D Printing of Praziquantel to Overcome Neglected Disease Formulation Challenges in Paediatric Populations, Pharmaceutics 2021, Vol. 13, Page 1114. 13 (2021) 1114. https://doi.org/10.3390/PHARMACEUTICS13081114.

[83] S.J. Kim, J.C. Lee, J.Y. Ko, S.H. Lee, N.A. Kim, S.H. Jeong, 3D-printed tablets using a single-step hot-melt pneumatic process for poorly soluble drugs, Int J Pharm. 595 (2021) 120257. https://doi.org/10.1016/j.ijpharm.2021.120257.

[84] B. Liu, X. Han, Z. Wang, H. Zhang, N. Liu, X. Gao, J. Gao, A. Zheng, Three-dimensional printing personalized acetaminophen sustained-release tablets using hot melt extrusion, J Drug Deliv Sci Technol. 66 (2021) 102855. https://doi.org/10.1016/j.jddst.2021.102855.

[85] M. Kuźmińska, B.C. Pereira, R. Habashy, M. Peak, M. Isreb, T.D. Gough, A. Isreb, M.A. Alhnan, Solvent-free temperature-facilitated direct extrusion 3D printing for pharmaceuticals, Int J Pharm. 598 (2021) 120305. https://doi.org/10.1016/J.IJPHARM.2021.120305.

[86] Z. Zheng, J. Lv, W. Yang, X. Pi, W. Lin, Z. Lin, W. Zhang, J. Pang, Y. Zeng, Z. Lv, H. Lao, Y. Chen, F. Yang, Preparation and application of subdivided tablets using 3D printing for precise hospital dispensing, European Journal of Pharmaceutical Sciences. 149 (2020) 105293. https://doi.org/10.1016/J.EJPS.2020.105293.

[87] H.K. Cader, G.A. Rance, M.R. Alexander, A.D. Gonçalves, C.J. Roberts, C.J. Tuck, R.D. Wildman, Water-based 3D inkjet printing of an oral pharmaceutical dosage form, Int J Pharm. 564 (2019) 359–368. https://doi.org/10.1016/j.ijpharm.2019.04.026.

[88] E.A. Clark, M.R. Alexander, D.J. Irvine, C.J. Roberts, M.J. Wallace, S. Sharpe, J. Yoo, R.J.M. Hague, C.J. Tuck, R.D. Wildman, 3D printing of tablets using inkjet with UV photoinitiation, Int J Pharm. (2017). https://doi.org/10.1016/j.ijpharm.2017.06.085.

[89] G.F. Acosta-Vélez, C.S. Linsley, M.C. Craig, B.M. Wu, Photocurable Bioink for the Inkjet 3D Pharming of Hydrophilic Drugs, Bioengineering 2017, Vol. 4, Page 11. 4 (2017) 11. https://doi.org/10.3390/BIOENGINEERING4010011.

[90] G.F. Acosta-Vélez, T.Z. Zhu, C.S. Linsley, B.M. Wu, Photocurable poly(ethylene glycol) as a bioink for the inkjet 3D pharming of hydrophobic drugs, Int J Pharm. 546 (2018) 145–153. https://doi.org/10.1016/J.IJPHARM.2018.04.056.

[91] G.F. Acosta-Vélez, C.S. Linsley, T.Z. Zhu, W. Wu, B.M. Wu, Photocurable Bioinks for the 3D Pharming of Combination Therapies, Polymers 2018, Vol. 10, Page 1372. 10 (2018) 1372. https://doi.org/10.3390/POLYM10121372.

[92] M. Madžarević, S. Ibrić, Evaluation of exposure time and visible light irradiation in LCD 3D printing of ibuprofen extended release tablets, European Journal of

Pharmaceutical Sciences. 158 (2021) 105688. https://doi.org/10.1016/J.EJPS.2020.105688.

[93] M. Krkobabić, D. Medarević, S. Cvijić, B. Grujić, S. Ibrić, Hydrophilic excipients in digital light processing (DLP) printing of sustained release tablets: Impact on internal structure and drug dissolution rate, Int J Pharm. 572 (2019) 118790. https://doi.org/10.1016/j.ijpharm.2019.118790.

[94] L. Rodríguez-Pombo, X. Xu, A. Seijo-Rabina, J.J. Ong, C. Alvarez-Lorenzo, C. Rial, D. Nieto, S. Gaisford, A.W. Basit, A. Goyanes, Volumetric 3D printing for rapid production of medicines, Addit Manuf. 52 (2022) 102673. https://doi.org/10.1016/J.ADDMA.2022.102673.

[95] L. Rodríguez-Pombo, L. Martínez-Castro, X. Xu, J.J. Ong, C. Rial, D.N. García, A. González-Santos, J. Flores-González, C. Alvarez-Lorenzo, A.W. Basit, A. Goyanes, Simultaneous fabrication of multiple tablets within seconds using tomographic volumetric 3D printing, Int J Pharm X. 5 (2023) 100166. https://doi.org/10.1016/J.IJPX.2023.100166.

[96] X. Xu, P. Robles-Martinez, C.M. Madla, F. Joubert, A. Goyanes, A.W. Basit, S. Gaisford, Stereolithography (SLA) 3D printing of an antihypertensive polyprintlet: Case study of an unexpected photopolymer-drug reaction, Addit Manuf. 33 (2020) 101071. https://doi.org/10.1016/j.addma.2020.101071.

[97] I. Adamov, G. Stanojević, D. Medarević, B. Ivković, D. Kočović, D. Mirković, S. Ibrić, Formulation and characterization of immediate-release oral dosage forms with zolpidem tartrate fabricated by digital light processing (DLP) 3D printing technique, Int J Pharm. 624 (2022) 122046. https://doi.org/10.1016/J.IJPHARM.2022.122046.

[98] J. Wang, A. Goyanes, S. Gaisford, A.W. Basit, Stereolithographic (SLA) 3D printing of oral modified-release dosage forms, Int J Pharm. (2016). https://doi.org/10.1016/j.ijpharm.2016.03.016.

[99] F. Fina, C.M. Madla, A. Goyanes, J. Zhang, S. Gaisford, A.W. Basit, Fabricating 3D printed orally disintegrating printlets using selective laser sintering, Int J Pharm. (2018). https://doi.org/10.1016/j.ijpharm.2018.02.015.

[100] A. Awad, A. Yao, S.J. Trenfield, A. Goyanes, S. Gaisford, A.W. Basit, 3D Printed Tablets (Printlets) with Braille and Moon Patterns for Visually Impaired

Patients, Pharmaceutics 2020, Vol. 12, Page 172. 12 (2020) 172. https://doi.org/10.3390/PHARMACEUTICS12020172.

[101] S.J. Trenfield, X. Xu, A. Goyanes, M. Rowland, D. Wilsdon, S. Gaisford, A.W. Basit, Releasing fast and slow: Non-destructive prediction of density and drug release from SLS 3D printed tablets using NIR spectroscopy, Int J Pharm X. 5 (2023) 100148. https://doi.org/10.1016/J.IJPX.2022.100148.

[102] Y. Yang, Y. Xu, S. Wei, W. Shan, Oral preparations with tunable dissolution behavior based on selective laser sintering technique, Int J Pharm. 593 (2021) 120127. https://doi.org/10.1016/J.IJPHARM.2020.120127.

[103] N. Allahham, F. Fina, C. Marcuta, L. Kraschew, W. Mohr, S. Gaisford, A.W. Basit, A. Goyanes, Selective Laser Sintering 3D Printing of Orally Disintegrating Printlets Containing Ondansetron, Pharmaceutics 2020, Vol. 12, Page 110. 12 (2020) 110. https://doi.org/10.3390/PHARMACEUTICS12020110.

[104] F. Fina, A. Goyanes, S. Gaisford, A.W. Basit, Selective laser sintering (SLS) 3D printing of medicines, Int J Pharm. 529 (2017) 285–293. https://doi.org/10.1016/j.ijpharm.2017.06.082.

[105] S. Infanger, A. Haemmerli, S. Iliev, A. Baier, E. Stoyanov, J. Quodbach, Powder bed 3D-printing of highly loaded drug delivery devices with hydroxypropyl cellulose as solid binder, Int J Pharm. (2019). https://doi.org/10.1016/j.ijpharm.2018.11.048.

[106] W.E. Katstra, R.D. Palazzolo, C.W. Rowe, B. Giritlioglu, P. Teung, M.J. Cima, Oral dosage forms fabricated by Three Dimensional Printing(TM), Journal of Controlled Release. 66 (2000) 1–9. https://doi.org/10.1016/S0168-3659(99)00225-4.

[107] K.A. van den Heuvel, M.T.W. de Wit, B.H.J. Dickhoff, Evaluation of lactose based 3D powder bed printed pharmaceutical drug product tablets, Powder Technol. 390 (2021) 97–102. https://doi.org/10.1016/J.POWTEC.2021.05.050.

[108] M. Kozakiewicz-Latała, K.P. Nartowski, A. Dominik, K. Malec, A.M. Gołkowska, A. Złocińska, M. Rusińska, P. Szymczyk-Ziółkowska, G. Ziółkowski, A. Górniak, B. Karolewicz, Binder jetting 3D printing of challenging medicines: From low dose tablets to hydrophobic molecules, European Journal of

Pharmaceutics and Biopharmaceutics. 170 (2022) 144–159. https://doi.org/10.1016/J.EJPB.2021.11.001.

[109] M. Tan, D. Dharani, X. Dong, C. Maiorana, B. Chaudhuri, K. Nagapudi, S.Y. Chang, A.W.K. Ma, Pilot-scale binder jet 3D printing of sustained release solid dosage forms, Int J Pharm. 631 (2023) 122540. https://doi.org/10.1016/J.IJPHARM.2022.122540.

[110] G. Cummins, M.P.Y. Desmulliez, Inkjet printing of conductive materials: A review, Circuit World. 38 (2012) 193–213. https://doi.org/10.1108/03056121211280413/FULL/PDF.

[111] List of 3D printing technologies - guide on all 3D printing technologies, (n.d.). https://www.aniwaa.com/guide/3d-printers/3d-printing-technologies/ (accessed January 5, 2023).

[112] S.A. Khaled, J.C. Burley, M.R. Alexander, C.J. Roberts, Desktop 3D printing of controlled release pharmaceutical bilayer tablets, Int J Pharm. (2014). https://doi.org/10.1016/j.ijpharm.2013.11.021.

[113] A. Goyanes, C.M. Madla, A. Umerji, G. Duran Piñeiro, J.M. Giraldez Montero, M.J. Lamas Diaz, M. Gonzalez Barcia, F. Taherali, P. Sánchez-Pintos, M.L. Couce, S. Gaisford, A.W. Basit, Automated therapy preparation of isoleucine formulations using 3D printing for the treatment of MSUD: First single-centre, prospective, crossover study in patients, Int J Pharm. 567 (2019) 118497. https://doi.org/10.1016/J.IJPHARM.2019.118497.

[114] D. Pedrosa de Oliveira, J.S.R. Costa, L. Oliveira-Nascimento, Sustainability of blisters for medicines in tablet form, Sustain Chem Pharm. 21 (2021) 100423. https://doi.org/10.1016/j.scp.2021.100423.

[115] F. Osei-Yeboah, C.C. Sun, Validation and applications of an expedited tablet friability method, Int J Pharm. 484 (2015) 146–155. https://doi.org/10.1016/j.ijpharm.2015.02.061.

[116] Triastek, Inc, (n.d.). https://www.triastek.com/ (accessed January 10, 2023).

[117] M3DISEEN, (n.d.). https://m3diseen.com/ (accessed February 18, 2023).

[118] M. Elbadawi, B. Muñiz Castro, F.K.H. Gavins, J.J. Ong, S. Gaisford, G. Pérez, A.W. Basit, P. Cabalar, A. Goyanes, M3DISEEN: A novel machine learning

approach for predicting the 3D printability of medicines, Int J Pharm. 590 (2020). https://doi.org/10.1016/j.ijpharm.2020.119837.

[119] DNA Studio 4 Vault - Bioprinting Software - CELLINK, (n.d.). https://www.cellink.com/software/dna-studio-4-vault/?utm_source=linkedin&utm_medium=social-organic (accessed February 26, 2023).

[120] 3D printing for flexible production of personalised medi, (n.d.). https://www.tno.nl/en/healthy/flexibele-en-vrije-vorm-producten/3d-printing-flexible-production/ (accessed February 28, 2023).

[121] Nourished | Nourished Personalised Gummy Vitamins, (n.d.). https://get-nourished.com/ (accessed February 26, 2023).

[122] Evonik Venture Capital invests in Laxxon - Evonik Industries, (n.d.). https://corporate.evonik.com/en/media/press-releases/corporate/evonik-venture-capital-invests-in-laxxon-170309.html (accessed January 26, 2023).

[123] Laxxon Medical | 3D Printed Pharmaceutical Solutions, (n.d.). https://www.laxxonmedical.com/ (accessed January 26, 2023).

[124] D. Moldenhauer, D.C.Y. Nguyen, L. Jescheck, F. Hack, D. Fischer, A. Schneeberger, 3D screen printing – An innovative technology for large-scale manufacturing of pharmaceutical dosage forms, Int J Pharm. 592 (2021) 120096. https://doi.org/10.1016/J.IJPHARM.2020.120096.

[125] H.K. Mamidi, S. Palekar, P.K. Nukala, S.M. Mishra, M. Patki, Y. Fu, P. Supner, G. Chauhan, K. Patel, Process optimization of twin-screw melt granulation of fenofibrate using design of experiment (DoE), Int J Pharm. 593 (2021) 120101. https://doi.org/10.1016/J.IJPHARM.2020.120101.

[126] E. Sipos, T. Csatári, A. Kazsoki, A. Gergely, E. Bitay, Z.I. Szabó, R. Zelkó, Preparation and characterization of fenofibrateloaded PVP electrospun microfibrous sheets, Pharmaceutics. 12 (2020) 8–10. https://doi.org/10.3390/pharmaceutics12070612.

[127] L. Hu, H. Wu, F. Niu, C. Yan, X. Yang, Y. Jia, Design of fenofibrate microemulsion for improved bioavailability, Int J Pharm. 420 (2011) 251–255. https://doi.org/10.1016/J.IJPHARM.2011.08.043.

[128] F. Li, X. Zheng, Y. Bao, T. Chen, J. Zeng, X. Xu, C. Yan, L. Feng, Fenofibrate modified-release pellets with lag phase and high oral bioavailability, Drug Des Devel Ther. 13 (2019) 141–151. https://doi.org/10.2147/DDDT.S179266.

[129] Y. Chen, Y. Lu, J. Chen, J. Lai, J. Sun, F. Hu, W. Wu, Enhanced bioavailability of the poorly water-soluble drug fenofibrate by using liposomes containing a bile salt, Int J Pharm. 376 (2009) 153–160. https://doi.org/10.1016/J.IJPHARM.2009.04.022.

[130] G. Torres-Flores, G.T. Nazende, T.A. Emre, Preparation of Fenofibrate loaded Eudragit L100 nanoparticles by nanoprecipitation method, Mater Today Proc. 13 (2019) 428–435. https://doi.org/10.1016/J.MATPR.2019.03.176.

[131] H. Patil, X. Feng, X. Ye, S. Majumdar, M.A. Repka, Continuous Production of Fenofibrate Solid Lipid Nanoparticles by Hot-Melt Extrusion Technology: a Systematic Study Based on a Quality by Design Approach, AAPS Journal. 17 (2015) 194–205. https://doi.org/10.1208/S12248-014-9674-8/TABLES/4.

[132] M. Patki, K. Patel, Development of a solid supersaturated self-nanoemulsifying preconcentrate (S-superSNEP) of fenofibrate using dimethylacetamide and a novel co-processed excipient, Https://Doi.Org/10.1080/03639045.2018.1546311. 45 (2018) 405–414. https://doi.org/10.1080/03639045.2018.1546311.

[133] M. Vogt, K. Kunath, J.B. Dressman, Dissolution enhancement of fenofibrate by micronization, cogrinding and spray-drying: Comparison with commercial preparations, European Journal of Pharmaceutics and Biopharmaceutics. 68 (2008) 283–288. https://doi.org/10.1016/J.EJPB.2007.05.010.

[134] L.M. Dwyer, V.K. Michaelis, M. O'Mahony, R.G. Griffin, A.S. Myerson, Confined crystallization of fenofibrate in nanoporous silica, CrystEngComm. 17 (2015) 7922–7929. https://doi.org/10.1039/c5ce01148e.

[135] B.N. Tran, Q. Van Pham, B.T. Tran, G. Thien Le, A.H. Dao, T.H. Tran, C.N. Nguyen, Supercritical CO2 impregnation approach for enhancing dissolution of fenofibrate by adsorption onto high-surface area carriers, J Supercrit Fluids. 184 (2022) 105584. https://doi.org/10.1016/J.SUPFLU.2022.105584.

[136] J. Bin Ahn, D.H. Kim, S.E. Lee, Y.C. Pyo, J.S. Park, Improvement of the dissolution rate and bioavailability of fenofibrate by the supercritical anti-

solvent process, Int J Pharm. 564 (2019) 263–272. https://doi.org/10.1016/J.IJPHARM.2019.04.051.

[137] C.N. Nguyen, C.V. Pham, G. Le Thien, B.T. Ngoc, H. Le Thi, C.P.T. Huyen, T.N. Thi, Immediate-released pelletized solid dispersion containing fenofibrate: Formulation, in vitro characterization, and bioequivalence studies in experimental beagle dogs, Int J Pharm. 570 (2019) 118661. https://doi.org/10.1016/J.IJPHARM.2019.118661.

[138] A. Lion, R.D. Wildman, M.R. Alexander, C.J. Roberts, Customisable Tablet Printing: The Development of Multimaterial Hot Melt Inkjet 3D Printing to Produce Complex and Personalised Dosage Forms, Pharmaceutics 2021, Vol. 13, Page 1679. 13 (2021) 1679. https://doi.org/10.3390/PHARMACEUTICS13101679.

[139] K. Vithani, A. Goyanes, V. Jannin, A.W. Basit, S. Gaisford, B.J. Boyd, A Proof of Concept for 3D Printing of Solid Lipid-Based Formulations of Poorly Water-Soluble Drugs to Control Formulation Dispersion Kinetics, Pharm Res. 36 (2019). https://doi.org/10.1007/S11095-019-2639-Y.

[140] D. Medarević, J. Djuriš, M. Krkobabić, S. Ibrić, Improving Tableting Performance of Lactose Monohydrate by Fluid-Bed Melt Granulation Co-Processing, Pharmaceutics 2021, Vol. 13, Page 2165. 13 (2021) 2165. https://doi.org/10.3390/PHARMACEUTICS13122165.

[141] G.A. Hebbink, M. Jaspers, H.J.W. Peters, B.H.J. Dickhoff, Recent developments in lactose blend formulations for carrier-based dry powder inhalation, Adv Drug Deliv Rev. 189 (2022) 114527. https://doi.org/10.1016/J.ADDR.2022.114527.

[142] J. Suárez-González, M. Magariños-Triviño, E. Díaz-Torres, A.R. Cáceres-Pérez, A. Santoveña-Estévez, J.B. Fariña, Individualized orodispersible pediatric dosage forms obtained by molding and semi-solid extrusion by 3D printing: A comparative study for hydrochlorothiazide, J Drug Deliv Sci Technol. 66 (2021) 102884. https://doi.org/10.1016/J.JDDST.2021.102884.

[143] S.Y. Chang, J. Jin, J. Yan, X. Dong, B. Chaudhuri, K. Nagapudi, A.W.K. Ma, Development of a pilot-scale HuskyJet binder jet 3D printer for additive manufacturing of pharmaceutical tablets, Int J Pharm. 605 (2021) 120791. https://doi.org/10.1016/J.IJPHARM.2021.120791.

[144] K. Kreft, Z. Lavrič, T. Stani´cstani´c, P. Perhavec, R. Dreu, L. Pharmaceuticals, Influence of the Binder Jetting Process Parameters and Binder Liquid Composition on the Relevant Attributes of 3D-Printed Tablets, Pharmaceutics 2022, Vol. 14, Page 1568. 14 (2022) 1568. https://doi.org/10.3390/PHARMACEUTICS14081568.

[145] M. Sadia, A. Sośnicka, B. Arafat, A. Isreb, W. Ahmed, A. Kelarakis, M.A. Alhnan, Adaptation of pharmaceutical excipients to FDM 3D printing for the fabrication of patient-tailored immediate release tablets, Int J Pharm. 513 (2016) 659–668. https://doi.org/10.1016/j.ijpharm.2016.09.050.

[146] G. Thoorens, F. Krier, B. Leclercq, B. Carlin, B. Evrard, Microcrystalline cellulose, a direct compression binder in a quality by design environment—A review, Int J Pharm. 473 (2014) 64–72. https://doi.org/10.1016/J.IJPHARM.2014.06.055.

[147] M. Cui, H. Pan, D. Fang, H. Sun, S. Qiao, W. Pan, Exploration and evaluation of dynamic dose-control platform for pediatric medicine based on Drop-on-Powder 3D printing technology, Int J Pharm. 596 (2021) 120201. https://doi.org/10.1016/J.IJPHARM.2021.120201.

[148] M. Cui, H. Pan, L. Li, D. Fang, H. Sun, S. Qiao, X. Li, W. Pan, Exploration and Preparation of Patient-specific Ciprofloxacin Implants Drug Delivery System Via 3D Printing Technologies, J Pharm Sci. 110 (2021) 3678–3689. https://doi.org/10.1016/J.XPHS.2021.08.004.

[149] U. Shah, L. Augsburger, Multiple Sources of Sodium Starch Glycolate, NF: Evaluation of Functional Equivalence and Development of Standard Performance Tests, Http://Dx.Doi.Org/10.1081/PDT-120005731. 7 (2002) 345–359. https://doi.org/10.1081/PDT-120005731.

[150] M. Đuranović, M. Madžarević, B. Ivković, S. Ibrić, S. Cvijić, The evaluation of the effect of different superdisintegrants on the drug release from FDM 3D printed tablets through different applied strategies: In vitro-in silico assessment, Int J Pharm. 610 (2021) 121194. https://doi.org/10.1016/J.IJPHARM.2021.121194.

[151] A. Hussain, F. Mahmood, M.S. Arshad, N. Abbas, N. Qamar, J. Mudassir, S. Farhaj, J.S. Nirwan, M.U. Ghori, Personalised 3D printed fast-dissolving tablets for managing hypertensive crisis: In-vitro/in-vivo studies, Polymers (Basel). 12 (2020) 1–15. https://doi.org/10.3390/polym12123057.

[152] P. Zarmpi, T. Flanagan, E. Meehan, J. Mann, N. Fotaki, Biopharmaceutical Understanding of Excipient Variability on Drug Apparent Solubility Based on Drug Physicochemical Properties: Case Study—Hypromellose (HPMC), AAPS J. 22 (2020). https://doi.org/10.1208/S12248-019-0411-1.

[153] T. Tagami, M. Ando, N. Nagata, E. Goto, N. Yoshimura, T. Takeuchi, T. Noda, T. Ozeki, Fabrication of Naftopidil-Loaded Tablets Using a Semisolid Extrusion-Type 3D Printer and the Characteristics of the Printed Hydrogel and Resulting Tablets, J Pharm Sci. (2019). https://doi.org/10.1016/j.xphs.2018.08.026.

[154] P. Chen, J. Liu, K. Zhang, D. Huang, S. Huang, Q. Xie, F. Yang, J. Huang, D. Fang, Z. Huang, Z. Lu, Y.Z. Chen, Preparation of clarithromycin floating core-shell systems (CSS) using multi-nozzle semi-solid extrusion-based 3D printing, Int J Pharm. 605 (2021) 120837. https://doi.org/10.1016/j.ijpharm.2021.120837.

[155] S. Migliozzi, G. Meridiano, P. Angeli, L. Mazzei, Investigation of the swollen state of Carbopol molecules in non-aqueous solvents through rheological characterization, Soft Matter. 16 (2020) 9799–9815. https://doi.org/10.1039/D0SM01196G.

[156] M. Suhail, P.C. Wu, M.U. Minhas, Using Carbomer-Based Hydrogels for Control the Release Rate of Diclofenac Sodium: Preparation and In Vitro Evaluation, Pharmaceuticals 2020, Vol. 13, Page 399. 13 (2020) 399. https://doi.org/10.3390/PH13110399.

[157] Carbopol® 974P NF Polymer - Oral controlled-release and Taste-masking formulations, Topical & Mucosal Applications - Lubrizol, (n.d.). https://www.lubrizol.com/Health/Pharmaceuticals/Excipients/Carbopol-Polymer-Products/Carbopol-974P-NF-Polymer (accessed October 14, 2022).

[158] J. dos Santos, G.S. da Silva, M.C. Velho, R.C.R. Beck, Eudragit®: A Versatile Family of Polymers for Hot Melt Extrusion and 3D Printing Processes in Pharmaceutics, Pharmaceutics 2021, Vol. 13, Page 1424. 13 (2021) 1424. https://doi.org/10.3390/PHARMACEUTICS13091424.

[159] EUDRAGIT® Functional Polymers for Oral Solid Dosage Forms - Evonik Industries, (n.d.). https://healthcare.evonik.com/en/drugdelivery/oral-drug-delivery/oral-excipients/eudragit-portfolio (accessed September 5, 2022).

[160] Y. Yang, H. Wang, X. Xu, G. Yang, Strategies and mechanisms to improve the printability of pharmaceutical polymers Eudragit® EPO and Soluplus®, Int J Pharm. 599 (2021) 120410. https://doi.org/10.1016/j.ijpharm.2021.120410.

[161] N. Gottschalk, M. Bogdahn, M. Harms, J. Quodbach, Brittle polymers in Fused Deposition Modeling: An improved feeding approach to enable the printing of highly drug loaded filament, Int J Pharm. 597 (2021) 120216. https://doi.org/10.1016/j.ijpharm.2021.120216.

[162] K. Ilyés, N.K. Kovács, A. Balogh, E. Borbás, B. Farkas, T. Casian, G. Marosi, I. Tomuță, Z.K. Nagy, The applicability of pharmaceutical polymeric blends for the fused deposition modelling (FDM) 3D technique: Material considerations–printability–process modulation, with consecutive effects on in vitro release, stability and degradation, European Journal of Pharmaceutical Sciences. (2019). https://doi.org/10.1016/j.ejps.2018.12.019.

[163] J. Krause, M. Bogdahn, F. Schneider, M. Koziolek, W. Weitschies, Design and characterization of a novel 3D printed pressure-controlled drug delivery system, European Journal of Pharmaceutical Sciences. 140 (2019) 105060. https://doi.org/10.1016/j.ejps.2019.105060.

[164] V. Linares, M. Casas, I. Caraballo, Printfills: 3D printed systems combining fused deposition modeling and injection volume filling. Application to colon-specific drug delivery, European Journal of Pharmaceutics and Biopharmaceutics. 134 (2019) 138–143. https://doi.org/10.1016/j.ejpb.2018.11.021.

[165] C.W. Rowe, W.E. Katstra, R.D. Palazzolo, B. Giritlioglu, P. Teung, M.J. Cima, Multimechanism oral dosage forms fabricated by three dimensional printing(TM), Journal of Controlled Release. 66 (2000) 11–17. https://doi.org/10.1016/S0168-3659(99)00224-2.

[166] Y. Yang, Y. Xu, S. Wei, W. Shan, Oral preparations with tunable dissolution behavior based on selective laser sintering technique, Int J Pharm. 593 (2021) 120127. https://doi.org/10.1016/j.ijpharm.2020.120127.

[167] H.E. Gültekin, S. Tort, F. Tuğcu-Demiröz, F. Acartürk, 3D printed extended release tablets for once daily use: An in vitro and in vivo evaluation study for a personalized solid dosage form, Int J Pharm. 596 (2021) 120222. https://doi.org/10.1016/J.IJPHARM.2021.120222.

[168] H. Sun, R. Yang, J. Wang, X. Yang, J. Tu, L. Xie, C. Li, Q. Lao, C. Sun, Component-based biocompatibility and safety evaluation of polysorbate 80, RSC Adv. 7 (2017) 15127–15138. https://doi.org/10.1039/C6RA27242H.

[169] A.N. Ghebremeskel, C. Vemavarapu, M. Lodaya, Use of surfactants as plasticizers in preparing solid dispersions of poorly soluble API: Selection of polymer–surfactant combinations using solubility parameters and testing the processability, Int J Pharm. 328 (2007) 119–129. https://doi.org/10.1016/J.IJPHARM.2006.08.010.

[170] R. Rashid, D.W. Kim, F.U. Din, O. Mustapha, A.M. Yousaf, J.H. Park, J.O. Kim, C.S. Yong, H.G. Choi, Effect of hydroxypropylcellulose and Tween 80 on physicochemical properties and bioavailability of ezetimibe-loaded solid dispersion, Carbohydr Polym. 130 (2015) 26–31. https://doi.org/10.1016/J.CARBPOL.2015.04.071.

[171] A.N. Ghebremeskel, C. Vemavarapu, M. Lodaya, Use of surfactants as plasticizers in preparing solid dispersions of poorly soluble API: stability testing of selected solid dispersions, Pharm Res. 23 (2006) 1928–1936. https://doi.org/10.1007/S11095-006-9034-1.

[172] A.A. D'souza, R. Shegokar, Polyethylene glycol (PEG): a versatile polymer for pharmaceutical applications, Http://Dx.Doi.Org/10.1080/17425247.2016.1182485. 13 (2016) 1257–1275. https://doi.org/10.1080/17425247.2016.1182485.

[173] M.S. Algahtani, A.A. Mohammed, J. Ahmad, E. Saleh, Development of a 3D printed coating shell to control the drug release of encapsulated immediate-release tablets, Polymers (Basel). 12 (2020). https://doi.org/10.3390/polym12061395.

[174] BIO X 3D Bioprinter - CELLINK, (n.d.). https://www.cellink.com/bioprinting/bio-x-3d-bioprinter/ (accessed October 14, 2022).

[175] S.E. Glassford, B. Byrne, S.G. Kazarian, Recent applications of ATR FTIR spectroscopy and imaging to proteins, Biochim Biophys Acta Proteins Proteom. 1834 (2013) 2849–2858. https://doi.org/10.1016/j.bbapap.2013.07.015.

[176] K.L. Andrew Chan, S.G. Kazarian, Attenuated total reflection Fourier-transform infrared (ATR-FTIR) imaging of tissues and live cells, Chem Soc Rev. 45 (2016) 1850–1864. https://doi.org/10.1039/c5cs00515a.

[177] J. Hapanowicz, Proposition of non-standard method useful for viscosity measurements of unstable two-phase systems coupled with examples of its application, Measurement (Lond). 164 (2020) 108113. https://doi.org/10.1016/j.measurement.2020.108113.

[178] F.D.C. Siacor, Q. Chen, J.Y. Zhao, L. Han, A.D. Valino, E.B. Taboada, E.B. Caldona, R.C. Advincula, On the additive manufacturing (3D printing) of viscoelastic materials and flow behavior: From composites to food manufacturing, Addit Manuf. 45 (2021) 102043. https://doi.org/10.1016/j.addma.2021.102043.

[179] M. Spiliopoulou, A. Valmas, D.P. Triandafillidis, C. Kosinas, A. Fitch, F. Karavassili, I. Margiolaki, Applications of X-ray Powder Diffraction in Protein Crystallography and Drug Screening, Crystals 2020, Vol. 10, Page 54. 10 (2020) 54. https://doi.org/10.3390/CRYST10020054.

[180] N.K. Thakral, R.L. Zanon, R.C. Kelly, S. Thakral, Applications of Powder X-Ray Diffraction in Small Molecule Pharmaceuticals: Achievements and Aspirations, J Pharm Sci. 107 (2018) 2969–2982. https://doi.org/10.1016/J.XPHS.2018.08.010.

[181] J.P. Real, M.E. Barberis, N.M. Camacho, S. Sánchez Bruni, S.D. Palma, Design of novel oral ricobendazole formulation applying melting solidification printing process (MESO-PP): An innovative solvent-free alternative method for 3D printing using a simplified concept and low temperature, Int J Pharm. 587 (2020) 119653. https://doi.org/10.1016/j.ijpharm.2020.119653.

[182] N. Gottschalk, J. Quodbach, A.G. Elia, F. Hess, M. Bogdahn, Determination of feed forces to improve process understanding of Fused Deposition Modeling 3D printing and to ensure mass conformity of printed solid oral dosage forms, Int J Pharm. 614 (2022) 121416. https://doi.org/10.1016/j.ijpharm.2021.121416.

[183] B.C. Pereira, A. Isreb, R.T. Forbes, F. Dores, R. Habashy, J.B. Petit, M.A. Alhnan, E.F. Oga, 'Temporary Plasticiser': A novel solution to fabricate 3D printed patient-centred cardiovascular 'Polypill' architectures, European

Journal of Pharmaceutics and Biopharmaceutics. 135 (2019) 94–103. https://doi.org/10.1016/j.ejpb.2018.12.009.

[184] B.R. Giri, E.S. Song, J. Kwon, J.H. Lee, J.B. Park, D.W. Kim, Fabrication of intragastric floating, controlled release 3D printed theophylline tablets using hot-melt extrusion and fused deposition modeling, Pharmaceutics. 12 (2020). https://doi.org/10.3390/pharmaceutics12010077.

[185] H. Kadry, T.A. Al-Hilal, A. Keshavarz, F. Alam, C. Xu, A. Joy, F. Ahsan, Multi-purposable filaments of HPMC for 3D printing of medications with tailored drug release and timed-absorption, Int J Pharm. (2018). https://doi.org/10.1016/j.ijpharm.2018.04.010.

[186] J.B. Park, B.J. Lee, C.Y. Kang, R. v. Tiwari, M.A. Repka, Process analytical quality control of tailored drug release formulation prepared via hot-melt extrusion technology, J Drug Deliv Sci Technol. 38 (2017) 51–58. https://doi.org/10.1016/J.JDDST.2017.01.007.

[187] N.G. Solanki, M. Tahsin, A. v. Shah, A.T.M. Serajuddin, Formulation of 3D Printed Tablet for Rapid Drug Release by Fused Deposition Modeling: Screening Polymers for Drug Release, Drug-Polymer Miscibility and Printability, J Pharm Sci. (2018). https://doi.org/10.1016/j.xphs.2017.10.021.

[188] P. Gill, T.T. Moghadam, B. Ranjbar, Differential Scanning Calorimetry Techniques: Applications in Biology and Nanoscience, J Biomol Tech. 21 (2010) 167.

[189] D. Fang, H. Pan, M. Cui, S. Qiao, X. Li, T. Wang, Q. Meng, L. Xu, W. Pan, Fabrication of three-dimensional-printed ofloxacin gastric floating sustained-release tablets with different structures, J Drug Deliv Sci Technol. 67 (2022). https://doi.org/10.1016/j.jddst.2021.102992.

[190] Z. Zheng, J. Lv, W. Yang, X. Pi, W. Lin, Z. Lin, W. Zhang, J. Pang, Y. Zeng, Z. Lv, H. Lao, Y. Chen, F. Yang, Preparation and application of subdivided tablets using 3D printing for precise hospital dispensing, European Journal of Pharmaceutical Sciences. 149 (2020) 105293. https://doi.org/10.1016/J.EJPS.2020.105293.

[191] R. Bottom, The role of modulated temperature differential scanning calorimetry in the characterisation of a drug molecule exhibiting polymorphic and glass

forming tendencies, Int J Pharm. 192 (1999) 47–53. https://doi.org/10.1016/S0378-5173(99)00271-9.

[192] G.C. Bazzo, B.R. Pezzini, H.K. Stulzer, Eutectic mixtures as an approach to enhance solubility, dissolution rate and oral bioavailability of poorly water-soluble drugs, Int J Pharm. 588 (2020) 119741. https://doi.org/10.1016/j.ijpharm.2020.119741.

[193] M.T. França, T. Martins Marcos, P.F.A. Costa, G.C. Bazzo, R. Nicolay Pereira, A.P. Gerola, H.K. Stulzer, Eutectic mixture and amorphous solid dispersion: Two different supersaturating drug delivery system strategies to improve griseofulvin release using saccharin, Int J Pharm. 615 (2022) 121498. https://doi.org/10.1016/j.ijpharm.2022.121498.

[194] A. Górniak, A. Wojakowska, B. Karolewicz, J. Pluta, Phase diagram and dissolution studies of the fenofibrate–acetylsalicylic acid system, Journal of Thermal Analysis and Calorimetry 2010 104:3. 104 (2010) 1195–1200. https://doi.org/10.1007/S10973-010-1148-3.

[195] Polarized Light Microscopy | Nikon's MicroscopyU, (n.d.). https://www.microscopyu.com/techniques/polarized-light/polarized-light-microscopy (accessed October 14, 2022).

[196] Polarized Light Microscopy - Microscope Configuration | Olympus LS, (n.d.). https://www.olympus-lifescience.com/pt/microscope-resource/primer/techniques/polarized/configuration/ (accessed October 14, 2022).

[197] M. Krkobabić, D. Medarević, S. Cvijić, B. Grujić, S. Ibrić, Hydrophilic excipients in digital light processing (DLP) printing of sustained release tablets: Impact on internal structure and drug dissolution rate, Int J Pharm. 572 (2019) 118790. https://doi.org/10.1016/J.IJPHARM.2019.118790.

[198] P. Inc, Thermogravimetric Analysis (TGA) TGA 8000 TGA 4000 STA 6000 / STA 8000 The Thermogravimetric Instrument Family, (n.d.).

[199] C.I. Gioumouxouzis, O.L. Katsamenis, N. Bouropoulos, D.G. Fatouros, 3D printed oral solid dosage forms containing hydrochlorothiazide for controlled drug delivery, J Drug Deliv Sci Technol. (2017). https://doi.org/10.1016/j.jddst.2017.06.008.

[200] Y. Yang, H. Wang, H. Li, Z. Ou, G. Yang, 3D printed tablets with internal scaffold structure using ethyl cellulose to achieve sustained ibuprofen release, European Journal of Pharmaceutical Sciences. (2018). https://doi.org/10.1016/j.ejps.2018.01.005.

[201] M. Cui, Y. Yang, D. Jia, P. Li, Q. Li, F. Chen, S. Wang, W. Pan, P. Ding, Effect of novel internal structures on printability and drug release behavior of 3D printed tablets, J Drug Deliv Sci Technol. (2019). https://doi.org/10.1016/j.jddst.2018.10.037.

[202] D. Chen, X.Y. Xu, R. Li, G.A. Zang, Y. Zhang, M.R. Wang, M.F. Xiong, J.R. Xu, T. Wang, H. Fu, Q. Hu, B. Wu, G.R. Yan, T.Y. Fan, Preparation and In vitro Evaluation of FDM 3D-Printed Ellipsoid-Shaped Gastric Floating Tablets with Low Infill Percentages, AAPS PharmSciTech. (2020). https://doi.org/10.1208/s12249-019-1521-x.

[203] A. Goyanes, H. Chang, D. Sedough, G.B. Hatton, J. Wang, A. Buanz, S. Gaisford, A.W. Basit, Fabrication of controlled-release budesonide tablets via desktop (FDM) 3D printing, Int J Pharm. (2015). https://doi.org/10.1016/j.ijpharm.2015.10.039.

[204] K. Keklikoglou, C. Arvanitidis, G. Chatzigeorgiou, E. Chatzinikolaou, E. Karagiannidis, T. Koletsa, A. Magoulas, K. Makris, G. Mavrothalassitis, E.D. Papanagnou, A.S. Papazoglou, C. Pavloudi, I.P. Trougakos, K. Vasileiadou, A. Vogiatzi, Micro-CT for Biological and Biomedical Studies: A Comparison of Imaging Techniques, Journal of Imaging 2021, Vol. 7, Page 172. 7 (2021) 172. https://doi.org/10.3390/JIMAGING7090172.

[205] Scanning Electron Microscopy | Principles of Scanning Electron Microscopy | Thermo Fisher Scientific - UK, (n.d.). https://www.thermofisher.com/uk/en/home/materials-science/learning-center/applications/scanning-electron-microscope-sem-electron-column.html (accessed October 14, 2022).

[206] K. Akhtar, S.A. Khan, S.B. Khan, A.M. Asiri, Scanning electron microscopy: Principle and applications in nanomaterials characterization, in: Handbook of Materials Characterization, Springer International Publishing, 2018: pp. 113–145. https://doi.org/10.1007/978-3-319-92955-2_4.

[207] MicroCT Imaging | PerkinElmer, (n.d.). https://www.perkinelmer.com/uk/category/microct-imaging (accessed October 6, 2022).

[208] A. du Plessis, C. Broeckhoven, A. Guelpa, S.G. le Roux, Laboratory x-ray micro-computed tomography: a user guideline for biological samples, Gigascience. 6 (2017) 1–11. https://doi.org/10.1093/GIGASCIENCE/GIX027.

[209] A. Zidan, A. Alayoubi, S. Asfari, J. Coburn, B. Ghammraoui, C.N. Cruz, M. Ashraf, Development of mechanistic models to identify critical formulation and process variables of pastes for 3D printing of modified release tablets, Int J Pharm. 555 (2019) 109–123. https://doi.org/10.1016/j.ijpharm.2018.11.044.

[210] A. du Plessis, I. Yadroitsev, I. Yadroitsava, S.G. le Roux, X-Ray Microcomputed Tomography in Additive Manufacturing: A Review of the Current Technology and Applications, 3D Print Addit Manuf. 5 (2018) 227–247. https://doi.org/10.1089/3DP.2018.0060/ASSET/IMAGES/LARGE/FIGURE13.JPEG.

[211] J.D. Boerckel, D.E. Mason, A.M. McDermott, E. Alsberg, Microcomputed tomography: approaches and applications in bioengineering, Stem Cell Res Ther. 5 (2014). https://doi.org/10.1186/SCRT534.

[212] Z. Gao, L.N.Y. Cao, X. Liu, L. Tian, J.D. Rodriguez, An In Vitro Dissolution Method for Testing Extended-Release Tablets Under Mechanical Compression and Sample Friction, J Pharm Sci. 111 (2022) 1652–1658. https://doi.org/10.1016/J.XPHS.2021.10.036.

[213] C.K. Brown, H. Dieter Friedel, A.R. Barker, L.F. Buhse, S. Keitel, T.L. Cecil, J. Kraemer, J. Michael Morris, C. Reppas, M.P. Stickelmeyer, C. Yomota, V.P. Shah, FIP/AAPS Joint Workshop Report: Dissolution/In Vitro Release Testing of Novel/Special Dosage Forms Meeting Report, Indian J Pharm Sci. 73 (n.d.) 338. https://doi.org/10.1208/s12249-011-9634-x.

[214] J. Østergaard, UV imaging in pharmaceutical analysis, J Pharm Biomed Anal. 147 (2018) 140–148. https://doi.org/10.1016/j.jpba.2017.07.055.

[215] M. Alhijjaj, P. Belton, S. Qi, A multi-technique characterization of the stability of surfactant containing solid dispersion based buccal patches prepared by hot melt injection moulding, Int J Pharm. 528 (2017) 547–562. https://doi.org/10.1016/J.IJPHARM.2017.06.048.

[216] D.T. Eduardo, S.E. Ana, F. José B., A micro-extrusion 3D printing platform for fabrication of orodispersible printlets for pediatric use, Int J Pharm. 605 (2021) 120854. https://doi.org/10.1016/J.IJPHARM.2021.120854.

[217] United States Pharmacopeia - Tablet Friability, in: 2016.

[218] S. Yamauchi, S. Hatakeyama, Y. Imai, M. Tonouchi, Nondestructive evaluation of crystallized-particle size in lactose-powder by terahertz time-domain spectroscopy, Optical Engineering. 53 (2013) 031203. https://doi.org/10.1117/1.OE.53.3.031203.

[219] C.R.M. Brambilla, O.L. Okafor-muo, H. Hassanin, A. Elshaer, 3DP Printing of Oral Solid Formulations: A Systematic Review, Pharmaceutics 2021, Vol. 13, Page 358. 13 (2021) 358. https://doi.org/10.3390/PHARMACEUTICS13030358.

[220] P. Tipduangta, K. Takieddin, L. Fábián, P. Belton, S. Qi, A New Low Melting-Point Polymorph of Fenofibrate Prepared via Talc Induced Heterogeneous Nucleation, Cryst Growth Des. 15 (2015) 5011–5020. https://doi.org/10.1021/ACS.CGD.5B00956.

[221] P. Costa, J.M. Sousa Lobo, Modeling and comparison of dissolution profiles, European Journal of Pharmaceutical Sciences. 13 (2001) 123–133. https://doi.org/10.1016/S0928-0987(01)00095-1.

[222] G. van den Mooter, The use of amorphous solid dispersions: A formulation strategy to overcome poor solubility and dissolution rate, Drug Discov Today Technol. 9 (2012) e79–e85. https://doi.org/10.1016/J.DDTEC.2011.10.002.

[223] J.B. Park, B.J. Lee, C.Y. Kang, R. v. Tiwari, M.A. Repka, Process analytical quality control of tailored drug release formulation prepared via hot-melt extrusion technology, J Drug Deliv Sci Technol. 38 (2017) 51–58. https://doi.org/10.1016/J.JDDST.2017.01.007.

[224] S. Feng, S. Bandari, M.A. Repka, Investigation of poly(2-ethyl-2-oxazoline) as a novel extended release polymer for hot-melt extrusion paired with fused deposition modeling 3D printing, J Drug Deliv Sci Technol. 74 (2022) 103558. https://doi.org/10.1016/J.JDDST.2022.103558.

[225] N.G. Patel, A.T.M. Serajuddin, Development of FDM 3D-printed tablets with rapid drug release, high drug-polymer miscibility and reduced printing

temperature by applying the acid-base supersolubilization (ABS) principle, Int J Pharm. 600 (2021) 120524. https://doi.org/10.1016/j.ijpharm.2021.120524.

[226] ICH Q1A (R2) Stability testing of new drug substances and drug products - Scientific guideline | European Medicines Agency, (n.d.). https://www.ema.europa.eu/en/ich-q1a-r2-stability-testing-new-drug-substances-drug-products-scientific-guideline#current-effective-version-section (accessed February 9, 2023).

[227] L. Greenspan, Humidity Fixed Points of Binary Saturated Aqueous Solutions, J Res Natl Bur Stand A Phys Chem. 81A (1977) 89. https://doi.org/10.6028/JRES.081A.011.

[228] Frequency sweeps :: Anton Paar Wiki, (n.d.). https://wiki.anton-paar.com/en/frequency-sweeps/ (accessed February 13, 2023).

[229] S. Bakrani Balani, F. Chabert, V. Nassiet, A. Cantarel, Influence of printing parameters on the stability of deposited beads in fused filament fabrication of poly(lactic) acid, Addit Manuf. 25 (2019) 112–121. https://doi.org/10.1016/J.ADDMA.2018.10.012.

[230] U. Sailaja, M.S. Thayyil, N.S.K. Kumar, G. Govindaraj, Molecular dynamics of amorphous pharmaceutical fenofibrate studied by broadband dielectric spectroscopy, J Pharm Anal. 6 (2016) 165–170. https://doi.org/10.1016/j.jpha.2014.09.003.

[231] M. Kyobula, A. Adedeji, M.R. Alexander, E. Saleh, R. Wildman, I. Ashcroft, P.R. Gellert, C.J. Roberts, 3D inkjet printing of tablets exploiting bespoke complex geometries for controlled and tuneable drug release, Journal of Controlled Release. (2017). https://doi.org/10.1016/j.jconrel.2017.06.025.

[232] T. Parikh, S.S. Gupta, A. Meena, A. Serajuddin, Investigation of thermal and viscoelastic properties of polymers relevant to hot melt extrusion - III: Polymethacrylates and polymethacrylic acid based polymers, Journal of Excipients and Food Chemicals. 5 (2014) 56–64.

[233] W. Fan, W. Zhu, X. Zhang, L. Di, The Preparation of Curcumin Sustained-Release Solid Dispersion by Hot Melt Extrusion— Ⅰ. Optimization of the Formulation, J Pharm Sci. 109 (2020) 1242–1252. https://doi.org/10.1016/J.XPHS.2019.11.019.

[234] W. Kempin, V. Domsta, G. Grathoff, I. Brecht, B. Semmling, S. Tillmann, W. Weitschies, A. Seidlitz, Immediate Release 3D-Printed Tablets Produced Via Fused Deposition Modeling of a Thermo-Sensitive Drug, Pharm Res. (2018). https://doi.org/10.1007/s11095-018-2405-6.

[235] H. Pan, D. Fan, Exploration of the pore-forming mechanisms of Tween80 and biocompatibility of the hydrogels in vivo, Chem Phys Lett. 743 (2020) 137175. https://doi.org/10.1016/J.CPLETT.2020.137175.

[236] G. van den Mooter, P. Augustijns, N. Blaton, R. Kinget, Physico-chemical characterization of solid dispersions of temazepam with polyethylene glycol 6000 and PVP K30, Int J Pharm. 164 (1998) 67–80. https://doi.org/10.1016/S0378-5173(97)00401-8.

[237] Bioprinting Thermoplastic Printhead - CELLINK, (n.d.). https://www.cellink.com/product/thermoplastic-printhead/ (accessed November 20, 2011).

[238] L.F.S. Carollo, A.L.F. Lima E Silva, S.M.M. Lima E Silva, Applying different heat flux intensities to simultaneously estimate the thermal properties of metallic materials, Meas Sci Technol. 23 (2012) 065601. https://doi.org/10.1088/0957-0233/23/6/065601.

[239] A. Melocchi, F. Parietti, A. Maroni, A. Foppoli, A. Gazzaniga, L. Zema, Hot-melt extruded filaments based on pharmaceutical grade polymers for 3D printing by fused deposition modeling, Int J Pharm. (2016). https://doi.org/10.1016/j.ijpharm.2016.05.036.